Pollution source identification and adequate design of a monitoring network in estuaries

Von der
Fakultät Architektur, Bauingenieurwesen und Umweltwissenschaften
der Technischen Universität Carolo-Wilhelmina
zu Braunschweig

zur Erlangung des Grades einer
Doktor-Ingenieurin (Dr.-Ing.)
genehmigte

Dissertation

von
Stephanie Zeunert
geboren am 02.05.1988
aus Rheda-Wiedenbrück

Eingereicht am:	03. Juli 2020
Disputation am:	27. November 2020
Berichterstatter:	Prof. Dr.-Ing. Günter Meon
	Prof. Dr. Michael Rode

2021

Danksagung

Diese Arbeit entstand während meiner Zeit als wissenschaftliche Mitarbeiterin an der Abteilung Hydrologie, Wasserwirtschaft und Gewässerschutz am Leichtweiß-Institut für Wasserbau der Technsichen Universität Braunschweig in der Zeit von 2018 bis 2020. Ich möchte mich an dieser Stelle bei all denjenigen bedanken, die mich auf meinem Weg begleitet und unterstützt haben.

Mein besonderer Dank geht hierbei an Herrn Prof. Dr.-Ing. Günter Meon für die Betreuung und fachliche Unterstützung bei der Anfertigung dieser Arbeit. Vielen Dank für die Freiheiten in der Bearbeitung, die stetige Motivation und das in mich gesetzte Vertrauen. Herrn Prof. Dr. Michael Rode danke ich für die bereitweilige Übernahme der Zweitbetreuung sowie die Unterstützung insbesondere zu Beginn der Arbeit was mir geholfen hat das Thema aus einem neuen Blickwinkel zu betrachten.

Danken möchte ich auch meinen aktuellen und ehemaligen Kollegen und Kolleginnen der Abteilung Hydrologie, Wasserwirtschaft und Gewässerschutz für die tolle Arbeitsatmosphäre und Zusammenarbeit. Namentlich hervorheben möchte ich dabei Malte Eley, Tobias Langmann, Dr.-Ing. Malte Lorenz, Patrick Nistahl, Dr.-Ing. Gerhard Riedel, Saskia Schimmelpfennig, Prof. Dr. Matthias Schöniger, Mannickam Somasundaram und Dr.-Ing. Karoline Stein. Ein besonderer Dank geht an Marlene Gelleszun, Dr.-Ing. Huyen Le, Tim Müller, Johanna Schwenkel und Susanne Festerling. Vielen Dank für eure Unterstützung!

Ein großer Dank geht an meine Familie, insbesondere meinen Eltern, die mich auf meinem Weg immer unterstützt haben. Meinem Bruder Matthias Zeunert danke ich sehr für das ausführliche Korrekturlesen. Ein liebevoller Dank geht an Brice Girol für die persönliche als auch fachliche Unterstützung während der gesamten Zeit sowie für das Korrekturlesen dieser Arbeit.

Summary

In the last decades, thousands of accidental pollution spills as well as intentional illegal discharges into surface waters have appeared all over the world. The identification of pollution source parameters (PSP), after these incidents has often proven difficult. However, this is an important aspect to mitigate the social, economic and ecological consequences. In recent years, several methods have been successfully developed to determine the unknown pollution source parameters including the source location and the release history. In the literature, this inverse problem is often referred to as pollution source identification (PSI). While numerous applications to rivers could be found in the literature, for estuaries only very little research has been carried out so far. This is mainly attributed to the higher complexity involved in modelling the pollutant transport processes.

Inverse problems like PSI heavily rely on pollutant concentration measurements collected in the course of the pollution incident. Previous works already indicated that the given monitoring data can significantly affect parameter identifiability and consequently the reliability of the obtained parameter estimates. However, a comprehensive analysis of the influence of the spatial and temporal monitoring design on identification results is missing both for unidimensional as well as for bidirectional flow systems in the literature. Consequently, the main objective of this thesis is to analyse the influence of the monitoring design on the identification process, and to improve the identification of PSP in the case of a spill incident through an adapted monitoring design, especially in estuaries. In this work, it is assumed that the pollutant is released instantaneously from a single point source. Consequently, the pollution spill can be described by four parameters, including the longitudinal and lateral source location, the release time, and the total pollutant mass.

To obtain basic knowledge regarding the influence of the spatial and temporal monitoring design on the identifiability of PSP, in a first step a synthetic unidirectional test case with a rectangular cross-section and a length of 55 km is considered. An analytical solution of the 2D advection-dispersion-reaction equation is used for the representation of the transport and mixing processes in the considered river section. Parameter identifiability under different monitoring configurations is analysed by using the profile likelihood approach. With the applied approach, the user is able to determine reasons in the case of non-identifiability and to derive likelihood-based confidence intervals. The obtained results indicate that parameter dependencies exist between different source parameters. An appropriate monitoring design can improve parameter identifiability and consequently lead to a more reliable parameter estimation. In general, monitoring stations closer to the release point will increase the accuracy in parameter estimates.

Subsequently, the identifiability analysis is extended to bidirectional flow systems. To represent the influence of tidal dynamics, a 2D numerical hydrodynamic transport model is set up for a simplified test case using the software suite Delft3D. The test case represents a simplified version of the Thi Vai Estuary and has a length of 30 km. Due to the high computational burden of the profile likelihood approach, a different approach is adopted for the identifiability analysis. The approach is based on a local sensitivity analysis at

multiple points in the parameter space. While the model output proved to be sufficiently sensitive to changes in all PSP, for the longitudinal source location and the release time a high correlation could be detected. The strengths of this interaction was dependent on the time of release in the tidal cycle. During times of higher currents (e.g. maximum ebb or flood tide) the interaction was stronger than at slack tide. For the comparison of different monitoring designs, two optimality criteria based on the Fisher-Information Matrix were derived. Results generally agree with those derived for the unidirectional test case and show that an early detection decreases uncertainties in the estimated parameters. However, compared to unidirectional flow systems, the periodically changing flow direction leads to a longer residence time of the pollutant plume in estuaries and a delayed detection at monitoring stations further downstream. The results of the sensitivity analysis have shown that a delayed detection reduces the sensitivity of the model output to changes in the source parameters.

For the identification of PSP several approaches exist in the literature. However, these have been rarely applied to bidirectional flow systems. In this work, the simulation-optimization approach is adopted as it can be easily linked to various transport models. The performance of two variants of the approach are compared for the two-dimensional bidirectional test case. While the usually applied approach corresponds to the simultaneous identification of all unknown source parameters, the modified version decouples the estimation of the release time from the other source parameters. Both approaches are applied to several pollution scenarios using perfect and noise perturbed monitoring data. While both optimization approaches performed well if perfect monitoring data were assumed, the simultaneous optimization approach showed signs of premature convergence in the presence of measurement noise. The calculated confidence intervals and correlation matrices indicated that the time of release plays an important role in the accurate identification of PSP, an observation that is consistent with the results of the identifiability analysis.

In a final step, both optimization approaches are transferred to a real-world estuary, the Thi Vai Estuary, located in South Vietnam. For the simulation of pollution scenarios a two-dimensional hydrodynamic transport model is set up. Compared to the test case, the bathymetry of the numerical model is much more complex and also takes into account the numerous meanders and the intertidal zone. The hydrodynamic transport model is calibrated based on monitoring data collected in the framework of the research project EWATEC-COAST. The joint research project was financed by the German Federal Ministry of Education and Research from 2012 to 2015 and managed by the Department of Hydrology, Water Management and Water Protection at the University of Braunschweig. Initially, an optimal monitoring network is developed for the Thi Vai Estuary based on the minimization of the mean detection time considering numerous pollution scenarios. Synthetically generated monitoring data of the optimized monitoring network are subsequently used for the identification of several theoretical spill incidents in the Thi Vai Estuary. Both optimization approaches performed generally well and could correctly identify 80% of the considered pollution scenarios. Reasons for premature convergence in the other cases were mostly due to the overall complexity of the optimization problem including parameter interactions, decreased parameter sensitivity and the spatial and temporal discretization of the numerical transport model.

Zusammenfassung

In den letzten Jahrzehnten kam es auf der ganzen Welt immer wieder zu zahlreichen Unfällen als auch illegalen Einleitungen, bei denen Schadstoffe in Oberflächengewässern eingeleitet wurden. Die Identifikation der Einleitungsparameter, insbesondere des Einleitungsortes, stellt hierbei eine große Herausforderung dar, ist aber sowohl unter ökonomischen als auch sozialen und umwelttechnischen Aspekte von großer Bedeutung. In den letzten Jahren wurden zahlreiche Methoden entwickelt, um die unbekannten Einleitungsparameter, zu denen neben dem Einleitungsort auch die zeitliche Einleitungsfunktion zählen, zu bestimmen. Die entwickelten Methoden beziehen sich dabei hauptsächlich auf Flüsse. Für Ästuare konnten in der Literatur bisher nur wenige Anwendungen gefunden werden. Dies ist häufig auf die höhere Komplexität bei der Modellierung der Transportprozesse zurückzuführen.

Inverse Probleme wie die Identifikation einer Verschmutzungsquelle hängen stark von den gesammelten Messdaten ab, die im Zuge des Schadstoffunfalls erhoben wurden. Frühere Arbeiten haben bereits gezeigt, dass die Monitoringdaten die Identifizierbarkeit der Einleitungsparameter und folglich die Verlässlichkeit der geschätzten Parametern erheblich beeinflussen können. Es fehlt jedoch momentan sowohl für uni- als auch bidirektionale Fließgewässer eine umfassende Studie, die den Einfluss des räumlichen und zeitlichen Monitoringdesigns auf die Identifizierbarkeit der Parameter bewertet. Folglich besteht das Hauptziel dieser Arbeit darin, den Einfluss des Monitorings auf den Identifkationsprozess zu analysieren und durch ein angepasstes Monitoringdesign die Identifikation der Einleitungsparameter im Falle eines Schadstoffeintrags insbesondere in Ästuare zu verbessern. In dieser Arbeit wird davon ausgegangen, dass die Schadstoffeinleitung ausschließlich durch eine momentane Einleitung aus einer einzelnen Punktquelle resultiert. Die zu bestimmenden Einleitungsparameter beinhalten somit die longitudinale und laterale Position der Einleitung, den Einleitungszeitpunkt und die eingeleitete Schadstoffmenge.

Um zunächst grundlegende Erkenntnisse bezüglich des Einflusses des räumlichen und zeitlichen Monitoringdesigns auf die Identifizierbarkeit der Einleitungsparameter zu erhalten, wird im ersten Schritt dieser Arbeit ein synthetischer Flussabschnitt mit einem rechteckigen Querschnitt und einer Länge von 55 km betrachtet. Zur Darstellung der Transport- und Mischungsprozesse wird auf eine analytische Lösung der 2D-Advektions-Dispersions-Reaktions-Gleichung zurückgegriffen. Die Identifizierbarkeit der Einleitungsparameter unter verschiedenen Monitoringkonfigurationen wird mit Hilfe der Profile-Likelihood-Methodik untersucht. Mit diesem Ansatz können sowohl Gründe im Falle einer Nicht-Identifizierbarkeit ermittelt werden als auch likelihood-basierte Konfidenzintervalle abgeleitet werden. Die Ergebnisse der Analyse zeigen, dass zwischen bestimmten Einleitungsparametern Korrelationen bestehen, die zu einer schlechteren Bestimmung der Parameter führen. Ein angepasstes Monitoringdesign kann allerdings die Identifizierbarkeit verbessern und folglich zu einer zuverlässigeren Parameterschätzung führen. Im Allgemeinen erhöhen Monitoringstationen in der Nähe des Einleitungsortes die Genauigkeit der Parameterschätzung.

Unter Nutzung der gewonnenen Erkenntnisse wird die Analyse der Identifizierbarkeit der Einleitungsparameter anschließend auf bidirektionale Gewässer wie Ästuare erweitert. Um den Einfluss der Gezeiten zu berücksichtigen, wird ein zweidimensionales numerisches Transportmodell mit der Software Delft3D für einen vereinfachten Testfall erstellt. Der Testfall stellt eine vereinfachte Version des Thi Vai Ästuars dar und besitzt eine Länge von 30 km. Da die Profile-Likelihood-Methode sehr rechenintensiv ist, wird auf einen anderen Ansatz für die Identifizierbarkeitsanalyse zurückgegriffen. Dieser basiert auf einer lokalen Sensitivitätsanalyse an mehreren Punkten im Parameterraum. Die Ergebnisse zeigen, dass der Output des Transportmodells generell sensitiv auf Änderungen in den Einleitungsparametern reagiert, es allerdings zu Parameterinteraktionen kommt, die die Identifizierbarkeit der einzelnen Parameter schwächt. So konnte für den longitudinalen Einleitungsort und den Einleitungszeitpunkt eine hohe Korrelation festgestellt werden, deren Stärke vom Einleitungszeitpunkt im Tidezyklus abhängig ist. Insgesamt war die Korrelation zu Zeiten der höchsten Strömungsgeschwindigkeiten (z. Bsp. während des maximalen Ebbe- bzw. Flutstroms) am stärksten. Bei Stillwasser konnte eine geringere Korrelation festgestellt werden. Für den Vergleich verschiedener Monitoringdesigns wurden zwei Optimalitätskriterien verwendet, die auf der Fisher-Informations-Matrix beruhen. Die erhaltenen Ergebnisse stimmen grundsätzlich mit denen des unidirektionalen Testfalls überein und zeigen, dass Unsicherheiten in den Einleitungsparametern reduziert werden können, je eher die Verschmutzungsfahne detektiert wird. Allerdings ist im Vergleich zu unidirektionalen Fließgewässern zu beachten, dass es durch die sich periodisch ändernde Fließrichtung zu einer längerern Verweilzeit des Schadstofffahne im Ästuar kommt, was zu einer verspäteteten Detektion an weiter unterhalb liegenden Monitoringstationen führt. Eine verspätete Detektion verringert die Sensitivität des Modelloutputs gegenüber Änderungen in den Einleitungsparametern.

Zur Identifikation von Einleitungsparametern im Zuge eines Schadstoffunfalls existieren in der Literatur verschiedene Ansätze. Diese wurden bisher jedoch selten auf Ästuare angewandt. In dieser Arbeit wird der Simulations-Optimierungsansatz ausgewählt, da er im Allgemeinen eine einfache Kopplung zwischen Optimierungsalgorithmus und unterschiedlichen Transportmodellen ermöglicht. In der Literatur existieren zwei Optimierungsvarianten, die in dieser Arbeit angewendet und verglichen werden. Während im ersten Ansatz alle Parameter simultan ermittelt werden, wird für das zweite Verfahren die Bestimmung des Einleitungszeitpunktes von den anderen Parametern entkoppelt. Beide Ansätze werden auf verschiedene Einleitungsszenarien angewandt, wobei sowohl perfekte als auch fehlerbehaftete Monitoringdaten betrachtet werden. Beide Optimierungsansätze liefern sehr gute Resultate unter der Annahme, dass die Monitoringdaten keine Fehler aufweisen. Allerdings zeigt der simultane Optimierungsansatz für ein Szenario Anzeichen von vorzeitiger Konvergenz bei einem Vorhandensein von Fehlern in den Messdaten. Die ermittelten Konfidenzintervalle und Korrelationsmatrizen zeigen, dass der Einleitungszeitpunkt eine wichtige Rolle in der Zuverlässigkeit der Parameterschätzung spielt, eine Beobachtung die mit den Ergebnissen der vorhergehenden Analyse übereinstimmt.

In einem letzten Schritt werden beide Optimierungsansätze auf einen realen Ästuar, den Thi Vai Ästuar in Südvietnam übertragen. Zur Simulation verschiedener Einleitungs szenarien wird ein zweidimensionales hydrodynamisches Transportmodell in der Software Delft3D aufgebaut. Im Vergleich zum Testfall ist die Bathymetrie des numerischen Modells deutlich komplexer und berücksichtigt auch die zahlreichen Mäander und die bei Ebbe trockenfallende Gezeitenzone. Daten, die im Rahmen des Forschungsprojektes EWATEC-COAST erhoben wurden, dienen zur Kalibrierung des Modells. Das Verbundforschungsprojekt wurde von 2012 bis 2015 durch das deutsche Bundesministerium für

Bildung und Forschung finanziert und von der Abteilung Hydrologie, Wasserwirtschaft und Gewässerschutz der TU Braunschweig geleitet. Zunächst wird für das Thi Vai Ästuar ein optimales Monitoringnetzwerk entwickelt, welches auf der Minimierung der mittleren Detektionszeit von zahlreichen Einleitungsszenarien beruht. Synthetisch erzeugte Monitoringdaten des optimierten Netzwerkes werden anschließend zur Identifikation mehrerer theoretischer Einleitungsszenarien verwendet. Beide Optimierungsansätze zeigen im Schnitt gute Ergebnisse und können die Parameter von 80% der betrachteten Einleitungsszenarien korrekt bestimmen. Eine frühzeitige Konvergenz in den anderen Fällen ist auf die Gesamtkomplexität des Optimierungsproblems zurückzuführen. Dies schließt Parameterwechselwirkungen, eine verringerte Parametersensitivität und die zeitliche und räumliche Diskretisierung des numerischen Modells mit ein.

Contents

1 Introduction

1.1 Background

In the last decades, the pollution of surface water bodies, including river systems, lakes, estuaries and coastal areas, has grown into a serious problem worldwide (FAO 2011). Economic development, intensive agriculture, population growth and climate change are leading to an increasing pressure on the available water resources, particularly in emerging countries such as in Southeast Asia (Visvanathan and Padmasri 2010). The strong industrial development in the vicinity of water courses increases the risk of accidental pollution spills and illegal wastewater discharges.

Since the implementation of reform policies in 1986 (Doi Moi), Vietnam has been one of the fastest growing countries in South East Asia with an annual economic growth rate of $\geq 5.2\%$ (Hoang et al. 2019). However, rapid urban and industrial development are severely threatening available water resources (World Bank Group 2019). One of the core regions of industrial development lies in the south of the country in the vicinity of Ho Chi Minh City (ICEM 2007). Ongoing industrial pollution is severely affecting the surrounding environment, including the Thi Vai Estuary, a branch of the Dong Nai river system. Since 1990, numerous industrial zones have been built adjacent to the estuary. In subsequent years, the water quality of the Thi Vai Estuary deteriorated significantly (Prilop et al. 2014; Le et al. 2017). However, only in 2008 the authorities uncovered that one of the adjacent companies was primarily responsible for the pollution. Over several years, the company illegally discharged large amounts of untreated wastewater into the estuary through an underground pipe system (Tran 2008; Nguyen and Pham 2012; Meon et al. 2017). Although wastewater treatment plants have been improved and stricter regulations were put into place, in recent years several other spill incidents occurred along the Thi Vai Estuary (Murray 2016) and the Dong Nai River (VietNamNews 2011). Another prominent incident is the Formosa steel plant incident at the coast of Central Vietnam, which led to thousands of fish kills (Trang 2017). The identification of the responsible source after these incidents has often proven difficult. However, this is an important aspect to mitigate the social, economic and ecological consequences.

1.2 Research objectives

In recent years, several methods have been successfully developed and applied in river systems to identify the pollutant source in the case of a spill incident. Depending on the spatial and temporal characteristics, the pollutant spill can be described by different parameters, including the source location. To identify the unknown parameters various methods have been applied, including the simulation-optimization approach (Han et al. 2014; Zhang and Xin 2017), the backward probability method (Cheng and Jia 2010; Ghane et al. 2016; Wang et al. 2018), Bayesian inference (Yang et al. 2016; Guozhen et al. 2016; Jiang et al. 2019) and the mathematical approach (El Badia and Hamdi 2007;

Mazaheri et al. 2015). In the literature, the problem is often referred to as pollution source identification (PSI).

However, for bidirectional flow systems like estuaries, only very little research has been carried out so far. This is partly due to the more complex transport processes. For a river stretch, assuming steady hydrodynamics, often an analytical solution of the advection-dispersion-reaction equation is used to describe the underlying transport processes (e.g. Guozhen et al. (2016), Zhang and Xin (2017) and Jiang et al. (2019)). In estuaries, due to the varying flow direction and often highly unsteady velocity, a numerical transport model has to be set up and calibrated for the particular system. For this task, an elaborate monitoring campaign is necessary beforehand. Additionally, when applying a numerical transport model, each model run needs a significant amount of computation time. Most PSI approaches rely on a vast number of model runs and the total computation time needs to be taken into account. Nevertheless, estuaries are particularly vulnerable to pollution due to the tide dependent change of flow direction, which leads to an overall longer residence time of pollutants inside the estuary. Therefore, spill incidents can have a severe effect on the water quality of estuaries and the identification of the pollution source should be of high priority.

As mentioned before, PSI relies on monitoring data which have to be collected in the event of a pollution incident. The considered spatial and temporal monitoring design can have a significant influence on the reliable estimation of the source parameters. When the observed data do not adequately define the actual source characteristics, multiple parameter sets might fit the data equally well (Amirabdollahian and Datta 2013). In this case, parameters are termed non-identifiable, leading to a non-unique solution of the inverse problem. Identifiability issues in PSI have already been encountered and reported by various authors. Ghane et al. (2016) applied the backward probability method to identify the parameters of an instantaneous pollution release in a river network. The analysis was based on a single monitoring station at the outlet of the river network. In the case that the river network contained multiple branches, the method was only able to state several potential source locations inside different branches, as these created similar concentration profiles at the monitoring point. Wang et al. (2018) used the same approach to identify the parameters of multiple instantaneous point sources based on a single monitoring station. The authors showed that the accuracy of source identification deteriorates when the number of point sources increases. Similar to Ghane et al. (2016), different parameter combinations led to a very close objective function value, impairing the accurate identification of source parameters. Increasing the number of monitoring stations could improve the identification results. Han et al. (2014) considered an instantaneous release from a single point source in a river stretch. Depending on the chosen monitoring design, the accurate identification failed even when perfect monitoring data were considered, implying that parameters are only poorly identifiable under certain monitoring configurations.

The previous examples indicate that the spatial and temporal monitoring design can have a significant influence on the accurate identification of pollution source parameters. However, existing studies mainly focused on the evaluation of the developed PSI approaches, and monitoring data were usually selected arbitrarily. Up to now, a comprehensive analysis of the influence of the spatial and temporal monitoring design on the identification results is missing both for uni- as well as for bidirectional flow systems.

Consequently, on the basis of a comprehensive literature review (Chapter 3), the following research objectives were identified for this thesis:

(i) Analysis of the influence of the spatial and temporal monitoring design on parameter identifiability and uncertainty for an instantaneous pollution spill under both uni- and bidirectional flow conditions.

(ii) Derivation of general guidelines and criteria for the design of an optimal monitoring network for pollution source identification.

(iii) Comparison of the performance of different pollution source identification approaches under bidirectional flow conditions using a numerical transport model.

(iv) Design of an optimal monitoring network for pollution source identification in the Thi Vai Estuary.

(v) Application of a selected pollution source identification approach for the identification of pollution spills in the Thi Vai Estuary.

1.3 Approach and thesis outline

The general concept for this thesis is depicted in Figure 1.1. It should be mentioned that this work only focuses on an instantaneous pollutant release from a single point source. The release can therefore be characterized by four source parameters, including the longitudinal and lateral source location, the release time and the total pollutant mass.

Most parts of this thesis deal with unsteady bidirectional flow systems. However, in a first step, to obtain general knowledge regarding the influence of the monitoring design on the identifiability of pollution source parameters, a synthetic river section (unidirectional flow) is considered (Chapter 6.1). Assuming steady flow conditions, an analytical solution of the two-dimensional advection-dispersion-reaction equation is used to model the pollutant transport in the river. The profile likelihood approach is adopted to determine structural and practical parameter identifiability, to analyse parameter interactions and to derive likelihood-based confidence intervals. With the adopted approach, the influence of the spatial and temporal monitoring design on parameter identifiability and uncertainty can be evaluated.

In a second step, the identifiability analysis is extended to bidirectional flow systems (Chapter 6.2). As before, a simplified synthetic test case is considered, which is based on the main properties of the Thi Vai Estuary. However, the geometry is simplified and does not contain the various meanders and the intertidal zone mainly covered by mangrove forest. The corresponding numerical hydrodynamic transport model is set up with the Delft3D software suite. Due to the high computational burden of the profile likelihood approach, a different approach is adopted for the identifiability analysis. The selected approach was originally proposed by Brun et al. (2001) and is based on a local sensitivity analysis at multiple points in the parameter space. Different monitoring designs are further compared using optimality criteria based on the Fisher Information Matrix. The results of the analysis provide important information regarding complexities arising in the identification process and the design of an optimal monitoring system.

As explained in the previous section, applications of PSI approaches to estuaries have only rarely been discussed in the literature up to now. In this work, the simulation-optimization approach is used for the identification of pollution source parameters. In the literature, two variants of this approach have been proposed. Usually, all unknown source parameters are simultaneously identified. In contrast, Jing et al. (2018) presented a modified approach, in which the estimation of the individual source parameters is decoupled from one another.

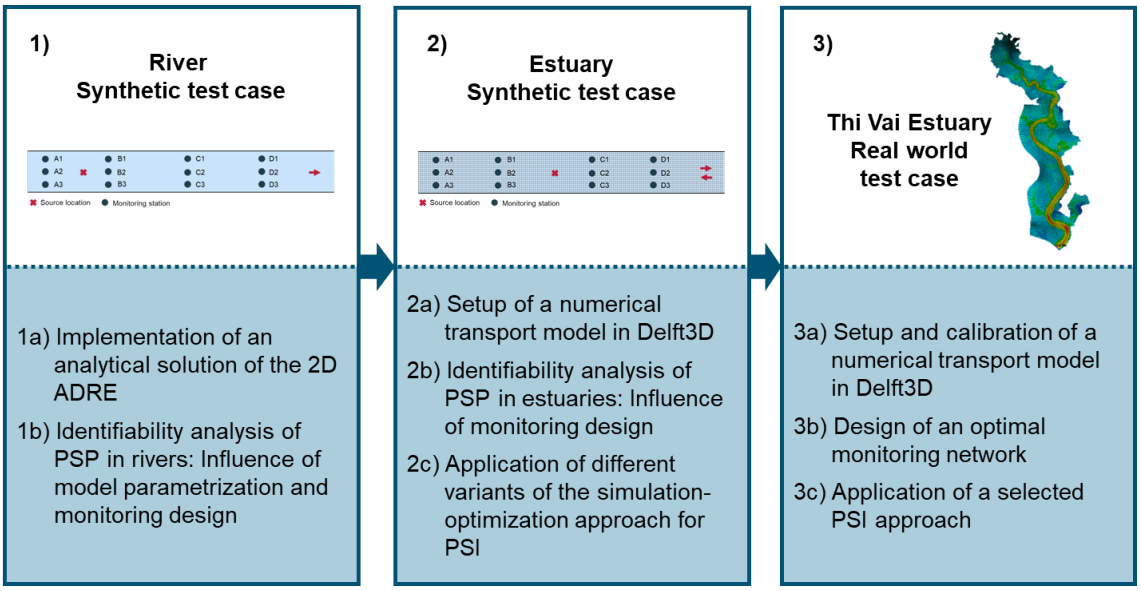

Figure 1.1: Overview of the three main work steps for the fulfilment of the stated research objectives. ADRE: Advection-dispersion-reaction equation, PSP: Pollution source parameters, PSI: Pollution source identification.

Both approaches are applied to the synthetic bidirectional test case using perfect and noise perturbed monitoring data. Several pollution scenarios are considered, which differ in the time of release in the tidal cycle.

In a third and final step, the simulation-optimization approach is transferred to a real world estuary, the Thi Vai Estuary in South Vietnam (Chapter 8). A two-dimensional hydrodynamic transport model is set up with the Delft3D software suite. The model is calibrated based on monitoring data collected as part of the research project EWATEC-COAST (Chapter 5). Based on the results of the identifiability analysis, an optimal monitoring network is designed for the Thi Vai Estuary. Synthetically generated monitoring data of the optimized monitoring network are used for the identification of several theoretical spill incidents.

Overall, the results of this thesis improve the understanding of the source identification problem and the influence of the spatial and temporal monitoring design on the identification results in both rivers and estuaries. The thesis ends with a summary and an outlook in Chapter 9. The outlook includes a detailed discussion of the given assumptions and possible extensions in future works.

2 Theoretical background

2.1 Estuaries

According to Pritchard (1967), an estuary is a semi-enclosed coastal body of water, which has a free connection with the open sea, and within which sea water is measurably diluted with fresh water derived from land drainage. In subsequent years this classic definition has been extended to include coastal waters such as bays and sounds that receive riverine discharge (Martin et al. 1999).

The following sections include a short description of the main hydrodynamic and mixing processes in estuaries. One significant difference to rivers is the tidal influence, which leads to alternating currents strongly affecting pollutant transport and mixing processes.

2.1.1 Tides

2.1.1.1 Tidal dynamics

Due to the connection to the open sea, estuarine hydrodynamics are strongly influenced by tides. Tides are defined by the periodic rise and fall of the water surface which is the result of the combined gravitational forces of the moon and the sun on the earth. Tidal waves originate in the deep ocean basins and then propagate into coastal waters and estuaries (Ji 2017, p. 382).

Tidal dynamics can be described in terms of tidal heights (the variation of the water level around a given datum level) and tidal currents (the variation in the velocity field) (Martin et al. 1999, p. 543). An overview of the typical relation between tidal heights and currents in estuaries is given in Figure 2.1. The figure also illustrates key terms, which will be further described in the consecutive text. Tidal currents are the horizontal water movement associated with the rise and fall of the water surface (Thomann and Mueller 1987). Ebb tide or ebb current correspond to the phase of seaward flow in estuaries or tidal rivers, while flood tide or flood current describe the landward flow of the water. The terms maximum ebb tide and maximum flood tide mark the points where the current velocity reaches its corresponding maximum value during ebb and flood tide, respectively. The small time period between ebb and flood tide (and vice versa), when the tidal current changes its direction, is known as slack water.

The tidal water level is defined by two main features, the tidal range or amplitude and the tidal period (Pugh 1987, p. 4). The tidal period is defined as the time between two consecutive high or low tides. Low tide or low water are the lowest water level reached at ebb tide, while high tide or high water correspond to the highest water level reached at flood tide. Tidal periods can be classified as diurnal (one high and one low tide per day), semidiurnal (two high and two low tides per day), and mixed (two high and two low tides per day with unequal heights) (Ji 2017, p. 382). Semidiurnal tides, which have a tidal

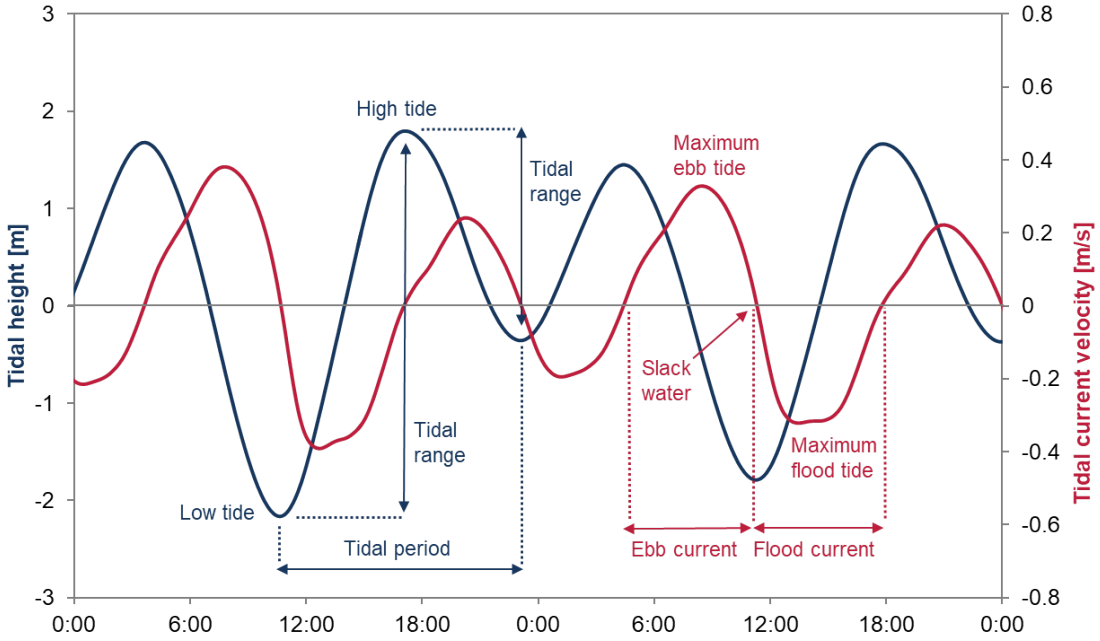

Figure 2.1: Schematic representation of the change in tidal height and tidal current velocity for a semidiurnal tidal regime.

period of 12.42 h, are the most frequently encountered tides on earth (Martin et al. 1999, p. 544; Ji 2017, p. 383).

The tidal range is defined as the difference between the water level at low tide and high tide. Based on the mean tidal range, microtidal (< 2 m), mesotidal (2-4 m), macrotidal (4-6 m) and hypertidal estuaries (> 6 m) can be distinguished (Bruner de Miranda et al. 2017, p. 37). The tidal range is usually not constant over time but varies in a cyclic fashion. All bodies in the solar system are in motion relative to one another, which leads to a continuous change in the gravitational forces acting on the earth (US EPA 1990). An example is the spring-neap-tide cycle, which occurs with a period of approximately 14.77 days (Ji 2017, p. 383). Spring tides are tides with tidal ranges greater than the average monthly range and occur when the earth, the moon and the sun are aligned (full and new moon) (Hicks 2006, p. 11; Ji 2017, p. 383). Neap tides are tides with ranges less than the average monthly range and occur when the sun and the moon are opposed (1st and 3rd quarter of the lunar phase) (Hicks 2006, p. 11; Ji 2017, p. 383).

2.1.1.2 Tidal constituents and harmonic analysis

In general, a measured tidal signal (either water level or velocity components) can be decomposed into (1) a value of longterm-mean, (2) a series of periodic components and (3) random fluctuations (Ji 2017, p. 387):

$$\zeta(t) = \zeta_0 + \sum_{i=1}^{N} A_i \cos(\omega_i t + \phi_i) + \eta_0 \tag{2.1}$$

where $\zeta(t)$ water level at time t [m]
ζ_0 mean height of water level above a given datum [m]
N number of tidal constituents
A_i amplitude of the ith constituent [m]
ω_i angular frequency of the ith constituent [$^\circ\,\mathrm{h}^{-1}$]
ϕ_i phase of the ith constituent [$^\circ$]
η_0 residual signal [m]

The summation of periodic components in Equation 2.1 represents the astronomical tidal motion which only results from gravitational effects and is therefore highly predictable (US EPA 1990). Each component represents a periodic change in the relative positions of the earth, moon and sun (Martin et al. 1999, p. 544) and can be expressed by a trigonometric function specified by its amplitude A_i, angular frequency ω_i and phase ϕ_i. The residual component η_0 represents effects which can not be predicted including meteorological effects, variations in river flow as well as measurement errors in the observed data leading to a difference between astronomical tides and actual tides (McDowell and O'Connor 1977, p. 5) .

Tidal harmonic analysis can be used to decompose the tidal signal and estimate the amplitudes and phases of the most important tidal constituents at a specific location. An overview of the most important tidal constituents and their characteristic tidal periods is given in Table 2.1. Using the tidal period T_i, the angular frequency can be specified as $\omega_i = \frac{2\pi}{T_i}$. While the tidal period is constant in time and space, the amplitude and phase are site-specific variables. These constituents can be extracted from measured tidal data (water level or velocity components). One of the most common approaches is the least-square approximation. The amplitude and phase of each tidal constituent are determined so that the sum between measured and modelled water levels is minimized (Malcherek 2018, p. 86).

Table 2.1: Most important tidal constituents (Ghosh 1998; Martin et al. 1999).

Constituent	**Description**	**Tidal period [solar h]**
M_2	Principal lunar semidiurnal component	12.42
S_2	Principal solar semidiurnal component	12.00
N_2	Longer lunar elliptic semidiurnal component	12.66
K_2	Solar lunar semidiurnal component	11.97
K_1	Solar-lunar component	23.93
O_1	Main lunar diurnal component	25.82
P_1	Main solar diurnal component	24.07

The index of the main tidal constituents in Table 2.1 shows the daily return of the partial tides (Malcherek 2018, p. 83). In addition to the listed components a multitude of further components are known, including long-period constituents and shallow water constituents. However, in general the listed components are often sufficient for an adequate representation of the tidal signal (Martin et al. 1999, p. 546).

The constituents calculated in the course of the harmonic analysis can be used to predict the tidal dynamics. Additionally, these can be used to analyse the form of the tidal wave

at a specific location. The tidal form factor F is calculated using the amplitudes of the two most important diurnal and semidiurnal constituents (Martin et al. 1999, p. 549):

$$F = \frac{K_1 + O_1}{M_2 + S_2} \tag{2.2}$$

With the quantification of the form factor a rough classification of the tidal wave into four categories, namely semidiurnal ($F < 0.25$), mixed, predominantly semidiurnal ($F = 0.25 - 1.5$), mixed, predominantly diurnal ($F = 1.5 - 3.0$), and diurnal ($F > 3.0$) can be carried out.

2.1.2 Basic transport and mixing processes

The transport and mixing of solutes in water bodies is governed by different processes. These include advection, molecular diffusion, turbulent diffusion, and dispersion. All processes apply in varying degrees to different types of water bodies (e.g. lakes, rivers, estuaries, coastal oceans, and groundwater) (Fischer et al. 1979, p. 7). A schematic representation of these processes is given in Figure 2.2.

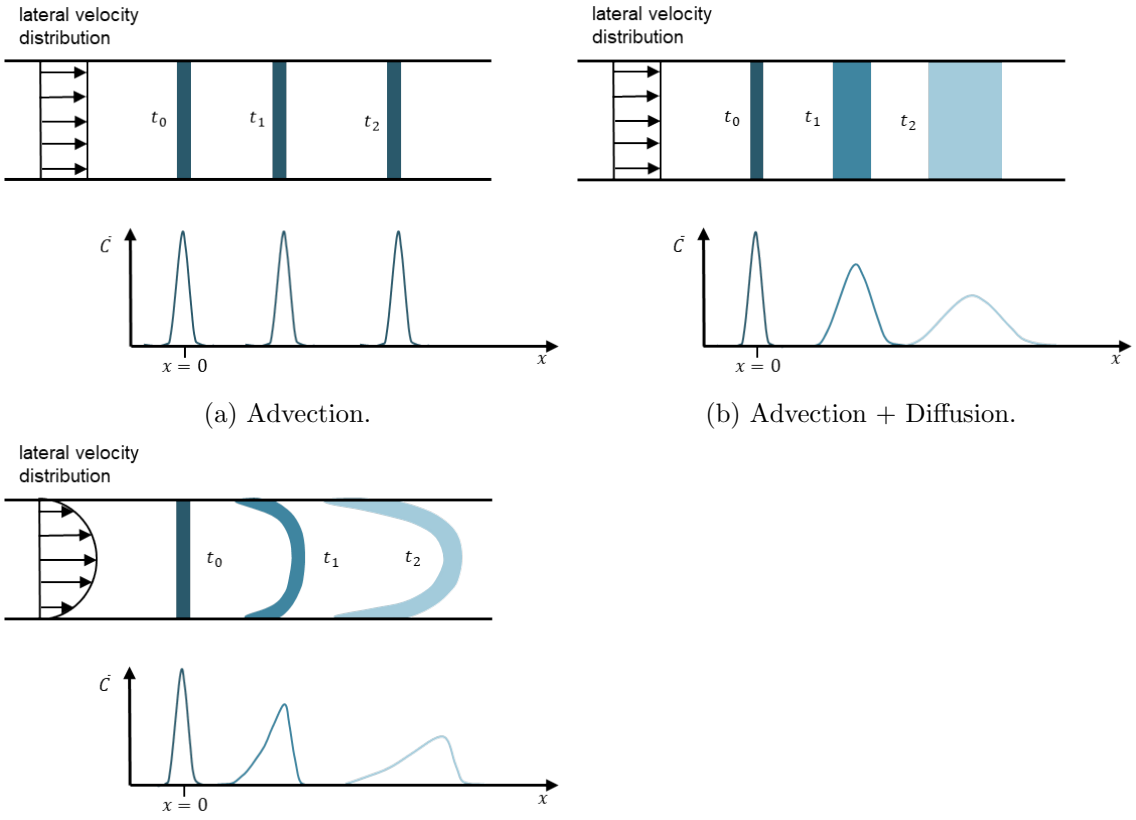

(a) Advection.

(b) Advection + Diffusion.

(c) Advection + Dispersion.

Figure 2.2: Schematic representation of transport and mixing processes (modified from Shanahan and Gaudet (2000) and Ji (2017)).

2.1.2.1 Advection

Advection is the transport of a solute with the mean water motion (same direction and speed (Shanahan and Gaudet 2000, 5B-5). The advective mass flux is dependent on the flow velocity v_x and can be described by:

$$J_x = v_x \cdot c \tag{2.3}$$

where J_x advective mass flux in x-direction $[\mathrm{g\,m^{-2}\,s^{-1}}]$
v_x flow velocity in x-direction $[\mathrm{m\,s^{-1}}]$
c solute concentration $[\mathrm{g\,m^{-3}}]$

In most situations in surface water, the movement of pollutants is dominated by advective flow (Shanahan and Gaudet 2000, 5B-5). An example for advective flow is the downstream transport of pollutants due to flow in a river or estuary (Chapra 1997, p. 138). As can be seen in Figure 2.2a, pure advection, when considering a uniform cross-sectional velocity profile, is only responsible for the solute movement, without distorting or diluting the solute plume (Ji 2017, p. 15).

2.1.2.2 Molecular diffusion

Molecular diffusion results from the random Brownian motion of molecules in a fluid and leads to a compensation of concentration gradients (Chapra 1997, p. 138). Mathematically, diffusion can be described by using Fick's law of diffusion (Fischer et al. 1979, p. 31):

$$J_x = -D_m \frac{\partial c}{\partial x} \tag{2.4}$$

where J_x diffusive mass flux in x-direction $[\mathrm{g\,m^{-2}\,s^{-1}}]$
D_m molecular diffusion coefficient $[\mathrm{m^2\,s^{-1}}]$
$\frac{\partial c}{\partial x}$ concentration gradient in x-direction

Fick's law states that the solute mass flux is proportional to the gradient of solute concentration (Shanahan and Gaudet 2000, 5B-5). Consequently, mass flows from regions of high to low concentrations (Chapra 1997, p. 141). The diffusion coefficient D_m quantifies the rate of the diffusive process, which depends on the fluid, the size of the particles, and the density and temperature of the fluid (Chapra 1997, p. 141; Fischer et al. 1979, p. 35). For example, salinity in water D_m has a value of $1.1 \cdot 10^{-9}\ \mathrm{m^2\,s^{-1}}$ (Malcherek 2018). In environmental problems, the process of molecular diffusion is generally unimportant to pollutant mixing due to the small size (Shanahan and Gaudet 2000, 5B-6).

2.1.2.3 Turbulent diffusion

In laminar flow, the only way a pollutant can spread is through molecular diffusion. However, in surface waters, fluid motions are usually turbulent, resulting in random and chaotic movement of water parcels in the fluid (Fischer et al. 1979, p. 55). Turbulent diffusion describes the random mixing of particles by small scale eddies due to turbulent flow. In contrast to laminar flow, mass will spread much faster in turbulent flow (Fischer et al.

1979, p. 55). In mathematical terms, turbulent diffusion can be described as roughly analogous to molecular diffusion by Fick's law:

$$J_x = -D_{t,x}\frac{\partial c}{\partial x} \tag{2.5}$$

where J_x diffusive mass flux in x-direction $[\mathrm{g\,m^{-2}\,s^{-1}}]$
$D_{t,x}$ turbulent diffusion coefficient in x-direction $[\mathrm{m^2\,s^{-1}}]$

Similar to molecular diffusion, it is assumed that mass is mixed by turbulence from areas of high concentration to areas of low concentration at a rate proportional to the concentration gradient (Shanahan and Gaudet 2000, 5B-6). In contrast to molecular diffusion, turbulent diffusion results in vastly greater rates of mixing. An overview of the range of diffusion coefficients in natural waters is given in Figure 2.3. In contrast to the molecular diffusion coefficient, the intensity of turbulent diffusion generally varies in different directions (Chatwin and Allen 1985). As can be seen in Figure 2.3, horizontal turbulent diffusion coefficients are usually much greater than vertical diffusion coefficients (Chapra 1997, p. 149).

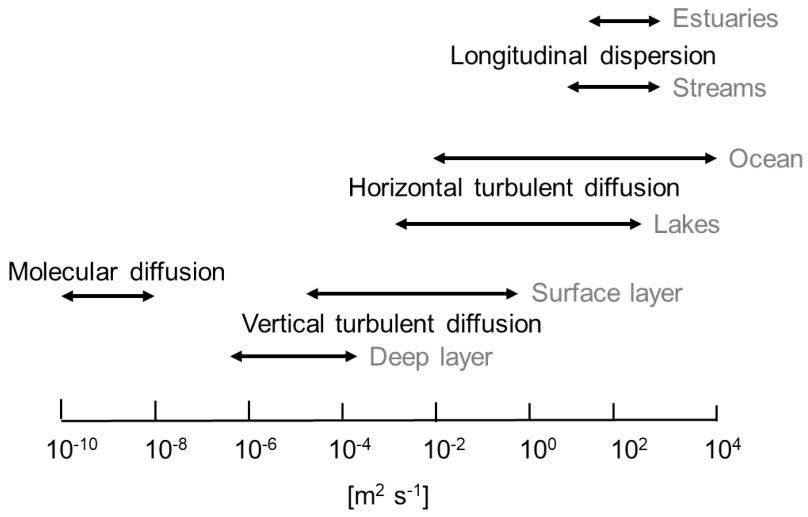

Figure 2.3: Typical ranges of diffusion and dispersion coefficients in natural waters (modified from Chapra (1997)).

2.1.2.4 Dispersion

Higher shear stresses due to the friction between the fluid and the lateral and vertical boundaries of a river or estuary, lead to a non-uniform cross-sectional velocity profile. This is exemplified for the lateral velocity distribution in Figure 2.2c. As a consequence, fluid is moving more slowly at the bottom and the banks than at the centre and top of the river. These velocity differences across the cross-section lead, in combination with turbulent diffusion, to increased mixing of pollutants in the longitudinal direction known as dispersion. Due to the dependence on the flow velocity, the process is sometimes also called shear-flow dispersion or advective dispersion (Chin 2013, p. 68).

The inclusion of a dispersion term in numerical transport models is a result of the spatial averaging (Shanahan and Gaudet 2000, 5B-7). If the model domain is adequately resolved

in three-dimensional space and small time steps are used, the governing equations contain only turbulent diffusion terms (US EPA 1990). Similar to the modelling of molecular and turbulent diffusion, dispersion is usually approximated using Fick's law in transport models:

$$J_x = -D_x \frac{\partial c}{\partial x} \tag{2.6}$$

where J_x dispersive mass flux in x-direction $[\mathrm{g\,m^{-2}\,s^{-1}}]$
D_x dispersion coefficient in x-direction $[\mathrm{m^2\,s^{-1}}]$

Approximate ranges for dispersion coefficients in natural waters and a comparison to molecular and turbulent diffusion coefficients can be found in Figure 2.3.

2.1.3 Main driving forces of mixing in estuaries

The transport and mixing processes described in the previous section, apply to both rivers and estuaries. In general, mixing is governed by both small-scale random processes (turbulent diffusion) as well as larger scale variations in the velocity field (dispersion). However, transport and mixing processes are much more complex in estuaries due to various additional driving forces which can have a significant influence on these processes. In general, two main driving forces controlling the transport and mixing processes in estuaries can be distinguished. These include the tidal dynamics and the riverine freshwater inflow. Additionally, for larger and shallow estuaries, wind forcing might also play a significant role (Martin et al. 1999, p. 543; Ji 2017, p. 379).

2.1.3.1 Influence of tidal dynamics

Tidal dynamics are usually considered the most important causes of mixing in estuaries, and can play a significant role in pollutant transport (Ji 2017, p. 385). Different tide-driven mechanisms of mixing can be distinguished including shear flow dispersion, tidal pumping, and tidal trapping.

Shear flow dispersion corresponds to the longitudinal dispersion of solutes due to velocity variations in the cross-sectional profile. This process occurs in estuaries in a similar way as in rivers. However, in estuaries the effect of reversing tidal currents has to be taken into account (Shanahan and Gaudet 2000). The generated turbulence associated with the shear stresses additionally causes turbulent mixing (Savenije 2012, pp. 10–11).

Superimposed on the oscillating tidal currents, there usually exists a steady net circulation also called residual circulation (Fischer et al. 1979, p. 237). The residual circulation can be calculated by averaging the velocity field at every point in the estuary over several tidal cycles (Fischer et al. 1979, p. 237; Day 2013, p. 27). Different causes are responsible for the development of a residual circulation, including density differences, which are further discussed in Section 2.1.3.2, as well as the interaction of tides, bathymetry and the Coriolis force. Due to the earth's rotation, currents are deflected to the right in the Northern hemisphere, and to the left in the Southern hemisphere (Fischer et al. 1979, p. 237). Therefore, in the Northern hemisphere, ebb tide currents will be deflected towards the right bank (when facing seawards), while flood tide currents will be deflected towards the left bank (McDowell and O'Connor 1977). This results in spatially asymmetric residual

flow patterns leading to a counter-clockwise net circulation in wide enough estuaries of the Northern hemisphere (Ji 2017, p. 385). A second cause for the development of a residual circulation is the interaction between tides and the often irregular bathymetry of most estuaries, a process which is also known as "tidal pumping" (Fischer et al. 1979, p. 237). Similar to the effect of the Coriolis force, ebb and flood currents often follow different flow paths, leading to the development of a residual flow pattern in the estuary (Shanahan and Gaudet 2000).

The bathymetry of the estuary further impacts circulation and mixing through the temporal trapping of pollutants inside side channels, embayments and tidal flats. The process is known as "tidal trapping" and leads, like dead zones in rivers, to an increase in longitudinal dispersion (Shanahan and Gaudet 2000). A schematic overview of the process is given in Figure 2.4. During flood tide, particles released into the main channel of the estuary move upstream (a). Some particles flow into a side channel or embayment (b). Due to phase differences between the main branch and the side channel, the side channel already starts emptying at slack tide while the water in the main stream is still flowing upstream (Savenije 2012, p. 107). As a result the pollutant parcel rejoins the main stream flow in a different part than it initially originated (c) (Shanahan and Gaudet 2000). The dominant length scale for tidal trapping is the tidal excursion, which is the maximum distance a particle can travel during one tidal cycle (Savenije 2012, p. 11; Martin et al. 1999, p. 561).

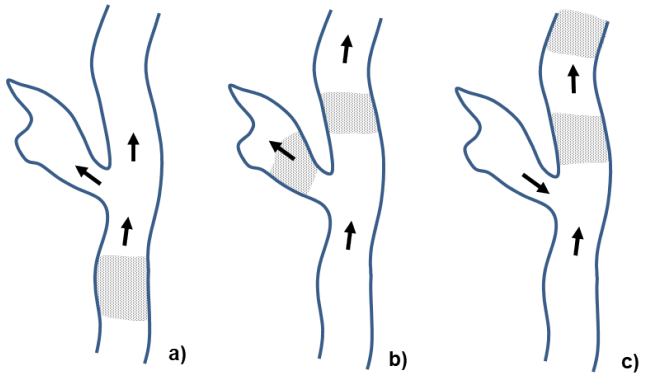

Figure 2.4: Schematic representation of tidal trapping in estuaries (modified from Fischer et al. (1979, p. 242)).

2.1.3.2 Influence of freshwater inflow

Although groundwater inflow, surface run-off and other sources can contribute as well, rivers are considered to be the primary source of freshwater to an estuary (Ji 2017, p. 379). The inflowing freshwater leads to the development of horizontal, lateral and vertical density gradients, resulting in complex circulation patterns in the estuary (Thomann and Mueller 1987). Density gradients are the results of salinity differences between freshwater and seawater. Freshwater usually has a density of $1\,\mathrm{g\,m^{-3}}$ at 20 °C. In contrast, seawater with an average salinity of 35 ppt is much heavier and has a density of $1.026\,\mathrm{g\,m^{-3}}$ at 20 °C (Ji 2017, p. 390). Due to these density differences, the incoming freshwater at the head of the estuary tends to flow above the denser seawater. When averaged over several tidal cycles, this results in a net seaward transport of freshwater in the surface layer, and a net landward transport of seawater in the deeper layers (Shanahan and Gaudet 2000). This

residual flow pattern is also referred to as estuarine or gravitational circulation (Bruner de Miranda et al. 2017, p. 49).

The freshwater inflow is further an important criterion which determines the flushing potential of estuaries. The flushing potential is highly dependent on the net flow out of the estuary which equals the riverine inflow when averaged over several tidal cycles (Thomann and Mueller 1987, p. 95; Martin et al. 1999). Different transport time scales exist to calculate the flushing characteristics of estuaries (e.g residence time, water age, flushing time) (Ji 2017, p. 394). In general, well-flushed estuaries are more robust against pollution than poorly flushed estuaries (Wolanski and Elliott 2015, p. 36).

2.1.4 Estuarine classification

The development of vertical stratification patterns primarily depends on the rate of the freshwater inflow, the tidal dynamics, and the geometry of the estuarine basin (Ji 2017, p. 391). Based on the given stratification patterns, estuaries can be divided into three different types, including (A) highly stratified, (B) partially stratified, and (C) well-mixed estuaries (Day 2013, pp. 33–34).

Highly stratified estuaries, also known as salt-wedge estuaries, are characterized by a very sharp vertical salinity gradient and mainly develop when forced by micro to meso tides and a high freshwater inflow (Bruner de Miranda et al. 2017, p. 80). A strong gravitational circulation pattern exist in these estuaries, with a landward flow of seawater in the bottom layer and a seaward flow of freshwater in the upper layer. The very sharp density gradient greatly inhibits vertical turbulent mixing across the interface (Ji 2017, p. 392). Due to increased shear stresses at the toe of the salt wedge, there is usually a unidirectional entrainment of saline water into the freshwater plume (Wolanski and Elliott 2015, p. 47).

Partially-stratified estuaries lie in between highly stratified and vertically well-mixed estuaries. Although significant vertical density gradients can be observed, these are less sharp than in highly stratified estuaries (Martin et al. 1999, p. 536). Typical for these kind of estuaries is a well-developed gravitational circulation (Day 2013, p. 34). Partially-stratified estuaries are usually characterized by a moderate to large tidal range and a moderate freshwater inflow, which result in both vertical turbulent mixing and entrainment (Day 2013, p. 34; Ji 2017, p. 392).

In well-mixed estuaries vertical mixing is almost complete, so that the vertical salinity distribution is approximately uniform with depth (Ji 2017, p. 393). This kind of estuary usually exists under meso- to macrotidal conditions and a low freshwater inflow, leading to vigorous vertical mixing (Bruner de Miranda et al. 2017, p. 84). In contrast to the other types, the net circulation is either characterized by a seaward flow in all depths, or tidal pumping is the dominant circulation mode (Day 2013, p. 34).

Between these three general types, any form of stratification may exist. It is important to note that stratification patterns are not steady but can change during the year due to changes in river inflow, tides and meteorological conditions (Martin et al. 1999, p. 558). Consequently, estuaries can exhibit different types of stratification throughout the year.

2.2 Parameter estimation

2.2.1 Inverse problems

In environmental systems, often mathematical models are used to simulate complex physical, chemical or biological processes. The results can be used within the framework of system management and risk analysis (Hill and Tiedeman 2007, p. 1). For example, in the case of a pollution incident in a river, pollutant transport models can be applied to predict concentration profiles at a water intake location further downstream. This is also called a forward problem. Forward problems are concerned with the prediction of a given state variable (e.g. concentration) based on a known model structure which includes an adequate parametrization of the given system. Nevertheless, for the application of these models in the first place, the model has to be sufficiently calibrated by adapting the model parameters to the given system. While some of these parameters can be measured directly in the field, others have to be estimated based on measured quantities of given state variables (Guillaume et al. 2019). This is called an inverse problem.

According to Sun and Sun (2015, p. 16), different types of inverse problems can be distinguished. These include, among others, the already mentioned identification of continuous or discrete model parameters. An example is the calibration of process rates in a water quality model based on measured outputs (e.g. the calibration of the nitrification rate based on measured ammonium and nitrate concentrations). Another type of inverse problem deals with the identification of distributed or point sources (or sinks) that may vary with time and/or location (Sun and Sun 2015, p. 16). This type of problem is also called sink/source identification and will be discussed in more detail in Chapter 3.1.

In mathematical terms, the relationship between the output of a deterministic model and measured data for a given state variable can be expressed by the following observation equation (Brun et al. 2001):

$$d = f(\theta) + \epsilon \tag{2.7}$$

where d measurement data $d = (d_1, \cdots, d_n)^T$
$f(\theta)$ corresponding model output $f(\theta) = (f_1(\theta), \cdots, f_n(\theta))^T$
θ unknown model parameters $\theta = (\theta_1, \cdots, \theta_p)^T$
ϵ measurement error $\epsilon = (\epsilon_1, \cdots, \epsilon_n)^T$
n number of measurement data
p number of unknown parameters

The function $f(\cdot)$ represents the underlying model structure used to generate the model output which corresponds to the collected measurement data. It implicitly includes all features of the model structure, including a corresponding set of spatial and time variables, control variables, model parameters, as well as initial and boundary conditions (Brun et al. 2001; Sun and Sun 2006). As can be seen in Equation 2.7, model output and actual measurement data are not equal but differ by a term ϵ, which represents the measurement error, when the model is assumed to be accurate.

The inverse problem deals with the estimation of θ based on available measurements d (Aster et al. 2013, p. 2). One approach to solve this kind of problem is through numerical optimization. The aim is to find the best possible values of the parameters θ according

to a predefined objective function which evaluates the fit between measured data d and model output $f(\theta)$ (Bard 1974, p. 83). The definition of the objective function is often based on maximum likelihood theory, considering that it has several beneficial statistical properties (Kreutz et al. 2015, p. 355).

2.2.2 Maximum likelihood estimation

Maximum likelihood estimation is a general method to obtain parameter estimates and is applicable to a wide range of problems. It is based on the likelihood function $L(\theta|d)$, with $\theta = (\theta_1, \cdots, \theta_p)^T$ being the parameter vector and $d = (d_1, \cdots, d_n)^T$ representing the observed data. Assuming that the observations are independent, the joint probability density function (pdf) $p(d|\theta)$ of the whole data set is the product of the individual pdf's of each observation $p_i(d_i|\theta)$ (Millar 2011, p. 21):

$$L(\theta|d) = p(d|\theta) = \prod_i^n p_i(d_i|\theta) \tag{2.8}$$

The likelihood function is identical in form to the joint pdf, except that $L(\theta|d)$ is regarded as a function of the parameters conditioned on the observed data (Bates and Watts 1988). For the application of maximum likelihood estimation, a joint pdf describing the statistical distribution of the error term needs to be assigned (Aster et al. 2013, p. 27). Usually, it is assumed that the errors follow a normal distribution. In practice, measurement errors are often the sum of a number of random errors from unknown sources, and, by the central limit theorem, the sum of these errors is approximately normally distributed independent of the distribution of the individual errors (Donaldson and Schnabel 1985). In the case that the errors are independent and follow a normal distribution ($\epsilon_i \sim N(0, \sigma_i^2)$), the likelihood function is given by (Aster et al. 2013, p. 28):

$$L(\theta|d) = \prod_i^n \frac{1}{\sqrt{2\pi\sigma_i^2}} \exp\left(-\frac{(d_i - f_i(\theta))^2}{2\sigma_i^2}\right) \tag{2.9}$$

When taking the natural logarithm of the likelihood function, one obtains the negative log-likelihood function:

$$-2\ln L(\theta|d) = \sum_{i=1}^n \left(\frac{d_i - f_i(\theta)}{\sigma_i}\right)^2 + \underbrace{2\sum_{i=1}^n \log(\sigma_i) + n\log(2\pi)}_{\text{independent of } \theta} \tag{2.10}$$

Since the last two terms of Equation 2.10 are independent of the parameter vector θ, they can usually be ignored in the optimization process. The maximum likelihood estimate (MLE) is the parameter vector which maximizes the given likelihood. To improve the numerical evaluation and the optimizer convergence, the MLE is usually determined by minimizing the negative log-likelihood function (Carrera and Neuman 1986a; Boiger et al. 2016):

$$MLE = \hat{\theta} = \arg\max_\theta(L(\theta|d)) = \arg\min_\theta(-2\ln L(\theta|d)) \tag{2.11}$$

Maximum likelihood estimation has several beneficial theoretical properties ensuring efficient and accurate statistical analyses and is therefore often used for parameter estimation (Kreutz et al. 2015). Among other properties, maximum likelihood estimates are asymptotically normally distributed around the true value of θ for large n (Dalitz 2017). This is an important aspect regarding the estimation of parameter uncertainty after the optimization process, as will be discussed in Section 2.2.4.

2.2.3 Numerical optimization

For the minimization of the objective function (e.g. the negative log-likelihood function) numerical optimization routines are usually applied. In the last decades, a wide variety of optimization algorithms and extensions have been proposed, all of which have their own strengths and weaknesses. In this section, only the most important properties of different classes of optimization algorithms and possible difficulties that can be encountered in the optimization process, are discussed. Extensive reviews of different optimization algorithms can be found elsewhere (e.g. Nocedal and Wright (2006), Wahde (2008), Weise (2009) and Rios and Sahinidis (2013)).

Overall, optimization algorithms can be classified into derivative-based and derivative-free methods. Derivative-based methods require the calculation of first and/or second derivatives of the objective function. If the derivatives cannot be derived analytically, finite differences can be used to calculate the derivatives numerically (Bard 1974, p. 117). Examples of derivative-based methods are steepest descent, conjugate gradient, Newton and quasi-Newton methods like the BFGS or DFP algorithm, or the Gauß-Newton method and its modified form, the Levenberg-Marquardt algorithm (Sun and Sun 2015). In contrast, when the calculation of derivatives is unavailable, unreliable or impractical to obtain, derivative-free methods might be applied (Rios and Sahinidis 2013). Derivative-free methods iteratively evaluate the objective function until a convergence criterion is met. Information regarding first or second order derivatives is not required. An example of a local derivative-free optimization algorithm is the Nelder-Mead simplex algorithm, described in more detail in Section 2.2.3.1. Other derivative-free local search methods are pattern search algorithms such as generalized pattern search (GPS) and mesh adaptive direct search (MADS), as well as trust region methods (Rios and Sahinidis 2013).

The methods described so far can be further classified as local optimization methods, as the optimization starts from a single initial parameter guess. While these methods work well in the case of convex functions with only one minimum, if the objective function exhibits multiple minima, convergence to the global minimum is not guaranteed (Knobloch et al. 2017). It is therefore strongly recommended to repeat the optimization based on several initial parameter guesses should indications for a multi-modal objective function exist (Bard 1974, p. 116).

Another option for the minimization of multi-modal objective functions is the application of global optimization methods. In contrast to local methods, global optimization methods start from multiple objective function evaluations in the parameter space. Several algorithms have been proposed in recent years including evolutionary algorithms like the genetic algorithm (GA) and differential evolution (DE) or swarm intelligence algorithms like particle swarm (PSO) and ant colony optimization (ACO) (Wahde 2008). In general, the search is based on two principles, the exploration and exploitation of the parameter space (Maier et al. 2019). While the process of exploration tries to find new points in areas of the parameter space which have not been investigated before, exploitation improves and

combines currently known solutions (Weise 2009, p. 60). The balance between those principles is usually based on the specific parametrization of the algorithm. Nevertheless, analogous to local methods, convergence to a global minimum cannot be guaranteed when using global optimization methods either. Premature convergence to a local minimum is often a problem when the surface of the objective function is rugged, discontinuous or has several local minima (Bolker 2008, pp. 319–326; Weise 2009, p. 56). This is often the case when the model is higher-dimensional, non-linear or when parameter dependencies exist (Schwaab et al. 2008; Kreutz et al. 2015, p. 368). An adequate parametrization of the mentioned algorithms can help to improve the convergence properties in these cases.

In contrast to local search methods, global optimization methods require a significant number of function evaluations. In addition, they often exhibit slow convergence (Kreutz et al. 2015, p. 368; Knobloch et al. 2017). Especially when the evaluation of the objective function is computationally demanding, parallelization routines are a suitable option to reduce the computational burden of global optimization algorithms (Maier et al. 2019).

In the following sections, the Nelder-Mead simplex algorithm and the global search method Differential Evolution are described in more detail, as these two optimization algorithms will be applied in this thesis.

2.2.3.1 Nelder-Mead simplex algorithm

The Nelder-Mead simplex algorithm is a local, derivative-free search method, devised in 1965 by Nelder and Mead (Nelder and Mead 1965). The algorithm starts by picking $p + 1$ parameter combinations that form the vertices of an initial simplex, with p being the dimension of the parameter vector (Bolker 2008, p. 303). Then, for each vertex of the initial simplex the objective function is evaluated. In the following iterations, the vertex with the highest objective function value is replaced by a new point. Candidate replacement points are obtained by transforming the worst vertex through a number of operations depicted in Figure 2.5.

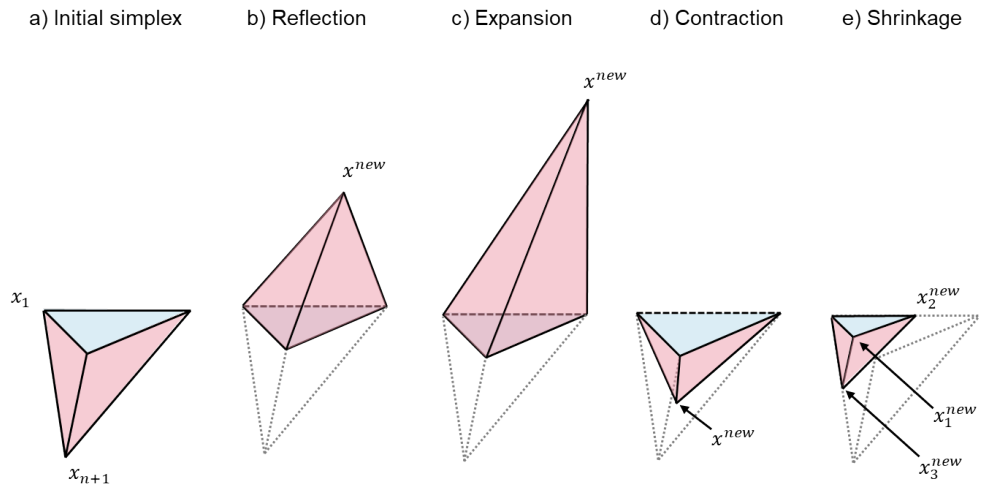

Figure 2.5: Operations in the Nelder-Mead simplex algorithm: original simplex, reflection, expansion, contraction, and shrinkage (modified from Larson et al. (2019)).

These operations start with the reflection of the current worst point in the simplex through the face opposite it (Bolker 2008, p. 303). If the new point improves the current best point, the Nelder-Mead simplex algorithm takes another step in the same direction, expanding

the current simplex. If this point also improves the current best point, the new point replaces the worst point in the simplex, and, together with the other points, generates a new simplex, for which the same procedure starts all over again (Price et al. 2005, p. 24). If no improvement can be observed for the expansion, the reflection point is taken for the next simplex. If reflection of the current worst point does not result in a better point, the simplex is contracted by moving the current worst point closer to the centroid of the simplex. If neither reflection nor contraction lead to a better point than the worst point, the simplex is shrunk around the current best point (Bolker 2008, p. 303). The algorithm stops when both the deviations between the function values of the simplex vertices and between the parameter values are sufficiently small.

Based on the described operations, the simplex can adapt itself to the local landscape of the objective function (Nelder and Mead 1965). The step size is not fixed, but based on the topography of the objective function (Price et al. 2005, p. 28). In contrast to derivative-based algorithms, the Nelder-Mead simplex algorithm has the advantage that it is less sensitive to discontinuities or noise in the objective function surface (Bolker 2008, p. 306). Nevertheless, because the number of sample points is restricted to $p + 1$, for complicated objective functions that require many more points to form a clear model of the surface topography, the Nelder-Mead algorithm might converge prematurely (Price et al. 2005, p. 28). It is therefore recommended, to test the algorithm several times with different initial values (Weise 2009, p. 283).

2.2.3.2 Differential Evolution

Differential Evolution (DE) is a population-based global optimization algorithm developed by Storn and Price (1997). For the optimization only direct function evaluations are necessary. Information about the gradient or higher derivatives of the objective function are not required. Accordingly, DE is classified as a direct search method.

DE starts by randomly generating an initial population, consisting of NP individuals. Each individual represents a parameter vector consisting of p parameters. Values for the generation of each parameter vector are randomly sampled from a uniform distribution which is bounded by previously specified lower and upper constraints for each parameter. Subsequently, the objective function is evaluated for each parameter vector. In the following, the individuals of a generation will be denoted as target vectors $x_{i,g}$. After an initial population is generated, the target vectors are compared to newly generated vectors using mutation and crossover operations. A flow chart of the operations in DE is shown in Figure 2.6. In the following, the depicted operations of mutation, crossover and selection are described in more detail.

Initially, for each target vector $x_{i,g}$ a mutant vector $v_{i,g}$ is created by combining three other, randomly chosen vectors from the current population. The mutant vector is generated by adding a scaled vector difference to a third vector (Price et al. 2005, p. 38). The size of the scaled difference is controlled by the user-defined variable $F \in [0, 2]$ (Storn and Price 1997). The created mutant vectors are transformed into trial vectors $u_{ij,g}$ by applying a crossover operation. In this step, parameter values from the target vector and the mutant vector are randomly copied into the trial vector. The operation is controlled by the user-defined crossover variable $CR \in [0, 1]$, which controls the fraction of parameter values that are copied from the mutant vector (Price et al. 2005, p. 39). Additionally, one parameter is randomly chosen and taken from the mutant vector to ensure that the trial vector does not duplicate the target vector (Price et al. 2005, p. 40).

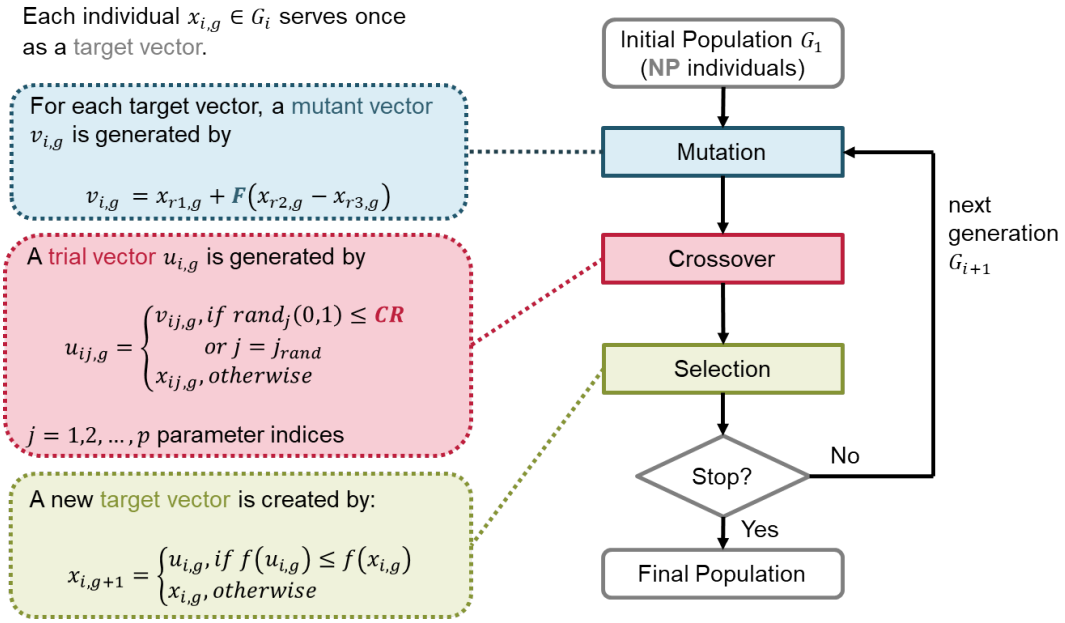

Figure 2.6: Flow chart for the Differential Evolution algorithm (modified from Chiang et al. (2013)). Equations are based on Price et al. (2005, pp. 38–41).

After the generation of NP trial vectors, the objective function is evaluated for each of them. In the final step, referred to as selection, the results are compared to the target vectors. If the trial vector $u_{i,g}$ yields an equal or lower objective function value than of its target vector $x_{i,g}$, it replaces the target vector in the next generation, otherwise the target retains its place in the population (Price et al. 2005, p. 40).

The described steps are repeated once the new population is obtained. As the solution matures, deviations between the individuals get smaller and the population converges to a small region in the parameter space. The algorithms stops when either the maximum number of iterations is reached or the deviations between function and/or parameter values are sufficiently small.

In summary, DE only needs a few user-defined control variables. These include the population size NP, the crossover rate CR and the scaling factor F. Suggestions for an appropriate parametrization of these variables are given in Price et al. (2005, pp. 166–167). Like all population-based optimization routines, DE requires a significant number of function evaluations until a convergence criterion is met. If the evaluation of the objective function is computationally demanding, which is often the case when coupled to environmental models, the total computational time can be considerable (Maier et al. 2019). Because each individual of a generation in DE can be evaluated independently of the other individuals, the incorporation of parallel computation routines is a viable option to reduce the computational time. Lastly, although evolutionary algorithms possess several advantages, it has to be emphasized that convergence to a global minimum is not ensured when using DE.

2.2.4 Parameter uncertainty

The minimization of the objective function via numerical optimization results in a point estimate. Since parameter estimation involves a variety of possible errors, including meas-

urement errors, model errors, and numerical errors, it is necessary to propagate the errors into the estimated parameters (Schwaab et al. 2008; Šimůnek and Hopmans 2002). The uncertainty in the estimated parameters can be derived by calculating confidence intervals. A confidence interval gives a region $[\theta_l;\ \theta_u]$ wherein the true parameter θ^* is most likely to fall (Dalitz 2017). More precisely, for repeated experiments, about $(1-\alpha)\%$ of the calculated confidence intervals will contain the true value θ^*, with $(1-\alpha)$ being the selected level of confidence (Bard 1974, p. 186).

Different methods have been proposed for the calculation of confidence intervals in nonlinear models. The method most frequently used is the linear approximation method, which is based on a linear approximation of the function f by a first-order Taylor series expansion about the parameter estimate $\hat{\theta}$ (Vugrin et al. 2007). The linear approximation of f about $\hat{\theta}$ leads to a quadratic approximation of the log-likelihood function resulting in ellipsoid contours centred at $\hat{\theta}$ (Bates and Watts 1988, p. 61; Vugrin et al. 2007). Similarly to the linear case, the approximate covariance matrix of the parameter estimate $\hat{\theta}$ can be derived by (Aster et al. 2013, p. 31):

$$\Sigma_p = (S^T \Sigma_\epsilon^{-1} S)^{-1} \tag{2.12}$$

where Σ_p covariance matrix of the parameter estimates $(p \times p)$
S Jacobian matrix calculated at $\hat{\theta}$ $(n \times p)$
Σ_ϵ error covariance matrix $(n \times n)$ with $\Sigma_\epsilon(ii) = \sigma_i^2$

The Jacobian matrix S, also denoted sensitivity or functional matrix, can be derived numerically by using the finite differences approach. A detailed description of its calculation is given in Chapter 6.2.1. In the case of independent and identically normally distributed errors ($\epsilon_i \sim N(0, \sigma^2)$), the error covariance matrix reduces to $\Sigma_\epsilon = \sigma^2 I$, and Σ_p can be written by (Donaldson and Schnabel 1985; Aster et al. 2013, p. 31):

$$\Sigma_p = \sigma^2 (S^T S)^{-1} \approx \frac{\epsilon^T \epsilon}{n-p} (S^T S)^{-1} \tag{2.13}$$

where σ^2 error variance
$\epsilon^T \epsilon$ sum of squared errors
n number of measurement data
p number of parameters

As σ is usually unknown in practice, it is typically estimated by dividing the sum of squared errors by the number of degrees of freedom $(n-p)$ (Witkowski and Allen 1993). The diagonal elements of the covariance matrix Σ_p equal the parameter variances and can be used to derive individual confidence intervals for the parameter estimates (Hill and Tiedeman 2007, p. 126):

$$CI_i(\alpha) = \hat{\theta}_i \pm t_{n-p}^{1-\alpha/2} \cdot \sqrt{\Sigma_p(ii)} \tag{2.14}$$

where	$\hat{\theta}_i$	parameter estimate
	$t_{n-p}^{1-\alpha/2}$	Student's t-distribution for a given confidence level $(1-\alpha)\%$ and $n-p$ degrees of freedom
	$\Sigma_p(ii)$	diagonal element of the parameter covariance matrix Σ_p

When σ is known, the Z-distribution can be applied instead of the Student's t-distribution. The entries in the parameter covariance matrix Σ_p can be further used to calculate the parameter correlation matrix below. The correlation between the ith and jth parameter can be calculated by (Šimůnek and Hopmans 2002, p. 147):

$$CM_{ij} = \frac{\Sigma_p(ij)}{\sqrt{\Sigma_p(ii)}\sqrt{\Sigma_p(jj)}} \tag{2.15}$$

Parameter correlations indicate whether coordinated changes in the parameter values could produce the same simulated results, and therefore the same model fit (Hill and Tiedeman 2007, pp. 127–128). When the estimates are correlated, the corresponding diagonal terms of the covariance matrix may be a poor approximation of the uncertainty in the parameters (Carrera and Neuman 1986a). Standard confidence intervals are further only exact in the case of linear models. For non-linear models, the calculated confidence intervals present only approximations. If the contours of the likelihood are roughly elliptical (at least near the MLE), the approach will work well (Bolker 2008, p. 265). Otherwise, a different approach for the calculation of confidence intervals should be applied.

A different approach to obtain confidence intervals for non-linear models is based on the definition of a threshold in the likelihood function (Raue et al. 2009). In the literature, these are also called likelihood-based confidence intervals. Likelihood-based confidence intervals are based on the likelihood-ratio test statistic, which is, under appropriate regularity conditions, approximately χ^2 distributed (Meeker and Escobar 1995, p. 50; Millar 2011). For a parameter vector θ, a likelihood-based confidence region to a confidence level $(1-\alpha)\%$ is defined by (Vugrin et al. 2007; Kreutz et al. 2015):

$$CR(\alpha) = \{\theta \mid 2\ln L(\hat{\theta}) - 2\ln L(\theta) \leq \chi^2(1-\alpha, df)\} \tag{2.16}$$

where $\chi^2(1-\alpha, df)$ corresponds to the $(1-\alpha)$th-percentile of the χ^2-distribution with df degrees of freedom (Meeker and Escobar 1995). The choice of $df = p$ yields confidence regions which hold jointly for all parameters, while $df = 1$ yields individual confidence intervals (Raue et al. 2010). Individual confidence intervals can be derived by calculating profile likelihoods after an optimal parameter set $\hat{\theta}$ has been obtained. For each parameter θ_i, a suitable set of values in in- and decreasing direction of the MLE is selected. Subsequently, for the selected values of θ_i, the other parameters $\theta_{j,j\neq i}$ are re-optimized (Maiwald et al. 2016):

$$PL(\theta_i) = \min_{\theta_{j,j\neq i}} (-2\ln L(\theta|d)) \tag{2.17}$$

According to Equation 2.16, a threshold in the likelihood profile, based on the desired level of confidence, can afterwards be used to compute profile likelihood-based confidence intervals (Kreutz et al. 2013):

$$CI_i(\alpha) = \{\theta|PL(\theta_i) \leq -2\ln L(\hat{\theta}|d) + \chi^2(1-\alpha, 1)\} \tag{2.18}$$

where $\chi^2(1-\alpha, 1)$ corresponds to the $(1-\alpha)$th-percentile of the χ^2-distribution with one degree of freedom.

In contrast to the calculation of standard confidence intervals, the technique to derive likelihood-based confidence intervals is much more computationally expensive (Meeker and Escobar 1995, p. 139; Hill and Tiedeman 2007). Nevertheless, the method provides more accurate confidence intervals as not only the curvature at the MLE is taken into account, but the complete geometry of the likelihood function. This is especially relevant in non-linear models or when only a small sample size is considered (Bates and Watts 1988; Vugrin et al. 2007). In these cases, parameters are not necessarily normally distributed and confidence intervals are typically not symmetric (Kreutz et al. 2015, p. 367).

2.2.5 Uniqueness, identifiability and stability

In mathematics, a problem is considered well-posed if (1) a solution to the problem exists (existence); (2) the solution of the problem is unique (uniqueness); and (3) the solution of the problem depends continuously on the data of the problem (stability) (Hadamard 1902). Conversely, if one of these conditions is violated, the problem is termed ill-posed. Inverse problems are often considered ill-posed, mainly due to non-unique solutions or instability problems (Aster et al. 2013, p. 22). Consequently, in the following, the causes and problems associated with an ill-posed problem are discussed in more detail.

According to Carrera and Neuman (1986b), a solution to an inverse problem is non-unique when the criterion to be minimized is non-convex, and, therefore exhibits local or global minima at more than one point in the parameter space. Solution uniqueness is inherently related to parameter identifiability. Parameters are termed non-identifiable when different parameter sets lead to the same model response (Šimůnek and Hopmans 2002). In this case, the solution to the inverse problem is non-unique, as different parameter vectors will result in the same value regrading the minimization criterion. Consequently, the inverse problem is considered ill-posed.

Parameter non-identifiability can have different sources and is often classified into structural and practical non-identifiability (Guillaume et al. 2019). The concept of structural identifiability was first introduced by Bellman and Åström (1970) and addresses the question whether model parameters can, in theory, be uniquely determined for a given model structure. A lack in structural parameter identifiability can exist if model predictions do not react to changes in the respective parameters (missing sensitivity) or if parameters compensate each other in their influence on model predictions (collinearity) (Brun et al. 2001). Structural identifiability analysis is usually based on the analysis of model equations and is independent of observational data (Guillaume et al. 2019).

Although necessary, structural identifiability is not sufficient to guarantee a reliable identification of model parameters in practice, when only a finite amount of noise-perturbed measurements are available (Miao et al. 2011). Therefore, the term practical identifiability has been introduced. In the literature, practical identifiability is often associated with the quantification of uncertainty in the estimated parameters (Raue et al. 2009; Miao et al. 2011; Marsili-Libelli et al. 2014). According to Raue et al. (2009), a parameter estimate is termed practically non-identifiable if, although a unique estimate could be obtained, only infinite confidence intervals in the de- and/or increasing direction of the parameter estimate can be derived. Large uncertainties can be due to a limited amount or quality of the given monitoring data collected for the given model structure (Raue et al. 2009). This

is a practical identifiability problem and a change in the monitoring design, i.e. an improvement in the amount and quality of the data, can resolve parameter non-identifiability in these cases. Nevertheless, unreliable parameter estimates might also be the result of structural identifiability problems.

Lastly, parameter estimates are said to be stable if they are insensitive to measurement errors (Šimůnek and Hopmans 2002). Consequently, small perturbations in the measurements should only lead to small changes in the estimated parameters. This is an important aspect in most practical applications, because measurement data usually contain measurement errors in real life. Instability often arises from a lack or poor degree of identifiability. In this case, the estimation criterion (e.g. objective function) will generally be characterized by elongated valleys or flat zones near the minimum, causing convergence problems in most minimization algorithms (Carrera and Neuman 1986b). To stabilize the inversion process, commonly regularization mechanisms are proposed, which impose additional constraints that bias the solution (Aster et al. 2013, p. 20).

Regarding parameter estimation, it is always essential to evaluate if an inverse problem might show signs of non-uniqueness, non-identifiability or instability. Prior analysis can be based on synthetically generated data and be carried out before monitoring data are collected (Guillaume et al. 2019). As pointed out by Sun and Sun (2015, p. 31), data insufficiency is the main factor that leads to non-uniqueness and instability of inverse solutions. The design of an optimal monitoring network, prior to parameter estimation, can therefore reduce the risk of obtaining an ill-posed problem.

3 State of the art

This chapter includes a detailed description of the pollution source identification (PSI) problem. Different methods to identify the source parameters of a pollution spill are presented and compared. In addition, the importance of monitoring data is emphasized. For this purpose, existing approaches for the design of a monitoring network in the context of PSI are presented.

3.1 Problem statement

It has become standard practice to use water quality models to predict the migration of contaminant plumes from known sources in surface water (Ren et al. 2007; Bahadur and Samuels 2015). Often, these models are part of an emergency response system (Grayman and Males 2002). The transport, mixing and transformation of the contaminant is governed by the advection-dispersion-reaction equation (ADRE). The two-dimensional (2D) ADRE has the following form:

$$\frac{\partial c}{\partial t} = D_x \frac{\partial^2 c}{\partial x^2} + D_y \frac{\partial^2 c}{dy^2} - v_x \frac{\partial c}{\partial x} - v_y \frac{\partial c}{\partial y} - kc + S \tag{3.1}$$

where

c	pollutant concentration	$[\mathrm{g\,m^{-3}}]$
D_x, D_y	dispersion coefficient in x- and y-direction	$[\mathrm{m^2\,s^{-1}}]$
v_x, v_y	depth-averaged flow velocity in x- and y-direction	$[\mathrm{m\,s^{-1}}]$
k	process coefficient (e.g. transformation, decay)	$[\mathrm{s^{-1}}]$
S	sinks and sources	$[\mathrm{g\,m^{-3}\,s^{-1}}]$

The term S represents mass additions and extractions to the modelled system. When describing a pollutant spill, the term S describes the characteristics of the spill. The mathematical expression of the source term S is dependent on the form of the release type. Under the assumption of a single instantaneous pollutant release, the source term S in the 2D ADRE is given by:

$$S = \frac{M_s}{h} \cdot \delta(x - x_s) \cdot \delta(y - y_s) \cdot \delta(t - t_s) \tag{3.2}$$

where

M_s	total pollutant mass	[g]
h	water depth at the source location	[m]
x_s	x-coordinate of the source location	[m]
y_s	y-coordinate of the source location	[m]
t_s	release time of the pollutant	[s]

In this case, the spill can be described by four parameters, including the release time t_s, the total pollutant mass M_s and the source location, specified by its x- and y-coordinate x_s and y_s. Note that the Dirac delta function $\delta(\cdot)$ always has the inverse dimension of its argument (Hahn and Özişik 2012, p. 313).

The pollution incident can be further classified as a continuous pollutant release. In this case, the Dirac delta function of the release time $\delta(t - t_s)$ is replaced by a release function $f(t)$ which considers a time-dependent release of the pollutant (Boano et al. 2005). Additionally, the pollution might stem from multiple point sources or a spatially distributed source, which further influences the mathematical expression of the term S.

If the source term S is known, contaminant concentration profiles at specific locations, e.g. water intake locations, can be predicted with the ADRE in the case of a pollution incident. Based on these simulations, mitigation measures might be put into place. This is also called forward modelling. In contrast, the corresponding inverse problem deals with the determination of the parameters of the source term S based on pollutant concentration measurements. In the literature, this problem is often referred to as pollution or contaminant source identification (PSI).

The determination of the number of sources and the corresponding release type is of central importance in PSI. As explained above, the mathematical expression of the source term S is dependent on the assumed spatial and temporal characteristics of the pollution sources. For the identification of source parameters, the expression has to be derived in advance. The number of sources and the release type will influence the number of source parameters which have to be identified. In the last decades, several approaches have been developed to identify the unknown source parameters. These are presented in the following sections.

3.2 Approaches for pollution source identification

Pollution source identification has been extensively studied in groundwater since the 1970s (Jiang et al. 2018). Only since the last decade approaches have been increasingly transferred and applied to the identification of spill incidents in surface water. Further fields of application are water distribution systems (Guan et al. 2006; Wagner et al. 2015; Seth et al. 2016) as well as indoor and outdoor air pollution (Liu and Zhai 2008; Kathirgamanathan et al. 2002).

For PSI, different methods have been developed over the last decades. These include probabilistic, mathematical, classification and optimization approaches. A detailed introduction to these methods will be given in the following sections. The literature cited in these sections contains mainly applications of PSI approaches to surface water systems. Reviews of approaches applied in groundwater or water distribution systems can be found in Atmadja and Bagtzoglou (2001) and Adedoja et al. (2018).

It has to be noted that the methods presented below rely on an appropriate flow and transport model, which has to be adapted to the specific characteristics of the flow system (e.g. river or estuary). The calibration of the flow and transport model usually needs to be carried out beforehand.

3.2.1 Linked simulation-optimization approach

Due to its simplicity, the simulation-optimization approach for pollution source identification can be found throughout the literature. For the approach, the numerical model for the simulation of flow and transport processes is externally linked to an optimization algorithm (Amirabdollahian and Datta 2013). A schematic overview of the linked simulation-optimization approach is given in Figure 3.1. At the beginning of the optimization, initial parameter values are randomly generated. These serve as input to the pollutant transport model and will be iteratively changed during the optimization process. After the model is run for the given set of parameters, the simulated concentrations of the transport model are compared to observed pollutant concentrations by calculating the value of a predefined objective function. Often, the objective function is derived from maximum likelihood theory and will be based on the summed squared errors (SSE) (Han et al. 2014; Parolin et al. 2015; Guneshwor et al. 2018). The aim is to find the best possible parameter values, which minimize the given objective function. Subsequently, parameters are updated according to the rules of the chosen optimization algorithm and the transport model is run again with the updated parameter sets. The steps are repeated until a stopping criterion is met. This will be either be based on a given threshold for the function or parameter tolerance, or on the maximum number of iterations or function evaluations. In the literature, different optimization algorithms have been used for the identification of source parameters. Examples are the genetic algorithm (Zhang and Xin 2017; Borah and Bhattacharjya 2016), differential evolution (Han et al. 2014; Gurarslan and Karahan 2015), particle swarm optimization (Guneshwor et al. 2018), or simulated annealing (Datta et al. 2013).

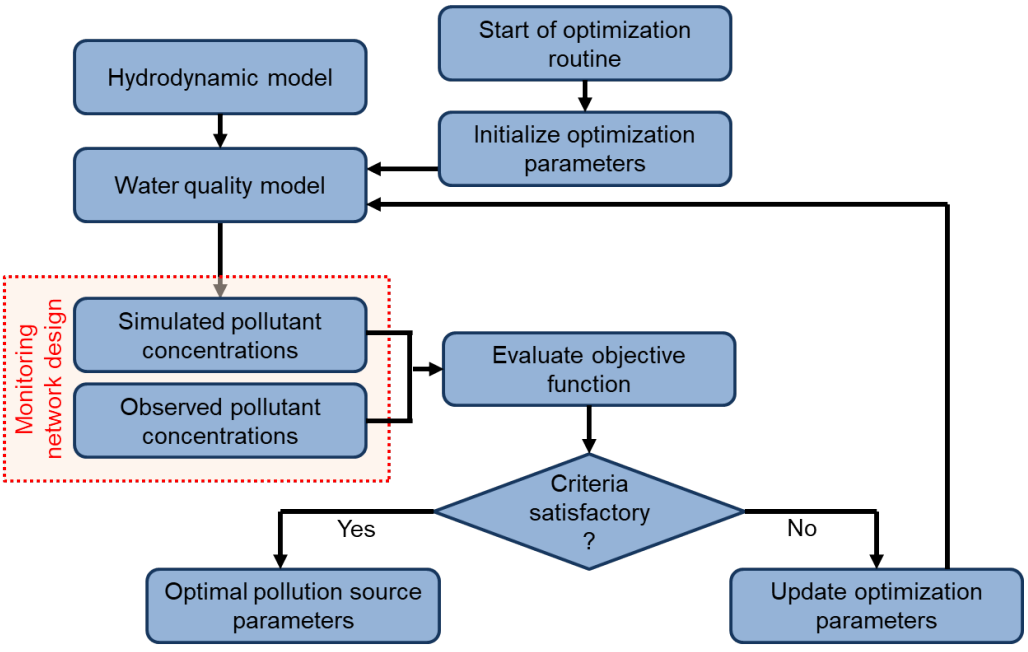

Figure 3.1: Schematic representation of the linked simulation-optimization approach for pollution source identification (modified from Amirabdollahian and Datta (2013)).

Zhang and Xin (2017) used an analytical solution of the 1D advection-dispersion equation and the basic genetic algorithm (BGA) to identify the source intensity and source location of a single continuous source and two continuous sources, respectively, in a small

straight river. The assumptions of a homogeneous channel, a constant flow field and almost immediate cross-sectional mixing justified the use of an analytical solution of the 1D advection-dispersion equation. When considering a single source, the inversion results agreed well with the real source parameters with relative errors smaller than 5%. It is noted that the population size used for BGA had a significant influence on the accuracy of inversion results. For cases of multi-point sources, the optimization approach was unable to identify the actual pollution sources due to the existence of multiple parameter combinations with almost identical values for the objective function.

Han et al. (2014) coupled an analytical solution of the 2D depth-averaged advection-dispersion equation with the Differential Evolution (DE) optimization algorithm. The authors considered an instantaneous pollution release from a single point source. The parameters to be identified included the x- and y-coordinates of the source location and the total pollutant mass. When perfect monitoring data were used, the estimated parameters agreed well with the actual parameter values. When considering monitoring errors in the data, the parameters could still be identified with relatively small errors. In addition, the authors analysed the influence of the number of monitoring sites, monitoring frequency and monitoring accuracy on the inversion results. It could be shown that these factors have a considerable influence on the results. In general, the more monitoring data were available and the better the accuracy of the data, the smaller the relative errors in the estimated source parameters.

Only two studies dealing with source identification in estuaries were found, namely Parolin et al. (2015) and Jing et al. (2018). Both studies used 2D numerical transport models as forward simulation models due to the unsteady flow conditions in estuaries. Parolin et al. (2015) used synthetic test data for the Macaé river estuary, Brazil to estimate the source location and intensity of a continuous pollution source. Three different optimization algorithms were compared for the estimation of the source location. The source intensity was estimated by golden section search. In summary, all methods performed equally well and were able to solve the inverse problem with at least 95% success when no errors were considered, and 80% success when artificial noise (relative noise level of 5%) was introduced into the monitoring data. The only difference was in the computational efficiency of the evaluated methods. Jing et al. (2018) decoupled the estimation of the source parameters. They considered a single instantaneous point source defined by its source location, release time and total pollutant mass. After a rough estimation of the release time, an improved version of the genetic algorithm (GA) was used for the estimation of the source location. In a third step the total pollutant mass was estimated. The approach was applied to Quanzhou Bay, China using synthetic test data. In general, the approach achieved good results, its accuracy was mainly influenced by the integrity and accuracy of the available monitoring data.

The main advantage of the simulation-optimization approach is its ability to link various different transport models and optimization algorithms. A direct access to the model programming code is not necessary. Thus, it can be applied to a diversity of problems and study areas. Disadvantages are the computational effort for the evaluation of the objective function and the possible convergence to a local minimum instead of a global minimum (Mazaheri et al. 2015). The computational time can be reduced when a surrogate model is used instead of the complex simulation model. Here, response surface surrogates (e.g. artificial neural networks (ANN) (Borah and Bhattacharjya 2016) or radial basis functions (RBF) (Guneshwor et al. 2018)), which were already applied to groundwater systems, or physically-based surrogates (e.g. the analytical solution of the ADRE) can be used to speed up the computation time.

3.2.2 Probabilistic approaches

3.2.2.1 Bayesian inference

In recent years, Bayesian inference has been increasingly applied to source identification problems. In this approach, all forms of uncertainty are expressed in terms of probability distributions (Yang et al. 2016). For example, prior knowledge regarding the source parameters can be incorporated through prior distributions. The result of the Bayesian approach is not a single parameter set, but the posterior parameter distribution of the source parameters from which uncertainties can be derived. The posterior probability distribution is calculated according to Bayes' theorem (Wang and Jin 2013):

$$P(\theta|d) = \frac{P(d|\theta)P(\theta)}{P(d)} \propto P(d|\theta)P(\theta) \tag{3.3}$$

where θ parameter vector containing the source parameters
d monitoring data
$P(\theta)$ prior probability distribution
$P(d)$ evidence
$P(d|\theta)$ likelihood probability distribution
$P(\theta|d)$ posterior probability distribution

In the Bayesian approach, expert knowledge regarding source parameters can be incorporated in the form of the prior probability distribution $P(\theta)$. Several alternatives are available for the assignment of the prior probability distribution. However, prior information regarding pollution source parameters is usually quite limited in real-life cases (Jiang et al. 2019). Therefore, for the identification of source parameters, often a uniform distribution within a predefined range is used (e.g Yang et al. (2016), Guozhen et al. (2016) and Jiang et al. (2019)). The likelihood probability distribution $P(d|\theta)$ describes the probability of the measured data d given a model with parameter values θ. The form of the likelihood function depends on the predefined error assumptions regarding monitoring errors and model errors, respectively. In Jiang et al. (2019) likelihood functions for both homoscedastic and heteroscedastic errors are defined. A pollutant transport model is required for the repetitive calculation of the likelihood. The denominator $P(d)$ can be regarded as a normalizing constant $P(d) = \int P(d|\theta)P(\theta)d\theta$.

Given an adequate prior distribution $P(\theta)$ and a likelihood probability distribution $P(d|\theta)$, the posterior probability distribution $P(\theta|d)$ of the pollution source parameters can be derived based on Bayes' theorem. However, as the calculation of multidimensional integrals is required, in general, the posterior distribution cannot be derived analytically. An alternative is the application of Monte Carlo Markov Chain (MCMC) sampling methods. MCMC methods provide the ability to characterize a probability distribution without knowing all of its mathematical properties, by randomly sampling values out of the distribution (van Ravenzwaaij et al. 2018). The samples are the states of a Markov chain which, after a sufficient number of steps, converges to an equilibrium distribution proportional to the posterior probability distribution (Yang et al. 2016). Various algorithms are available for the construction of a Markov chain including the Gibbs and the Metropolis-Hastings sampling algorithms. For the final inference of source parameters, statistical measures of the obtained samples of the posterior probability distribution are calculated. The first

part of the Markov chain is ignored in this analysis, because these early samples cannot be guaranteed to be drawn from the target distribution (van Ravenzwaaij et al. 2018).

Up to now, the approach is applied mainly to source identification in groundwater systems (Wang and Jin 2013; Hazart et al. 2014), but in recent years a few authors also applied the approach to surface water systems. Yang et al. (2016) used the approach to identify source parameters of multi-point water pollution accidents. An analytical solution of the 1D ADRE for multi-point sources was used as a transport model. For the derivation of the posterior probability distribution a new method called DEMH-MCMC was designed which combines the Differential Evolution (DE) algorithm and Metropolis-Hastings-Markov Chain Monte Carlo (MH-MCMC) to improve the convergence rate of the Markov chain. Real data of a small tracer experiment in a 100 m long test channel with two release points were used to test the ability of the approach. Within the Bayesian framework, the source location and the source intensity of the two sources were identified. The results show that DE helps to improve the sampling efficiency of MH-MCMC due to its strong global searching ability. Thus, a vast number of calculations can be saved and the convergence rate of the MH-MCMC can be improved. Additional tests showed that DEMH-MCMC has better noise immunity in comparison to the application of the DE algorithm or the traditional MH-MCMC method.

In practice, the model parameters (e.g. flow velocity, dispersion coefficient, decay rate), which are used inside the pollutant transport model, can not be estimated accurately and therefore include uncertainties. Guozhen et al. (2016) used prior probability distributions instead of constant values for sensitive model parameters and included these in the Bayesian framework. These were used additionally to the uniform prior distributions of the source parameters to calculate the posterior probability distribution of the source parameters. An analytical solution of the 2D ADRE was applied to model a number of synthetic instantaneous pollutant releases inside a river. Two methods were used to approximate the posterior probability distribution, including the traditional Metropolis algorithm and the Delayed Rejection and Adaptive Metropolis (DRAM) algorithm. The results showed that the DRAM-MCMC method improved the efficiency and accuracy of the source identification in comparison to the traditional MCMC. Besides, the incorporation of sensitive model parameters inside the Bayesian framework got more accurate results as when constant parameter values were considered.

Jiang et al. (2019) recently applied the Bayesian framework to an actual nitrobenzene spill in the Songhua River, China. In addition to a detailed deduction of the Bayesian approach for pollution source identification in rivers, the authors put a special focus on the error assumptions used for the formation of the likelihood function. Here, the results of homoscedastic and heteroscedastic error assumptions were compared. To model the pollutant transport in the Songhua River, an analytical solution of the 1D ADRE was used. The Metropolis algorithm was used inside the Bayesian framework for the construction of Markov chains. In Figure 3.2, the obtained posterior probability distributions of the source parameters using the heteroscedastic error assumption are presented. To infer the most likely values for the estimated source parameters, the mean of the samples of the posterior probability distribution was calculated. In general, the estimated source parameters for both error assumptions were relatively close to their real values. Nevertheless, the heteroscedastic error assumption seemed to be more acceptable and provided slightly better results.

Using the Bayesian approach, different sources of uncertainty can be incorporated into the solution. This is a major advantage in comparison to simulation-optimization ap-

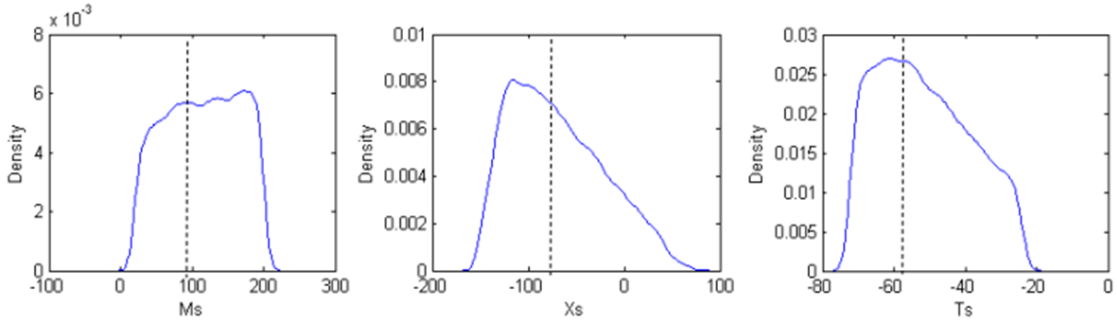

Figure 3.2: Posterior probability density functions for the total pollutant mass M_s, the longitudinal source location X_s and the release time T_s under the assumption of heteroscedastic errors. The dashed lines denote the real values. Modified from Jiang et al. (2019) under the terms and conditions of the Creative Commons Attribution (CC BY) license (http://creativecommons.org/licenses/by/4.0/).

proaches where only a single parameter set is obtained in the end. Nevertheless, to reach convergence, the constructed Markov chain needs a vast number of calculations. Thus, in general, the Bayesian method is usually regarded as a computationally very expensive approach (Zhang et al. 2015). For convergence of the Markov chain, it has to be ensured that the posterior probability distribution is proper. Non-identifiable parameters cause the posterior to be non-proper (Berger and Bayarri 2004). Thus, before an MCMC technique can be used securely, the user must ensure parameter identifiability (Raue et al. 2013).

3.2.2.2 Backward probability method

The backward probability method (BPM) was originally developed and employed to backtrack pollutant plumes in groundwater systems. In this method, the forward governing equation, with the pollutant concentration as the dependent variable, is replaced by the adjoint equation, with the adjoint state as the dependent variable (Bagtzoglou and Atmadja 2005). A detailed derivation of the governing equations can be found in Neupauer and Wilson (1999). In a two-dimensional system the adjoint equation of the advection-dispersion equation has the form (Neupauer and Wilson 2001):

$$\frac{\partial \psi}{\partial \tau} = v_x \frac{\partial \psi}{\partial x} + v_y \frac{\partial \psi}{\partial y} + D_x \frac{\partial^2 \psi}{\partial^2 x} + D_y \frac{\partial^2 \psi}{\partial^2 y} + \frac{\partial h}{\partial c} \tag{3.4}$$

where ψ adjoint state
τ backward time ($\tau = t_d - t$)
$\frac{\partial h}{\partial c}$ load term

The adjoint equation models the same physical processes as the forward equation (e.g. advection and dispersion); however, the flow field is reversed in both time and space. In addition, the boundary conditions are modified and a new load term is introduced (Neupauer and Wilson 2004). As in the forward model, the hydrodynamic variables need to be determined prior to parameter identification. However, the included dispersion term in the adjoint equation does not represent a temporally inverted dispersion mechanism, but characterizes the uncertainty in the former position of the particle (Stollberg 2012; Neupauer and Wilson 2001).

The adjoint equation describes a family of adjoint states ψ, with a particular adjoint state defined by the load term $\frac{\partial h}{\partial c}$ through the choice of the performance functional h (Neupauer and Wilson 2004). The backward location probability (BLP) and the backward travel time probability (BTTP) are two possible adjoint states. According to Neupauer and Wilson (1999), the BLP is the probability where the particle was located at some prior time. The BTTP is the probability of when the particle was located at some position upgradient of the detection point and can be determined after the source location has been identified. To derive the BLP, the load term in Equation 3.4 needs to be replaced by (Neupauer and Wilson 2001):

$$\frac{\partial h}{\partial c} = \delta(x - x_{obs})\delta(y - y_{obs})\delta(\tau) \tag{3.5}$$

where x_{obs} x-coordinate of the monitoring station
y_{obs} y-coordinate of the monitoring station

The load term is a product of Dirac delta functions, which represent an instantaneous mass impulse at the beginning of the backward simulation at the observation station. This pollution release is propagated backwards in time from the measurement station to the possible pollution source using the adjoint equation.

For the use of the BPM in source identification, the relation between forward and backward location probability is of importance. The forward location probability (FLP) describes the position of a solute parcel at a fixed time after its release from the source. In Figure 3.3, the relationship between FLP and BLP is illustrated. Unit probability magnitude is considered at the source point and detection point, respectively, as an initial condition for both kinds of probabilities. While for the FLP the pollutant distribution is tracked forward in time, for the BLP the distribution is allowed to advect upgradient in backward time. The BLP density function will only be equal to the FLP density function at the source location (Ghane et al. 2016).

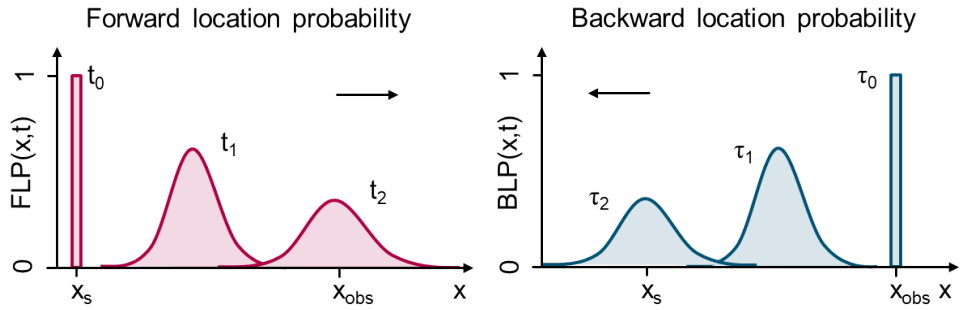

Figure 3.3: Schematic representation of the relationship between forward and backward location probability. x_s: pollution source, x_{obs}: monitoring station, t: forward time, τ: backward time.

One helpful feature of the FLP is its relation to the pollutant concentration. The normalized concentration distribution released from an instantaneous point source is equivalent to the forward location probability density function at time t given by (Cheng and Jia 2010; Neupauer and Wilson 2001):

$$FLP(x, y, t) = \frac{c(x, y, t)}{M_s} \tag{3.6}$$

where $FLP(x, y, t)$ forward location probability
$c(x, y, t)$ concentration distribution
M_s total pollutant mass

Thus, if the BPM is used for source identification, measured concentrations of the pollutant at at least one downstream location are necessary. The similarity between observed concentrations and computed BLP serves as the basis for the identification of the source location. Because the total pollutant mass is unknown, the correlation coefficient is used as an objective function (Cheng and Jia 2010; Wang et al. 2018):

$$r = \frac{\sum_{i=1}^{n}(c_i - \overline{c})(BLP_i - \overline{BLP})}{\sqrt{\sum_{i=1}^{n}(c_i - \overline{c})^2}\sqrt{\sum_{i=1}^{n}(BLP_i - \overline{BLP})^2}} \tag{3.7}$$

where c_i ith observation value
BLP_i ith corresponding solution of the BLP
n number of monitoring data

It is assumed that the location which maximizes the correlation coefficient identifies the source location. The release time and total pollutant mass can be calculated after the source location has been successfully identified.

Cheng and Jia (2010) were the first to apply this approach to surface water. A finite element based 2D depth-integrated free-surface flow model was used to derive the velocity field. The pollutant transport was governed by the 2D depth-averaged advection-dispersion equation. Several test cases were used to validate the relation between FLP and BLP in surface water. In general, the solutions of the BLP transport equation agreed well with the FLP, which was computed using the pollutant concentration at the monitoring stations. Several sensitivity tests indicated that the numerical errors for identifying a known source are affected by different parameters such as the diffusivity, mesh irregularity and local velocity gradient.

The approach was extended by Ghane et al. (2016) to pollution source identification in river networks. The BPM was applied to a 1D hypothetical test case of a river network with irregular cross-sections and variable hydrodynamic parameters. The BLP was propagated backwards in time and computed reach by reach. All potential source locations could be identified, using only one backward simulation. However, because each of the identified potential sources creates a similar effect at the detection point, the method is unable to state which node is the actual source location. It has to be noted that other approaches for pollution source identification would exhibit the same problem due to the non-unique solution. The identification of the source location can be improved when additional monitoring stations are installed inside the river network.

Wang et al. (2018) applied the BPM to multi-point source pollution incidents in a river stretch. In the case of multiple sources, the simulation of the pollutant transport follows the superposition principle. The total pollutant concentration in the river can be described as the sum of the pollutant concentration caused by several individual sources. In the same way, this principle can be applied to the BLP. The authors showed that the accuracy of source identification deteriorates when the number of point sources increases. As in the case of Ghane et al. (2016), different parameter combinations led to very close

objective function values. Averaging the results of repeated tests greatly reduces the errors. Furthermore, increasing the number of monitoring stations can additionally improve the identification results.

So far, all applications of the BPM to surface waters only considered conservative pollutants. Nevertheless, a direct application of the approach to reactive transport is possible if the governing equation is linear (1st-order decay) (Neupauer and Wilson 2003; Neupauer and Wilson 2004).

In conclusion, the main advantage of the BPM is its computational efficiency. It takes considerably less time in contrast to other approaches because only one simulation backwards in time is necessary for each data point to derive the adjoint states. Thus, the BPM is preferable for problems that are time-consuming and where poor prior information is available (Wang et al. 2018). According to Neupauer and Wilson (2004), any numerical code that can simulate contaminant transport (forward model) can be used to simulate backward probabilities. Nevertheless, the numerical implementation is non-trivial, since numerous configurations in space and time concerning the flow field reversal and boundary conditions need to be carried out (Stollberg 2012).

3.2.2.3 Other probabilistic approaches

There are a handful of other methods which can be classified as probabilistic approaches but which have been only seldom applied for pollution source identification in surface water.

Jiang et al. (2018) primarily analysed the uncertainty characteristics of the pollution source inversion problem. The authors used the Direct Monte Carlo method to identify the source parameters and propagate uncertainties. In a first step, a large number of random source parameter sets was generated. For every parameter set, the analytical solution of the 1D ADRE considering an instantaneous pollutant release, was used to model the pollutant concentration at the given monitoring locations. The results were compared to the actual observed data by calculating the value of a predetermined objective function. In contrast to other methods, the generation of different parameter sets is purely random. Therefore, a vast number of random parameter sets is necessary to have a sufficient density in the multidimensional parameter space and to derive meaningful results regarding the identification of source parameters. Nevertheless, in contrast to other methods, the Direct Monte Carlo method does not rely on the objective function being smooth in any sense, nor does it involve any potentially numerical unstable processes such as matrix inversion.

The geostatistical approach is another probabilistic approach which was mainly applied in groundwater systems (Snodgrass and Kitanidis 1997; Sun 2007). Boano et al. (2005) used the approach to recover the release history of a spatially distributed source as well as multiple independent point sources in a river. It has to be stressed that for the application of this approach, the spatial distribution or, in the case of point sources, the release locations were considered to be known. The method relies on a probabilistic description of both the observations and the release function, and estimates a release function that is consistent with the observations. The release function to be estimated is discretized into components that are assigned a known stochastic structure with unknown stochastic parameters (Bagtzoglou and Atmadja 2005). In a first step, called structural analysis, the unknown stochastic parameters are estimated from the data based on the principle of maximum likelihood. In a second step, the release history is determined by means of a kriging estimator (Boano et al. 2005). The method could be applied successfully by

Boano et al. (2005) to both cases. The number of data points and measurement errors were important factors which influence the success in recovering the release history.

3.2.3 Mathematical approach

The mathematical approach is often referred to as direct approach as no iterative procedure is necessary to determine the pollutant source characteristics (Atmadja and Bagtzoglou 2001). In general, the mathematical approach is based on the integral equation obtained from applying the Green's function method (Mazaheri et al. 2015). The convolution integral is subsequently approximated using the trapezoidal or rectangle rule (El Badia et al. 2005). The application of one of the quadrature rules leads to a linear, over-determined and ill-posed system of algebraic equations (Mazaheri et al. 2015). To stabilize the solution of the inverse problem, regularization methods, most often Tikhonov regularization, are applied (El Badia and Hamdi 2007; Hamdi and Mahfoudhi 2013). The resulting quadratic minimization problem has an explicit closed-form solution, which can be directly computed without any iterative procedure (El Badia et al. 2005; Mazaheri et al. 2015).

Initially, the approach was developed by Skaggs and Kabala (1994) to reconstruct the release function of a contaminant plume in groundwater. In the last two decades, several works have been published that have also applied the approach in surface water. In addition to determining the source position, the aim is to reconstruct the release function which is assumed to vary over time. This is different to most other approaches, in which assumptions regarding the release type are usually made beforehand to reduce the number of source parameters.

El Badia et al. (2005) were some of the first to apply the mathematical approach to the identification of the location and release history of a point source in a river stretch. The source was assumed to emit organic matter represented by the biological oxygen demand (BOD) in the study. A mathematical proof for identifiability and stability could be established under the consideration of two monitoring stations, located up- and downstream of the source. The approach was adopted by El Badia and Hamdi (2007) who used dissolved oxygen (DO) concentration data instead of direct BOD measurements. In comparison to El Badia et al. (2005), results were a little less accurate and the recovered intensity function was more sensitive with respect to the introduction of noise into the data. In further works, the approach was extended and applied to more difficult settings. These include applications in 2D (Hamdi 2012), with spatially varying velocity, dispersion, and reaction coefficients (Hamdi and Mahfoudhi 2013), and to moving point sources (Ben Belgacem et al. 2013).

Mazaheri et al. (2015) applied the approach to reconstruct the release functions of multiple point sources with varying time patterns. The number and position of pollution sources were assumed to be known. The proposed method was validated by using hypothetical and real examples. The authors could show that to appropriately recover the release functions of all pollution sources, it is necessary to locate one measurement station downstream of each source. The reconstruction of two or more release functions of different sources with only one monitoring station failed due to non-unique solutions.

In contrast to other methods presented in this work, the mathematical approach is much less time consuming as the solution can be computed in one stage and does not rely on any iterative procedure (El Badia et al. 2005; Mazaheri et al. 2015). Nevertheless, the underlying mathematics and formulations are much more complex with respect to other

methods and require advanced knowledge in linear algebra for their application (Mazaheri et al. 2015).

3.2.4 Classification approach

The classification approach is used seldom for pollution source identification in the literature. The applications presented in this section comprise two studies, namely Telci and Aral (2011) and Lee et al. (2018), which both applied the approach to the Altamaha river system, USA. In general, the approach consists of two steps: (i) pre-processing of data sets, and (ii) training and testing of a classification model.

Both studies used the EPA storm water management model (SWMM) to generate a large set of pre-run contaminant scenarios for training purposes. These scenarios are random combinations of spill characteristics (location, time, mass) and spatial variable rainfall patterns. For each scenario, breakthrough curves were obtained at specified monitoring locations. Both studies used monitoring network designs of previous studies (Telci et al. 2009; Park et al. 2014), where the mean detection time and the detection reliability of the system served as design criteria. The obtained breakthrough curves can be characterized by a series of statistical moments, which are saved for each spill scenario. These characteristics are used to train the classification models being applied.

Telci and Aral (2011) used the adaptive sequential feature selection (ASFS) algorithm as a classification model for the identification of the source location. The algorithm sequentially screens potential candidate locations and results in the end in a single source index. Lee et al. (2018) argued that with the final result of the ASFS algorithm one cannot evaluate how reliable the identified location is. As a potential improvement, they proposed the application of random forest models as classification models which contain a collection of tree-structured classifiers. In contrast to the ASFS algorithm, this method provides quantitative measures indicating that a selected location is the correct spill location. Both approaches could be successfully applied to the Altamaha river system, with the random forest models performing slightly better than the ASFS algorithm. As expected, Lee et al. (2018) observed that the more monitoring locations were used for the identification, the better the classification results.

In summary, classification approaches need a considerable amount of pre-run scenarios for training purposes. However, when a pollution incident occurs, no new simulations need to be carried out. When applying the approach to a real spill incident, it has to be considered that external factors (e.g. rainfall patterns) might differ from the randomly created training data sets.

3.3 Monitoring network design for pollution source identification

When a pollutant is introduced into a water body, the physical and chemical processes of molecular and turbulent diffusion as well as dispersion and decay lead to a deformation of the pollutant plume in time and space. This is exemplified for both rivers and estuaries in Figure 3.4 for three monitoring stations, located in increasing distance to the pollution source. Due to the deformation of the pollutant plume, it is possible to draw conclusions where the plume might have originated.

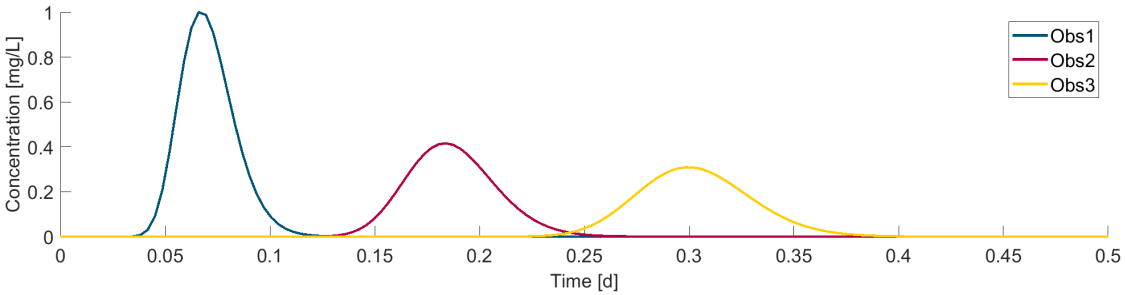

(a) River.

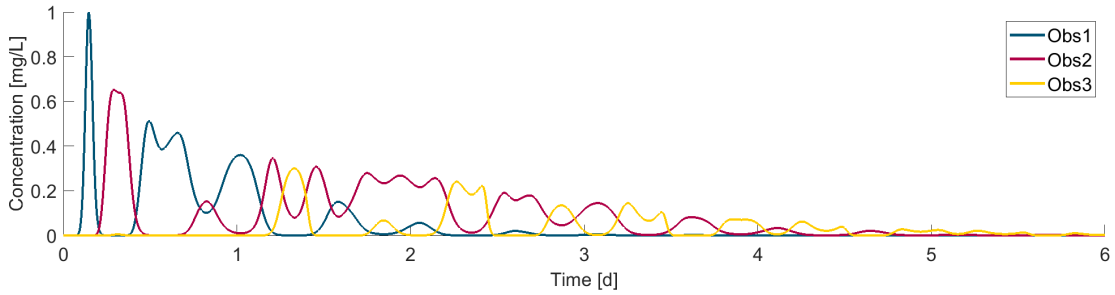

(b) Estuary.

Figure 3.4: Examples of pollutant concentration time series at three monitoring stations (a) in a river and (b) and in an estuary.

Monitoring data form the basis for the application of all presented pollution source identification approaches and can greatly influence the accuracy of inversion results. In this section, the influence of monitoring data on the accuracy of source identification results and reasons for the possible ill-posedness of the considered problem are discussed. Additionally, existing approaches for the design of an optimal monitoring network for pollution source identification are presented.

3.3.1 Influence of monitoring data on source identification

In the literature dealing with the identification of pollution sources in surface water, very different and versatile monitoring network designs have been applied. An overview of the spatial and temporal monitoring designs considered in selected studies is given in Table 3.1.

In most studies, measurement data were generated synthetically using the simulated concentration data of the considered transport model. To correspond to more realistic conditions, usually, a perturbation term was added to the data. The perturbation was either based on an additive (Parolin et al. (2015)) or multiplicative error model (Cheng and Jia (2010), Han et al. (2014) and Li et al. (2016)). Only Jiang et al. (2019) used data of a real nitrobenzene spill in the Songhua River, China to validate the applied Bayesian approach. Two other studies included in Table 3.1 used real data of a tracer experiment to validate their approaches, namely Ghane et al. (2016) and Yang et al. (2016).

Table 3.1: Overview of different spatial and temporal monitoring designs applied for the identification of pollution source parameters in selected studies. The table is not assumed to be comprehensive.

Literature	**Transport model**	**Source characteristics**	**Application area**	**Spatial monitoring design**	**Temporal monitoring design**
Ghane et al. (2016)	1D analytical solution of the ADRE	single, instantaneous point source (x_s= 0 m, t_s=7:07)	River Severn, Wales, real tracer data	individual data of 7 monitoring stations (7.2 to 13 km)	no information
Yang et al. (2016)	1D analytical solution of the ADRE	multiple instantaneous point sources (x_s=35, 79 m, t_s=0 s)	experimental channel, real tracer data	longitudinal measurements every 10 m from 0 to 100 m, 10 measurements	t=90 s, 1 measurement
Zhang and Xin (2017)	1D analytical solution of the ADRE	multiple continuous point sources, (x_s=300, 500 m, t_s=0 s)	river stretch, synthetic data	longitudinal measurements every 100 m from 0 to 1000 m, 10 measurements	t=4000 s, 1 measurement
Wang et al. (2018)	1D analytical solution of the ADRE	multiple instantaneous point sources (x_s= 1, 2.5, 4 km, t_s=8:00, 8:30, 9:30 h)	river stretch, synthetic data	1 to 3 monitoring stations (5, 6, 7 km)	Period: no information, Frequency: 15 min
Jiang et al. (2019)	1D analytical solution of the ADRE	single, instantaneous point source (x_s=0 km, t_s=13.11.05 14:00)	Songhua River, China, real spill data	4 monitoring stations (155, 276, 281 and 336 km)	Period: 18.11.05 18:00 to 19.11.05 19:00, 25 h; Frequency: 2 to 6 h
Han et al. (2014)	2D analytical solution of the ADRE	single, instantaneous point source (x_s=500 m, y_s=50 m, t_s = 0 s)	river stretch, synthetic data	3 monitoring stations: M1(2000,40), M2(2000,80), M3(2000,120)	Period: 1200 to 3700 s, Frequency: 500 s, 6 measurements
Guozhen et al. (2016)	2D analytical solution of the ADRE	single, instantaneous point source (x_s=5 km, t_s=120 min, no information on y_s)	river stretch, synthetic data	1 monitoring station, no information on position (presumably 20 km)	no information (presumably Period: 4 h, Frequency: 5 min)
Jing et al. (2018)	2D numerical transport model	single, instantaneous point source	Quanzhou Bay, China, synthetic data	2 monitoring stations	no information
Parolin et al. (2015)	2D numerical transport model	single continuous point source	Macae river estuary, Brazil, synthetic data	5 monitoring stations	Period: 0 to 24 h, Frequency: 60 min, 24 measurements

3.3.1.1 Spatial design

In most studies it is assumed that concentration data were collected at predetermined monitoring stations. The number of monitoring stations as well as their distance to the source location, greatly differed between the considered studies. For example, Guozhen et al. (2016) only used one monitoring station 15 km downstream of the source location. In contrast, in Jiang et al. (2019) four monitoring stations were considered, which were located 155 to 336 km downstream of the release point. Both studies considered the problem of identifying an instantaneous pollutant release from a single point source.

Several studies indicated that the number and position of monitoring stations can greatly influence the accuracy of pollution source identification. Ghane et al. (2016) used real data from a tracer experiment of the River Severn, England, where measurements were taken at 7 monitoring stations located 7200 m to 13 000 m downstream of the injection point. A comparison of the identification results, where each monitoring station was taken separately, implied that the errors in source parameters increases when more distant monitoring stations were used. This was confirmed by Wang et al. (2018), who analysed the influence of different spatial monitoring designs on the identification of multiple point sources, and Mazaheri et al. (2015), who focused on the recovery of the release history of multiple point sources. Regarding the number of considered monitoring stations, according to Jiang et al. (2018) and Wang et al. (2018), data from multiple stations lead to more accurate inversion results.

Table 3.1 implies that often one-dimensional transport models are considered for PSI in rivers. Consequently, the influence of the mixing zone and the position of monitoring stations in the lateral direction on inversion results have hardly been investigated up to now. Only Han et al. (2014) analysed the influence of the number of monitoring stations in the lateral direction on the identification of an instantaneous point source. In their work, the authors considered three monitoring stations inside one cross-section. The monitoring stations were located inside the mixing zone, 1.5 km downstream of the pollutant source. For the analysis, monitoring data were assumed to be without any errors. Errors resulted especially in the identification of the total pollutant mass when only a single monitoring station in the middle of the cross-section was considered. With two to three stations inside the cross-section, all source parameters could be determined almost without any errors. However, a comprehensive analysis of the influence of the position of monitoring stations with regard to the mixing zone is missing in the literature up to now.

In the case of an emergency, pollutant concentrations can not only be measured at a predetermined monitoring station over a given time period, but also at various locations in the longitudinal direction within a very short period of time. For the identification of multiple continuous pollution sources, Zhang and Xin (2017) used pollutant concentrations measured at 10 locations along the river which were placed 100 m apart from each other. Measurements were taken 4000 s after the source release. The two sources to be identified, were located inside the considered longitudinal measurement profile. A similar approach was adopted by Yang et al. (2016) for the identification of multiple instantaneous sources. Concentration measurements were taken 90 seconds after the pollutant release at 11 measuring points 10 m apart from each other. The smaller temporal and spatial scale in comparison to Zhang and Xin (2017) is due to the the application to a channel irrigation test field which was only 100 m in length. Up to now, an analysis of the influence of the point of time when the longitudinal measurements were taken and a comparison to the measurement at a predetermined monitoring station is lacking in the literature.

3.3.1.2 Temporal design

The temporal monitoring design includes the start time of the monitoring, the monitoring frequency and the monitoring duration. In the literature, the influence of the temporal design on source identification results in surface waters has not been extensively evaluated. Only Han et al. (2014) briefly analysed the influence of the monitoring frequency on inversion results. The authors considered three monitoring stations located in the lateral direction of a single cross-section. Monitoring frequencies of 400 s to 2400 s were used, resulting in 6 to 2 measurements at each monitoring station, respectively. As expected, the lower the monitoring frequency, the greater the errors in the identified pollution source parameters. When less than 4 measurements were collected at each monitoring station, very large deviations could be observed between the estimated and real source parameters, leading to a failure of the identification process. How the start time of the monitoring or the monitoring duration affects the inversion results has not been evaluated in the literature up to now.

3.3.2 Ill-posedness of the source identification problem

Inverse problems like pollution source identification are often considered ill-posed (Boano et al. 2005; Wang and Liu 2012). According to Chapter 2.2.5, a well-posed problem satisfies three conditions: (1) a solution exists, (2) the solution is unique, and (3) the solution depends continuously on the input data. If a problem violates any of these conditions, it is termed ill-posed. Solution uniqueness is inherently related to parameter identifiability. Parameters are termed non-identifiable when different parameter sets lead to the same model response (Šimůnek and Hopmans 2002). Identifiability issues in PSI have already been encountered and reported by various authors.

Wang et al. (2018) used the backward probability method to identify the parameters of multiple instantaneous point sources based on a single monitoring station. The authors showed that the accuracy of source identification deteriorates when the number of point sources increases. In this case, different parameter combinations lead to a very close objective function value, impairing the accurate identification of pollution source parameters. Increasing the number of monitoring stations could improve the identification results. Mazaheri et al. (2015) used the mathematical approach to recover the release history of multiple point sources. Similar to Wang et al. (2018), if only one monitoring station but multiple point sources were considered, the mathematical approach failed to provide accurate results for the release histories. The authors stated that for an appropriate recovery of the release history of multiple pollutant sources, one measurement station downstream of each source is necessary. A mathematical proof can be found in El Badia et al. (2005). Ghane et al. (2016) applied the backward probability method to identify the parameters of an instantaneous pollution release in a river network. The analysis was based on a single monitoring station at the outlet of the river network. In the case that the river network contained multiple branches, the method was only able to state several potential source locations inside different branches, as these created similar concentration profiles at the monitoring point. Multiple monitoring stations in different branches of the river network can effectively reduce the number of potential source locations.

These examples already imply that the monitoring design greatly influences parameter identifiability and solution uniqueness of the inverse problem. This is not only the case when multiple point sources or complex river networks are considered, but also for a single instantaneous point source in a simple river stretch, as described in Han et al. (2014). Here,

the analysis showed that depending on the chosen spatial and temporal monitoring design, high errors did exist between actual and estimated source parameters, although perfect monitoring data were considered. In this case, the global optimization algorithm did not converge to the true global minimum, a sign that parameters are only poorly identifiable.

In the cases mentioned, it is irrelevant which approach is used for PSI as identifiability is a property of the problem itself and does not depend on the method used to identify the parameters (Olivier and Smyth 2017).

In summary, the spatial and temporal monitoring design will highly influence the accurate identification of pollution source parameters. A well-designed monitoring network can reduce the risks of obtaining an ill-posed problem. Considerations and possible approaches for the design are discussed in the following section.

3.3.3 Approaches for an optimal monitoring design

Although most authors are in agreement that monitoring data have a major influence on the accurate identification of pollution source parameters, up to now, studies in surface waters were mainly based on an arbitrarily chosen monitoring design. Only two studies, namely Telci and Aral (2011) and Lee et al. (2018), considered synthetic data collected from a real-time monitoring network, which was assumed to be implemented prior to the release of the pollutant. In contrast, for groundwater systems, the use of a well-designed monitoring network to improve the efficiency in source identification has already been emphasized by several authors (Datta et al. 2009; Amirabdollahian and Datta 2013). In recent years, several approaches for the optimal design of a monitoring network have been proposed (Datta et al. (2009), Chadalavada et al. (2012) and Jin et al. (2014)). Similarly, in water distribution systems the dependence of the source identification problem on the monitoring design has been addressed in several studies (Tryby et al. 2010; Liu and Auckenthaler 2014). However, approaches for the monitoring network design will greatly differ between groundwater, surface water and water distribution systems due to the different temporal and spatial dynamics.

3.3.3.1 Emergency response vs. real-time monitoring

For the design of a monitoring network in all considered systems, two cases have to be distinguished. Monitoring data can either be collected by a real-time monitoring network already installed before the spill occurs or as part of the emergency response after the pollutant plume has been detected.

In most surface waters, monitoring is usually only started when information on a potential spill is available. This information might be derived directly from the responsible discharger, via public reports or randomly from collected monitoring data (Grayman and Males 2002). An example is the monitoring in response to the nitrobenzene spill in the Songhua River, China, which served as the basis for the identification of source parameters in Jiang et al. (2019). When a pollution incident has been detected in a river or estuary, there is usually too little time to carry out a detailed analysis on the optimal design of the monitoring network. Therefore, the design will be usually based mainly on subjective criteria and economic resources. This is a fundamental difference to groundwater systems, where several approaches for an adequate design of a monitoring network after the detection of a pollutant plume, have been presented in the literature (Datta et al. 2009; Chadalavada et

al. 2012; Jha and Datta 2014)). This is due to the much slower transport processes in comparison to rivers or estuaries. Usually, pollutants can be tracked over several years, which results in a considerably longer response time to implement a well-designed monitoring network.

In the last several years, there have been considerable advances in real-time water quality monitoring (Storey et al. 2011; Park et al. 2020). A real-time monitoring network consists of permanently installed monitoring devices which continuously measure certain water quality variables. If abnormalities are observed in the measured data, or a predefined threshold value is exceeded, the system can set off an alarm. Real-time water quality monitoring is frequently employed in water distribution systems, where the early detection of potential contaminants is of major importance (Storey et al. 2011). Nevertheless, for surface water bodies, which serve as a source of drinking water or are located in the vicinity of industrial agglomerations, the installation of a real-time monitoring network might be equally appropriate to rapidly detect and identify a possible pollutant spill. For example, real-time monitoring networks have been installed along the Rhine River or the Ohio River (Grayman et al. 2000; Diehl et al. 2006). Data from these networks can either be used directly for PSI, or additional sampling can be carried out in the case of an alarm. For the optimal design of a real-time monitoring network used for PSI, two approaches could be identified in the literature. These rely on different design criteria and will be presented in the following sections.

3.3.3.2 Detection time and detection probability

For pollution source identification in surface water systems, up to now, only two studies, namely Telci and Aral (2011) and Lee et al. (2018), considered theoretical data collected from an optimal real-time monitoring network, which was assumed to be implemented beforehand. The design of the monitoring networks was based on the mean detection time and the detection reliability of the systems, and is presented in Telci et al. (2009) and Park et al. (2014), respectively. A monitoring network based on these criteria is often part of an early-warning system (EWS). Typically, EWS are implemented to rapidly detect a deterioration in water quality resulting from accidental or intentional discharges of toxic and hazardous materials (Gullick et al. 2003). The faster a spill can be detected, the more time exists to put mitigation measures into place or announce public warnings (Grayman and Males 2002; Aral and Nam 2016). EWS are mainly implemented in systems which provide drinking water. These can include groundwater systems (Bode et al. 2016), water distribution networks (Rathi and Gupta 2015) or surface water systems (Gullick et al. 2003). However, even if not originally intended in the design process, monitoring data collected from an EWS might also be used to identify a pollution source in the case of a spill incident.

According to Telci et al. (2009), the approach for the design of the monitoring network is usually based on two steps. The first step is concerned with the selection, preparation and simulation of potential pollution scenarios. This step usually requires a sufficiently calibrated model for the simulation of flow and transport processes in the considered system (Bode et al. 2016). In the second step, optimal monitoring locations are determined by using numerical optimization algorithms. The main objective is usually the minimization of the mean detection time of the previously selected scenarios. Additionally, the maximization of reliability of the system can be taken into consideration, resulting in a multi-objective optimization problem.

The selection of pollution scenarios is a crucial step in the design of the monitoring network. Each system is highly variable and uncertainties in hydrodynamics as well as spill characteristics have to be taken into account (Bode et al. 2016; Aral and Nam 2016). Regarding the spill characteristics, most designs focus on an accidental or intentional instantaneous pollution release from a point source. In addition to potential source locations, different spill times have to be selected if it is assumed that the underlying hydrodynamics are unsteady. Hydrodynamics are highly dependent on external forces (e.g. rainfall, freshwater inflow, tidal dynamics). Spatial and temporal variations in these factors have to be properly represented in the considered pollution scenarios. As mentioned before, for the simulation of selected pollution scenarios, a well-calibrated flow and transport model is necessary. The processes of advection and dispersion will affect the detection times at potential monitoring stations and therefore, have to be accurately resolved (Zhu et al. 2018).

Scenarios can either be selected manually or based on the results of a Monte Carlo analysis (Grayman and Males 2002; Bode et al. 2018). After a given given number of spill scenarios are selected, each scenario is computed and simulated pollutant concentrations are recorded and stored for N potential monitoring locations. The location of potential monitoring stations has to be considered beforehand. The results form the basis for the second step, the actual optimization of the monitoring network. Using numerical optimization routines, out of N potential monitoring locations, M monitoring locations are selected which optimize the given objective function. The number M is usually considered beforehand and will mostly depend on budgetary constraints. However, it is also possible to include the number in the design process (Aral and Nam 2016).

As mentioned before, the main objective is usually the minimization of the mean detection time of the considered scenarios. In general, the detection time $t_{d,s}(x_i)$ for a single scenario s, given the monitoring station x_i, is the time elapsed between the release of the pollutant and the first detection at the respective monitoring station (Aral and Nam 2016). The pollutant is considered detected if the measured pollutant concentration $c_{obs,i}$ exceeds a given concentration threshold value c_{th}. Likewise, for a monitoring network $X = \{x_1, \cdots, x_i, \cdots, x_M\}$, consisting of several stations, the detection time $t_{d,s}(X)$ is the minimum time elapsed between the release and the first detection at one of the monitoring stations (Telci et al. 2009):

$$t_{d,s}(X) = \min\{t_{d,s}(x_1), \cdots, t_{d,s}(x_i), \cdots, t_{d,s}(x_M)\} \tag{3.8}$$

For the design of an optimal monitoring network several pollution scenarios have to be considered. Based on the definitions above, the mean detection time of the monitoring network X for all scenarios can be calculated by (Telci et al. 2009; Aral and Nam 2016):

$$\bar{t}_d(X) = \frac{1}{W} \sum_{s=1}^{S} w_s \; t_{d,s}(X) \tag{3.9}$$

where

S	number of all considered scenarios
w_s	weight assigned to the sth scenario
W	sum of weights of all scenarios $W = \sum_{s=1}^{S} w_s$
X	monitoring network $X = \{x_1, \cdots, x_i, \cdots, x_M\}$
$t_{d,s}(X)$	detection time of the monitoring network X for the sth scenario

As can be seen from Equation 3.9, different weights w_s can be assigned to the considered scenarios. These can on the one hand include the probability of occurrence of a spill at the considered source locations (Park et al. 2014; Aral and Nam 2016). On the other hand, the weights can be used to describe the hazard associated with each source and reflect factors like the stored contaminant mass, mobility and toxicity (Bode et al. 2018). Different weighting schemes will usually lead to different monitoring designs (Aral and Nam 2016).

A successful monitoring network must not only detect a contaminant spill as early as possible, but also provide maximum reliability regarding the detection of various spill incidents (Aral and Nam 2016). Therefore, often, additionally the reliability of the system is taken into account during optimization. The reliability of a monitoring design $R(X)$ is defined as the ratio of detected contamination scenarios to the total scenarios considered in the analysis and can be computed by (Telci et al. 2009; Aral and Nam 2016):

$$R(X) = \frac{1}{W} \sum_{s=1}^{S} w_s \delta_s(X) \tag{3.10}$$

where $\delta_s(x)$ is an indicator variable which takes either the value 0 for non-detected scenarios or 1 for detected scenarios (Telci et al. 2009).

The consideration of the mean detection time as well as the detection probability will result in a multi-objective optimization problem. It should be noted that the mean detection time and detection probability are competing objectives. Monitoring devices located further downstream will increase the reliability but tend to increase the expected detection time (Park et al. 2014). Consequently, the multi-objective optimization of both criteria will result in a pareto front (Telci et al. 2009). For the optimization of the monitoring network different optimization algorithms have been proposed. Telci et al. (2009) and Aral and Nam (2016) used a genetic algorithm, while Zhu et al. (2018) applied the Multi-Objective Particle Swarm Optimization (MOPSO) algorithm. In contrast, Park et al. (2014) formulated the problem as a stochastic discrete optimization via simulation (OvS) problem.

Overall, the mean detection time and the detection reliability will primarily depend on the number of monitoring stations to be installed. The higher the number of monitoring stations, the lower the mean detection time and the higher the probability of detecting all spill scenarios. In practice, it has to be considered that the estimated detection time and detection probability should not be regarded as absolute measures of the monitoring network. Both criteria depend not only on the distribution of considered source locations but also on the mass of the spill, the detection threshold, and the detection time limit (Aral and Nam 2016).

3.3.3.3 Data information content

The second approach for the design of an optimal monitoring network is directly related to the problem of PSI. The aim of the optimal monitoring network is to improve the source identification performance in the case a spill incident occurs (Jin et al. 2014). The performance of the monitoring design can be evaluated by the uncertainty in the

estimated source parameters. Monitoring data which minimize parameter uncertainty are preferred.

Problems of this kind are usually attributed to the field of optimal experimental design (OED). OED is concerned with increasing the information content in the collected data of an experiment in such a way that unknown model parameters can be estimated with the best possible statistical quality. This is usually a measure of the accuracy and/or de-correlation of the estimated parameters (Banga and Balsa-Canto 2008). Approaches for OED are usually based on the Fisher Information Matrix (FIM), which quantifies the information content included in the observations of a monitoring design for the estimation of unknown model parameters (Sun and Sun 2015). The FIM is the inverse of the approximate parameter covariance matrix defined in Equation 2.12, which is frequently used to obtain parameter confidence intervals (Li et al. 2018). Maximizing the information content in the data is therefore equivalent to minimizing the uncertainty in the unknown model parameters (Sun and Yeh 1990). The information content of different monitoring designs can be compared by so-called optimality criteria. Optimality criteria are scalar functions based on the trace (A-optimality), the determinant (D-optimality) or the eigenvalues (E-optimality) of the FIM (Marsili-Libelli and Giusti 2008). A more detailed description of the calculation of the FIM and of different optimality criteria is given in Chapter 6.2.1.

In surface waters, the approach based on the FIM has for example been used to analyse the influence of the number and location of monitoring stations on parameter identifiability of a water quality model (Freni and Mannina 2012). Similarly, the approach can be used to design an optimal monitoring network for PSI. So far, no applications could be found in the literature regarding PSI in surface waters. However, in the following, two studies are presented which applied the approach to design an optimal monitoring network for a groundwater system (Jin et al. 2014) and a water distribution network (Tryby et al. 2010). Both approaches can easily be transferred to surface water systems.

Similar to the design of an early-warning monitoring network described in Section 3.3.3.2, the general approach for the design of the monitoring network is based on two steps. The first step is concerned with the selection, preparation and simulation of potential pollution scenarios. In the second step, numerical optimization routines are applied to determine optimal monitoring locations which minimize the overall uncertainty in the considered pollution scenarios.

Jin et al. (2014) proposed an approach for the optimal placement of monitoring wells in a groundwater system. The aim of the proposed monitoring network was the accurate identification of potential contaminant scenarios. While most works regarding the design of an optimal monitoring network for PSI in groundwater systems are based on a spill that has already occurred, the work of Jin et al. (2014) is based on several potential spills which could occur in a larger region in the future. In a first step, a large number of random pollution scenarios were generated and computed with the PGREM3D transport model. The authors included uncertainties in source characteristics (location and intensity), as well as in the hydraulic conductivity field in their investigation. Simulated concentration data at potential monitoring stations were stored for each scenario, as these were needed in the second step of the approach. The second step was concerned with the optimization of the monitoring network. The objective function used in the optimization process was a weighted product of two individual objectives. These included the determinant of the FIM, equivalent to the D-optimality criterion, as well as the distance between selected

monitoring wells:

$$O_i(X) = (det(FIM(X)_i))^a \cdot (D(X)_i)^b \tag{3.11}$$

where $O_i(X)$ objective function value for the ith scenario considering the monitoring network X

$det(F(X)_i)$ determinant of the FIM for the ith scenario considering the monitoring network X

$D(X)_i$ distance metric for the ith scenario considering the monitoring network X

a, b weight assigned to each objective

During the optimization process, $O_i(X)$ was calculated for each scenario iteratively for a given monitoring design X. As the optimization focuses on several pollution scenarios, the individual values $O_i(X)$ corresponding to each scenario were integrated into one objective function value $O_{opt}(X)$. The value $O_{opt}(X)$ represents the 25%-quantile of the sorted values of $O_i(X)$, which is maximized in the optimization process.

The source identification performance of the resulting monitoring network was subsequently compared to a monitoring network consisting of uniformly placed wells. For the evaluation of the performance of both designs, 30 random spill incidents were considered. Overall, in comparison to uniformly placed wells the optimal design could improve the accuracy in source identification. This was especially relevant when only a small amount of monitoring wells could be installed.

Tryby et al. (2010) developed an approach for the design of a monitoring network for source identification in water distribution systems (WDS). According to the authors, the approach involves the selection of monitoring locations that are best suited to generate a well-conditioned source identification problem. As a transport model, an input/output water quality model was used, which represents the WDS in discrete form as a system of linear algebraic equations. In compact matrix notation the model can be expressed by:

$$Am = c \tag{3.12}$$

where A matrix of response coefficients ($n_s T \times nT$)

m vector of contaminant mass injections ($1 \times nT$)

c vector of contaminant concentrations ($n_s T \times 1$)

n_s number of monitoring sensors

n number of potential contamination sources

T number of injection periods

The design of the monitoring network was based on the analysis of the eigenvalue spectrum of the matrix $A^T A$, which is equivalent to the FIM. The eigenvalues of $A^T A$ provide information on the conditioning of the underlying inverse problem (Tryby et al. 2010). Very small eigenvalues close to zero result when the matrix $A^T A$ is almost singular. In this case, the inverse solution may become unstable, and the accuracy of one or more estimated parameter values will be questionable (Tryby et al. 2010; Schenk et al. 2018).

Consequently, it is desirable to maximize the eigenvalues of $A^T A$. The objective function maximized in Tryby et al. (2010) is given by:

$$O_{opt}(X) = \frac{1}{nT\lambda_{max}(X)} \sum_{i=1}^{nT} \lambda_i(X) \tag{3.13}$$

where $\lambda_{max}(X)$ largest eigenvalue of $A^T A$
$\lambda_i(X)$ eigenvalue of the ith column of $A^T A$

The performance of the developed monitoring network was compared to two other monitoring designs, including an ad hoc network and one whose design was based on nodal demands. Each monitoring network was designed including a total number of 3, 6, and 12 sensors. To evaluate the source identification performance of each monitoring design, an ensemble of 200 random contamination events was generated. Overall, only minor differences could be observed between the different monitoring designs. The results of the analysis imply that the number of monitoring sensors installed in the network was more important than the network used to locate the source (Tryby et al. 2010). This is because the number of sensors heavily influences the detection probability, which is a necessary criterion for source identification.

4 Conclusions from the literature review

Chapter 3 provided an overview of the state of the art regarding pollution source identification (PSI) in surface waters and emphasized the importance of the monitoring design. The further discussion will be based on three main elements of the source identification problem. These include (i) the pollutant transport model, (ii) the identification approach and (iii) the monitoring design.

4.1 Selection of an appropriate transport model

The pollution source identification approaches presented in Chapter 3.2 rely on a pollutant transport model, which simulates the transport and mixing of a pollutant inside the water body. Frequently, an analytical solution of the advection-dispersion-reaction equation (ADRE) is employed in the literature. In comparison to a numerical transport model, the analytical solution is computationally fast and numerical errors and instabilities due to the spatial and temporal discretization do not occur.

Several studies applied an analytical solution of the one-dimensional (1D) ADRE (Ghane et al. 2016; Jiang et al. 2018; Wang et al. 2018). When using a 1D transport model, it has to be considered that immediate mixing in the lateral and vertical direction is assumed. Thus, in practice, this equation can only be applied to very narrow and shallow rivers, or when observation points are located further away from a potential release location and mixing in the lateral and vertical directions has already taken place.

Because the lateral mixing zone can have a considerable length, for larger rivers the use of a two-dimensional (2D) transport model is recommended (Jiang et al. 2018). One problem of the analytical solution of the 2D ADRE usually applied in the literature is that it typically considers an infinite domain in the longitudinal and lateral flow direction (e.g. Han et al. (2014) and Guozhen et al. (2016)). However, in reality, lateral boundaries in the form of river banks exist and further movement of the constituent across the banks can not take place. Using the analytical solution of the 2D ADRE without lateral boundaries would therefore underestimate the real concentrations inside the river. To introduce a no-flux boundary condition at the lateral boundaries, the mirror-image technique can be used (Fischer et al. 1979; Chin 2013). It ensures that the constituent beyond the river bank is reflected back by introducing additional sources also called image sources, which balance the mass loss inside the river section. Up to now, this technique has not been used when a 2D analytical solution of the ADRE was applied as a transport model in PSI.

Although the analytical solution of the ADRE is computationally fast, its application is based on several assumptions which limits its use in more complex study areas (Chadalavada et al. 2012; Jiang et al. 2019). In general, the analytical solution is based on a straight and homogeneous river section with no tortuosity, steady-state in hydrodynamics and consequently spatial and temporal constant model coefficients for the flow velocity, dispersion coefficients and decay rate.

If unsteady flow or more complex river geometries are investigated, more sophisticated numerical hydrodynamic and water quality models are required to adequately represent the pollutant transport processes (Jiang et al. 2019). This is especially relevant for estuaries, where the changing flow direction due to the tidal influence plays an important role in pollutant transport and mixing. Consequently, unsteady flow conditions and varying flow directions have to be considered and a numerical transport model has to be applied. Up to now, the identification of a pollutant release under bidirectional flow conditions has only been investigated by Parolin et al. (2015) and Jing et al. (2018). Both studies used a numerical transport model to adequately represent the underlying transport and mixing processes.

4.2 Comparison of pollution source identification approaches

In Chapter 3.2, different approaches for the identification of pollution source parameters in surface water systems haven been presented. Table 4.1 summarizes the main strengths and weaknesses of the presented approaches.

Table 4.1: Comparison of the strengths and weaknesses of different approaches for pollution source identification.

Approach	**Strengths**	**Weaknesses**
Simulation-optimization approach	- easy implementation - linkage to various transport simulation models possible	- high computational effort - convergence to a global minimum not guaranteed
Bayesian inference	- consideration of parameter uncertainties - linkage to various transport simulation models possible	- very high computational effort - posterior probability function has to be proper
Backward probability method	- small computational effort - consideration of parameter uncertainties	- numerical implementation non-trivial
Mathematical approach	- small computational effort	- complex mathematics require advanced knowledge
Classification approach	- small computational effort in case of pollution accident - linkage to various transport simulation models possible	- very high computational effort for training phase - uncertainties in boundary conditions can not be eliminated completely

In general, all presented approaches have individual strengths and weaknesses that determine the scope in which they can be applied for PSI. Methods like the simulation-optimization approach or Bayesian inference are considered very time consuming because

of their high computational demand. For the simulation-optimization approach a considerable number of function evaluations have to be carried out before an optimization algorithm meets convergence. For the Bayesian approach an even higher number of simulations are necessary for a proper representation of the posterior parameter probability distribution. To reduce the computational effort, a surrogate model might be used instead of a more time consuming numerical simulation model. Nevertheless, the named approaches have the advantage that the linkage to different numerical transport models is generally easy. A direct access to the source code is not required, but only to the input files of the pollutant transport model. This is different to the backward probability method or the mathematical approach, whose implementation is non-trivial.

In summary, the choice of an appropriate PSI approach mainly depends on the selected transport model, the mathematical knowledge and programming experience of the user and the available time for the implementation and computation of the chosen approach. It has to be noted that for all approaches a calibrated transport model is necessary to simulate the pollutant concentration distribution in the considered system (Amirabdollahian and Datta 2013). This has to be set up and calibrated beforehand.

4.3 Design of an optimal monitoring network

The literature review has shown that the design of the monitoring network is an important aspect in the successful identification of pollution source parameters. Often, the PSI problem is considered to be ill-posed due to solution non-uniqueness and instability issues (Tryby et al. 2010). However, a well-designed monitoring network can reduce the risks of obtaining an ill-posed problem.

In the literature, different spatial and temporal monitoring designs have been adopted for PSI in surface waters. However, up to now, the influence of the monitoring design on source identification results has rarely been evaluated. In existing studies, monitoring data were usually selected arbitrarily. Most authors mainly focused on the evaluation of the developed PSI approach and not on the monitoring design. Only a few authors performed some minor test to evaluate the influence of the monitoring design on the inversion results. However, how the considered monitoring data correspond to practical implementations in the context of emergency monitoring has usually not been discussed.

Up to now, a comprehensive analysis on the influence of the spatial and temporal monitoring design on source parameter identification is missing for unidirectional as well as for bidirectional flow systems. The following questions will be of particular importance regarding the design of the monitoring network:

- Influence of the number and location of monitoring stations: How does the position of monitoring stations in relation to the source location affect the inversion results? Can multiple stations improve the accuracy in inversion results?
- Influence of the location of monitoring stations in regard to the mixing zone: Does the mixing zone affect parameter estimation? Where should stations ideally be located?
- Influence of the monitoring frequency and monitoring period: At what times should monitoring data be collected? How do the start time and the duration of the monitoring affect the inversion results?

- Comparison of different monitoring approaches: Does a concentration time series recorded at a single monitoring station provide the same amount of accuracy as a longitudinal concentration profile?

Based on the results, practical guidelines for the design of a monitoring network in the case of a pollution incident can be developed. Especially in highly industrialized areas, a robust monitoring plan should be developed in advance (Jiang et al. 2019)

For the design of a real-time monitoring network, different design criteria have been proposed in the literature. Up to now, only Telci and Aral (2011) and Lee et al. (2018) used results of an optimal real-time monitoring network for PSI in a river network. The design of the monitoring network was based on the minimization of the mean detection time and the maximization of the reliability of the system. Additionally, for groundwater and water distribution systems, optimal monitoring networks have been developed which aim at the minimization of uncertainties in source parameter identification in the case of a pollution incident (e.g. Tryby et al. (2010) and Jin et al. (2014)). In contrast to the minimization of the detection time, the approach is directly related to the problem of source identification. However, both criteria might lead to a very similar monitoring design. An evaluation of the relationship between the early detection and the minimization of uncertainties in PSI is missing in the current literature.

In estuaries, the optimal monitoring design regarding PSI has not received any attention. While in rivers a detected pollutant plume can only originate from an upstream location, in estuaries due to the change in flow direction it is also possible that the detected pollutant was introduced in the downstream parts and then transported upstream during flood tide. Consequently, in contrast to rivers, the release time in the tidal cycle will be of major importance for the optimal design.

4.4 Conclusions and further work flow

Up to now, general guidelines regarding the influence of monitoring data on pollution source identification are missing even for relatively simple river systems. Consequently, this work initially analyses the impact of the spatial and temporal design on PSI results for a synthetic unidirectional case. To simulate the transport and mixing processes in the considered river section, an analytical solution of the 2D ADRE is applied. In contrast to other works, the mirror-image technique is used to capture no-flux conditions at the lateral boundaries. Due to the application of a 2D transport model, the influence of the mixing zone can be taken into account in the analysis. Based on the results of the analysis, general recommendations regarding the design of a monitoring network in the case a pollution incident occurs, are developed. The analysis is further extended to bidirectional flow systems (e.g. estuaries). Due to the consideration of unsteady hydrodynamics, a numerical synthetic test case is set up with the Delft3D software suite. Results are used to derive general guidelines and criteria for an optimal monitoring network design in the context of PSI.

The literature review has further revealed that PSI approaches have only rarely been applied to bidirectional flow systems like estuaries. Because this work uses the commercial software suite Delft3D to simulate unsteady transport conditions, the simulation-optimization approach is selected for the identification of source parameters. As explained in Section 4.2, the approach is well suited to be coupled to an external transport model.

In the literature, two variants of the simulation-optimization approach have been proposed. The approach usually applied in the literature, corresponds to the simultaneous identification of all unknown source parameters. In contrast, Jing et al. (2018) presented a modified approach, in which the estimation of the source parameters is decoupled from one another. Both approaches are applied to the synthetic bidirectional test case to compare their performance.

In a final step, the identification approach is transferred to a real-world estuary, the Thi Vai Estuary, located in South Vietnam. Based on the results regarding the spatial and temporal monitoring design, a real-time monitoring network is designed for the Thi Vai Estuary. Synthetically generated monitoring data of the optimized monitoring network are used for the identification of several theoretical spill incidents. The schematic diagram in Figure 4.1 visualizes the link between the initial pollutant release, the pollutant detection by the installed monitoring design and the source identification by the simulation-optimization approach.

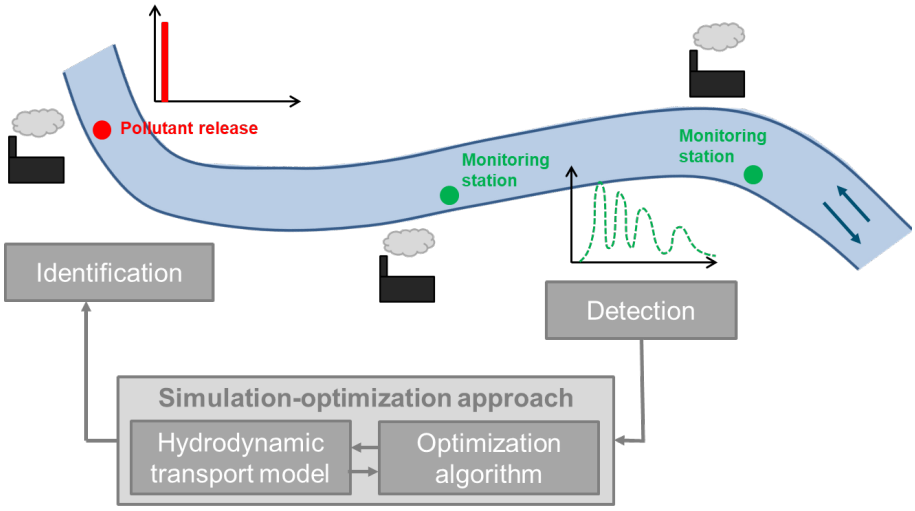

Figure 4.1: Schematic diagram of the link between the initial pollutant release, the pollutant detection by the installed monitoring design and the source identification by the simulation-optimization approach.

The literature review has revealed that PSI is regarded as a complex inverse problem which is frequently ill-posed. To simplify the source identification problem, this work is based on several assumptions regarding the source and pollutant characteristics as well as the pollutant transport model:

- Single point source: The pollutant can only stem from a single point source in the considered flow system.
- Instantaneous pollutant release: The whole pollutant mass is introduced into the water immediately. In the transport model this is represented by a Dirac impulse.
- Conservative substance: The pollutant is not assumed to be subject to any decay or transformation processes.

- Accurate transport model: The transport and mixing processes are assumed to be accurately represented by the transport model. Uncertainties in model parameters are not considered.

Chapter 9 includes a detailed discussion of the given assumptions and possible extensions in future works.

5 Setup and calibration of a hydrodynamic transport model for the Thi Vai Estuary

The Thi Vai Estuary is located in South Vietnam, one of the core regions of industrial development in the country. The overall aim of this thesis is the application of a pollution source identification (PSI) approach to the estuary, described in detail in Chapter 8. In the upcoming chapters, previous work including an identifiability analysis (Chapter 6) and the comparison of different PSI approaches (Chapter 7) are based on a hypothetical numerical test case, built using the software suite Delft3D. Because the test case is based on the main characteristics of the Thi Vai Estuary, the study area and the calibration of the hydrodynamic transport model for the Thi Vai Estuary are already presented here.

5.1 Study area

5.1.1 The Thi Vai Estuary

The Thi Vai Estuary and its catchment are located in the provinces Dong Nai, Ba Ria-Vung Tau and Ho Chi Minh City in South Vietnam, one of the core regions of industrial development in the country. The total catchment has a size of 625 km^2. Ho-Chi-Minh-City, the biggest city in Vietnam, lies approx. 40 km northwest of the catchment.

The Thi Vai Estuary is formed by the confluence of the Ba Ky channel and the tributary Suoi Ca. After about 32 km the estuary joins the river Go Gia. Together they drain into the Ganh Rai Bay, a shallow bay in the South China Sea (Figure 5.1). In the upper reaches, at the monitoring station Long Tho, the Thi Vai Estuary has a width of 75 m and a depth of 2 m below sea level. In the downstream direction, the estuary gets gradually wider and deeper. The middle to lower reaches of the estuary have a width of 400 to 700 m at the stations Vedan and Cai Mep, respectively. The depth increases further from approximately 10 to 20 m below sea level. The most profound areas are located at the outer side of the bends (cutbanks) in the middle to downstream parts of the estuary. Here, the elevation can reach up to 32 m below sea level as observed near the port Cai Mep.

The Thi Vai Estuary can be described as a meso-tidal estuary with a semi-diurnal tidal regime and typical tidal ranges between 2 m (neap tide) and 4 m (spring tide) at the station Cai Mep before the estuary joins the Go Gia. The intertidal flats, which are mainly located on the west side of the estuary, are covered by mangroves and flooded at every high tide. In contrast, the eastern banks are dominated by ports and industrial areas.

Five tributaries are draining into the Thi Vai Estuary. The rivers Bung Mon, Suoi Ca, Ben Ngu, Cau Vac and Muong enter the estuary from the north and the east side (Figure 5.1). The weir Ba Ky in the North prevents saltwater from entering the channel Ba Ky, which collects the discharge of the river Bung Mon before it enters the estuary. Only at ebb tide water can pass the weir.

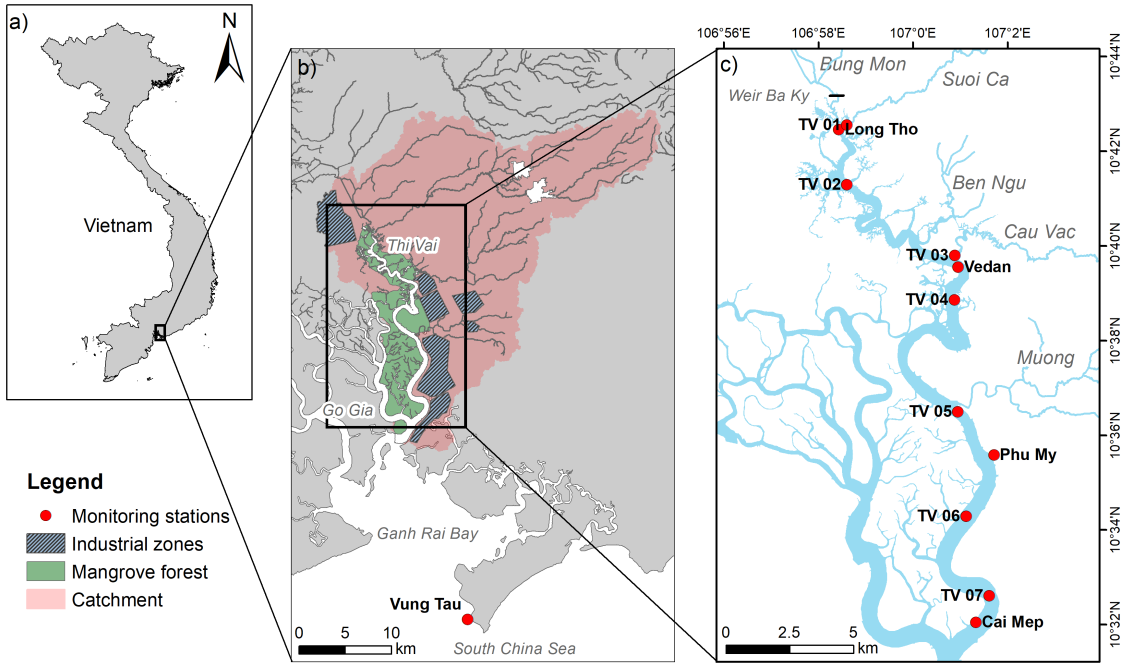

Figure 5.1: Overview of the Thi Vai and its catchment. a) Location of the Thi Vai catchment in Vietnam. b) Detailed map of the catchment with locations of mangrove forests and industrial zones along the estuary. c) Location of monitoring stations and tributaries.

5.1.2 Climate and catchment hydrology

The catchment of the Thi Vai Estuary is located in the northern tropics (Latitude: 10° 30' N to 10° 50' N). It is affected by a tropical monsoon climate with a characteristic rainy season from May to November and a dry season from December to April. Figure 5.2 shows the mean monthly precipitation for the meteorological station Bien Hoa, which is located about 25 km north-west of the Thi Vai catchment. For the analysis, the time period from 1998 to 2013 was considered. On average, the annual rainfall is 1980 mm. More than 80 % falls in the rainy season. The months from July to September represent the time with the highest monthly precipitation lying in a range from 290 to 300 mm. The months with the lowest rainfall amount ($\leq$ 15 mm) are January and February.

Precipitation has a pronounced effect on the freshwater inflow into the estuary. The main tributaries are the rivers Bung Mon, Suoi Ca, Ben Ngu, Cau Vac and Muong, which enter the estuary from the north and east side (Figure 5.1). The average discharge of the five main tributaries during the year is shown in Figure 5.2. These discharges were calculated by the hydrological model PANTA RHEI for the period from 1998 to 2013 (Lorenz 2015). A clear relationship between the mean precipitation and the mean discharge of the tributaries can be observed. The highest discharges can be found in the rainy season from July to October. From December to March precipitation is very small, leading to a very small freshwater discharge into the estuary. On average, the tributaries have a mean total flow rate of 28.2 $m^3 s^{-1}$ and 5.7 $m^3 s^{-1}$ in the rainy and dry season, respectively (Table A.1). The freshwater discharge is an important factor regarding the transport and residence time of pollutants inside the estuary. It further influences the stratification characteristics inside the estuary, which are discussed in detail in Section 5.1.4.

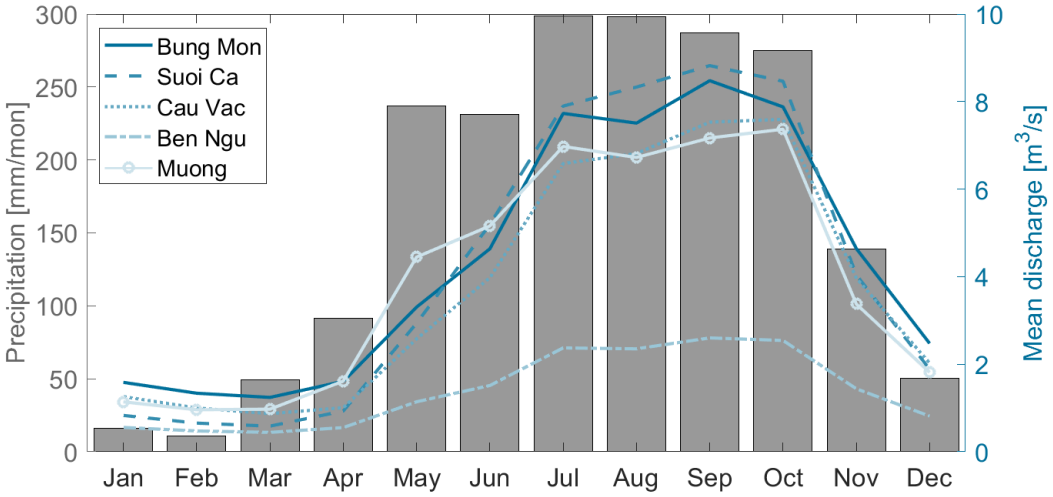

Figure 5.2: Mean monthly precipitation [mm] for the meteorological station Bien Hoa and mean discharge [$m^3\,s^{-1}$] for the main tributaries of the Thi Vai Estuary calculated by the hydrological model PANTA RHEI. The analysis considered the time period from 1998 to 2013.

Minor differences in the mentioned long-term meteorological values in comparison to Lorenz (2015) are the result of the application of a different time span, which is due to the data period of the modelled freshwater inflow which was only available form 1998 to 2013.

5.1.3 Tidal dynamics

The Thi Vai Estuary is strongly influenced by the tidal dynamics of the South China Sea. In the course of the research project EWATEC-COAST, data loggers were installed at three stations inside the estuary, namely Long Tho, Vedan and Cai Mep, to continuously measure the water level over a time period of almost two years. In addition, hourly data of the tide gauge Vung Tau were obtained, which can be freely downloaded from the website of the Research Quality Database of the University of Hawaii Sea Level Center (UHSLC) (https://uhslc.soest.hawaii.edu).

The MATLAB program UTide, written by Codiga (2011), was used to perform a harmonic analysis of tidal components, described in Chapter 2.1.1.2. For the tide gauge Vung Tau, a timespan of 5 years (2012-2016) was considered, consisting of hourly data. The constituents of the tide gauge Vung Tau were compared to literature values (Hak et al. 2016) beforehand, to ensure that the methodology was applied correctly. For the monitoring stations inside the estuary hourly data form October 2013 to March 2015 (1.5 years) were considered. The amplitudes and phases of the most important tidal constituents are presented in Figure 5.3. Exact values and the calculated tidal form factor (Equation 2.2) can be found in Table A.2 of the Appendix.

As expected, the constituents M_2, K_1, O_1 and S_2 are the most important tidal constituents in the Thi Vai Estuary. The amplitudes of most constituents, especially of semidiurnal components, increase the further the station is located away from the estuary mouth. This amplification is a result of the interaction between the up estuary tidal wave propagation and the estuarine morphology. Due to the increasing convergence of the estuary upstream,

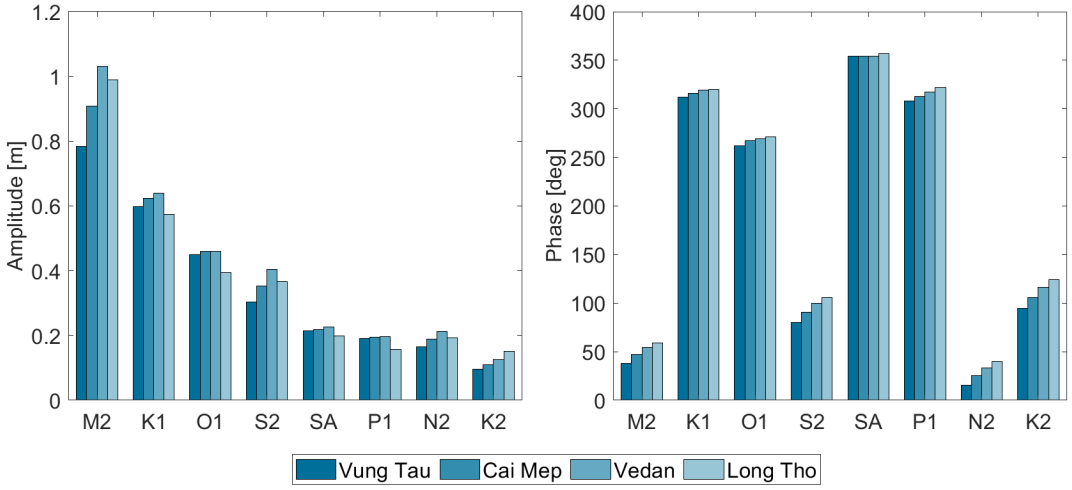

Figure 5.3: Amplitudes and phases of the most important tidal constituents in the Thi Vai Estuary.

the tidal wave is laterally compressed in the absence of friction, leading to an increase in its height (Bruner de Miranda et al. 2017, p. 38). For the station Long Tho, the amplitudes are dampened due to the enhanced effect of friction and an increased freshwater inflow. For the phases of all constituents, an increasing phase lag, especially of semidiurnal components, can be observed. Due to the travel velocity of the tidal wave, the further a station is located away from the estuary mouth, the later the peak of the tidal wave will arrive there.

The tidal form factor F (Equation 2.2) lies in the range of 0.72 to 0.96, showing a mixed tidal signal, with predominantly semidiurnal tides for all stations (Table A.3a). For systems with predominantly semidiurnal tides, the two high and low tides each day can show conspicuous inequalities in successive high and low water levels, respectively. This is in agreement with the visual inspection of the measured tidal water levels.

The harmonic constituents of the station Cai Mep are used in this work for the seaward boundary condition of a simplified numerical test case representing the Thi Vai Estuary. It should be noted that the calculated constituents might include uncertainties, due to the short considered time span, minor data gaps and measurement errors. However, an influence on the results of the following work steps is not expected.

5.1.4 Mixing processes

The mixing processes in the Thi Vai Estuary are mainly influenced by the tidal dynamics and the freshwater inflow of the tributaries. A considerable influence of wind on the mixing processes can be disregarded due to the bathymetric features of the Thi Vai Estuary. In contrast, in estuaries which either consist of large open areas or are very shallow, the effect of wind on mixing processes and stratification might not be ignored.

In Figure 5.4, the longitudinal salinity variation along the Thi Vai Estuary for the dry and rainy season is compared. The data were provided by the DONRE Dong Nai, which carries out monthly water quality measurements at the depicted monitoring stations. As expected, in both seasons, an increase in salinity in the longitudinal direction from the

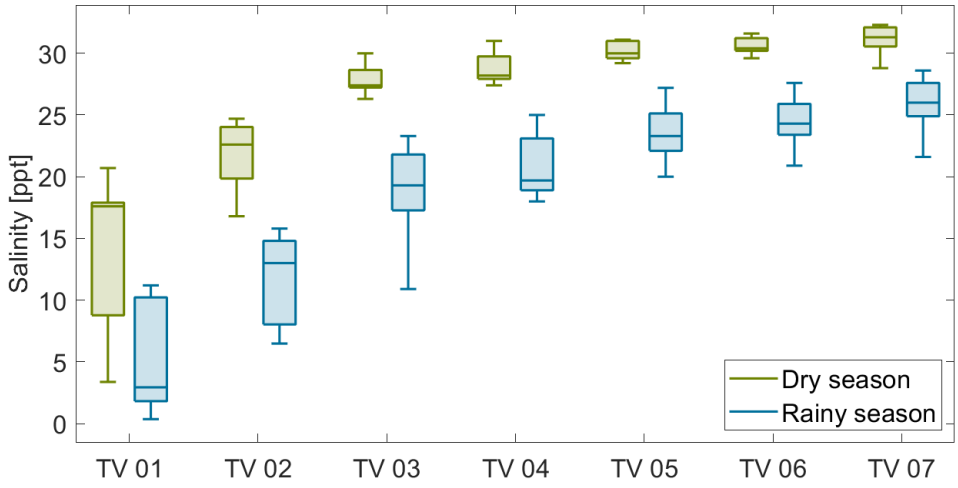

Figure 5.4: Comparison of longitudinal salinity variation in the Thi Vai Estuary between the dry and rainy season in 2012 (Data were provided by the DONRE Dong Nai).

head to the mouth of the estuary can be observed. The monitoring stations in the upper parts of the estuary additionally show higher salinity variations during both seasons. This is due to the smaller water volume at these stations in addition to their proximity to the freshwater inlets, leading to higher salinity variations when freshwater enters the estuary.

At all monitoring stations, a distinctive seasonal pattern with higher salinity levels in the dry season and lower salinity in the rainy season can be observed. This is the result of the much higher freshwater inflow in the rainy season, as already detected in Figure 5.2. In the upper parts of the estuary, at the station TV 01, the mean salinity ranges between 5 and 14 ppt in the rainy and the dry season, respectively. In the lower parts, at the station TV 07, only small changes can be observed over the year. Here, the mean salinity ranges between 26 ppt and 31 ppt, respectively. A further difference between the rainy and dry season is the salinity variation during the season, which is in the rainy season at almost all seven stations higher than during the dry season. This is due to the very small freshwater volume in the dry season, leading to nearly constant salinity conditions inside the estuary.

The vertical salinity distribution measured at three stations, namely Long Tho, Vedan and Phu My, for four specific dates, is shown in Figure 5.5. Data were recorded in the course of the research project EWATEC-COAST using a multiparameter sonde. During the dry season (04.12.13 & 18.12.2013), almost no vertical differences can be observed at the three stations. The vertical profiles show a homogeneous distribution and are nearly identical for the two dates in the dry season. In the rainy season, an overall decrease in salinity can be observed at all stations. The salinity profiles, measured in the middle of the rainy season (22.08.13), are the result of a longer-lasting precipitation period beforehand. In contrast, the salinity profiles at the end of the rainy season (27.11.13) were mainly caused by a short but intense precipitation event, only observed at the rainfall station Long Thanh, shortly before the salinity measurement. For both dates, at the station Long Tho, stratification of the water column can be observed. The salinity differences between surface and bottom layer are in the range of 10 to 15 ppt. At the stations Vedan and Phu My only for November 27th, 2013 a slight increase in salinity in the downwards direction

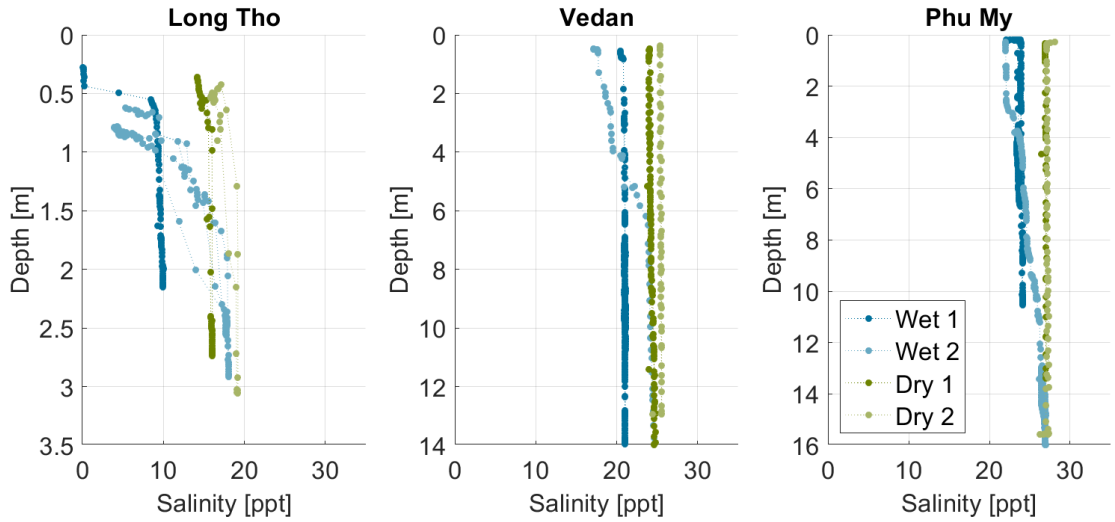

Figure 5.5: Measured depth profiles of salinity at three stations along the Thi Vai Estuary (Wet 1: 22.08.13, Wet 2: 27.11.13, Dry 1: 04.12.13, Dry 2: 18.12.13).

can be observed. The difference between surface and bottom layer is for Vedan and Phu My on average 7 and 5 ppt, respectively. Due to the lack of measurement data, it is unknown whether this pattern exists in the longer term or occurs only very briefly after precipitation events.

In summary, due to the small freshwater inflow through the tributaries, stratification can only be observed in the rainy season from May to November, and then most of the time only locally, especially in the upper reaches of the Thi Vai Estuary. As the estuary gets more wide and profound, stratification patterns are only rarely and very likely only temporarily observed in these areas.

5.1.5 Point and non-point pollution sources

The Thi Vai Estuary lies in one of the core regions of industrial development in Vietnam. Since 1990, as part of Vietnam's economic opening, numerous industrial zones have been built adjacent to the estuary. An impression of the degree of industrial development in the vicinity of the Thi Vai Estuary in the years from 2000 to 2014 is given in Figure 5.6.

Among others, the company Vedan, which specializes in the production of the flavour enhancer monosodium glutamate, was officially put into operation in 1993. Gradually, more and more companies and industrial zones emerged. Due to the numerous wastewater discharges, which were often not properly cleaned, the water quality of the Thi Vai deteriorated significantly. In hindsight it can be concluded, that the main reason was the company Vedan which discharged large amounts of uncleaned wastewater, containing high concentrations of ammonium and organic matter, into the estuary through an underground pipe system over several years (Nguyen and Pham 2012). The scandal was uncovered by the authorities in 2008. After the discovery, stricter regulations by the local authorities and the implementation of enhanced wastewater treatment plants for most of the adjacent industrial zones led to an improvement of the water quality of the Thi Vai Estuary. Nevertheless, the water quality is still affected by ongoing pollution. Especially the water quality parameters dissolved oxygen, ammonium, nitrite, and total suspended solids frequently exceed the national threshold values (Le et al. 2017).

In 2014, the Thi Vai Estuary received wastewater from 14 industrial zones including the company Vedan (Source: Institute for Environment and Resources, National University Ho Chi Minh City). The industrial zones are situated mainly along the east side of the estuary (Figure 5.1). Most of these industrial zones are equipped with centralized wastewater treatment plants. The companies, located inside the industrial parks, work in the fields of mechanical engineering, textile manufacturing, chemistry, agricultural products, flavours, pharmaceuticals, etc. Due to the fast industrial development in this region, further industrial zones are already planned along the Thi Vai Estuary.

(a) 2000. (b) 2014.

Figure 5.6: Satellite images of the Thi Vai Estuary and its vicinity for the years 2000 and 2014 (Source: Google Earth, Landsat/Copernicus).

Agricultural and urban wastewater is mainly introduced through the tributaries of the estuary. The catchment of the Thi Vai Estuary is intensively used for agriculture. Rubber plantations predominate on a large part of the area (42% of total catchment area). Additionally, annual crops (6.7%) like corn and cassava, as well as rice (5%), are grown (Lorenz 2015). 10% of the catchment area is covered by rural settlements. Most are located close to the industrial zones and have considerably grown over the last years. The results of the research project EWATEC-COAST have shown that the pollution loads from the catchment are contributing more and more to the overall pollution of the estuary, especially in the upper parts where most of the freshwater inflow enters (Lorenz et al. 2017). While in the dry season the pollution input from the industrial zones still considerably contributes to the overall load to the estuary, in the rainy season the load from the tributaries dominates.

In addition to the sources already mentioned, in some parts of the Thi Vai Estuary there exist several aquacultures that mainly specialize in shrimp farming. Most of the wastewater of these farms arises after harvest when the water inside the ponds is changed. The wastewater is almost always directly discharged into the environment without proper treatment. It contains not only food and shrimp residues, but also medical residues and antibiotics. Thus, after harvest, which is carried out approximately every four months, a local contamination of the Thi Vai Estuary might take place.

5.2 Hydrodynamic transport model

The application of a pollution source identification approach to the Thi Vai Estuary in Chapter 8, is based on a two-dimensional depth-integrated hydrodynamic and transport model. The setup and calibration using the Delft3D software suite are described in detail in the following sections.

5.2.1 Delft3D

The Delft3D modelling software is developed by WL | Delft Hydraulics in the Netherlands and consists of several integrated modules including Delft3D-FLOW and Delft3D-WAQ.

Delft3D-FLOW is a hydrodynamic simulation program, which solves the unsteady shallow water equations in two (depth-averaged) or three dimensions. The equations can be derived from the Navier-Stokes equations for incompressible free surface flow. The system of equations consists of the continuity equation, the horizontal momentum equations, and the transport equations for conservative constituents. In Delft3D, the equations are formulated in orthogonal curvilinear coordinates or spherical coordinates on the globe. Nevertheless, in the following, the hydrodynamic equations used in Delft3D-FLOW are presented for simplicity in Cartesian coordinates (Gerritsen et al. 2008):

Continuity equation

$$\frac{\partial \zeta}{\partial t} + \frac{\partial (d+\zeta) v_x}{\partial x} + \frac{\partial (d+\zeta) v_y}{\partial y} = Q \tag{5.1}$$

where ζ water level above a reference plane [m]
d depth below the reference plane [m]
v_x, v_y depth-averaged flow velocity in x- and y-direction [$\mathrm{m\,s^{-1}}$]
Q contributions per unit area due to the discharge or withdrawal of water, precipitation and evaporation [$\mathrm{m\,s^{-1}}$]

Momentum equations

$$\frac{\partial v_x}{\partial t} + v_x \frac{\partial v_x}{\partial x} + v_y \frac{\partial v_x}{\partial y} - f v_y = -\frac{1}{\rho} P_x + \frac{\tau_{sx} - \tau_{bx}}{\rho (d+\zeta)} + F_x \tag{5.2}$$

$$\frac{\partial v_y}{\partial t} + v_x \frac{\partial v_y}{\partial x} + v_y \frac{\partial v_y}{\partial y} - f v_x = -\frac{1}{\rho} P_y + \frac{\tau_{sy} - \tau_{by}}{\rho (d+\zeta)} + F_y \tag{5.3}$$

where f Coriolis parameter [$\mathrm{s^{-1}}$]
ρ water density [$\mathrm{kg\,m^{-3}}$]
P_x, P_y horizontal pressure terms [$\mathrm{kg\,m^{-2}\,s^{-2}}$]
F_x, F_y horizontal Reynolds stresses [$\mathrm{m\,s^{-2}}$]
τ_{bx}, τ_{by} bed shear stresses [$\mathrm{kg\,m^{-1}\,s^{-2}}$]
τ_{sx}, τ_{sy} free surface (wind) stresses [$\mathrm{kg\,m^{-1}\,s^{-2}}$]

The momentum equations (Eq. 5.2 and Eq. 5.3) include variable forcings due to the Coriolis force, horizontal Reynolds stresses, which are modelled using the eddy viscosity concept, water-surface and bed shear stresses, and horizontal pressure terms, which are given by Boussinesq approximations. For a detailed description of these terms, the reader is referred to Gerritsen et al. (2008) and Deltares (2018b). The set of partial differential equations in combination with an appropriate set of initial and boundary conditions is solved on a finite difference grid using an Alternating Direction Implicit method for time integration (Deltares 2018b).

The module Delft3D-FLOW provides the hydrodynamic basis for the far-field water quality module Delft3D-WAQ. Information regarding the flow velocity, water level, density etc. is transferred via a communication file. The 2D depth-integrated advection-diffusion-reaction equation forms the basis of the Delft3D-WAQ module (Deltares 2018a):

$$\frac{\partial c}{\partial t} = D_x \frac{\partial^2 c}{\partial x^2} + D_y \frac{\partial^2 c}{dy^2} - v_x \frac{\partial c}{\partial x} - v_y \frac{\partial c}{\partial y} - kc + S \tag{5.4}$$

where

c	substance concentration	$[\mathrm{g\,m^{-3}}]$
D_x, D_y	dispersion coefficient in x- and y-direction	$[\mathrm{m^2\,s^{-1}}]$
v_x, v_y	depth-averaged flow velocity in x- and y-direction	$[\mathrm{m\,s^{-1}}]$
k	process coefficient (e.g. transformation, decay)	$[\mathrm{s^{-1}}]$
S	sinks and sources	$[\mathrm{g\,m^{-3}\,s^{-1}}]$

The flow velocities in Equation 5.4 are derived from the Delft3D-FLOW hydrodynamic model. Dispersion coefficients in the horizontal directions are specified by the user. The dispersion term considers all transport that could not be resolved with the finite grid of the Delft3D-FLOW module and includes turbulent diffusion as well as dispersion which accounts for depth averaging, but also for horizontal integration over the size of each computational grid cell (Deltares 2018a). The process coefficient k can represent various physical, chemical and biological water quality processes (e.g. reaeration, adsorption, decay). The selection of these processes is substance-specific. Sinks and sources like the addition of mass by waste loads or the extraction of mass by intakes are summarized by the term S.

For the numerical discretization in space and time, several numerical schemes are available in Delft3D-WAQ. These differ in their accuracy, robustness (stability and positivity) and efficiency.

Delft3D-FLOW is used in this study for the hydrodynamic simulations, including the effect of density differences due to temporal and spatial variations in salinity. The water quality module Delft3D-WAQ is used to simulate the transport of a conservative tracer. It can be expanded to non-conservative tracers when a 1^{st}-order decay rate is included. As such, this tracer is a substitute for various pollutants (e.g. organic matter). Although both modules can simulate the transport and 1^{st}-order decay of a tracer, the advantage in using the water quality model for the simulation of the transport processes lies in the much shorter computation time in comparison to the hydrodynamic model. This is a considerable advantage in the further work of this thesis as several model runs (e.g. optimization) will be necessary.

5.2.2 Model setup

5.2.2.1 Computational grid and bathymetry

The computational grid for the numerical model of the Thi Vai Estuary was created using the grid generation module RGFGRID of the Delft3D software suite. According to Chapter 5.1.4, most of the year the Thi Vai Estuary can be considered as well-mixed. Consequently, a two-dimensional depth-averaged model was used to simulate the hydrodynamics and pollutant transport of the estuary. For the representation of the model area, an orthogonal curvilinear grid was used. The model includes the part of the estuary from the upper tributaries Suoi Ca and Bung Mon to the station Cai Mep, which is located before the confluence of the Thi Vai Estuary and the Go Gia River (Figure 5.7). In the lower parts, the grid was slightly extended beyond the tide gauge Cai Mep to avoid the influence of the nearby bend which can lead to numerical instabilities in the hydrodynamic model. In the lateral direction, the computational grid was expanded beyond the banks of the estuary, to include the intertidal areas covered mainly by mangroves, which are regularly flooded at high tide. These areas can have a significant influence on hydrodynamics and matter transport, and can serve as storage areas for pollutants during low tide. In the course of the grid generation, it was ensured that the quality criteria (e.g. orthogonality, smoothness, aspect ratio) were sufficiently satisfied. In total, the computational grid consists of $\sim 13\,000$ grid elements, which correspond to an area of $80\,\mathrm{km}^2$. In comparison to Zeunert et al. (2017), the computational grid was modified to reduce the computational effort of a single run, an important criterion for the use in the optimization process at a later stage.

For the interpolation of bathymetric data onto the computational grid, the software module QUICKIN was used. Bathymetric data of the Thi Vai Estuary were obtained during a hydrographic survey in the course of the project EWATEC-COAST in 2013. For the surrounding parts, including the intertidal areas, elevation data were provided by the Institute for Environmental Resources (IER, University of Ho-Chi-Minh-City). All elevation data are vertically referenced to the national datum Hon Dau 1992. The interpolated bathymetry of the Thi Vai Estuary is depicted in Figure 5.7. Note, that in Delft3D the sign convention for bathymetry is positive downwards, i.e. larger values indicate lower elevations.

5.2.2.2 Initial and boundary conditions

The open boundaries of the model consist of five tributary inflows from the north and east and one seaward boundary in the south, which connects the Thi Vai Estuary to the South China Sea. The flow conditions of the five main tributaries Bung Mon, Suoi Ca, Cau Vac, Muong and Ben Ngu, were simulated by the hydrological model PANTA RHEI for the period from 01.01.1998 to 30.09.2014 (Lorenz et al. 2017). For the lower seaward boundary condition, a tide gauge (Cai Mep) was installed in the course of the research project EWATEC-COAST, which automatically measured the water level in the period from March 2013 to April 2015. Initially, the water level was set to 2 m in the whole computational space.

For the simulation of salinity inside the estuary, the boundary conditions for the tributaries were set to 0 ppt. For the seaward boundary condition, a constant salinity of 30 ppt was used to account for the remaining flow distance to the open sea. The initial salinity in the model domain was set to 20 ppt. To reduce the influence of initial conditions on the

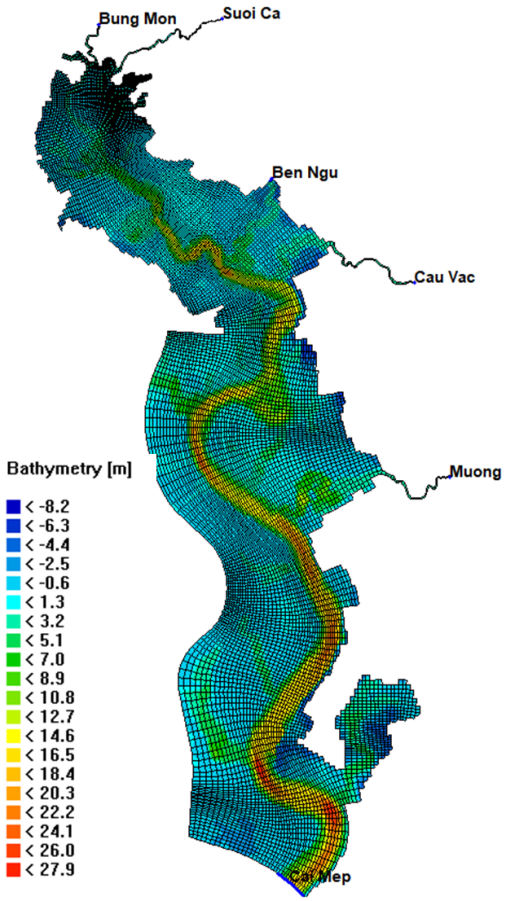

Figure 5.7: Computational grid and interpolated bathymetry of the hydrodynamic transport model for the Thi Vai Estuary.

model results, it was ensured that a sufficiently long warm-up time was considered, before the model results were used for calibration.

5.2.2.3 Parametrization

The model was run from 01.12.2012 to 30.09.2014 with a time step of 30 seconds. Only the model results from 01.01.2013 to 30.09.2014 were used for the calibration of the hydrodynamic transport model. The model was calibrated manually using the method of trial and error to find the best fitting coefficients. The calibration parameters include the horizontal eddy viscosity coefficient, the horizontal eddy diffusivity coefficient, and for the representation of the bottom roughness the Manning coefficient. Both, the horizontal eddy viscosity and the horizontal diffusivity coefficient, were set to a value of $2\,\mathrm{m^2\,s^{-1}}$. Regarding the Manning coefficient, for the flow channel, a uniform value of $0.02\,\mathrm{s\,m^{-1/3}}$ was chosen, while for the intertidal zones, which are mainly covered by mangrove forest, a value of $0.095\,\mathrm{s\,m^{-1/3}}$ was used, to account for the higher flow resistance in this area.

5.2.3 Model calibration

5.2.3.1 Statistical performance criteria and error indices

Different statistical performance criteria were used to compare observed and model-predicted data regarding water level, discharge, and salinity. These include the two dimensionless measures, the index of agreement d_2 and the modified index of agreement d_1 (Willmott et al. 1985):

$$d_2 = 1 - \frac{\sum_{i=1}^{n}(P_i - O_i)^2}{\sum_{i=1}^{n}(|P_i - \overline{O}| + |O_i - \overline{O}|)^2} \tag{5.5}$$

$$d_1 = 1 - \frac{\sum_{i=1}^{n}|P_i - O_i|}{\sum_{i=1}^{n}(|P_i - \overline{O}| + |O_i - \overline{O}|)} \tag{5.6}$$

where n number of measurements
P_i ith model predicted value
O_i ith observed value
$\overline{O}$ mean of the observed values

Both measures are bounded between 0 and 1 with higher values indicating a better agreement between model predictions and observations. The original version d_2 is, like the Nash-Sutcliffe Efficiency, sensitive to extreme outliers, owing to the squared differences (Legates and McCabe 1999). Thus, relatively high values can be observed even for poor model fits (Krause et al. 2005). In contrast, in the modified version d_1, differences between model results and measured data are given their appropriate weighting (Legates and McCabe 1999). Consequently, d_1 approaches 1.0 more slowly than d_2, and therefore provides greater separation when comparing models that perform relatively well (Willmott et al. 2012).

Additionally, the errors should be quantified in terms of the units of the variable (Legates and McCabe 1999). In this study, the mean absolute error (MAE) and the root mean squared error (RMSE) are considered:

$$MAE = \frac{1}{n}\sum_{i=1}^{n}|P_i - O_i| \tag{5.7}$$

$$RMSE = \sqrt{\frac{1}{n}\sum_{i=1}^{n}(P_i - O_i)^2} \tag{5.8}$$

Both error indices evaluate the differences between the output of the hydrodynamic transport model and the measured data in the units of the variable, thus facilitating their interpretation. The smaller the MAE and the RMSE, the better the calibration of the model to the observed data. A perfect fit is indicated by a value of 0 for both indices. In

general RMSE ≥ MAE. The degree to which RMSE exceeds MAE is an indicator of the variance in the errors (Legates and McCabe 1999). If all errors have the same magnitude, MAE is equal to RMSE.

Lastly, the percent bias (PBIAS) is considered, which measures the average tendency of the model to over- or underpredict the simulated quantities in respect to the measured data:

$$PBIAS = \frac{\sum_{i=1}^{n}(O_i - P_i) \cdot 100}{\sum_{i=1}^{n} O_i} \tag{5.9}$$

Ideally, PBIAS should be equal to 0. Positive values indicate that, on average, the measured data are underpredicted by the model. In contrast, negative values result when model predictions are, on average, larger than their corresponding measured values (i.e. overprediction) (Gupta et al. 1999).

5.2.3.2 Results of the hydrodynamic model

The hydrodynamic model was calibrated using measured water level and discharge data collected during a monitoring program as part of the research project EWATEC-COAST. As discussed in Chapter 5.1.3, the water level was recorded automatically every 10 minutes by a data logger at the stations Long Tho and Vedan from March 2013 to September 2014. Although earlier measurements were available, only the data from October 2013 to September 2014 were used for the calibration of the hydrodynamic model, due to the presence of ambiguities in the earlier data. Figure 5.8 shows the model-predicted and observed water level at both stations for October 2013, a small part of the actual calibration period. Alongside the visual inspection, several statistical performance criteria and error indices were calculated (Section 5.2.3.1). The calculation of the statistical criteria for the water level was based on the whole calibration period from October 2013 to September 2014. Both, the direct visual comparison, as well as the statistical performance criteria shown in Table 5.1, indicate that the simulation results are in good agreement with the measured data. At both stations, an index of agreement d_2 of 0.99 and a value of 0.95 to 0.96 for the modified version d_1 could be achieved. The MAE ranges between 0.07 and 0.08 m at both stations. These values are in the range proposed by Bartlett (1998), according to whom the deviations between simulated and measured water levels should be lower than 0.1 m at the mouth, and 0.3 m at the head of estuaries. While for the station Vedan, the water level is slightly underpredicted, for Long Tho the PBIAS shows, on average, an overprediction of $\sim 5\%$. Differences in measured and simulated water levels can, among other things, be attributed to uncertainties in the conversion of the water pressure, initially measured by the data loggers, to the actual water level.

The discharge was measured on several occasions at the station Phu My over the tidal cycle using an acoustic Doppler current profiler (ADCP). Figure 5.9 compares measured and predicted discharge for two time periods at the station Phu My. The simulated discharge is in good agreement with the measured data, which is confirmed by a value of 0.99 and 0.94 for the original and the modified index of agreement, respectively (Table 5.1). The MAE of 354 $m^3 s^{-1}$ is low in comparison to the total measured discharge variations which range approximately from -4400 to +6800 $m^3 s^{-1}$ in the two measurement campaigns.

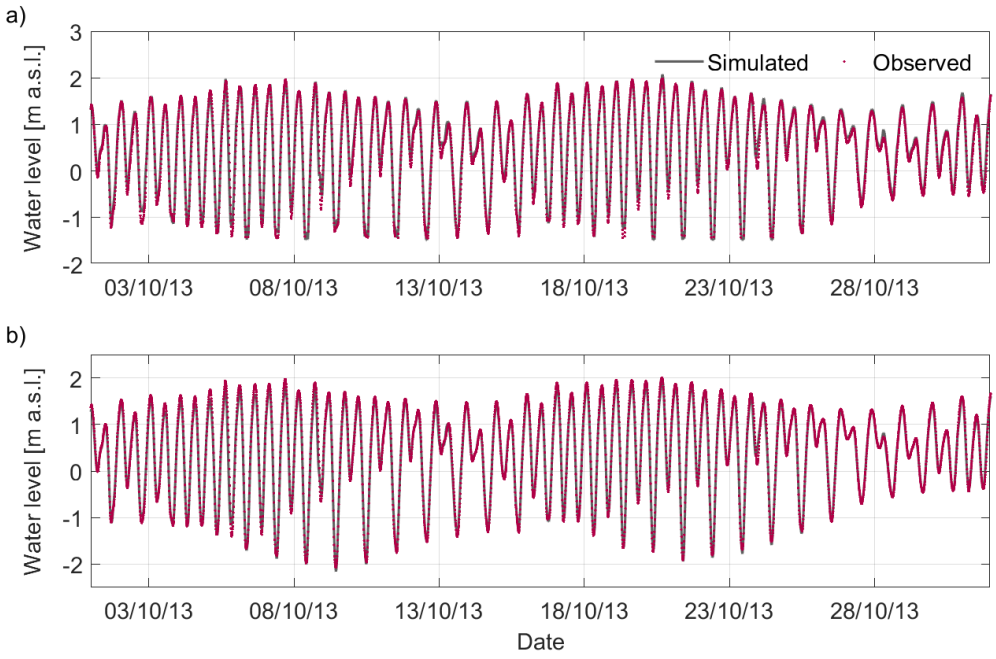

Figure 5.8: Comparison of measured and simulated water levels for October 2013 (a small part of the actual calibration period) at the stations a) Long Tho and b) Vedan.

5.2.3.3 Results of the transport model

Because no tracer experiments were carried out in the estuary, salinity data were used to verify if the transport and mixing processes in the Thi Vai Estuary are reproduced correctly by the hydrodynamic transport model. As part of the EWATEC-COAST project, salinity was measured weekly at the stations Long Tho, Vedan and Phu My from March 2013 to June 2014 using a multiparameter probe (V2 6600, YSI). Data were collected in two to three different depths in the centre of each cross-section. The output of the two-dimensional model was compared to depth-averaged salinity data. Figure 5.10 includes a visual comparison between measured and simulated salinity at the stations Long Tho, Vedan and Phu My. As discussed in Chapter 5.1.4, the temporal dynamics of salinity in the

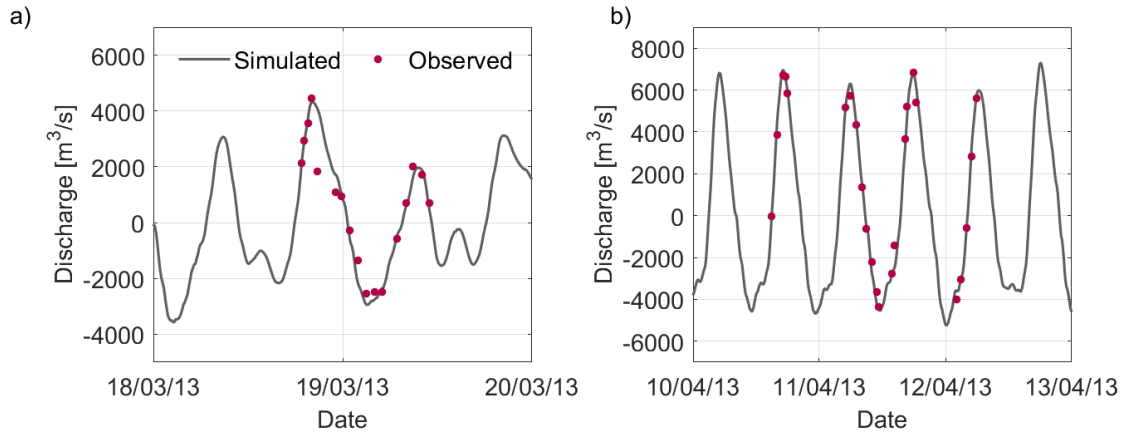

Figure 5.9: Comparison of measured and simulated discharge at the station Phu My for the period from a) 18.03.13 to 20.03.13 and b) 10.04.13 to 13.04.13.

Thi Vai Estuary are characterized by a periodic pattern with high salinity levels in the dry season and lower levels in the rainy season. The results show that the model was able to capture these variances in the course of the simulation period. In comparison to the other monitoring stations, significantly higher daily salinity deviations in the modelled data can be observed for the station Long Tho. The station is located in the upper reaches of the Thi Vai Estuary close to the confluence of the tributaries Bung Mon and Suoi Ca. Due to the lower water volume in these parts of the estuary, higher salinity variations during the day can be observed here. These findings are confirmed by the results of Chapter 5.1.4.

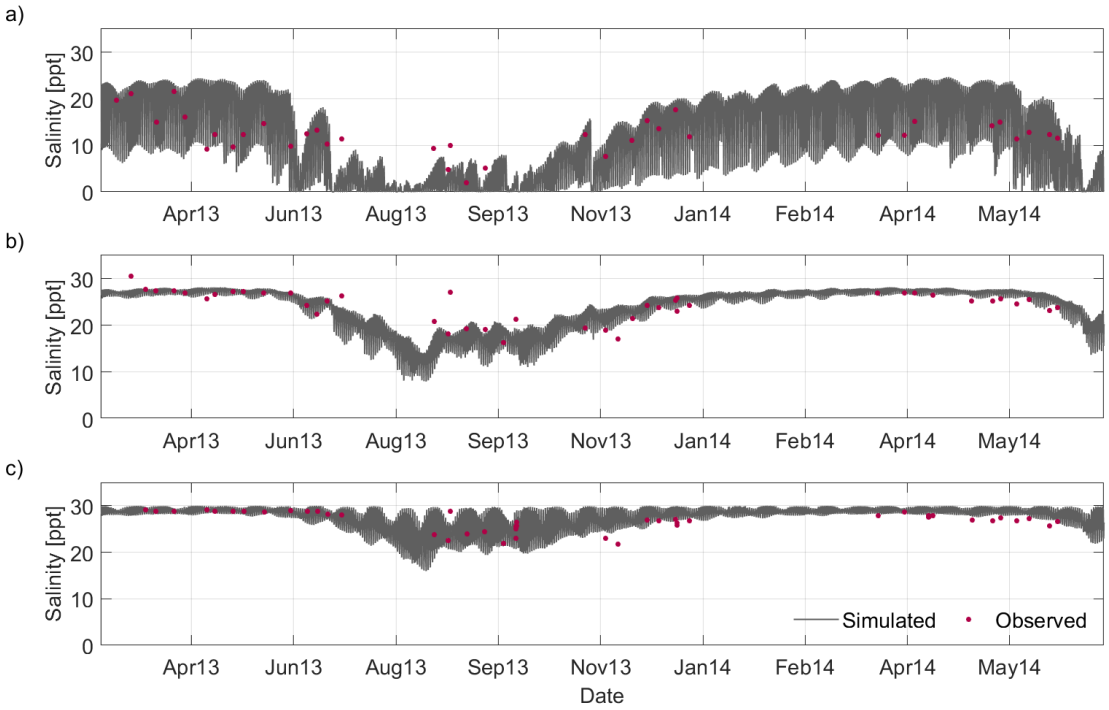

Figure 5.10: Comparison of measured and simulated salinity at the stations a) Long Tho, b) Vedan and c) Phu My.

The statical performance criteria regarding the calibration of salinity indicate that values of 0.66 to 0.86 could be achieved for the index of agreement d_s at the three stations (Table 5.1). The mean absolute error ranges between 1.76 and 5.41 ppt. Higher deviations could be observed at the station Long Tho. Here, in addition to the overall higher daily salinity deviations, in the rainy season temporary vertical stratification patterns might exist (compare Chapter 5.1.4). At the other two stations, the performance criteria indicate a good representation of salinity. According to Bartlett (1998), salinity deviations should be lower than 1 ppt at the estuary mouth, and 5 ppt or more in the region of most rapid change. These values are only slightly exceeded by the transport model. Overall, the PBIAS is negative for all stations and indicates that the salinity is slightly over-predicted by the model.

To further validate the transport and mixing processes, salinity data of five additional monitoring stations, which were provided by the DONRE Dong Nai, were used. Here, salinity was measured monthly in 2013, along with other water quality parameters. For each measurement, only the date of the measurement but not the exact time was given. Therefore, the validation is based on a visual inspection. In Figure 5.11, model-predicted and observed salinities are compared for the five monitoring stations. The simulated daily minimum, mean, and maximum salinity are represented as solid lines. Overall, most of

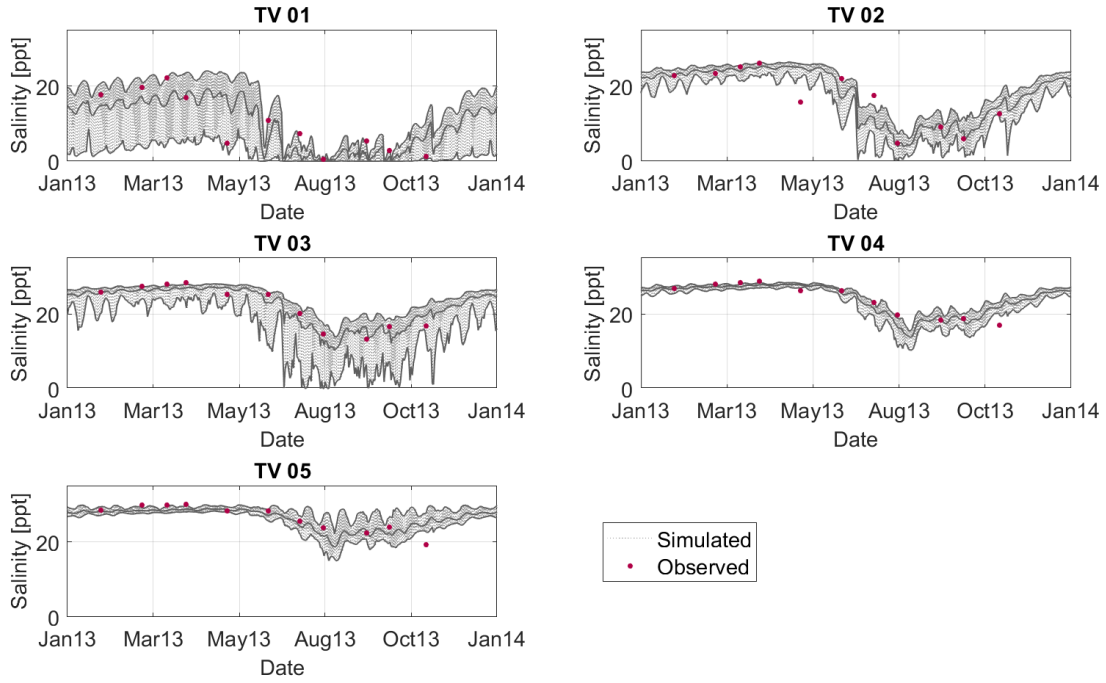

Figure 5.11: Comparison of measured and simulated salinity at the stations TV 01 to TV 05 (Data were provided by the DONRE Dong Nai). The grey dashed line represents the simulated salinity. The solid lines represent the simulated minimum, mean and maximum daily salinity.

the time, measured salinity lies in the model predicted range at all monitoring stations. Especially in the upper reaches, the daily salinity variation can be significant, as already observed at the station Long Tho. The higher salinity variations at the station TV 03 in comparison to TV 02 are explained by its location in the vicinity of the tributary inflow Cau Vac.

Based on the calibration results, it can be concluded that the spatial and temporal salinity patterns are represented correctly by the transport model in the middle to lower reaches of the Thi Vai Estuary. The results in the upper reaches have to be handled with care, because here temporary stratification might exist after intense precipitation events. Freshwater discharge plays a significant part in the development of temporal and spatial salinity patterns in the estuary. It has to be considered that the freshwater discharge is model-predicted, and therefore includes higher uncertainties than measured discharge, which leads to higher uncertainties in model-predicted salinity, especially in the vicinity of tributary inflows.

Because in the further work the pollutant transport is simulated using the water quality module Delft3D-WAQ, it was ensured that Delft3D-WAQ produces the same model results regarding salinity predictions as the hydrodynamic transport model. Here, the horizontal dispersion coefficient in both directions was set to $2\,\mathrm{m^2\,s^{-1}}$ equal to the calibrated horizontal eddy diffusivity coefficient.

Table 5.1: Statistical performance criteria for the calibration of the hydrodynamic transport model of the Thi Vai Estuary.

Parameter	Monitoring station	d_2	d_1	MAE	RMSE	PBIAS
Water level [m]	Long Tho	0.99	0.95	0.08	0.11	-4.71
	Vedan	0.99	0.96	0.07	0.10	1.41
Discharge [$m^3 s^{-1}$]	Phu My	0.99	0.94	354	539	-2.95
Salinity [ppt]	Long Tho	0.66	0.45	5.41	6.56	-3.94
	Vedan	0.86	0.68	1.87	2.53	-1.31
	Phu My	0.75	0.56	1.76	2.21	-25.75

6 Identifiability analysis of pollution source parameters

Parameter estimation is inherently related to parameter identifiability (Olivier and Smyth 2017). As explained in Chapter 2.2.5, if model parameters are not identifiable, the solution to the inverse problem is non-unique, and the problem is consequently termed ill-posed. Furthermore, even if a unique solution exists, only poorly identifiable parameters lead to high uncertainties in the estimated parameters, instability issues, and slow convergence of the optimization algorithm (Carrera and Neuman 1986b). To ensure a reliable estimation of model parameters, it is therefore strongly recommended to perform an identifiability analysis (Miao et al. 2011). The analysis can be performed based on synthetically generated data. This additionally allows to evaluate the influence of the monitoring design on parameter identifiability (Guillaume et al. 2019).

Several approaches exist to determine if the parameters of a model are identifiable. Comprehensive reviews of different methods can be found for example in Walter and Pronzato (1996), Miao et al. (2011) and Guillaume et al. (2019). In the following sections, two different approaches are selected and applied to an unidirectional and bidirectional test case, representing a river and an estuary, respectively.

6.1 Unidirectional flow

In the first part of this chapter, an instantaneous pollutant release in a unidirectional two-dimensional flow system is considered. The pollutant transport and mixing processes are represented by an analytical solution of the 2D advection-dispersion-reaction equation. Up to now, the identifiability of pollution source parameters and the influence of the monitoring design has not been analysed in the literature.

The presented section has been submitted and accepted in the Journal *Advances in Water Resources* and can be found in Zeunert and Meon (2020).

6.1.1 Identifiability analysis

One approach for the evaluation of parameter identifiability is the profile likelihood (PL) approach, which is frequently adopted in systems biology (Raue et al. 2009; Kreutz et al. 2013). Because the PL approach does not pose any restrictions on the algebraic form of the model equations, it can also be applied to other research areas (Raue et al. 2014). The PL approach is based on the likelihood function $L(\theta|d)$ given in Equation 2.8. After the determination of the MLE, likelihood-based confidence intervals can be derived by calculating profile likelihoods. The procedure is described in more detail in Chapter 2.2.4.

The derived likelihood profiles and confidence intervals can be used to assess both structural and practical parameter identifiability as well as parameter uncertainty. An overview

of three possible cases is given in Figure 6.1. A perfectly flat profile indicates a structural non-identifiable parameter (Figure 6.1b). Profiles that have a unique minimum, but do not cross the confidence threshold in decreasing and/or increasing direction, reveal practically non-identifiable parameters (Figure 6.1d). If parameters are both structurally and practically identifiable, finite confidence intervals can be derived (Figure 6.1f).

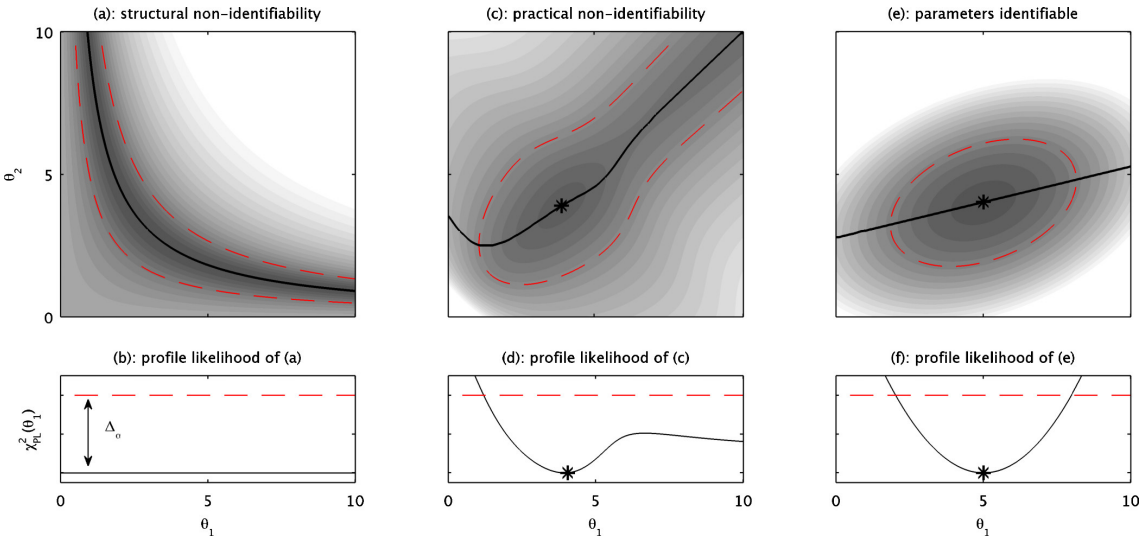

Figure 6.1: Assessment of parameter identifiability from calculated profile likelihoods (b,d,f) and corresponding traces in the parameter space (a,c,e). Reprinted from Raue et al. (2010), with the permission of AIP Publishing.

6.1.2 Pollutant transport model

In this work, it is assumed that the pollutant is released instantaneously from a single point source. Consequently, the pollution spill is described by four parameters including the x- and y-coordinate of the source location x_s and y_s, the release time t_s and the total pollutant mass M_s. The approach can be easily transferred to other source characteristics, e.g. continuous sources or multiple point sources. To model the transport and mixing of the pollutant in the river, an analytical solution of the advection-dispersion-reaction equation (ADRE) is applied. In comparison to a numerical transport model, the analytical solution is computationally fast and numerical errors and instabilities due to the spatial and temporal discretization do not occur. Nevertheless, if unsteady flow or more complex river geometries are investigated, a numerical transport model is necessary.

In the literature regarding PSI, the transport and mixing inside the river is often modelled by using the one-dimensional (1D) ADRE (Ghane et al. 2016; Jiang et al. 2018; Wang et al. 2018). When applying this equation, it has to be considered that immediate mixing in the lateral and vertical direction is assumed. Thus, in practice, this equation can only be applied to very narrow and shallow rivers or when observation points are located further away from a potential release location and mixing in lateral and vertical direction has already taken place. Because the lateral mixing zone can have a considerable length, the use of a two-dimensional (2D) model is recommended (Jiang et al. 2018). For an instantaneous pollution release at time t_s with a total pollutant mass M_s introduced at a source location specified by its coordinates x_s and y_s, the analytical expression of the 2D

ADRE has the form (van Genuchten et al. 2013):

$$c(x,y,t) = \frac{M_s}{4h\pi t^* \sqrt{D_x D_y}} \exp\left[-\frac{(x - x_s - v_x t^*)^2}{4D_x t^*} - \frac{(y - y_s - v_y t^*)^2}{4D_y t^*} - kt^*\right] \tag{6.1}$$

where h water depth [m]
D_x, D_y dispersion coefficient in x- and y-direction [$\mathrm{m^2\,s^{-1}}$]
v_x, v_y depth-averaged flow velocity in x-and y-direction [$\mathrm{m\,s^{-1}}$]
k decay rate [$\mathrm{s^{-1}}$]
t^* time since the pollutant release $t^* = t - t_s$ [s]

Equation 6.1 considers an infinite domain in the longitudinal and lateral flow direction. Nevertheless, in reality, a further movement of the constituent across the river banks can not take place. Using Equation 6.1 without lateral boundaries would therefore underestimate the real concentration inside the river. To introduce a no-flux boundary condition at the lateral boundaries, the mirror-image technique is used in this work (Fischer et al. 1979; Chin 2013). It ensures that the constituent beyond the river bank is reflected back by introducing additional sources also called image sources which balance the mass loss inside the river section. Usually, it is sufficient to only use a small number of mirror reflections (Fischer et al. 1979). Based on Chin (2013), in this work, the number of mirror reflections is set to four on the left- and right-hand boundary.

6.1.3 Monitoring data

For the identifiability analysis, a discrete number of synthetically generated noise perturbed data is considered. Monitoring data are derived using the results of the transport model described in Section 6.1.2 and adding a perturbation term. For the identifiability analysis, a reference scenario is defined, having the system and pollutant characteristics shown in Table 6.1. The analytical solution considers a straight river section with no tortuosity, a constant rectangular cross-sectional profile and steady-state in hydrodynamics. Thus, constant values for the longitudinal and lateral flow velocities and dispersion coefficients in respect to both time and space are applied. In general, v_y is set to zero, because no significant advective transport takes place in the lateral direction. The river depth h is set to 2 m. When using the 2D ADRE, it is assumed that the pollutant is mixed instantly in the vertical direction. If a pollutant with a different density than water (e.g. oil derivative) is considered, the 3D ADRE should be applied instead. The river width W, which is not a direct parameter of Equation 6.1, is used for the placement of image sources. For the reference scenario, an instantaneous pollutant release in the centre of the cross-section at KM 7 is considered. Here, at time 12:00 h, a total pollutant mass of 500 kg is introduced into the river. The pollutant is considered to be conservative. In Section 6.1.5.2, additionally, the influence of a decay rate is evaluated.

Regarding the spatial design of the monitoring network, two different configurations are considered in this work. These include concentrations measurements at predetermined monitoring stations and measurement campaigns along the longitudinal direction of the river for a given point in time. Both approaches rely on the knowledge that a pollutant release has already occurred further upstream in the river. The detection of a potential pollutant release (e.g early-warning system) is not part of this study. Monitoring is only conducted after the information that a pollutant release has occurred somewhere upstream.

Table 6.1: Parametrization of the reference scenario for the unidirectional test case.

Parameter	Description	Value
System- and pollutant-dependent model parameters		
h	river depth	$2\,\mathrm{m}$
W	river width	$300\,\mathrm{m}$
v_x	flow velocity in x-direction	$0.5\,\mathrm{m\,s^{-1}}$
v_y	flow velocity in y-direction	$0\,\mathrm{m\,s^{-1}}$
D_x	dispersion coefficient in x-direction	$25\,\mathrm{m^2\,s^{-1}}$
D_y	dispersion coefficient in y-direction	$0.4\,\mathrm{m^2\,s^{-1}}$
k	decay rate	$0\,\mathrm{d^{-1}}$
Pollution source parameters		
M_s	total pollutant mass	$500\,\mathrm{kg}$
x_s	x-coordinate of source location	$7000\,\mathrm{m}$
y_s	y-coordinate of source location	$150\,\mathrm{m}$
t_s	release time	12 h

Knowledge of a potential release might be derived from the responsible discharger itself, from public complaints or available monitoring data (Grayman and Males 2002).

6.1.3.1 Monitoring stations

In this work, the single and combined influence of different monitoring stations on parameter identifiability and uncertainty is analysed. The location of the considered pollutant source and the monitoring stations can be retrieved from Figure 6.2, which includes a schematic representation of the synthetic river section. Corresponding concentration time series at the monitoring stations are presented in Figure A.1 of the Appendix. It is assumed that monitoring starts at the considered monitoring stations 4 h before the corresponding maximum pollutant concentration is reached. The sampling frequency and duration are set constant to 15 min and 8 h, respectively, to enable a comparison of different monitoring designs. In total, 33 observations were used for each monitoring station. Because less data is generally collected in practice, Section 6.1.5.4 includes an analysis of the influence of the monitoring frequency and duration on PSP identification.

Only the monitoring stations B1 and B2 are considered for the analysis of the likelihood profiles of the reference scenario in Section 6.1.5.1 and the influence of system- and pollutant-dependent model parameters in Section 6.1.5.2. The further monitoring stations (A1, A2, C1, C2) shown in Figure 6.2 are used in Section 6.1.5.3 to assess the influence of the spatial monitoring network design on the identifiability of pollution source parameters (PSP).

6.1.3.2 Longitudinal measurements

For the identification of PSP, Zhang and Xin (2017) and Yang et al. (2016) did not use concentration time series collected at selected locations, but longitudinal concentration

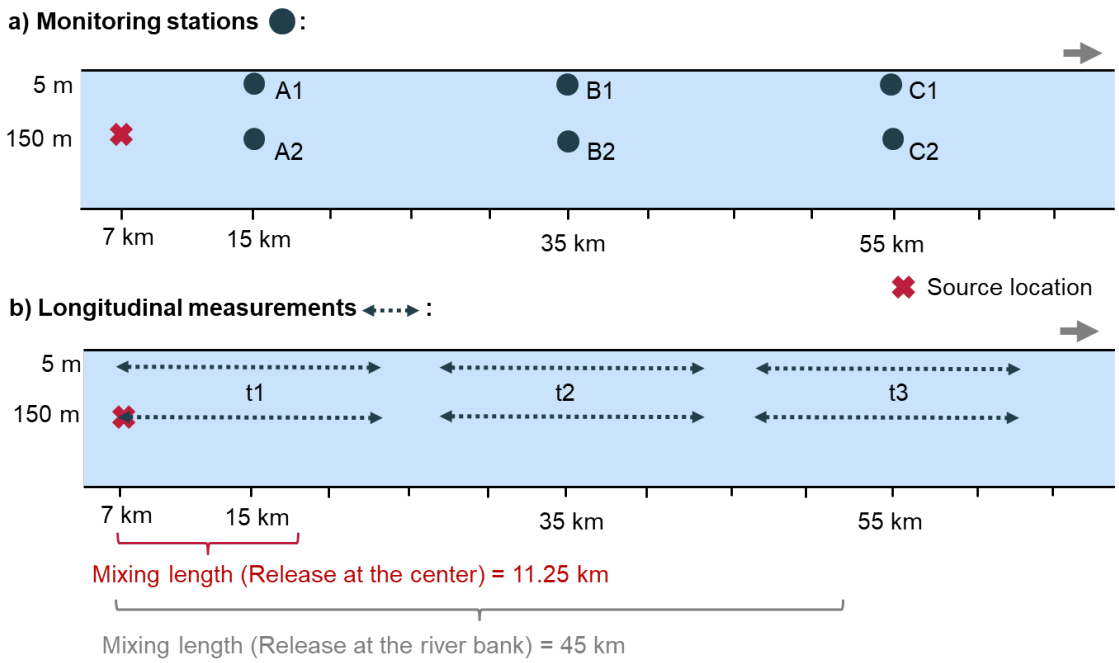

Figure 6.2: Schematic representation of the considered river section, position of the source location and spatial monitoring design of the unidirectional test case. a) Location of monitoring stations; b) Location of longitudinal measurement campaigns.

measurements where pollutant concentrations were measured along the longitudinal direction over a very small time period. To compare the influence of both data collection approaches on the identifiability of PSP, additionally longitudinal concentration measurements were considered in the analysis. In this work, it was assumed that data were collected at three different points in time, namely $t_1 = 4.4$ h, $t_2 = 15.6$ h and $t_3 = 26.7$ h after the pollutant release. The considered times determine the moments where the peak of the pollutant plume arrives at the cross-section A, B and C, respectively. For all designs, a monitored river section with a total length of 16 km and an equidistant discretization of 500 m was considered. The centre of each section was located at the cross-section A, B and C, respectively. It was assumed that concentration profiles were taken either close to the bank (y_{obs} =5 m) or in the centre of the river stretch (y_{obs} =150 m) (Figure 6.2). Corresponding concentration data are presented in Figure A.2 of the Appendix. In total, for every longitudinal measurement series 33 observation data were considered.

6.1.3.3 Integration of measurement errors

As monitoring data are seldom perfect, an error model was used to perturb the simulated concentration data generated by the analytical solution of the 2D ADRE. for the identifiability analysis, it was assumed that measurement noise is multiplicative, an often applied assumption when concentration data are used (Cheng and Jia 2010; Han et al. 2014; Li et al. 2016):

$$\epsilon_i = f_i(\theta) \cdot \epsilon_{rel} \quad \text{with} \quad \epsilon_{rel} \sim N(0, \sigma_{rel}^2) \tag{6.2}$$

Consequently, σ_i is set to $f_i(\theta) \cdot \sigma_{rel}$ in Equation 2.8. The relative standard deviation σ_{rel} of the measurement noise is set to 0.1. Corresponding noise perturbed observation data used in the further analysis are depicted in Figure A.1 and A.2 of the Appendix. In this work a constant value for σ_{rel} is used. Higher values for the relative standard deviation will lead to larger uncertainties in the estimated parameters.

Synthetically generated concentration data can be very small. This is not representative of actual monitoring data, whose accuracy is influenced by the monitoring device. Therefore, a concentration threshold value c_{th}, e.g. limit of detection, is defined. Concentration data below the predefined value were set to the respective value. In this work, a value of 10^{-4} $\mathrm{g\,m^{-3}}$ was adopted after careful inspection of all considered monitoring data. As the chosen value can have an influence on the results, it should be chosen with care.

6.1.4 Software

All calculations were carried out in MATLAB 2018b. For the optimization of parameters the MATLAB function *fminsearchbnd* based on the Nelder and Mead Simplex algorithm was employed (D'Errico 2020). The algorithm is described in detail in Chapter 2.2.3.1. The following parameter boundaries are used for the estimation of optimal parameter sets and calculation of likelihood profiles: x_s: 0-14 000 m, y_s: 0-300 m, t_s: 0-24 h and M_s: 0-1000 kg.

In general, optimization results have to be handled with care, due to the existence of local minima. Therefore, likelihood profiles were carefully inspected after their calculation. Firstly, the MLE should be the lowest point in all parameter profiles. Secondly, likelihood profiles should be relatively smooth. Sudden changes or spikes might be the result of premature convergence of the optimization algorithm. In this case, it is necessary to repeat profile calculations from different initial values to enhance robustness of the results (Raue et al. 2014).

The analytical solution of the 2D ADRE was implemented based on a vectorized approach, resulting in a fast computation of simulated concentrations. When a single monitoring station with 33 data points is considered, the analytical solution of the 2D ADRE is computed on average in less than 0.001 s. For the calculation of the corresponding likelihood profiles of one scenario, on average less than 30 s were needed when using parallel computation for the different likelihood profiles. As can be expected, the more monitoring data are included in the analysis, the higher will be the computational time.

6.1.5 Results and Discussion

6.1.5.1 Identifiability of pollution source parameters in the reference scenario

In Figure 6.3, the resulting likelihood profiles of each pollution source parameter (PSP) for the reference scenario, defined in Section 6.1.3, are displayed. Three monitoring configurations are compared, considering on the one hand the individual monitoring stations B1 and B2, and, on the other hand a combination of both monitoring stations. The grey dashed line represents the 95% confidence level. In general, parameters are termed structurally identifiable if the MLE is a unique minimum of the likelihood profile. Profiles that have a unique minimum, but do not cross the confidence threshold in decreasing and/or

increasing direction, are often termed practically non-identifiable (Raue et al. 2009). Nevertheless, as this can also be the result of poor structural identifiability, further analysis should be carried out in this case.

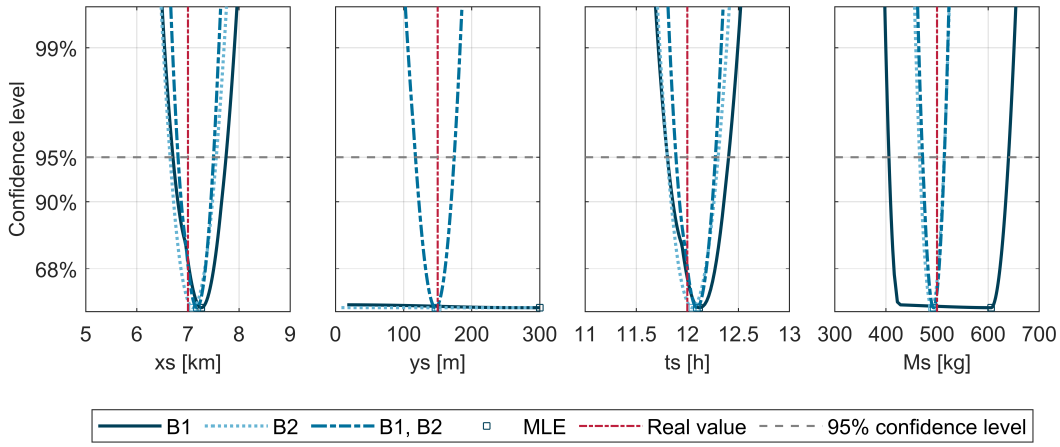

Figure 6.3: Likelihood profiles for the pollution source parameters of the reference scenario considering the individual monitoring stations B1 and B2, as well as a combination both monitoring stations.

If monitoring data are collected at both monitoring stations B1 and B2, the derived likelihood profiles for the four PSP exhibit a unique minimum and exceed the 95% confidence level in both directions, resulting in finite confidence intervals. In this case the parameters can be termed both structurally and practically identifiable. In contrast, if only one of the monitoring stations either at the bank or in the centre of the cross-section is considered, the likelihood profiles of the lateral source location y_s show a unique minimum (when observed in detail), but are very flat in decreasing direction. Additionally, for the monitoring station B1, the likelihood profile for the total pollutant mass M_s is very flat in decreasing direction leading to significantly wider confidence intervals in comparison to the other monitoring configurations. The poor identifiability of the parameters y_s and M_s under the discussed monitoring configurations is also the reason for the large deviation between real and estimated parameter values for y_s and M_s.

Reasons for parameter non- as well as poor identifiability can be further analysed by plotting the fixed parameter θ_i against the re-optimized parameters θ_j. This provides an overview of possible parameter interactions and can determine functionally related groups when structurally non-identifiable parameters are observed (Raue et al. 2014). A straight horizontal line indicates that no interaction between the correspondent source parameters exists. In contrast, if the line continuously deviates from zero, a change in the parameters θ_j can at least partially balance a change in the parameter θ_i in regards to the likelihood function.

In Figure 6.4a, the traces of M_s for the profile calculation of y_s are presented, considering the individual monitoring stations B1 and B2. For the monitoring station B1, a non-linear interaction effect between y_s and M_s can be observed, which explains the poor identifiability of these parameters. Relating these results to practice, if a higher pollutant mass is introduced not in the centre but at the river banks, due to lateral mixing, similar pollutant concentrations could be observed at the monitoring station B1. In contrast, for the monitoring station B2 no interaction could be observed between y_s and M_s. In this

case, the poor identifiability of y_s is due to a lack of sensitivity of the model output to changes in the parameter y_s. In both cases, an improvement in data quantity or quality could not improve the identifiability of y_s as this is the result of a structural problem due to the defined model input, i.e. the considered monitoring locations.

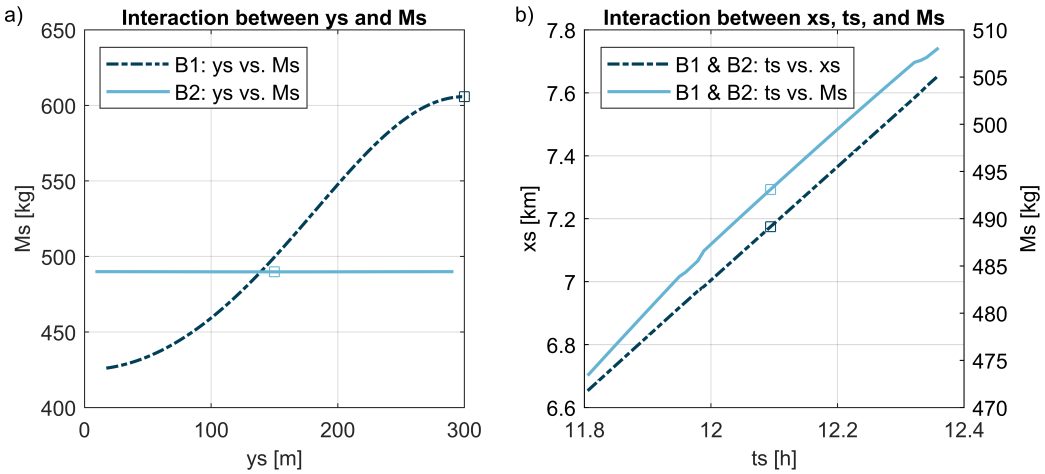

Figure 6.4: Change of the re-optimized parameters in respect to their original values along the likelihood profile for the reference scenario. The square denotes the corresponding MLE estimated for each monitoring configuration. a) Traces of M_s for the profile calculation of y_s. b) Traces of x_s and M_s for the profile calculation of t_s.

The results are in agreement with Han et al. (2014), who used the simulation-optimization approach for the identification of source parameters of an instantaneous pollutant release. In the case that the pollution source was located in the centre of a cross-section and only a single monitoring station in the lateral direction was used, the accurate identification of the total pollutant mass M_s and the lateral source location y_s failed and led to very high errors in the estimated parameters. If two or more monitoring stations were considered inside one cross-section both parameters could be determined with very small errors.

The results already imply that the identifiability and reliable estimation of PSP is influenced by the monitoring network design. Parameter interactions between PSP can lead to flatter profiles of the likelihood function, resulting in poor identifiability and inaccurate estimation of parameters.

6.1.5.2 Influence of system- and pollutant-dependent model parameters

In the further course of this work, the influence of the monitoring design will only be analysed based on a specific river system and pollutant defined in the reference scenario. However, system- and pollutant-dependent model parameters as the flow velocity, the longitudinal and lateral dispersion coefficients or the decay rate might influence the identifiability of PSP. To assess if the results obtained in this study can be transferred to other river systems, the influence of the mentioned model parameters on the identifiability of PSP is analysed.

For every considered scenario only one model parameter was changed, while the other parameters were held constant.Two monitoring configurations were considered and maintained for all scenarios, including the individual station B2 as well as a combination of

the stations B1 and B2. In contrast to the information given in the description of the reference scenario, the monitoring duration was extended to 16 h so that the full pollutant concentration profiles were measured for each of the considered scenarios. This is especially relevant when the dispersion coefficient is very high or when the flow velocity is small. It is noted that in practice this many measurements are unlikely to be available, but only in this way different scenarios can be compared independent of the monitoring duration.

The results are presented in Figure 6.5. To make the scenarios easier to compare, instead of showing the full likelihood profile, only the MLE and the likelihood-based confidence intervals for a confidence level of 95% are presented for each scenario. While the solid lines represent the monitoring design consisting of both monitoring stations B1 and B2, for the dashed lines only the monitoring station B2 is taken into account. In general, very wide confidence intervals represent non- or only poorly identifiable parameters. A further sign of poor identifiability is a large deviation between the MLE and the real parameter value.

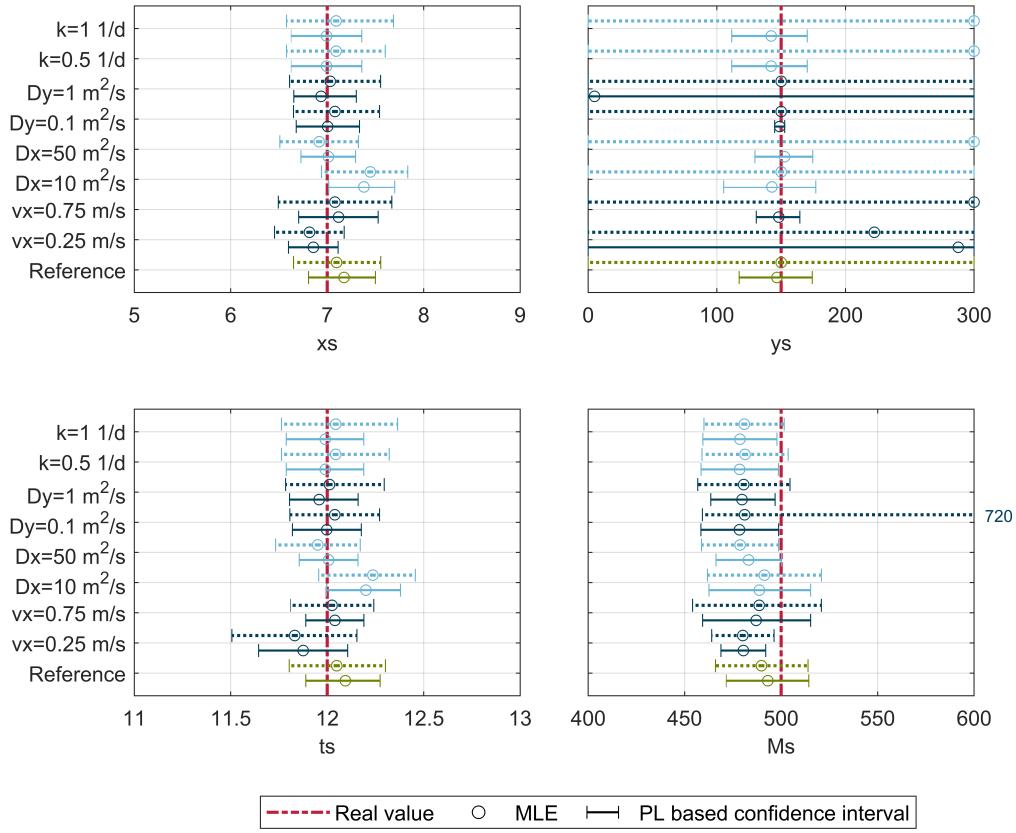

Figure 6.5: Influence of system- and pollutant-dependent model parameters on the identification of pollution source parameters. Solid lines: Monitoring stations B1 and B2; Dashed lines: Monitoring station B2. The circle represents the MLE and the error bar the profile likelihood based 95% confidence interval for each scenario.

Regarding the parameters y_s and M_s, significant changes in the width of the derived confidence intervals can only be observed if the flow velocity v_x or the lateral dispersion coefficient D_y are modified. The accurate identification of y_s and M_s is dependent on

the length of the mixing zone and the associated position of the considered monitoring stations. The model parameters v_x, D_y and W affect the total mixing length. A decrease in v_x or an increase in D_y will lead to a decreased length of the mixing zone. If D_y is changed to $0.1\,\mathrm{m^2\,s^{-1}}$ the mixing zone has a length of 45 km. In this case, the monitoring stations B1 and B2 are still located inside the mixing zone. As described in Section 6.1.5.2, if only one monitoring station is considered, the confidence interval for M_s is very wide due to interaction effects with y_s. If both monitoring stations are considered, both parameters can be determined with relatively small uncertainties. The results further show that y_s, regardless of the considered scenario, can only be determined if two monitoring stations are used inside the cross-section. In the case that D_y is set to $1\,\mathrm{m^2\,s^{-1}}$ or v_x to $0.25\,\mathrm{m\,s^{-1}}$, y_s can only be termed poorly identifiable even when two monitoring stations are considered. This is explained by the fact that full longitudinal mixing would have occurred even when a release from the bank of the river stretch is considered. Thus, different lateral release locations could not be distinguished any more at the cross-section B.

For the parameters x_s and t_s only minor changes can be observed between different scenarios. Both parameters can be termed identifiable and estimated with high accuracy under the given scenarios. Slight differences can be observed for changes in the flow velocity v_x or the longitudinal dispersion coefficient D_x. In Figure 6.4b, traces of x_s and M_s for the profile calculation of ts for the reference scenario are shown. Slight linear interaction effects can be observed between the three parameters. In practice, a source located a little bit further downstream with a later release time and a higher pollutant mass will lead to a similar concentration profile at the observation stations. Nevertheless, under the given hydrodynamic conditions, these effects do not influence parameter identifiability. When v_x or D_x are varied, the interaction between x_s, t_s and M_s changes. In the case that v_x is increased, the uncertainty in t_s slightly decreases, while for the other source parameters the opposite is the case. In comparison, for an increase in D_x, the uncertainty in all three parameters is slightly reduced. The process of dispersion, whose strength is represented by the parameter D_x, is an important process, which enables the identifiability of x_s and t_s in the first place. If only advection would be considered, infinite combinations would exist for x_s and t_s, which could not be determined separately.

As already emphasized, the presented results are only valid under the specified monitoring configurations which included the monitoring stations B1 and B2. The results have shown, that parameter identifiability and uncertainty can be affected by the parametrization of the pollutant transport model. Nevertheless, the model parametrization can not be chosen arbitrarily but depends on the underlying system and pollutant characteristics. Therefore, an identifiability analysis should always be part of the parameter estimation process (Miao et al. 2011). Only if parameter identifiability is ensured, a reliable estimation of the unknown source parameters can be expected.

6.1.5.3 Influence of the spatial monitoring design

Up to now, only monitoring data collected at the cross-section B were considered in the analysis. The results have already shown that parameter identifiability is influenced by the monitoring network design. In the following section, the influence of the spatial monitoring design is further evaluated.

For the parametrization of the different scenarios, the system- and pollutant-dependent model parameters of the reference scenario (Table 6.1) were applied. Again, in the upcom-

ing figures, for reasons of better comparison, for every scenario not the likelihood profile but the MLE and the resulting confidence intervals in both directions, are presented.

Monitoring stations

In Figure 6.6, the resulting confidence intervals for various monitoring networks are compared, which differ in the number and location of considered monitoring stations. Regarding the uncertainty in the parameters x_s and t_s, when the cross-sections A to C are considered, the farther the monitoring station is located away from the source, the higher the uncertainty in both parameters. This could be confirmed by Ghane et al. (2016) and Wang et al. (2018), who observed increasing deviations between estimated and actual PSP values the further downstream the monitoring station was located. The lateral location of the monitoring station does not seem to significantly influence the results. The consideration of two monitoring stations in one cross-section can slightly reduce parameter uncertainties. The same holds for the consideration of more than one station in the longitudinal direction.

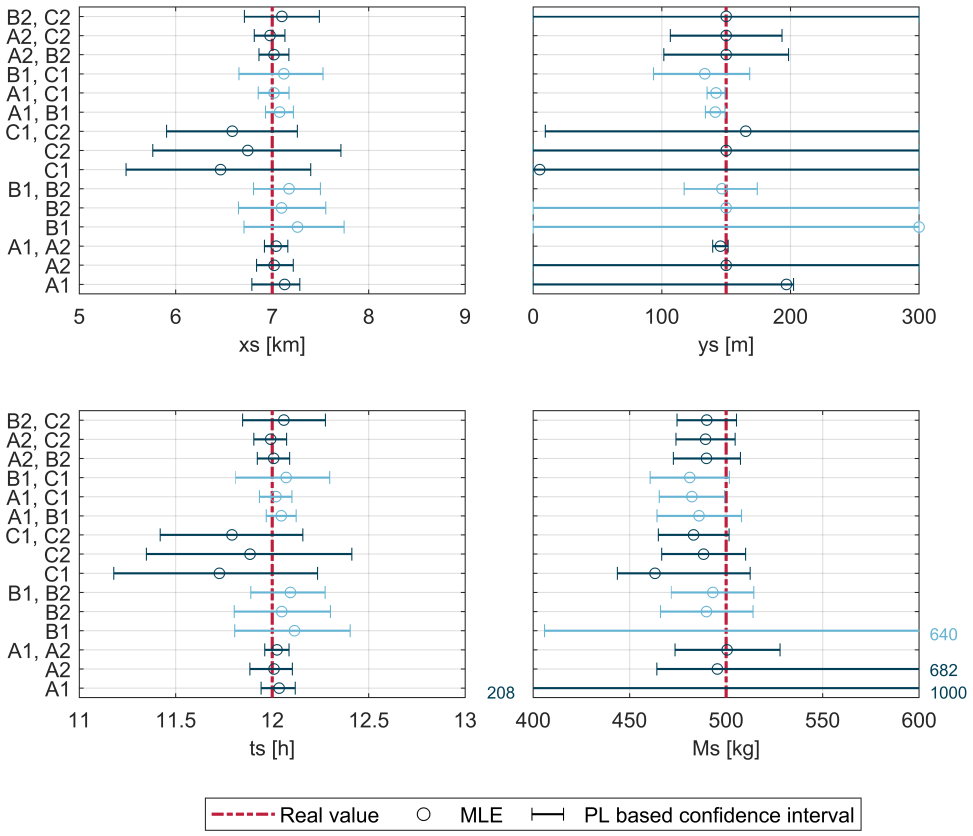

Figure 6.6: Influence of the number and location of different monitoring stations on the identification of pollution source parameters. The circle represents the MLE and the error bar the profile likelihood based 95% confidence interval for each scenario.

As already discussed in Section 6.1.5.1, the parameters y_s and M_s, show poor identifiability under certain monitoring configurations resulting in very wide confidence intervals. The lateral source location y_s can only be reliably estimated if more than one station is considered in cross-section A and B, or when multiple stations in the longitudinal direction

are incorporated in the monitoring network. As explained before, the accurate identification of y_s is dependent on the lateral mixing length. For the reference scenario the estimated mixing length is approx. 11.25 km, as depicted in Figure 6.2. Due to increasing lateral mixing, information regarding the identification of y_s is lost, resulting in increasing uncertainty the further downstream the monitoring station is located. Although full mixing has already taken place when the pollutant plume arrives at cross-section B, y_s is still identifiable when two monitoring stations are used at the named cross-section. This might be surprising at first, but can be explained by the longer mixing length in case the pollutant is introduced at the river banks. In this case the mixing zone would extend up to approx. 45 km downstream of the release point, thus creating different signals at the two monitoring stations inside the cross-section, in contrast to a release in the centre of the cross-section. Large confidence intervals exist for the monitoring cross-section C where full lateral mixing would have already taken place, even if a release from the bank of the river stretch is considered.

Regarding the identification of the total pollutant mass M_s the opposite can be observed. With increasing distance between source location and monitoring station, the confidence intervals become more narrow. This can be explained by a decreasing interaction effect between y_s and M_s. The consideration of more than one monitoring station only has an influence if full lateral mixing has not taken place yet.

Longitudinal measurements

The derived confidence intervals for the four pollution source parameters, when using longitudinal measurements, are displayed in Figure 6.7. For the longitudinal source location x_s and the release time t_s finite confidence intervals can be obtained for all scenarios. The closer the time of the measurement to the release time of the pollutant the narrower the confidence intervals. The lateral location, i.e. if the monitoring is performed along the centre or the river bank, has not a significant influence on the results. The consideration of an additional measurement campaign further downstream can lead to a slight reduction in the uncertainty of estimated parameters.

Regarding the identifiability of the parameters y_s and M_s, similar conclusions as to the measurement at monitoring stations can be drawn. If only a single longitudinal measurement campaign is performed before full lateral mixing has taken place, the total pollutant mass M_s can only be identified with large uncertainties. Measurements later in time can significantly reduce uncertainties, especially if these are carried out in the river centre, instead of the river bank. In contrast, the lateral source location y_s can only be estimated with acceptable uncertainties if at least two measurement campaigns are carried out which should be located at the river bank.

The results show that both monitoring approaches can be used equally in pollution source identification. It has to be considered, that in this work, it is assumed that data are collected at a single time which is not representative in practice. Nevertheless, for the collection of longitudinal concentration profiles, in contrast to the measurement at predetermined monitoring stations, a minor amount of time is needed for data collection. For the measurement at monitoring stations, the monitoring frequency and duration have to be set according to the system characteristics to prevent the pollutant plume not being detected.

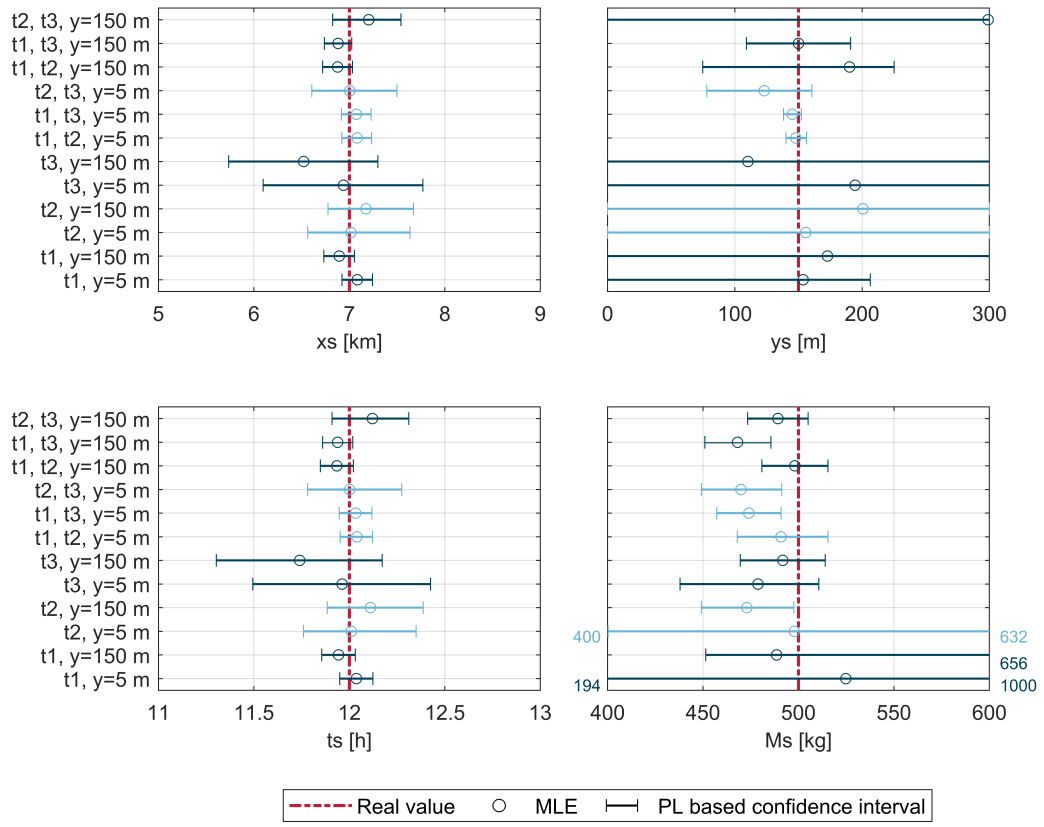

Figure 6.7: Influence of the design of longitudinal measurement campaigns on the identification of pollution source parameters. The circle represents the MLE and the error bar the profile likelihood based 95% confidence interval for each scenario. Time of data collection: $t_1 = 4.4$ h, $t_2 = 15.6$ h, and $t_3 = 26.7$ h after the pollutant release.

6.1.5.4 Influence of the temporal monitoring design

Not only the spatial design, but also the temporal monitoring design will influence the uncertainty in the estimated parameters. In this work, the temporal design is evaluated with regard to the monitoring frequency and the start of the monitoring. The analysis is based on the monitoring stations B1 and B2. For comparison, the reference scenario considers a monitoring frequency of 15 min, a start of the monitoring 11.5 h after the release and a total monitoring duration of 8 h.

For the analysis of the temporal design, a monitoring frequency of 30 min and 60 min is considered, resulting in a total number of 17 and 9 measurements, respectively, at each monitoring station. Additionally, the influence of the start time of the monitoring is analysed. Here, three different points in time are considered, including a start of the monitoring 14.5 h, 15.5 h and 16.5 h after the initial release of the pollutant. The considered times refer to a start of the monitoring when the concentration time series have reached half of their maximum value, when the maximum concentration is reached, and when the concentration time series have decreased to half of their maximum value. In total, 21, 17 and 13 measurements are considered at each monitoring station for the corresponding start times.

The results for the analysis of the temporal design are presented in Figure 6.8. Regarding

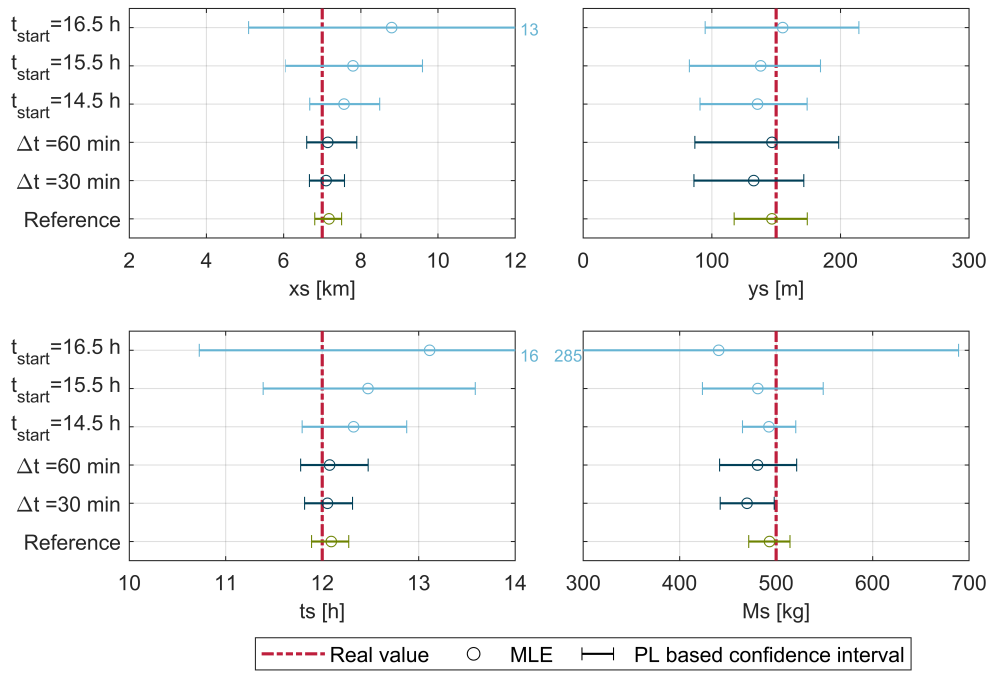

Figure 6.8: Influence of the temporal monitoring design on the identification of pollution source parameters. The circle represents the MLE and the error bar the profile likelihood based 95% confidence interval for each scenario. The analysis is based on the monitoring stations B1 and B2. The reference scenario considers a monitoring frequency of 15 min and a start of the monitoring 11.5 h after the release.

the monitoring frequency, a decrease in the monitoring frequency leads to increased uncertainties in the estimated parameters. This is to be expected, as the number of available monitoring data influences the width of the confidence intervals. Nevertheless, all PSP can still be estimated with relatively small uncertainties and the MLE does not deviate significantly from the real parameter values even if a monitoring frequency of 60 min is used. In practice, the monitoring frequency has to be chosen according to the hydrodynamic characteristics (e.g. flow velocity, longitudinal dispersion). A highly advective system will require a higher monitoring frequency to avoid that the pollutant plume might not be detected.

Regarding the start of the monitoring, a significant impact can be observed on the MLE and the derived confidence intervals of the considered source parameters. The later the monitoring starts at the stations B1 and B2, the larger the confidence intervals for the parameters x_s, t_s and M_s. In contrast, for the parameter y_s only a minor impact can be observed. Based on the results, it is strongly recommended to start the monitoring before the pollutant plume actually arrives at the considered monitoring stations. A reliable estimation of source parameters can only be expected when the complete concentration profile is recorded.

6.1.5.5 Practical guidelines for the monitoring design

Given the results of the preceding analysis, some practical guidelines for the design of a monitoring network in the case of a pollution incident can be summarized. It has to be noted that the considered river stretch represents idealized conditions assuming a straight river section with no tortuosity, a rectangular cross-section, and steady hydrodynamics. Therefore, the given suggestions can only be understood as general guidelines.

Regarding the longitudinal source location x_s and the release time t_s, monitoring stations should be located as close as possible to the potential source. The monitoring program should therefore be started as soon as possible after detection. Multiple stations in one cross-section or along the longitudinal direction can reduce uncertainties in the estimated parameters. The results imply that the location of the monitoring location in the lateral direction does not significantly affect the results. Under economical considerations, a station at the river bank might be more suitable. Nevertheless, it has to made certain that the pollutant can actually be measured there, as lateral mixing up to this location might not have taken place yet. For the application of longitudinal measurements the same guidelines can be applied. The earlier the measurement the more accurate the identification of x_s and t_s. Additional measurement campaigns at a later time further downstream can further reduce uncertainties.

In contrast to the identification of x_s and t_s, the uncertainty in the estimated total pollutant mass M_s reduces the further the monitoring station is located away from the source. This is due to the interaction with the lateral source location y_s. If full lateral mixing has not taken place yet, measurements should be collected at at least two monitoring stations in one cross-section or at multiple stations along the longitudinal direction of the river stretch. The same holds for longitudinal measurement campaigns, which should be carried out at at least two different points in time.

The accurate identification of the lateral source location y_s is the most difficult as it is connected to the lateral mixing length. In practice, the identification of y_s might often be regarded as negligible. Nevertheless, y_s should always be incorporated in the identification process. If monitoring stations are still located inside the mixing zone and y_s is falsely set constant to a wrong value, due to interaction effects, errors will be present in the other source parameters, especially in M_s. For an accurate identification of y_s, monitoring should be started as soon as possible after detection at a minimum of two monitoring stations either located in the lateral or longitudinal direction of the river stretch.

The given summary already implies that, depending on the chosen monitoring design, there is a trade-off in the accuracy of different source parameters. Therefore, it should be determined beforehand, which parameter will be the most important in the identification process. Most often, this will be the longitudinal source location, which can be used to identify the responsible polluter. On the other hand, it might also be necessary to estimate the pollutant mass introduced into the river for the planning of mitigation measures. A different monitoring design might be necessary in either of these cases. The design of the monitoring network will further depend on economic considerations. In general, the results imply that the more monitoring data are collected the smaller the uncertainties in the estimated parameters. Nevertheless, economic resources are often limited, which results in a trade-off between cost and parameter uncertainty.

When considering an even longer river stretch with high industrial activity along the river banks, it might be appropriate to design and install an early-warning monitoring network before an actual pollution incident has occurred. In groundwater systems several

authors have already emphasized the use of scientifically designed monitoring networks for pollution source identification (Datta et al. 2009; Amirabdollahian and Datta 2013). Regarding the application in surface waters, Telci et al. (2009) and Park et al. (2014) developed optimal monitoring networks for the Altamaha river system (USA) based on the mean detection time and detection probability. Telci and Aral (2011) and Lee et al. (2018) later applied the designed monitoring networks for pollution source identification in the considered river network. Results of this study indicate that for the identification of the longitudinal source location x_s and the release time t_s the detection time might be an appropriate criterion. Regarding the identification of M_s and y_s, the influence of the mixing length has to be taken into consideration.

6.2 Bidirectional flow

One of the drawbacks of the analytical solution of the 2D ADRE is the consideration of spatial and temporal constant model coefficients. Especially in estuaries, the changing flow direction plays an important role in pollutant transport and mixing. Therefore, for the simulation of pollutant concentrations, unsteady flow conditions and varying flow directions have to be considered . Consequently, for the identifiability analysis of pollution source parameters in a bidirectional flow system, a numerical transport model is set up using the Delft3D software suite.

6.2.1 Methodology

6.2.1.1 Sensitivity and collinearity analysis

For the profile likelihood approach, which is used for the identifiability analysis in unidirectional flow systems in Section 6.1, a significant number of model runs and re-optimizations are necessary. In the case of computationally intensive numerical transport models, other approaches for the identifiability analysis have to be applied. In this work, the approach described by Brun et al. (2001) is adopted to analyse the identifiability of PSP in bidirectional flow systems. The approach was developed to analyse the sensitivity and collinearity of model parameters in large and complex environmental simulation models.

According to Brun et al. (2002), a parameter set θ has to fulfil two conditions to be termed identifiable. First, the model output $f(\theta)$ has to be sufficiently sensitive to individual changes of each parameter in θ. Second, changes in the model output due to changes in single parameters may not be cancelled by appropriate changes in other parameters of θ. The approach, subsequently described, is based on a local approximation of the sensitivity matrix at selected points in the parameter space, and can help assess if these two conditions are satisfied. The sensitivity matrix can be obtained by calculating the first-order partial derivatives at a selected parameter vector θ_0 (Brun et al. 2001):

$$s_{ij} = \left.\frac{\partial f_i(\theta)}{\partial \theta_j}\right|_{\theta=\theta_0} \qquad i = 1, \cdots, n \text{ and } j = 1, \cdots, p \tag{6.3}$$

where s_{ij} coefficients of the sensitivity matrix $S = \{s_{ij}\}$
n length of the model outcome vector $f(\theta) = (f_1(\theta), \cdots, f_n(\theta)^T$
p length of the parameter vector $\theta = (\theta_1, \cdots, \theta_p)^T$

The resulting $n \times p$ sensitivity matrix S is also known as Jacobian or functional matrix. The sensitivity coefficients s_{ij} provide information on the dependency of the modelling output on the parameters. Values close to zero reflect a scarce impact of the jth parameter on the ith modelling output. In contrast, high absolute values of s_{ij} reflect a strong dependency of the jth parameter on the ith modelling output (Freni and Mannina 2012).

The coefficients of the sensitivity matrix S can be approximated numerically using the finite difference method. Usually, a central difference scheme is used, as this provides a better approximation of the sensitivity coefficients (Šimůnek and Hopmans 2002; Li et al. 2018):

$$s_{ij} \approx \frac{f_i(\theta_j - \Delta\theta_j) - f_i(\theta_j + \Delta\theta_j)}{2\Delta\theta_j} \tag{6.4}$$

In this work, the perturbation factor $\Delta\theta_j$ is set to 100 m, 5 min, and 30 g m^{-3} for the release location x_s, the release time t_s, and the pollutant concentration C_s, respectively. The choice of absolute deviations is different from the usually applied relative deviation of 1%, and a result of the spatial and temporal discretization of the numerical transport model. In order to obtain dimension-free sensitivity information that enables the comparison between different parameters, the scaled sensitivity matrix $\overline{S} = \{\overline{s}_{ij}\}$ is calculated (Brun et al. 2001; Shahmohammadi and McAuley 2019):

$$\overline{s}_{ij} = s_{ij}\frac{s_{\theta_j}}{s_{y_i}} \quad i = 1, \cdots, n \quad j = 1, \cdots, p \tag{6.5}$$

where s_{θ_j} scaling factor related to the uncertainty in the initial value of the jth parameter value

s_{y_i} estimate of the standard deviation of the ith measurement

In cases where there is only little prior knowledge available, a reasonable choice of s_{θ_j} can be the value θ_{0_j} itself (Brun et al. 2001). s_{y_i} mainly accounts for different scales of different outputs or weights when data are not identically distributed. In this work, s_{θ_j} is set to θ_{0_j}. The scaling factor s_{y_i} is set constant to unity, implying that all observation values exhibit the same standard deviation.

By visualizing the columns of $\overline{S}$ one can analyse the sensitivity of the model output to individual changes in each parameter. Additionally, pairwise scatter plots of the columns of $\overline{S}$ allow the assessment whether near-linear dependencies exist between pairs of parameters. To detect dependencies between more than two parameters the joint influence of the parameter subset K on the model output has to be considered. By checking the degree of near-linear dependence within the column subsets S_K of the scaled sensitivity matrix, joint parameter interactions can be detected (Brun et al. 2001). Because the norm of the columns can largely influence the results, the normalized sensitivity matrix $\tilde{S} = \{\tilde{s}_{ij}\}$ is considered in the analysis, containing the normalized columns (Brun et al. 2001):

$$\tilde{s}_j = \frac{s_j}{\|s_j\|} \quad j = 1, \cdots, p \tag{6.6}$$

where $\tilde{s}_j$ jth column of the normalized sensitivity matrix $\tilde{S}$

$\|s_j\|$ Euclidean norm of the jth column of S

Based on the normalized sensitivity matrix, the collinearity index for a subset of parameters K can be derived (Brun et al. 2001; Reichert and Vanrolleghem 2001):

$$\gamma_K = \frac{1}{\sqrt{\min EV[\tilde{S_K}^T \tilde{S_K}]}} = \frac{1}{\sqrt{\lambda_{min,K}}} \tag{6.7}$$

where $\tilde{S_K}$ $n \times k$ submatrix of $\tilde{S}$, containing only those columns that correspond to the parameters in K

$\lambda_{min,K}$ smallest eigenvalue of $\tilde{S_K}^T \tilde{S_K}$

The collinearity index γ_K measures the degree of near-linear dependence of the columns of $\tilde{S_K}$. If the columns are orthogonal γ_K equals unity, with increasing degree of linear dependence γ_K approaches infinity (Reichert and Vanrolleghem 2001). In this case, changes in the model output due to small changes in a parameter θ_j can largely be compensated by appropriate changes in other parameters in K (Brun et al. 2002). According to Brun et al. (2002) and Reichert and Vanrolleghem (2001), a parameter subset K is termed poorly identifiable if γ_K exceeds an empirically determined threshold of approximately 10 to 15. The collinearity index γ_K is usually calculated for all subsets of the full parameter set in order to get an overview of the near-linear dependence of different parameter subsets.

6.2.1.2 Optimal experimental design

As already discussed in Chapter 2.2.5, parameter identifiability can be influenced by the monitoring design. An adequate selection of sampling sites, sampling times and frequencies can determine if parameters are identifiable, and increase the accuracy in the estimated parameters (Iliadis 2019; Marsili-Libelli et al. 2014). The research field of optimal experimental design (OED) is concerned with increasing the information content in the collected data such that the parameters can be estimated with the best possible statistical quality. This is usually a measure of the accuracy and/or de-correlation of the estimated parameters (Banga and Balsa-Canto 2008). Approaches for OED in the literature are often based on the Fisher Information Matrix (FIM), which quantifies the information content included in the observations of a monitoring design for the estimation of unknown model parameters (Sun and Sun 2015). The FIM is based on the sensitivity matrix S defined in Equation 6.4 (Shahmohammadi and McAuley 2019):

$$FIM = S^T \Sigma_\epsilon^{-1} S \tag{6.8}$$

with Σ_ϵ^{-1} being the variance-covariance matrix of the measurement noise. In the case that the scaled sensitivity matrix is used, Σ_ϵ^{-1} can be ignored, because the variance-covariance information is already incorporated via the scaling factors s_{y_i} (Shahmohammadi and McAuley 2019).

It can be noted, that the inverse of the FIM yields the approximate covariance matrix Σ_p of the parameter estimate $\hat{\theta}$, which is usually used to obtain confidence intervals (compare Equation 2.12 of Chapter 2.2.4):

$$FIM = \Sigma_p^{-1} \tag{6.9}$$

The information content of different monitoring designs can be compared using a scalar function $\phi[\cdot]$ which can be based on the trace, the determinant or the eigenvalues of the FIM. The scalar functions are also called optimality criteria. A popular criterion is the D-optimality criterion, which is based on the determinant of the FIM (Sun and Sun 2015; Marsili-Libelli and Giusti 2008):

$$\phi[FIM] = \max(\det(FIM)) \tag{6.10}$$

The determinant of a matrix gives information regarding the linear dependency between the matrix columns. If $\det(F) = 0$, at least two columns of the sensitivity matrix are linear combinations of each other; the matrix is singular. In this case, it is not possible to obtain unique parameter values from the observation data. Otherwise, if $\det(F) \neq 0$, the parameters are identifiable (Li et al. 2018). For identifiable parameters, a greater determinant value indicates smaller uncertainties in the estimated parameters (Li et al. 2018). From a geometric perspective, the D-optimality criterion seeks to minimize the volume of the confidence ellipsoid (Sun and Sun 2015; Banga and Balsa-Canto 2008).

Another criterion is the E-optimality criterion, which is based on the maximization of the smallest eigenvalue of the FIM (Sun and Sun 2015):

$$\phi[FIM] = \max(\lambda_{min}(FIM)) \tag{6.11}$$

In the case of linear dependence amongst two or more columns of the FIM, at least one of the corresponding eigenvalues is equal to zero. Regarding parameter identifiability, larger eigenvalues correspond to a decreased correlation between different model parameters. In geometrical terms, the E-optimality criterion seeks to minimize the length of the largest axis length of the confidence ellipsoid, which is equivalent to minimizing the largest variance in the estimated parameters (Sun and Sun 2015, p. 466).

Different optimality criteria can lead to different monitoring designs (Atkinson et al. (2007), as cited in Sun and Sun (2015, p. 470)). Therefore, in this work, both the D- and the E-optimality criteria are compared. In general, the D-optimality criterion improves overall information content, while the E-optimality criterion builds a compromise between improving information and parameter de-correlation (García et al. 2017).

6.2.2 Setup of a synthetic test case in Delft3D

To analyse parameter identifiability in bidirectional flow systems, a hypothetical two-dimensional test case is set up in Delft3D. The test case is based on the main characteristics of the Thi Vai Estuary, for which a source identification approach will be applied in Chapter 8 of this thesis.

The hypothetical test case is based on a rectangular river stretch with a width of 500 m and a river length of 30 km. The cell size is set to 50 m and 100 m in the lateral and longitudinal directions, respectively. In total, the computational grid consists of 3000 grid cells. The computational grid possesses two open boundaries. The upstream boundary represents the freshwater inflow into the estuary. For the Thi Vai Estuary, the mean freshwater inflow is very small and only about 17.6 $\mathrm{m^3\,s^{-1}}$ (Table A.1). Consequently, for the upstream boundary of the synthetic test case a constant freshwater inflow of 20 $\mathrm{m^3\,s^{-1}}$

Table 6.2: Main characteristics of the synthetic two-dimensional bidirectional test case.

	Parameter	**Value**
Geometry	Length	30 km
	Width	500 m
	Depth	10 m
	Cell size in longitudinal direction	100 m
	Cell size in lateral direction	50 m
	Total grid cells	3000 cells
Boundary conditions	Upper boundary	$20\,m^3\,s^{-1}$
	Lower boundary	Tidal constituents of tide gauge Cai Mep
Model parameters for Delft3D-FLOW	Roughness (Manning)	$0.02\,s\,m^{-1/3}$
	Horizontal eddy viscosity	$1\,m^2\,s^{-1}$
Model parameters for Delft3D-WAQ	Longitudinal dispersion	$25\,m^2\,s^{-1}$
	Lateral dispersion	$0.5\,m^2\,s^{-1}$
	Decay rate	$0\,d^{-1}$

is considered. The lower boundary represents the tidal influence of the open sea. Here, astronomical components of the station Cai Mep are applied (Table A.2).

The modelling program Delft3D-FLOW is used for the hydrodynamic simulations. The communication files created in Delft3D-FLOW serve as input to the transport model Delft3D-WAQ, which is used for all subsequent pollutant transport simulations. The pollutant is considered to be conservative. An overview of the described properties of the synthetic test case is given in Table 6.2

6.2.3 Reference scenarios

The identifiability analysis in the bidirectional flow system is based on an instantaneous pollutant release. The source term is defined by the longitudinal source location x_s, the lateral source location y_s, the release time t_s and the total pollutant mass M_s. For non-linear models, the sensitivity coefficients calculated at different points in the parameter space will differ (Hill and Tiedeman 2007). Therefore, four reference scenarios are selected, which differ in their pollutant release time, due to the consideration of an unsteady flow system. On the one hand, a pollutant release at slack water before ebb tide (SET) and flood tide (SFT) is considered. The time of release is initiated by a change in the flow direction in these scenarios. On the other hand, the time of release is set to the point in time where ebb and flood tide reach their corresponding maximum flow velocity. The scenarios are referred to as maximum ebb tide (MET) and flood tide (MFT), respectively. The definition of release times is based on the simulated discharge at the source location. The discharge time series and the corresponding release times are depicted in Figure 6.9.

While the release times differ in the four scenarios, the source location and the total pollutant mass are kept constant. In all scenarios, the pollutant release takes place at the south bank of the river stretch at KM 15 (Figure 6.10). It is further assumed that the pollutant release can only take place from the right bank of the river stretch. Thus,

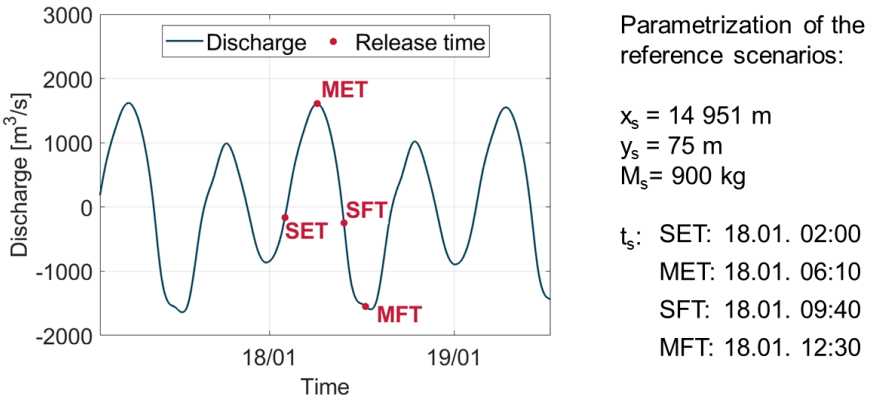

Figure 6.9: Parametrization of the four reference scenarios for the bidirectional synthetic test case and discharge measured at the source location with pollutant release times marked in red.

interaction effects between the total pollutant mass M_s and the lateral source location y_s, discussed in Section 6.1 can be ignored. The identifiability analysis focuses instead only on the parameters x_s, t_s and M_s. In each scenario, during one simulation time step (equal to 5 min) a conservative tracer with a discharge of $1\,\mathrm{m^3\,s^{-1}}$ and a pollutant concentration of $3000\,\mathrm{g\,m^{-3}}$ is released into the estuary. This leads to a total pollutant mass M_s of 900 kg. A summary of the parametrization of the four reference scenarios is given in Figure 6.9.

6.2.4 Monitoring data

All analysis steps, including the sensitivity and collinearity analysis, as well as the calculation of the FIM, are based on the sensitivity matrix. In this work, the sensitivity matrix is evaluated at the true parameter vector of each reference scenario. Measurement errors are not considered in the analysis. Consequently, the covariance matrix of the measurement errors, which is used for the calculation of the FIM, is set equal to the identity matrix (Jin et al. 2014). In comparison, under the assumption that measurement errors are independent and identically normally distributed, the FIM would become $FIM = \sigma^{-1} S^T S$ (Sun and Sun 2015). As σ would only influence the absolute values of the FIM, the assumption of perfect monitoring data would lead to the same conclusions regarding the comparison of different monitoring designs. Therefore, the monitoring design can already be validated, before actual measurements are conducted in the field.

For the sensitivity and collinearity analysis of the described reference scenarios two monitoring stations, one upstream (C1) and one downstream (F1) of the source location, are considered. The other monitoring stations depicted in Figure 6.10 are further used to compare the influence of the spatial monitoring design on the identifiability of pollution source parameters in Section 6.2.5.3 using optimality criteria which are based on the FIM.

The total simulation time extends over two months (15.01. to 15.03.). The simulation time step is set to 5 min. For the sensitivity and collinearity analysis, the results of the entire simulation period are used. The same holds for the comparison of the spatial design of the monitoring network. Further, in Section 6.2.5.4, the influence of the temporal monitoring design on parameter identifiability is assessed. Here, varying monitoring durations and frequencies are considered.

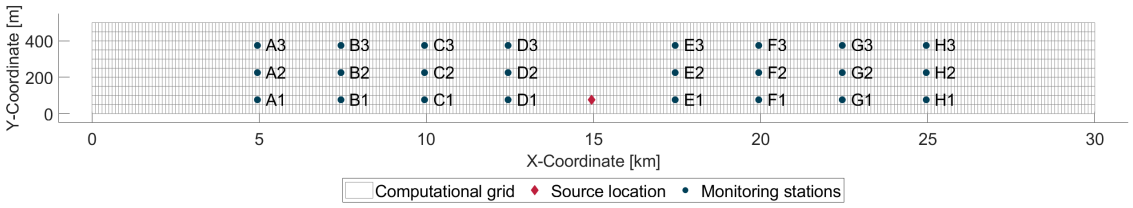

Figure 6.10: Position of the source location and the monitoring stations in the two-dimensional test case representing the bidirectional flow system.

6.2.5 Results and Discussion

6.2.5.1 Sensitivity and collinearity analysis

In this section, the sensitivity and collinearity of the source parameters of an instantaneous pollutant release in a bidirectional flow system are evaluated. As described in Section 6.2.3, four reference scenarios are considered. In the subsequent sections, the following abbreviations will be used for these reference scenarios: Slack water before ebb tide (SET), Maximum ebb tide (MET), Slack water before flood tide (SFT), and Maximum flood tide (MFT).

In Figure 6.11, the columns of the calculated scaled sensitivity matrix are plotted against time for each reference scenario. The sensitivity matrix describes the influence of small changes in the parameter values on the model output, in this thesis the simulated pollutant concentrations. The analysis is based on the monitoring stations C1 and F1, which are located up- and downstream of the source, respectively. Based on Figure 6.11, it can be stated that the model output is sensitive to all three source parameters, although this is a little bit difficult to observe for the pollutant mass M_s. Insensitivity to one of the parameters would result in a constant value of zero over time, entailing that the parameter is non-identifiable. Overall, it can be concluded that each parameter can be considered as potentially identifiable at least on an individual basis in all four scenarios.

Depending on the considered scenario, the sensitivity is higher at the up- or downstream monitoring station. For the scenarios SET and MET, the model is more sensitive at the downstream monitoring station F1, because the pollutant plume passes this station first. In contrast, for the scenario SFT the model shows a higher sensitivity at the upstream station C1. In this case, the pollutant plume is initially transported upstream after its release, due to the reversed flow direction. For the scenario MFT, both monitoring stations show similar, but in comparison to the other scenarios, reduced sensitivities. The results imply, that the sensitivity of the model output to parameter changes is dependent on the time of detection at the monitoring stations. This is further discussed in Section 6.2.5.3.

It can further be observed, that especially the parameters x_s and t_s show their highest sensitivity at the beginning, when the pollutant is initially detected at the monitoring stations. The sensitivity tends towards zero approximately two days after detection for almost all scenarios, although concentration measurements are still well above zero. This implies that monitoring has to be started immediately after detection of the pollutant plume. Otherwise, the parameters can not be accurately estimated because the concentration profiles of different scenarios will become more and more similar after a short period of time.

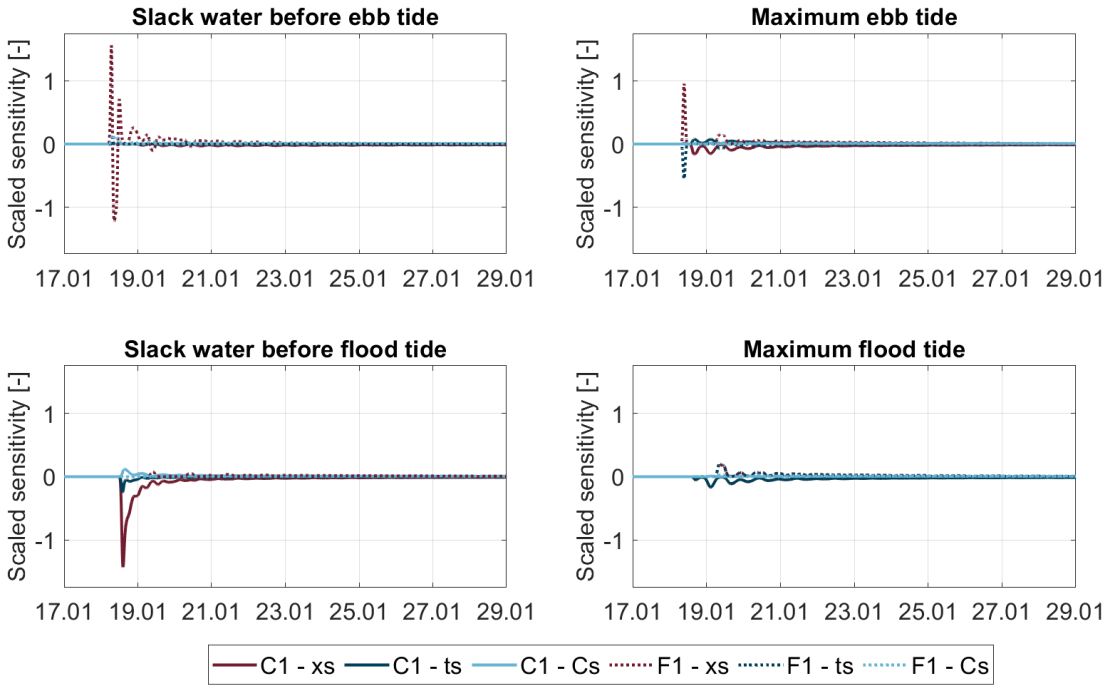

Figure 6.11: Scaled sensitivities for the pollution source parameters x_s, t_s and M_s considering the monitoring stations C1 (solid) and F1 (dashed).

The scaled sensitivity matrix is further used to derive pairwise scatter plots which are presented in Figure 6.12. With the help of these plots, linear dependencies between pairs of parameters can be detected. Especially for the scenarios MET and MFT, a distinct linear interaction between the parameters x_s and t_s can be observed. For the scenario BFT the interaction is still visible, but not as strong as in the other two scenarios. Additionally, in some of the scenarios slight interaction effects can be observed between C_s and the other two source parameters. However, this interaction is not as strong as for x_s and t_s. Strong interaction effects between different model parameters are problematic, because in this case a change in one parameter value can be compensated by a change in another parameter.

To quantify existing interaction effects, and to further assess joint interaction effects between more than two parameters, collinearity indices are calculated for all parameter subsets. Results for the considered reference scenarios are presented in Table 6.3. According to Brun et al. (2002) and Reichert and Vanrolleghem (2001), critical values for the collinearity index lie in the range of 5 to 20. The collinearity indices confirm the findings from Figure 6.12. As can be observed in Table 6.3, for the scenarios SET and SFT, the collinearity indices are sufficiently small. In contrast, for the scenarios MET and MFT, collinearity indices of 14.83 and 41.54 were derived for the full parameter set. This is a result of near collinearity between the columns of S corresponding to the parameters x_s and t_s. High collinearity indices indicate that parameters are only poorly identifiable.

In summary, the results of the sensitivity analysis imply that the model output is sufficiently sensitive to changes in the considered source parameters. Nevertheless, a strong linear dependency between the longitudinal source location x_s and the release time t_s could be detected. Jha and Datta (2014) already addressed the arising complexities in PSI due to the interrelation between the spatial location and the time of activity. However, they discussed this in the context of groundwater systems, and so far this has not

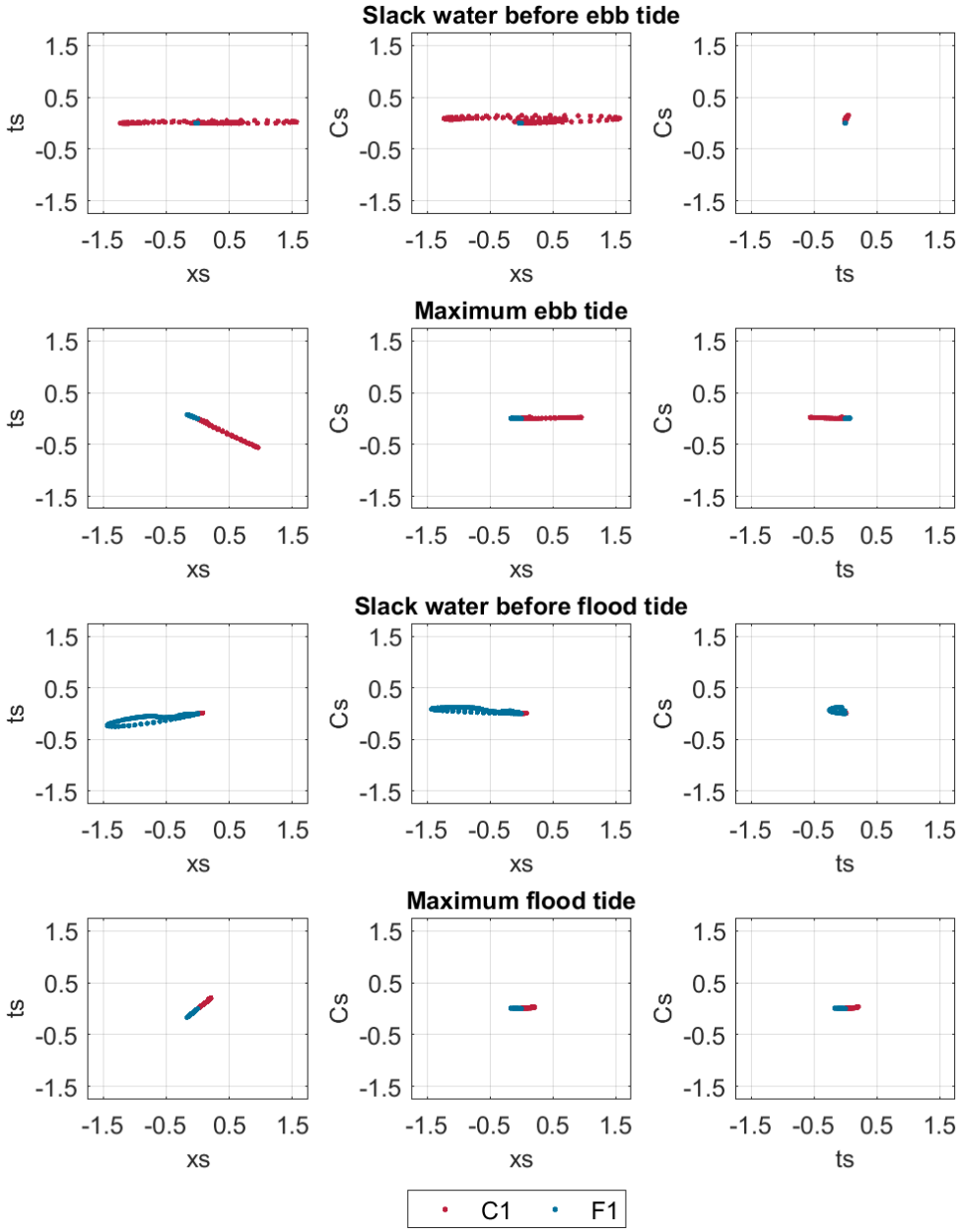

Figure 6.12: Pairwise scatter plots of the columns of the calculated scaled sensitivity matrix $\overline{S}$ for the pollution source parameters x_s, t_s and M_s considering the monitoring stations C1 and F1.

Table 6.3: Collinearity indices for specific parameter subsets including the pollution source parameters x_s, t_s and M_s. For the calculation the monitoring stations C1 and F1 are considered.

Parameters	SET	MET	SFT	MFT
x_s, t_s	1.20	14.68	4.15	41.15
x_s, C_s	1.02	1.00	1.79	1.02
t_s, C_s	1.59	1.01	1.54	1.02
x_s, t_s, C_s	1.81	14.83	4.62	41.54

been discussed in the literature for surface water systems. In unsteady bidirectional flow systems like estuaries, the strength of this interaction is dependent on the time of the release in the tidal cycle. Around times where the flow velocity reaches its corresponding maximum value (e.g. MET or MFT), a stronger correlation exists. Regarding parameter estimation, poor parameter identifiability will decrease the accuracy and precision in the obtained parameters. Additionally, the optimization procedure will be affected and might show signs of slow and possibly premature convergence.

6.2.5.2 Visualization of the response surface

To further analyse the dependency between the longitudinal source location x_s and the release time t_s, the response surface of a selected objective function is visualized. A response surface depicts the shape of the objective function with respect to a pair of selected model parameters (Maier et al. 2019). It is obtained by solving the model equations with the appropriate initial and boundary conditions, for a predefined set of possible parameter combinations (Hopmans et al. 2002).

In this work, a total of 6018 different parameter combinations were considered for the visualization of the response surface of the parameters x_s and t_s. The predefined range and discretization of both parameters can be found in Table 6.4. As a response surface can only depict the behaviour of two parameters, the total pollutant mass M_s and the lateral source location y_s were set constant to 900 kg and 75 m, respectively. After the simulation of all scenarios, the simulated concentration data were compared to the concentration data of the defined reference scenarios. For each scenario, the value of the objective function, in this work the sum of squared errors (SSE), was evaluated. To calculate the objective function values, two monitoring stations, namely C1 and F1, located up- and downstream of the actual pollution source, were considered.

Table 6.4: Scenario definition for the visualization of the response surface for the parameters x_s and t_s.

Parameter	Lower bound	Upper bound	Discretization
x_s	10 km	20 km	200 m
t_s	17.01. 02:00	19.01. 12:30	30 min

In Figure 6.13, the response surface of the objective function for each of the four reference scenarios is illustrated. As already discussed in the previous section, a strong interaction between the two pollution source parameters can be observed. The response surface exhibits a flat valley representing the dependency between x_s and t_s. The results show that the valley is much more pronounced for the scenarios MET and MFT and extends over a larger parameter range. This is in accordance with the results of the previous section, where higher collinearity indices could be observed for the mentioned scenarios. In the case the valley is very flat, a large number of potential parameter combinations with very similar objective function values exist which complicate an accurate and precise estimation of source parameters. In contrast to the results of the sensitivity and collinearity analysis in the previous chapter, the dependency between x_s and t_s is only close to linear in the vicinity of the optimum. When considering the entire parameter range, the interaction is clearly non-linear, a result of the unsteady hydrodynamics. This should be taken into consideration when calculating confidence intervals after parameter estimation.

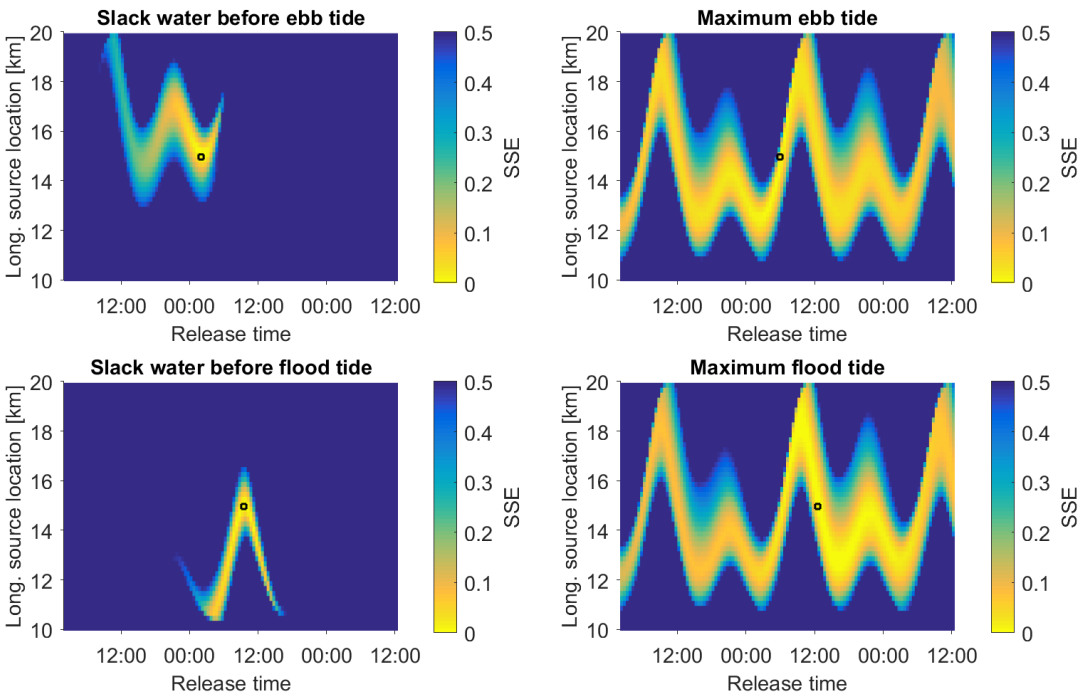

Figure 6.13: Response surface plots of the objective function (SSE) for the source parameters x_s and t_s considering the monitoring stations C1 and F1. The black square marks the location of the global minimum.

6.2.5.3 Influence of the spatial monitoring design

The results of the sensitivity analysis already demonstrated that the sensitivity of the model output to changes in the pollution source parameters is influenced by the location of the considered monitoring station. Therefore, in this section, different monitoring designs are compared using the D- and E-optimality criterion which are based on the FIM. The results are depicted in Figure 6.14. While for the dashed line all three monitoring stations of the respective cross-section are taken into account, for the solid line only the respective monitoring station at the south bank is considered. Additionally, the detection time is plotted for the different monitoring designs, defined as the point in time when the pollutant concentration exceeds a threshold value of 10^{-4} g m^{-3} at the respective monitoring stations.

Regarding the interpretation of the optimality criteria, higher values of the D- and E-optimality criterion indicate a better identifiability of PSP, which results in smaller uncertainties in the estimated parameters. The location of the optimal sampling location is dependent on the time of the pollutant release in the tidal cycle. While for the scenarios SET and MET, the monitoring stations at the cross-section E maximize both optimality criteria, for the scenarios SFT and MFT the upstream stations at the cross-section D is preferred. The further the stations are located away from the source location, the smaller are the values of both optimality criteria. Considering more than one monitoring station in the cross-section can improve parameter identifiability. Nevertheless, the improvement of using three monitoring stations is smaller than using a single station located closer to the actual source. Both optimality criteria show very similar characteristics for the four reference scenarios and will probably produce a very similar monitoring network design

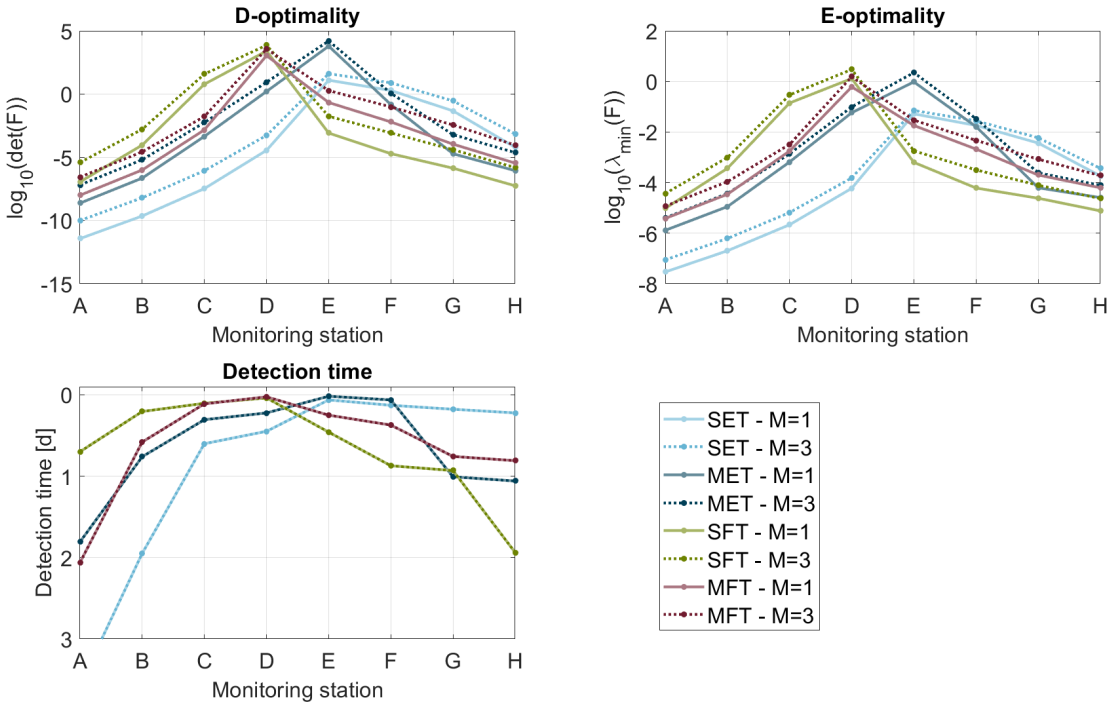

Figure 6.14: Influence of the spatial monitoring design on the identifiability of the pollution source parameters in a bidirectional flow system. For the dashed lines all three monitoring stations of the respective cross-section are taken into account. For the solid lines only the respective monitoring station at the south bank is considered.

when used as design criteria. This is also due to the strong correlation between x_s and t_s, which will have the most influence on the optimality criteria.

When comparing the profiles of the optimality criteria to the detection time, it can be observed that both optimality criteria are closely connected to the detection time of the pollutant plume. The monitoring stations at the cross-sections D and E exhibit the lowest detection time for the four reference scenarios. At the same time, both cross-sections maximize the considered optimality criteria. This leads to the conclusion that the faster the detection through a monitoring location the better the identifiability of pollution source parameters. Monitoring stations located further up- or downstream will lead to higher uncertainties in the estimated parameters. Therefore, the application of the detection time as a design criterion for an optimal monitoring network in the context of PSI, as already considered in Telci and Aral (2011) and Lee et al. (2018), poses an alternative to the D- and E-optimality criteria.

Nevertheless, it has to be stated that although the optimality criteria can be improved through the choice of the spatial monitoring design, it is not possible to de-correlate the longitudinal source location x_s and the release time t_s. For some scenarios (e.g. MET and MFT) uncertainties in the estimated pollution source parameters will naturally be higher.

6.2.5.4 Influence of the temporal monitoring design

In addition to the spatial monitoring design, the temporal monitoring design, including the sampling frequency and duration, can also influence the identifiability and uncertainty in pollution source parameters. As before, to compare different monitoring designs, the D-optimality and E-optimality criterion are considered. For the temporal analysis, the spatial monitoring design is set fixed. Only the monitoring stations C1 and F1 are considered. The influence of the sampling frequency and the monitoring duration on the D- and E-optimality criteria is presented in Figure 6.15.

Regarding the monitoring duration, a slight increase in the D-optimality criterion can be observed up to two weeks for all scenarios. Increasing the monitoring duration further, only has a very minor influence, although pollutant concentrations are still above the detection limit of 10^{-4} g m^{-3} at the monitoring stations C1 and F1. For the E-optimality criterion, the effect of an increase in the monitoring duration is even smaller. Especially for the scenario MET and MFT, almost no changes in the E-optimality criterion can be observed, when increasing the monitoring duration from 0.5 up to 6 weeks.

In contrast, for the monitoring frequency, a significant influence on both optimality criteria can be observed for all four scenarios. An increase in the monitoring frequency leads to a continuous increase in both optimality criteria. At first glance this might be explained by a higher number of observation data which are considered in the analysis. Therefore, for Figure 6.15c the number of data points considered in the analysis is set constant, while the monitoring duration and frequency are changed accordingly. The highest values for both optimality criteria can be observed for the highest monitoring frequency associated with the shortest monitoring duration. The results imply that the information content in the data is significantly higher immediately after detection, which can be confirmed by the results of the sensitivity analysis in Section 6.2.5.1.

6.3 Conclusions

In the case of a pollution incident, the overall aim is the fast and accurate identification of pollution source parameters (PSP), so that the responsible parties can be found and mitigation measures put into action. In this section, two different approaches were applied to analyse the identifiability and uncertainty of the source parameters belonging to an instantaneous pollutant release in a uni- and bidirectional flow system. Additionally, the influence of the spatial and temporal monitoring design was evaluated. For unidirectional flow systems, under the assumption of steady hydrodynamics, an analytical solution of the two-dimensional advection-dispersion-reaction-equation was applied to model the pollutant transport inside the river. The profile-likelihood approach was adopted to determine parameter identifiability and uncertainty. To represent the tidal influence on the hydrodynamics, for bidirectional systems, a numerical transport model was set up. Due to the high computational demand of the profile likelihood approach, a different approach was applied for the evaluation of parameter identifiability. The selected approach is based on a local approximation of the sensitivity matrix at selected points in the parameter space which enables the evaluation of parameter sensitivity and collinearity. For the comparison of different monitoring designs, optimality criteria based on the FIM were derived. It has to be noted that both approaches address parameter identifiability on a local scale.

For both systems, a linear dependency between the longitudinal release location x_s and the release time t_s could be observed. In bidirectional flow systems, the strength of this

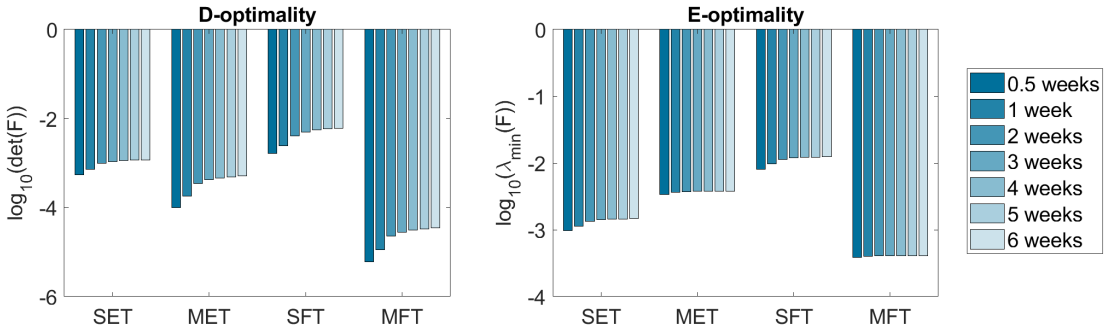

(a) Calculated D- and E-optimality criteria for different monitoring durations. The monitoring frequency is set constant to 1 h.

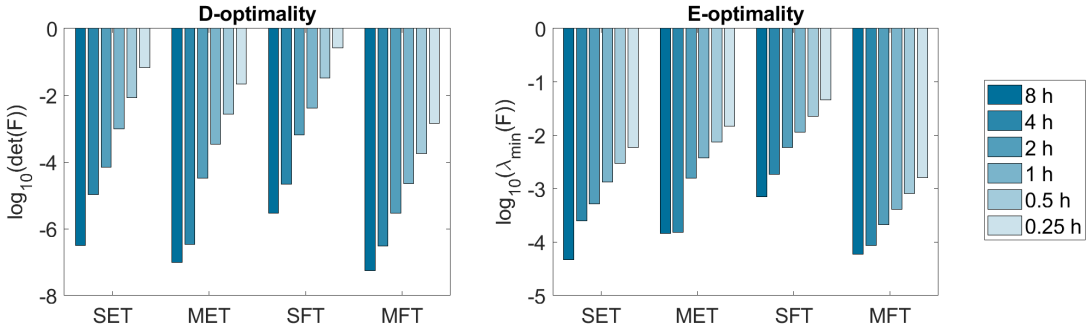

(b) Calculated D- and E-optimality criteria for different monitoring frequencies. The monitoring duration is set constant to two weeks.

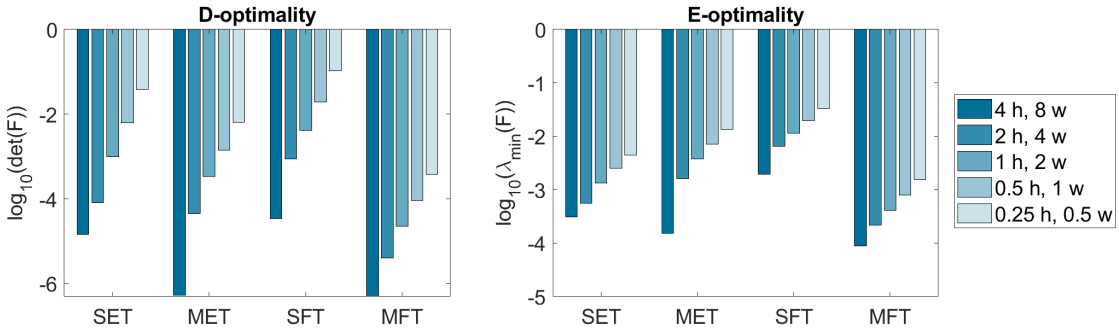

(c) Calculated D- and E-optimality criteria for different monitoring durations and frequencies. The total number of considered observation data is constant for all scenarios.

Figure 6.15: Influence of the temporal monitoring design on the identifiability of pollution source parameters in a bidirectional flow system. The analysis is based on the monitoring stations C1 and F1.

interaction is dependent of the time of release in the tidal cycle. If the release occurs at the time of maximum ebb or flood tide current, the correlation between both source parameters is higher than when the release occurs around slack tide. Additionally, for unidirectional flow systems a non-linear interaction effect between the lateral source location y_s and the total pollutant mass M_s could be detected, which depends on the mixing length and the corresponding position of the considered monitoring station. For the analysis in bidirectional systems, the lateral source location was set constant, so that this interaction

was not taken into account.

A comparison of different monitoring designs further indicates that in both systems, the spatial and temporal design of the monitoring network have a significant influence on the uncertainty in PSP. Regarding the spatial design, in general, monitoring stations located closer to the source location improve the estimation of source parameters. This applies to all parameters except to the total pollutant mass. Due to the interaction of the pollutant mass and the lateral source location, the uncertainty reduces the further the station is located away from the source. In bidirectional systems, the position of the optimal monitoring location is dependent on the time of release in the tidal cycle and can either be located up- or downstream of the source location.

Regarding the temporal design, the analysis in both systems has shown that information content in observation data is at its highest immediately after detection at the monitoring stations. It is therefore strongly recommended to start with the monitoring before the pollutant plume actually arrives at the considered monitoring stations. In unidirectional flow systems, the whole concentration profile should be measured at the considered monitoring stations. In bidirectional systems, it is sufficient to only measure the first part of the concentration profiles as the sensitivity of observations to a change in the parameters reduces to zero over time. A high temporal frequency can additionally lead to a reduction in parameter uncertainties in both systems.

In the upcoming section, the efficiency of two numerical optimization approaches regarding the estimation of pollution source parameters of an instantaneous pollutant release are compared. The results obtained in this section help to understand the complexities arising in the estimation process and facilitate the interpretation of estimation results. As pointed out in Chapter 2.2.5, the design of an optimal monitoring network, prior to parameter estimation, can reduce the risk of obtaining an ill-posed problem. The results of this section give valuable advice regarding the optimal design of a monitoring network for the reliable estimation of PSP in the case of a pollution incident. Results are used in Chapter 8.1 to design an optimal monitoring network for the Thi Vai Estuary.

7 Comparison of source identification approaches under bidirectional flow conditions

In this chapter, the simulation-optimization approach is applied to identify the unknown source parameters of an instantaneous pollutant release under bidirectional flow conditions. Two optimization approaches, which were both applied in existing literature, are compared. The approach usually applied in the literature is based on the simultaneous identification of all unknown source parameters. In contrast, Jing et al. (2018) presented a modified approach, in which the estimation of the source parameters is decoupled from one another. Both approaches are applied to the previously presented synthetic bidirectional test case using perfect and noise perturbed monitoring data. Several pollution scenarios, which differ in the release time, are considered.

7.1 Optimization approaches

7.1.1 Simultaneous optimization

In general, when the simulation-optimization approach is applied to identify the source parameters of a spill incident, all parameters are estimated simultaneously. Usually, a global optimization algorithm is used for this task. For example, Han et al. (2014) applied the Differential Evolution (DE) algorithm to identify a single instantaneous pollutant release in a river stretch. Zhang and Xin (2017) applied the genetic algorithm to identify multiple continuous pollutant releases from different point sources. Both studies assumed steady flow and used an analytical solution of the ADRE. Parolin et al. (2015) compared three different optimization algorithms for the estimation of the source location of a continuous point source in an estuary. These include the Luus-Jaakola method, the particle collision algorithm, and the ant colony optimization algorithm. In contrast to the previous works, Parolin et al. (2015) used a numerical transport model to simulate the pollutant transport inside the estuary under consideration. All mentioned works could provide accurate results under the specified assumptions regarding the hydrodynamic properties and pollutant characteristics. It has to be noted that global optimization algorithms need a considerable number of model runs and are not guaranteed to converge to the global minimum.

Up to now, the simultaneous optimization approach has not been applied to identify the source parameters of an instantaneous pollutant release in an estuary. Therefore, in this work, the approach is applied to the previously presented synthetic bidirectional test case. The results are compared to the decoupled optimization approach, presented in the following section. For the simultaneous identification of the release time t_s, the source location x_s and the total pollutant mass M_s the DE algorithm is chosen. The optimization algorithm is described in more detail in Chapter 2.2.3.2. Other optimization

algorithms, e.g. the genetic algorithm (GA) or particle swarm optimization (PSO) were also tested and provided similar results. The number of individuals in each population NP is set to 30. Following the advice for dependent parameters in Price et al. (2005, p. 166), the scaling factor S and the crossover rate CR are set to 0.8 and 0.9, respectively. The algorithm stops if either the function or parameter tolerance is smaller than 10^{-6}, or if the maximum number of iterations (150) is reached. For a faster computation, individuals of each population are calculated in parallel.

7.1.2 Decoupled optimization

The results of the identifiability analysis in Section 6.2 have shown that a dependency exists between the release time and the longitudinal source location. For unsteady flow systems, this interaction leads to a complex shape of the response surface, which exhibits a flat valley across a large range of the parameter space (Figure 7.1). The difficulty of the problem is increased by the spatial discretization of the numerical model. Because the longitudinal source location x_s is not a continuous variable, multiple local minima or saddle points might exist in the response surface. In this case, the global optimization algorithm might converge prematurely to a local instead of a global minimum.

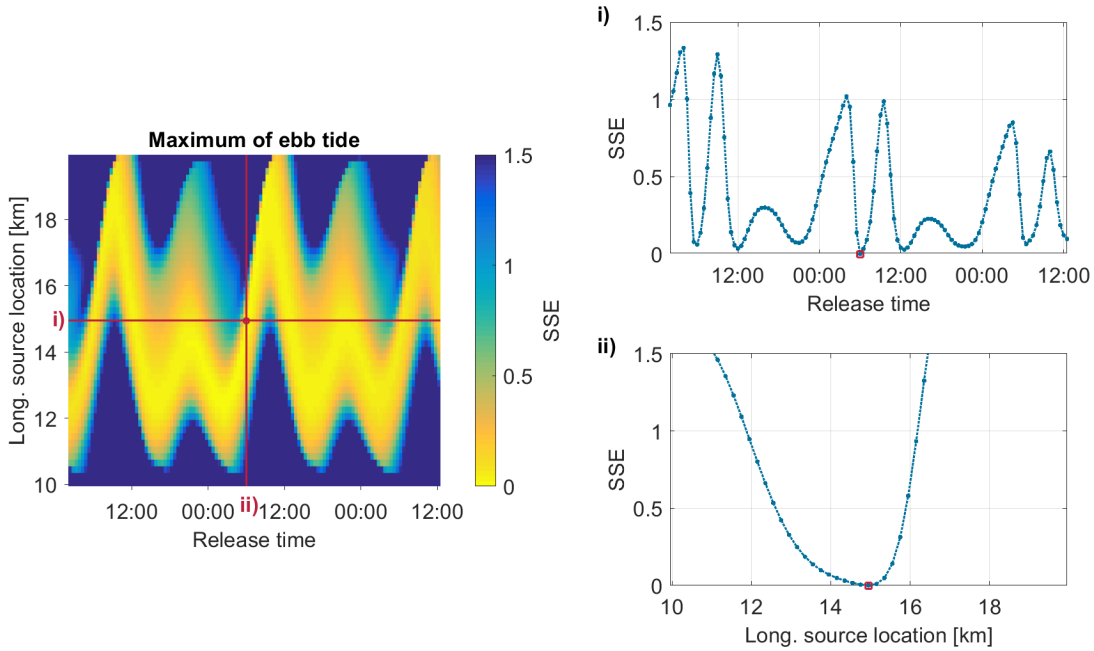

Figure 7.1: Profiles of the objective function setting (i) the longitudinal source location x_s and (ii) the release time t_s constant. (Considered monitoring stations: C1 and F1).

Therefore, a different strategy is proposed, decoupling the optimization of the release time and of the other source parameters. The approach was originally proposed by Jin et al. (2014) and applied to a theoretical instantaneous pollutant release in the Quanzhou Bay, China. The authors decoupled the optimization of all three source parameters, including release time, source location and total pollutant mass. In a first step, the range of potential release times was roughly estimated based on collected observation data. Second, potential release times were selected based on the estimated parameter range. For each potential release time, the source location was estimated using a modified version of the genetic

algorithm and the correlation coefficient as an objective function. In a third step, due to the linear relationship between measured pollutant concentrations and total pollutant mass, the mass could be determined.

In Figure 7.1, two profiles of the objective function are displayed, when either the release time t_s or the source location x_s is set constant. The profile of the objective function for x_s is convex and exhibits only one minimum under the condition that t_s is assumed to be known. In contrast, if x_s is set constant, the profile of t_s is characterized by multiple local minima. It is therefore advantageous to set t_s fixed to a constant value, while optimizing the other source parameters, as considered in Jing et al. (2018).

This work adopts a similar approach to identify the source parameters of an instantaneous point source. As in Jing et al. (2018), based on the collected observation data and installed monitoring system, a range for the potential release time is determined. The range is divided into a set of potential release times based on a predefined discretization. For each of the selected release times, the other source parameters, including the source location and the total pollutant mass, are optimized. Gradually, the discretization of t_s is further decreased from initially 2 h over 30 min to 5 min. The computational effort can be significantly reduced by solving the optimization problems in parallel.

For the optimization, the MATLAB function *fminsearchbnd* based on the Nelder-Mead simplex algorithm is employed (D'Errico 2020). The Nelder Mead simplex algorithm is a local search algorithm. In contrast, a global search algorithm would require a significantly higher number of function evaluations. As multiple optimization problems are considered for the decoupled approach, the use of a global optimization algorithm would result in an enormous increase in computation time. The Nelder-Mead simplex algorithm is a constrained direct method and does not use numerical or analytical gradients of the objective function. The algorithm is described in more detail in Chapter 2.2.3.1. The function tolerance and the parameter tolerance are both set to 10^{-6}. The algorithm *fminsearchbnd* stops when either both criteria are satisfied or the maximum number of iterations (100) is exceeded.

7.2 Coupling between Delft3D and MATLAB

For the simulation-optimization approach, the transport model needs to be directly linked to the optimization algorithm. In this work, the transport model Delft3D-WAQ is linked to the MATLAB environment. During the optimization process, the input file of the transport model is changed in an iterative manner and adapted to new source parameter combinations.

The main input file of Delft3D-WAQ (.inp) is an ASCII file and contains all information about the water quality model, including its linkage to the hydrodynamic model, boundary and initial conditions, and the model parametrization. In addition, information regarding the definition of sources and sinks is included. In the case of an instantaneous point source, the file includes the source location, the release time, and the pollutant concentration. The section of the input file containing the information is displayed in Figure 7.2. Usually, the input file is created and changed using the graphical user interface (GUI) of Delft3D-WAQ. However, for the optimization of pollution source parameters, the named parameters need to be changed in the file and subsequently, the file needs to be run automatically in the MATLAB environment.

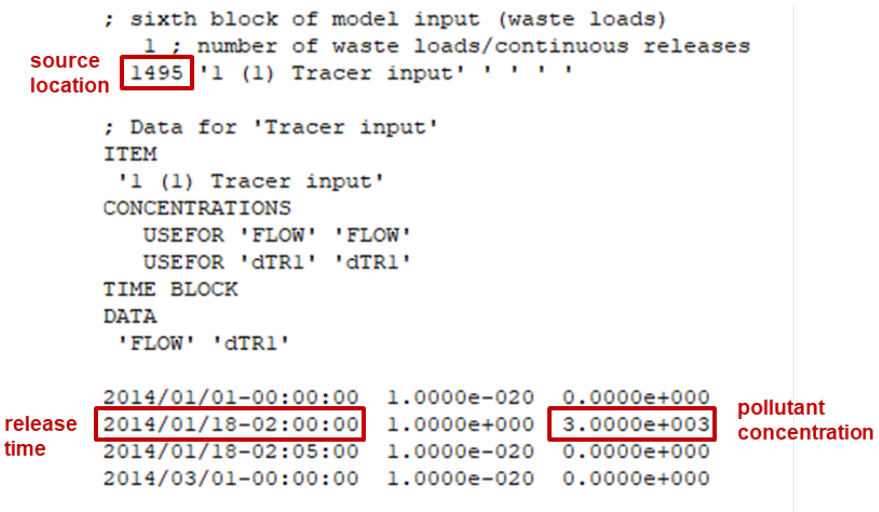

Figure 7.2: Section of the input file of the water quality model Delft3D-WAQ containing the definition of the pollution source parameters.

Therefore, for each function evaluation in the optimization process, the input file of a reference scenario with the same hydrodynamic settings is loaded into the MATLAB environment. The input file of Delft3D-WAQ does not contain direct coordinates for the source location but an integer value for the computational cell, in which the pollutant was released. The link between the x- and y-coordinates of each cell to the integer value is contained in the model schematisation file (.lga), created in the course of the hydrodynamic simulation. Here, the cell with the smallest euclidean distance to the proposed source location is selected. The release time can be directly included in the input file. Because an instantaneous pollutant release is considered, the release duration is set to one simulation time step (e.g. 5 min). Further, the discharge and corresponding pollutant concentration are necessary to fully describe the instantaneous release. In this work, the discharge is set constant and only the pollutant concentration is changed for each model run. After all pollution source parameters are adapted in the input file, it is saved and run automatically inside the MATLAB environment via a batch file.

7.3 Further considerations for the application of both optimization approaches

7.3.1 Scenario definition

Both optimization approaches are applied to the synthetic test case, described in Section 6.2.2. The results of the identifiability analysis in Chapter 6.2 have shown that the identifiability of PSP changes according to the release time. Thus, for the application of both approaches, not one but four reference scenarios are considered, which are defined in Chapter 6.2.3. Furthermore, it is assumed that a pollutant release can only take place from the south bank of the estuary. Thus, the lateral source location y_s is set constant. This reduces the optimization problem to the estimation of only three parameters, namely the longitudinal source location x_s, the release time t_s, and the total pollutant mass M_s.

7.3.2 Monitoring data

For this study, monitoring data are synthetically generated using the simulation results of the pollutant transport model. The results of two monitoring stations, namely C1 and F1, are considered in the optimization process. The monitoring stations are located at the right bank of the river stretch, 5 km up- and downstream of the source location, respectively. It is assumed that the pollution is detected quickly and that monitoring starts one hour after the release. The monitoring frequency is set to 1 h. Regarding the duration of the monitoring the results of Section 6.2.5.4 have shown that the data at the beginning are the most crucial and that sensitivity reduces to zero after a short amount of time. Therefore, the monitoring duration is set to 3 d. Concentration data below a given threshold concentration, e.g. the limit of detection, are set to zero. In this work, a threshold value of 10^{-4} g m^{-3} is adopted. Corresponding concentration time series for the monitoring stations C1 and F1 are presented in Figure A.3.

In the first step, it is assumed that monitoring data are perfect and correspond exactly to the simulated data. In this case, both optimization approaches should converge to the global minimum and lead to an exact identification of the actual source parameters. Nevertheless, in real life, measurement data will certainly contain errors. Therefore, in the second step, artificial noise is introduced into the simulated monitoring data. Errors in the data are considered to be independent and identically distributed, corresponding to a normal distribution with zero-mean and a standard deviation of 0.001 g m^{-3}. Although the estimated parameter values will most likely deviate from the actual values, small changes in the measured values should not lead to significant changes in the estimated parameters; otherwise the problem is termed unstable (Aster et al. 2013).

7.3.3 Objective function

For both optimization approaches, the summed squared error (SSE) is used as the objective function:

$$SSE = \sum_{i=1}^{n} (c_{sim,i} - c_{obs,i})^2 \tag{7.1}$$

where n number of monitoring data
$c_{obs,i}$ observed concentration corresponding to the ith measurement
$c_{sim,i}$ simulated concentration corresponding to the ith measurement

The SSE can be derived from the likelihood function under the assumption that errors are independent and identically normal distributed (see Chapter 2.2.2).

7.3.4 Boundary constraints and initial values

Both selected optimization algorithms require boundary constraints for the parameters to be estimated. In general, boundary constraints help to minimize the set of possible solutions and ensure physical meaning of the estimated parameters. Regarding the bidirectional test case considered in this chapter, it is assumed that the pollutant source is located between the monitoring stations C1 and F1. The upper constraint for the release

time t_s is given by the earliest time of detection at one of the monitoring stations. It is further assumed that the pollutant was introduced into the estuary no more than 12 h before it was detected. If a permanent monitoring network is installed inside the estuary, the lower boundary constraint can also be derived based on the maximum detection time. This will be further discussed in Section 8.2. One option to approximate the total pollutant mass is the simultaneous measurement of the pollutant concentration and the discharge at the lower monitoring station. For simplicity, in this work it is assumed that the total pollutant mass lies in a range ± 150 kg of the actual pollutant mass. The considered lower and upper parameter constraints are summarized in Table 7.1.

Table 7.1: Lower and upper boundary constraints for the optimization of pollution source parameters in the synthetic bidirectional test case.

Parameter	Lower bound	Upper bound
x_s	10 km	20 km
t_s	DT* - 12 h	DT*
M_s	750 kg	1050 kg

*DT: Detection time

For DE, the initial population is created internally by a random selection of parameter values. Regarding the decoupled optimization approach, *fminsearch* is a local optimization algorithm and the initial parameter values can strongly influence the convergence of the algorithm. Therefore, before the start of the optimization, the objective function is evaluated for 10 random parameter combinations. The best parameter combination is selected and used as initial values in the optimization algorithm.

7.4 Results and discussion

In the following, the results of both optimization approaches are presented. In the case when noise-free monitoring data are considered, PSP should be identified correctly without any errors by both approaches. In the case of noise perturbed monitoring data, estimated values for PSP should not deviate significantly from the actual values. Both approaches should converge to the same global minimum for all scenarios.

7.4.1 Perfect monitoring data

In Table 7.2, the results of the simultaneous and decoupled optimization when considering perfect monitoring data are presented. As can be seen by the attained minimum value of the objective function, both approaches could converge to the global minimum for all four considered pollution scenarios. Estimated parameter values are equal or close to their actual values. Minor differences in x_s are due to the spatial model discretization of the numerical transport model. Each grid cell has a length of 100 m in the longitudinal direction. Therefore, the source location can only be located up to an accuracy equal to the grid cell size as all locations inside a grid cell will have the same objective function value. The absolute differences are smaller than 50 m and indicate that the correct grid cell could be found for both optimization approaches in all four pollution scenarios. Regarding the simultaneous optimization, for the scenarios SET and MET the release time slightly

differs from the actual release time. This is due to the temporal discretization of the transport model in which a time step of 5 min is considered.

For the simultaneous optimization approach, in total 3480 to 4170 function evaluations were necessary until the algorithm met one of the convergence criteria. The speed of convergence depends, among other things, on the parametrization of the optimization algorithm. In this work, relatively high values were chosen for the mutation and crossover coefficient. This leads to a higher rate of exploration of the parameter space but at the same time slows down convergence. Nevertheless, earlier tests have shown that the algorithm tends to converge prematurely when coefficients are set to a smaller value. This is mainly due to the dependency between the source location and the release time, as discussed in Chapter 6.2. In comparison to the simultaneous optimization approach, for the decoupled approach the number of function evaluations is slightly smaller and very similar across all four scenarios.

Table 7.2: Results of the simultaneous and decoupled optimization approach considering perfect monitoring data.

Scenario	Absolute error			Obj. func.	Function
	x_s [m]	t_s [min]	M_s [kg]	minimum	evaluations
Simultaneous optimization					
SET	9.83	0.82	0.00	0	3570
MET	21.92	4.15	0.00	0	3480
SFT	18.92	0.00	0.00	0	4170
MFT	10.37	0.00	0.00	0	3840
Decoupled optimization					
SET	10.09	0.00	0.00	0	3184
MET	11.01	0.00	0.00	0	3234
SFT	10.46	0.00	0.00	0	3221
MFT	12.47	0.00	0.00	0	3225

As examples, for the scenarios SET and MFT, the results of the considered optimization steps in the decoupled approach are presented in Figure 7.3. In both cases, the objective function for the release time t_s is convex and possesses a unique global minimum. Similarly to the profile likelihood approach applied in Chapter 6.1, the interaction of t_s with the other source parameters can be evaluated based on the results of each optimization step. Regarding the scenario MFT, the values for the optimal source location x_s are dependent on the tidal dynamics but only vary by 2 km for the considered release times. In contrast, for the scenario SFT, the optimal source location shows a more pronounced dependency with the release time and lies in a range between 12 and 18 km. This already implies that in the case when noise perturbed data are considered, the source location will exhibit larger uncertainties for the scenario MFT. For the scenario SFT, the introduced pollutant mass is almost constant for all release times. In contrast, for the scenario MET, a significant interaction between t_s and M_s can be observed. These observations are in accordance with the results of the collinearity analysis in Section 6.2.5.1.

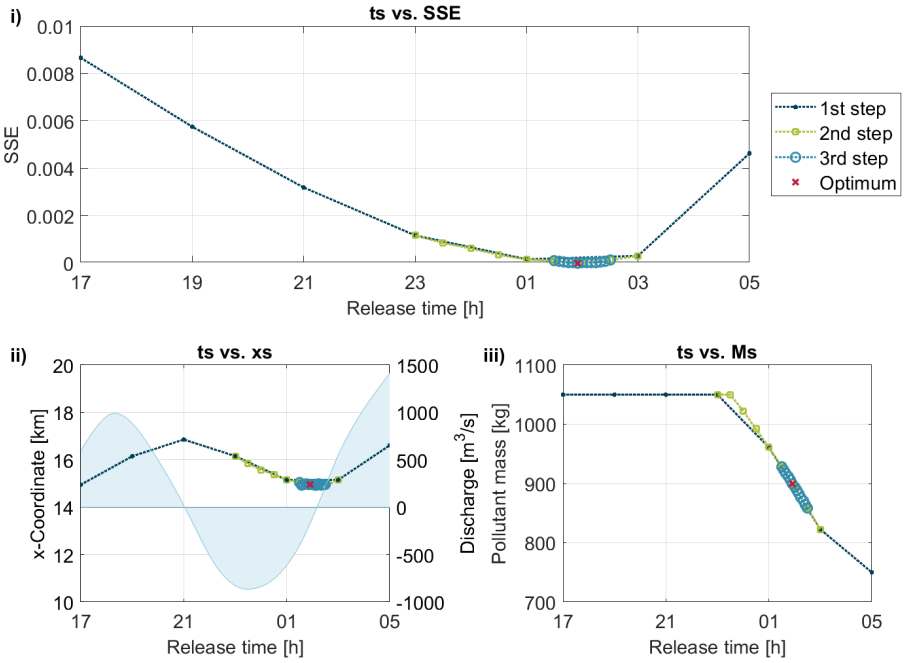

(a) Scenario "Slack water before ebb tide".

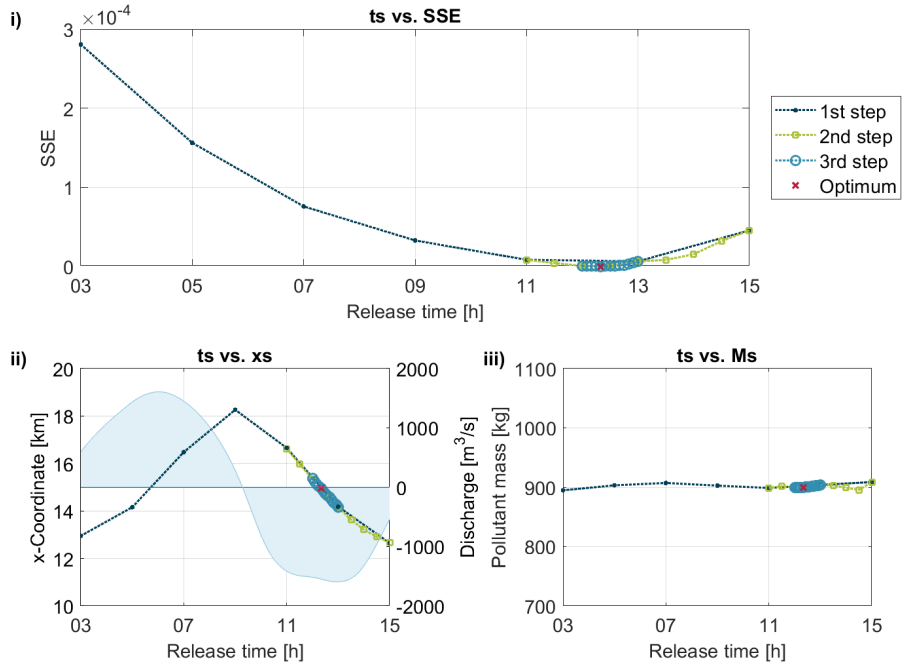

(b) Scenario "Maximum flood tide".

Figure 7.3: Results of the decoupled optimization approach for the scenarios "Slack water before ebb tide" and "Maximum flood tide". i) Change of objective function (SSE) for different release times; ii) Change in the source location for different release times; iii) Change in the pollutant mass for different release times.

In summary, under the assumption of perfect monitoring data, both optimization approaches were able to locate the global minimum of the objective function and estimate the actual source parameter values for all considered pollution scenarios.

7.4.2 Integration of measurement errors

In practical applications, monitoring data contains measurement errors. Therefore, artificial noise was introduced into the synthetically generated monitoring data. Results of both optimization approaches when considering noise-perturbed data are presented in Table 7.3. For the scenarios SET, MET and SFT, both optimization approaches converged to the same minimum. The estimated parameter values are still close to their actual values. As before, slight deviations between the estimated and actual source location x_s are due to the spatial discretization of the numerical transport model. The same holds for the release time t_s. Only in the scenario SFT, a different grid cell and release time were estimated by both optimization approaches.

Regarding the scenario MFT, a comparison of the minimum objective function value obtained by both approaches indicates that the global optimization algorithm converged prematurely to a local instead of the global minimum. The estimated values for the source parameters deviate significantly between both approaches. Reasons for the premature convergence of the global optimization algorithm are most likely the strong dependency between the longitudinal source location and the release time. This was already discussed in Chapter 6.2.

Table 7.3: Results of the simultaneous and decoupled optimization approach considering noise perturbed monitoring data. If the estimated grid cell does not correspond to the actual grid cell, absolute errors for x_s are marked in bold.

Scenario	Absolute error			Obj. func.	Function
	x_s [m]	t_s [min]	M_s [kg]	minimum	evaluations
Simultaneous optimization					
SET	36.21	3.78	9.62	$1.24 \cdot 10^{-4}$	4530
MET	35.68	2.82	0.71	$1.31 \cdot 10^{-4}$	2730
SFT	**89.79**	14.63	9.51	$5.89 \cdot 10^{-5}$	3630
MFT	**297.40**	19.05	10.51	$1.15 \cdot 10^{-4}$	3240
Decoupled optimization					
SET	13.86	0.00	9.60	$1.24 \cdot 10^{-4}$	3181
MET	30.48	0.00	0.70	$1.31 \cdot 10^{-4}$	3200
SFT	**138.88**	15.00	9.51	$5.89 \cdot 10^{-5}$	3283
MFT	4.89	0.00	4.84	$6.15 \cdot 10^{-5}$	3201

Table 7.4 includes, in addition to the actual and estimated parameter values, approximated standard confidence intervals and the parameter correlation matrix for each pollution scenario. Approximated standard confidence intervals are calculated according to Equation 2.13. The correlation matrix is obtained from Equation 2.15. The results indicate that uncertainties are lowest when the pollutant release occurs at slack water before ebb tide (SET). If the pollutant release occurs when the flood tide reaches its corresponding maximum flow velocity (MFT), the longitudinal source location x_s and the release time t_s can only be estimated with very high uncertainties. As standard confidence intervals are only valid if the likelihood function can be approximated by a quadratic function at the parameter estimate $\hat{\theta}$, the resulting confidence intervals were compared to likelihood-based confidence intervals. Following Schwaab et al. (2008), these were calculated based on the saved parameter sets and corresponding objective function values evaluated by the

global optimization algorithm. Both, standard and likelihood-based confidence intervals provided very similar results.

Table 7.4: Actual and estimated parameter values, approximated standard confidence intervals, and correlation matrix for the source parameters of each pollution scenario under the consideration of measurement noise ($\sigma = 0.001$).

			Confidence	Correlation matrix		
Parameter	Actual	Estimate	interval	x_s	t_s	C_s
Slack water before ebb tide						
x_s [km]	14.95	14.91	± 0.02	1.00	-0.56	0.47
t_s [hh:mm]	02:00	01:56	± 00:08		1.00	-0.83
M_s [kg]	900.00	909.62	± 11.45			1.00
Maximum ebb tide						
x_s [km]	14.95	14.91	± 0.26	1.00	0.99	0.16
t_s [hh:mm]	06:10	06:07	± 00:11		1.00	0.18
M_s [kg]	900.00	900.71	± 19.20			1.00
Slack water before flood tide						
x_s [km]	14.95	14.86	± 0.11	1.00	-0.98	0.74
t_s [hh:mm]	09:40	09:55	± 00:12		1.00	-0.61
M_s [kg]	900.00	890.49	± 15.19			1.00
Maximum flood tide						
x_s [km]	14.95	14.95	± 1.09	1.00	-0.99	-0.01
t_s [hh:mm]	12:30	12:30	± 00:56		1.00	0.01
M_s [kg]	900.00	895.16	± 19.25			1.00

As expected, the correlation between x_s and t_s is rather high, leading to a correlation coefficient of 0.99 for the release at maximum ebb and flood tide, respectively. This high correlation is an indication that non-unique parameter estimates might exist (Hill and Tiedeman 2007, p. 135)

7.5 Conclusions

Usually, in the literature, the parameters of a single or multiple pollutant sources are identified simultaneously using a global optimization algorithm (Han et al. 2014; Zhang and Xin 2017). The decoupled approach has only been applied for PSI in Jing et al. (2018). A comparison of the accuracy and efficiency of both approaches has not been carried out up to now. Therefore, in this work, both approaches were applied to identify the source parameters of a single instantaneous spill in a 2D synthetic estuary.

When monitoring data were assumed to be perfect, both approaches were able to detect the global minimum of the objective function and to identify the real source parameters. Under the consideration of measurement noise, in general, both approaches provided very similar results. Estimated parameters were still in proximity to their real values, but depending on the scenario, could possess higher uncertainties. This is supported by the results of the identifiability analysis in Chapter 6.2. Nevertheless, for the scenario MFT,

the global optimization converged prematurely. This is a result of the strong interaction between the source location x_s and the release time t_s as already indicated in Chapter 6.2. This leads to a poor identifiability of both parameters and instability issues due to the very flat shape of the objective function in the vicinity of the global minimum.

Regarding the efficiency of both optimization approaches, a smaller number of model evaluations was needed for the decoupled approach. This is especially important when a complex numerical model with a high computational time is used. In contrast to Jing et al. (2018), in this work a local instead of a global optimization algorithm was used for the decoupled approach. In the decoupled approach, several individual optimization problems are solved. The total number of optimization problems will depend on the initially estimated range of the release time and the required accuracy in the results. The application of a global optimization algorithm like GA will not be feasible if a large number of individual optimization problems are considered. In comparison, the Nelder-Mead simplex algorithm will result in a smaller number of function evaluations. However, it should be noted that a local search algorithm should always be started from several initial values to guarantee that the algorithm actually converged to the global minimum. In this work, it was sufficient to create a random set of initial values and use the best value for the start of the optimization process.

In summary, both approaches showed very similar results. Consequently, the simultaneous as well as the decoupled approach will be transferred and applied to a real-world estuary, the Thi Vai Estuary, in Chapter 8 to further validate both approaches.

8 Pollution source identification in the Thi Vai Estuary

In this chapter, the simulation-optimization approach is transferred to the Thi Vai Estuary. In a first step, an optimal real-time monitoring network is developed for the Thi Vai Estuary. The monitoring network provides the monitoring data to identify the pollution source parameters (PSP) in the case of a pollution incident. Subsequently, several synthetic pollution scenarios are considered to evaluate whether the optimization approach is successful in a real-world estuary.

8.1 Design of an optimal monitoring network

Based on the results of the identifiability analysis in Chapter 6, it can be concluded that the chosen monitoring data can have a significant influence on the accurate identification of source parameters in both rivers and estuaries. The results have shown that data should be collected as early as possible in the case of a pollution spill. For the early detection of a pollutant plume and the provision of data for the identification process, the installation of a real-time monitoring system can be beneficent. This is especially relevant in water bodies which are located in highly industrialized areas, or which serve as a source of drinking water or for the production of food. In this case, an early detection of potential harmful concentration levels and an accurate identification of pollution source parameters is of high importance.

The Thi Vai Estuary is located in one of the core regions of industrial development in Vietnam. Over the last decades, numerous industrial zones have been built in close vicinity to the estuary. Despite this, large parts of the tidal flats in the upper to middle reaches of the estuary are used for the cultivation of fish and shrimps. These have already been severely affected once due to the poising of the Thi Vai Estuary by the company Vedan (Nguyen and Pham 2012). The installation of an on-line water quality monitoring network could present an option for the early detection of possible pollution spills and provide data for the identification of the spill parameters, including the source location.

Consequently, in a first step, an optimal monitoring network is developed for the Thi Vai Estuary. Data from the monitoring network will be used in Section 8.2 for the identification of potential pollution spills. The design of the monitoring network will be based on the following assumptions:

- The pollutant can be detected with an automatic measurement device at pre-defined monitoring stations.
- The pollutant background concentration in the estuary lies below a given threshold concentration.
- A release can only take place in the main stream of the estuary. Tributaries are not considered in the analysis.

Practical limitations of these assumptions will be further discussed in Chapter 9.

8.1.1 Methodology

An overview of the approach for the design of an optimal monitoring network is given in Figure 8.1. According to Telci et al. (2009), the general approach consists of two steps. Step 1 is concerned with the selection, preparation and simulation of potential pollution scenarios. For this task, a sufficiently well-calibrated flow and transport model is necessary (Bode et al. 2016). In this work, the calibrated hydrodynamic transport model of the Thi Vai Estuary, described in detail in Chapter 5, is used for the simulation of potential pollution scenarios. Step 2 is concerned with the optimization of the monitoring network, which includes the selection of optimal monitoring locations. Based on the scenario simulations from the first step, a chosen design criterion is optimized using a numerical optimization algorithm. For the optimization, the number of monitoring stations which can actually be installed has to be determined beforehand. In the following sections, the individual steps for an application to the Thi Vai Estuary will be described in more detail.

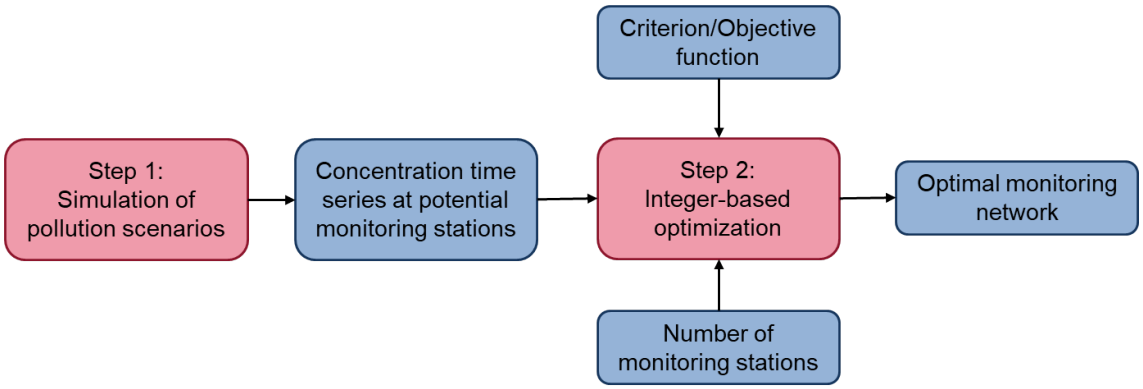

Figure 8.1: Approach for the design of an optimal real-time monitoring network for pollution source identification in surface waters.

8.1.1.1 Simulation of potential pollution scenarios

As explained above, in a first step, numerous potential pollution scenarios have to be simulated by using the calibrated transport model. These scenarios build the database for the design of the monitoring network. Each of these scenarios results in a multitude of concentration time series at potential monitoring stations which are stored for the optimization process in the second step.

For the selection of potential pollution scenarios, several factors have to be considered. These include the influence of external forces (e.g. freshwater inflow, tidal dynamics) on the pollutant transport in the considered system, as well as the adequate parametrization of potential spills (e.g. location, release time, pollutant mass). As these factors can be highly uncertain in practice, the design of the monitoring network must properly account for the probabilistic nature of these factors (Grayman and Males 2002).

In this study, only single instantaneous pollutant spills are considered, which differ in the source location and the release time. The total pollutant mass is set constant to 900 kg for all scenarios. For the selection of potential source locations only the main stream of

the Thi Vai Estuary is considered. Tributaries and secondary channels are ignored. It is further assumed that inside the main stream, pollution spills can occur at any location along the longitudinal direction, but only from the eastern bank. This is a reasonable assumption since most of the industrial zones are located there. By taking into account the entire main stream, industrial zones that might be built in the future or possible other pollution incidents (e.g. ship accident) can already be incorporated, and would not lead to a change in the monitoring design. This applies particularly to rivers or estuaries whose surroundings are exposed to a high degree of industrial development.

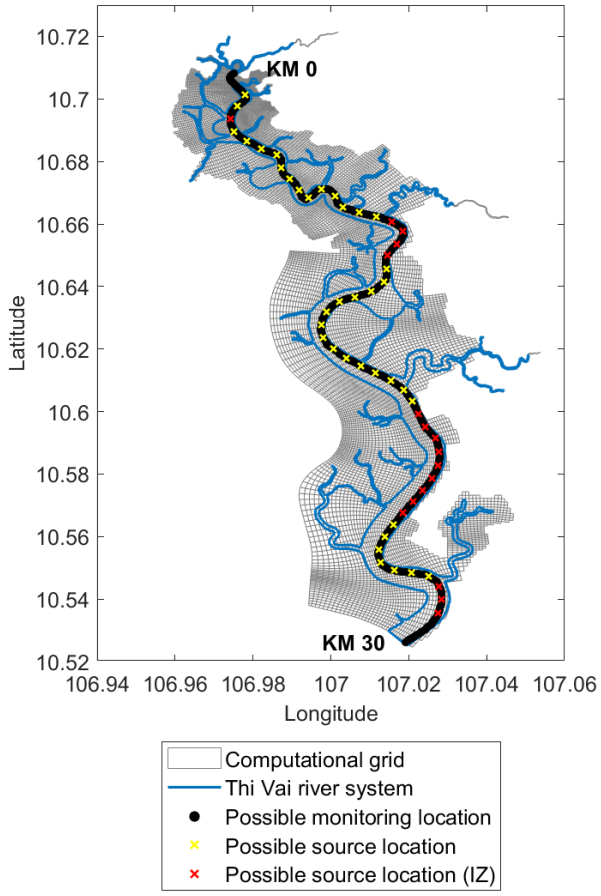

Figure 8.2: Location of potential pollution source locations as well as monitoring stations for the design of a monitoring network for the Thi Vai Estuary. Red: Potential source locations in the vicinity of already exiting industrial zones ($w_s = 5$); Yellow: Other potential source locations ($w_s = 1$).

To reduce the computational burden, not all grid cells along the east bank of the Thi Vai Estuary are considered, but only a total of 54 potential release locations. These are evenly distributed along the main stream from KM 5 to KM 25 with a distance of 500 m. Potential source locations are depicted in Figure 8.2.

As the transport simulations are based on unsteady hydrodynamics, different release times of the pollutant have to be considered. In this study, in total, eight different release times have been included in the analysis, which are divided between spring and neap tide. The release times include a release at slack water before ebb tide, at maximum ebb tide, at slack water before flood tide, and at maximum flood tide. The considered release times are based on the simulated discharge time series in the middle section of the Thi Vai Estuary. An overview of the discharge time series and the corresponding release times is given in Figure A.4 of the Appendix.

In addition to the tidal dynamics, the variability in the freshwater inflow has to be taken into account in the pollution scenarios. Regarding the Thi Vai Estuary, it could be observed in Chapter 5.1.2 that the freshwater inflow is low in comparison to the total volume of the estuary, but highly variable throughout the year due to dependence on the dry and rainy season. Because of the difficulty in representing this high variability in the considered scenarios, the mean freshwater discharge for each tributary is used instead. In total, approximately 17.8 $m^3 s^{-1}$ freshwater enter the Thi Vai Estuary from the five major tributaries (Table A.1). To determine whether the use of a constant freshwater inflow presents a valid assumption, the results will be compared to the

results when using the mean freshwater discharge of the dry and rainy season, which is approximately 5.7 and 28.2 $m^3 s^{-1}$, respectively.

In total, 432 scenarios are considered for the design of the monitoring network. These scenarios are run using the calibrated transport model of the Thi Vai Estuary. For each scenario, the simulation period is set to one month from 15.01. to 15.02. with a time step of 5 min. The resulting concentration time series are stored for each potential monitoring station and can subsequently be used in the second step, the actual optimization of the monitoring network. Potential monitoring stations are assumed to be located at the eastern bank of the main stream of the estuary (Figure 8.2). This is a valid assumption as monitoring stations are, in general, located at the bank due to economical considerations and better accessibility. In total, 580 potential monitoring locations are considered in the analysis. Due to the spatial discretization, it is assumed that the sensors are located at the centre of the grid cells of the computational grid.

8.1.1.2 Choice of the design criterion

For the optimization of the monitoring network, an optimization criterion has to be selected. As discussed in Chapter 3.3.3, up to now, the design of an optimal monitoring network for PSI has been rarely addressed in the literature. Approaches which could be found were either based on the mean detection time (Telci and Aral 2011; Lee et al. 2018) or on optimality criteria based on different properties of the Fisher information matrix (FIM) (Tryby et al. 2010; Jin et al. 2014).

When designing an optimal monitoring network for the task of PSI, the collected data should lead to an accurate identification of the unknown source parameters. Based on the theory of optimal experimental design (compare Chapter 3.3.3.3), a monitoring design which maximizes the information content in the data will lead to improved parameter identifiability and reduce parameter uncertainty (Sun and Yeh 1990; Banga and Balsa-Canto 2008). In Chapter 6.2.5.3, two optimality criteria, namely D- and E-optimality, have been compared for different monitoring designs. Both criteria led to similar results and can be considered as appropriate measures for the design of a monitoring network. Nevertheless, both criteria require the calculation of the Fisher information matrix (FIM) for each pollution scenario. A comparison of these criteria to the detection time at different monitoring stations has shown that, the earlier the pollutant plume is detected by a monitoring station, the higher the information content in the data. Thus, the detection time can be considered as an alternative measure for the design of the monitoring network. In contrast to the use of optimality criteria like D- or E-optimality, fewer simulation runs are necessary when using the detection time as a design criterion. When using the optimality criteria, the FIM has to be evaluated for each considered pollution scenario. The FIM is based on the sensitivity matrix, which has to be evaluated using the finite difference approach in the case of numerical transport models. This results in $p + 1$ simulations for each scenario, with p being the number of source parameters. In contrast, if the detection time is considered as the optimization criterion, only one simulation is necessary for each pollution scenario. Consequently, for the design of a monitoring network for the Thi Vai Estuary the mean detection time is chosen as the design criterion.

8.1.1.3 Optimization problem

Based on the computed pollution scenarios and the selected design criterion, the optimization of the monitoring network can take place. As discussed in the previous section, the mean detection time will serve as a design criterion for the optimal monitoring network in this work. The computation of the mean detection time $\bar{t}_d(X)$ for several pollution scenarios is presented in detail in Chapter 3.3.3.2. Based on the definition of the mean detection time, the objective function to be minimized can be written as:

$$f(X) = \min\{\bar{t}_d(X)\} \tag{8.1}$$

Although theoretically feasible, the use of a combinatorial analysis instead of a numerical optimization routine is not recommended due to the high number of potential monitoring locations, which lead to millions of possible combinations of monitoring stations. The potential combinations can be calculated by $\binom{N}{M}$, with N being the number of potential monitoring stations, and M being the number of monitoring stations to be installed. A short example: When considering 580 potential monitoring stations from which 3 can be selected, the number of potential combinations is equal to 32 350 660. Therefore, numerical optimization routines are used in this work.

Important for the calculation of the detection time is the concentration threshold c_{th}. Depending on the chosen threshold the detection time can vary significantly. In general, the larger the threshold, the later the time of detection by the considered monitoring system. A larger threshold additionally increases the probability that a monitoring network will miss a spill (Park et al. 2014). For its selection in practice, the background concentration, the toxicity of the chemical monitored, as well as the sensitivity and specificity of the monitoring method have to be taken into account (Gullick et al. 2003). In this work, the detection threshold is set to $10^{-3}\,\mathrm{g\,m^{-3}}$. In the event that the threshold is not exceeded once at a monitoring station during the entire simulation period, a penalty value of 48 h is used instead for the detection time. Similarly, if the detection time at a monitoring station exceeds the detection time limit of 24 h, the penalty value of 48 h is used instead of the actual detection time to further penalize a very late detection by the monitoring network.

To increase the importance of already existing industrial zones, appropriate weights can be considered in the optimization (Aral and Nam 2016; Park et al. 2014; Bode et al. 2018). In this work, for scenarios including source locations at already existing industrial zones, the weight w_s of the respective scenarios is set to 5, equal to a five times higher probability of occurrence for a spill at these locations. Consequently, for all other scenarios a weight w_s of 1 is used.

In general, the single-objective function can be solved using a multitude of optimization methods. It should be noted that potential monitoring stations are represented as integer values $(1, \cdots, N)$ in the optimization. Therefore integer-based optimization routines have to be used. In this work, the differential evolution (DE) algorithm, described in detail in Chapter 2.2.3.2, is applied. The classical DE algorithm is developed for continuous parameter optimization. For the application to a discrete optimization problem, the available script for DE was slightly modified, incorporating rounding routines to only obtain integer values. Regarding the parametrization of DE, the population size NP was set to $10 \cdot M$, while the mutation and crossover coefficients F and CR were both set to 0.8.

8.1.2 Results

8.1.2.1 Influence of the total number of monitoring stations on the network design

The optimization of the monitoring network is carried out several times, each time taking a different number of monitoring stations into account. In Figure 8.3, the location of optimal monitoring stations are presented, considering one to five monitoring stations to be installed inside the estuary. Overall, the stations are evenly distributed along the main stream of the Thi Vai Estuary. This is to be expected since the underlying flow patterns are in general symmetric, and potential pollution sources are evenly distributed along the eastern bank of the estuary.

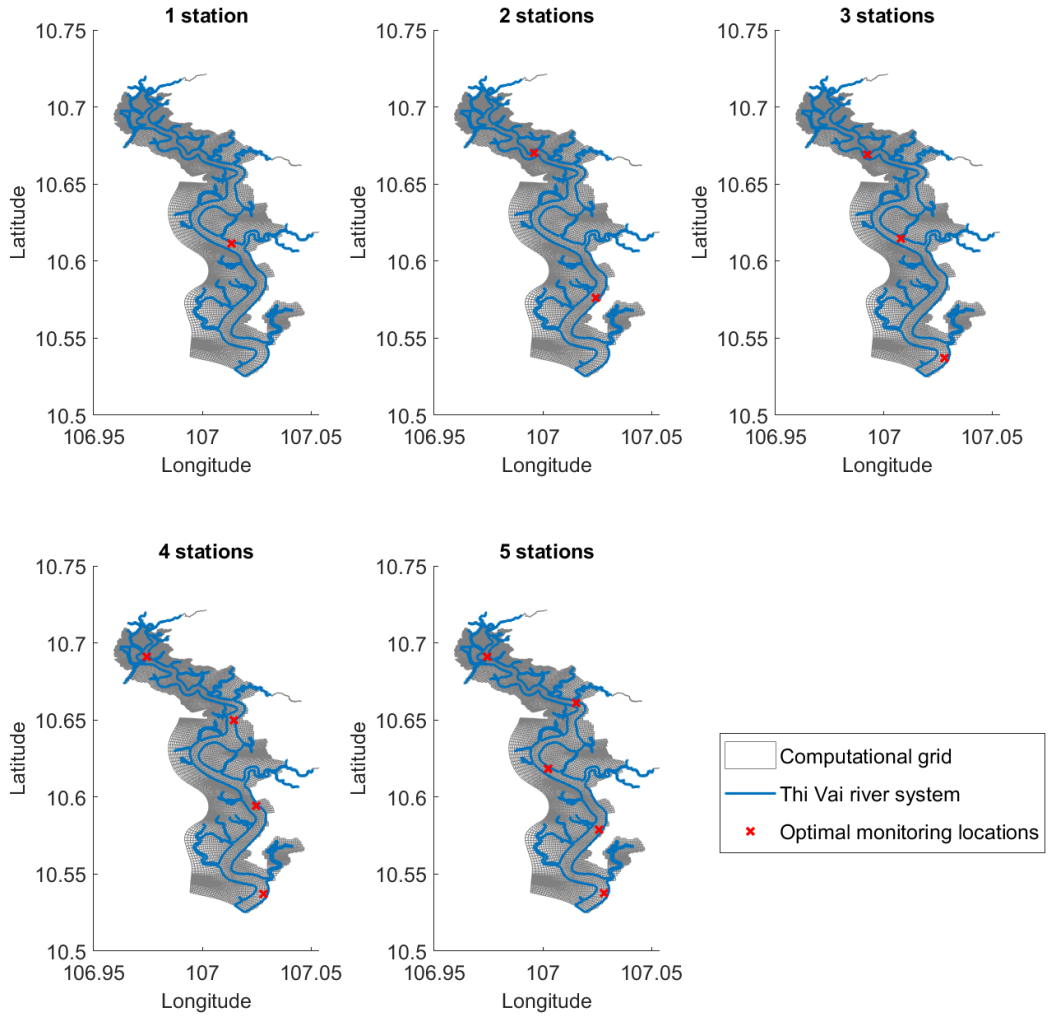

Figure 8.3: Locations of optimal monitoring stations inside the Thi Vai Estuary based on the numerical optimization of the mean detection time.

In Table 8.1, the mean detection time is presented for the considered monitoring networks. With an increase in the number of installed monitoring stations from one to five stations, the mean detection time decreases from 22.82 h to 2.09 h. In addition, the maximum detection time and the detection probability are presented. The maximum detection time is defined as the maximum time the optimized monitoring network needs to detect all considered scenarios. The detection probability represents the reliability of the monitoring

Table 8.1: Influence of the number of considered monitoring stations on the average and maximum detection time, and detection probability.

Number of monitoring stations	Mean detection time [h]	Maximum detection time [h]	Detection probability [%]
1	22.82	> 24	63.19
2	10.36	> 24	91.44
3	5.06	> 24	99.31
4	3.02	19.33	100
5	2.09	14.00	100

system. It is defined as the ratio of detected pollution scenarios to total scenarios (Telci et al. 2009). As can be seen in Table 8.1, if less than four stations are included in the design, only 63.19% to 99.31 % of all considered scenarios can be detected within 24 hours. When including four or more monitoring stations, all considered pollution scenarios can be detected by the monitoring network in less time than the desired detection time limit of 24 h. The maximum detection time is an important property of the monitoring network. In the case of a spill incident, it can give guidance on how long ago a pollutant was maximally introduced into the estuary before being detected by the monitoring network. The maximum detection time can therefore be used together with the absolute detection time to determine a lower bound for the release time.

In the analysis, it has to be considered, that the average detection time and the detection probability are not absolute measures but depend on the pollutant mass introduced during a spill, the detection threshold and the detection time limit (Aral and Nam 2016). For example, if the introduced pollutant mass is only small, the spill might not be detected. The detection threshold represents the concentration above which the pollutant can be detected by a monitoring device. If a higher detection threshold is used in the analysis, the average detection time will certainly increase. A larger threshold value additionally increases the probability that a monitoring network will miss a spill (Park et al. 2014).

Although the results clearly indicate that an increase in the number of monitoring stations reduces the average detection time and increases detection probability, the number of monitoring stations installed in practice will generally be dictated by budgetary constraints. Nevertheless, a comparison of different monitoring designs can give guidance on the minimum number of stations to be installed to achieve a given system performance.

In the further work, data collected by the designed monitoring network will be used for the identification of potential pollution spills in the Thi Vai Estuary. For the identification, an optimal monitoring network consisting of four monitoring stations is considered. The selected monitoring network has average and maximum detection times of 3.02 h and 19.33 h, respectively, with a detection probability of 100% for the considered pollution scenarios. In Chapter 8.2, the performance of the optimal monitoring network will be evaluated based on several random spill scenarios.

8.1.2.2 Influence of hydrodynamic conditions on the network design

As already mentioned, the selection of appropriate pollution scenarios, including uncertainties in hydrodynamics and source characteristics, is of major importance for the design

of an optimal monitoring network and the actual application in the real world. Up to now, optimal monitoring networks have been primarily developed for river systems. Therefore, this section includes a short analysis on how different hydrodynamic conditions influence the results. The factors influencing the hydrodynamics are the freshwater inflow and the tidal dynamics, which are both dependent on the specified boundary conditions of the hydrodynamic model. The analysis can give valuable guidelines on which pollution scenarios should be included in the design of an optimal monitoring network in an estuary.

In terms of tidal dynamics, the timing of the spill in the tidal cycle can play a significant role in the design of the monitoring network. Therefore, the first analysis is based on the influence of pollution spills exclusively during flood or ebb tide on the design. A second analysis is performed for pollution spills exclusively during neap and spring tide. The results regarding the position of optimal monitoring stations as well as the mean and maximum detection times are presented in Figure 8.4.

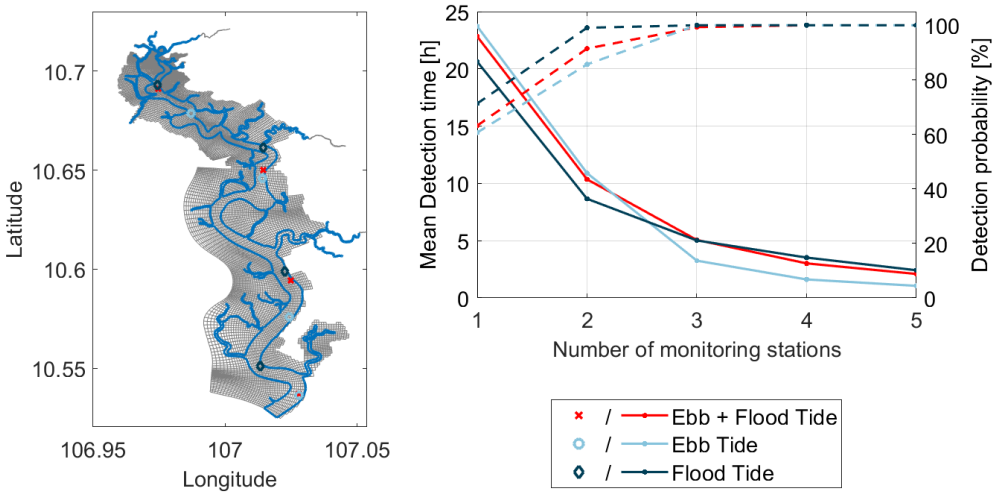

(a) Influence of ebb and flood tide.

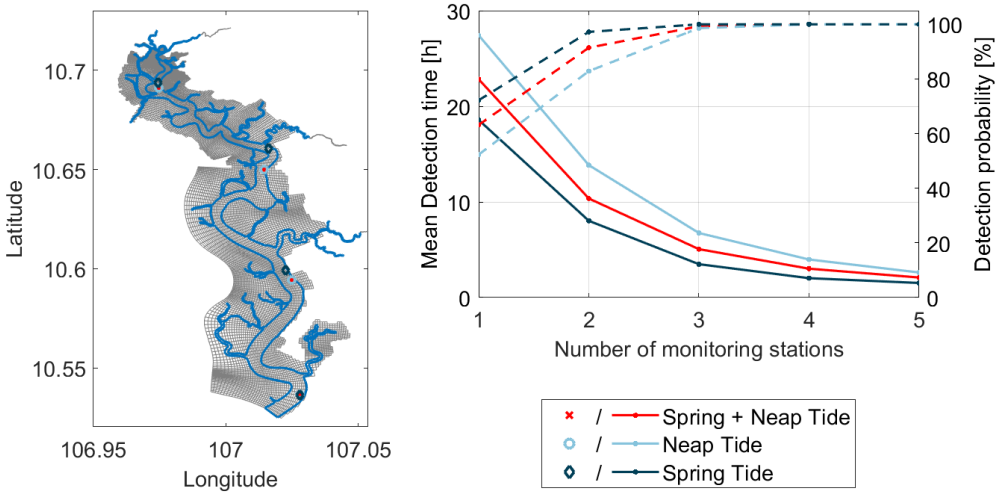

(b) Influence of spring and neap tide.

Figure 8.4: Influence of tidal dynamics on the design of the monitoring network for the Thi Vai Estuary.

If only pollutions spills during ebb or flood tide are considered, the location of optimal

monitoring stations can vary considerably 8.4a. For flood tide, monitoring locations are generally located further upstream, while for ebb tide monitoring stations are located further downstream. No clear relationship can be detected between the mean detection time and the time of release in the tidal cycle. If a smaller number of monitoring stations (≤ 2) is considered, a smaller mean detection time can be observed for flood tide scenarios. In contrast, if the number of monitoring stations is increased further, a smaller detection time can be observed for ebb tide scenarios.

In Figure 8.4b, the results regarding the influence of spring and neap tide on the optimal monitoring network are presented. The location of optimal monitoring stations is only slightly influenced if pollution spills exclusively during spring or neap tide are considered. This is in accordance with Aral and Nam (2016). It can be observed that the mean detection time for spring tide is generally smaller than for neap tide. This is due to the higher tidal excursion in the case of spring tide, which leads to an earlier detection by the monitoring network.

Finally, the influence of the freshwater inflow of the tributaries on the east and north side of the Thi Vai Estuary, is analysed. Three different freshwater discharge rates are compared. These include the mean freshwater discharge Q_{mean} for the entire year, the mean discharge in the dry season Q_{dry} and the mean discharge in the rainy season Q_{wet} (Table A.1). Results are presented in Figure A.5 of the Appendix. Overall, the freshwater discharge has only a very small influence on the monitoring network. No significant changes in mean detection time, detection probability, or location of the monitoring stations can be observed. For the Thi Vai Estuary, the freshwater inflow is very small in comparison to the total volume of the estuary. The pollutant transport is dominated by tidal currents, and the freshwater inflow only plays a minor role when selecting optimal monitoring stations. Consequently, the consideration of the mean freshwater inflow is an appropriate assumption in this work. For other estuaries, this might be different and should be analysed before designing a monitoring network.

8.2 Pollution source identification

Given the optimal monitoring network, both optimization approaches presented in Chapter 7, are applied to the Thi Vai Estuary to identify the source parameters of several theoretical pollution spill incidents. It has to be noted that this represents a first attempt to apply the simulation-optimization approach to the Thi Vai Estuary. The numerical transport model of the Thi Vai Estuary is much more complex than the two-dimensional test case from Chapter 7. Therefore, a number of assumptions and simplifications are considered in the application, which are described in the following sections.

8.2.1 Methodology

8.2.1.1 Challenges in the transfer

The hydrodynamic transport model of the Thi Vai Estuary differs in certain aspects from the two-dimensional test case considered in Chapter 7. First, due to the use of an orthogonal curvilinear grid in a spherical coordinate system, the coordinates of the source location x_s and y_s are not directly related to the longitudinal and lateral flow direction.

Second, in the numerical model of the Thi Vai Estuary tidal flats are integrated to correctly represent the underlying hydrodynamics. The influence of tidal flats has not been evaluated in the preceding analysis. These might act as temporary sinks, leading to a further dispersion of the pollutant plume as discussed in Chapter 2.1.3.

Because of the complex geometry of the Thi Vai Estuary, it was assumed that potential source locations only exist at the eastern bank of the estuary. This is a reasonable assumption since most industrial zones are located here. Consequently, the lateral source location can be ignored, leading to a reduction of the optimization problem to only three parameters, the longitudinal source location, the release time and the total pollutant mass. Additionally, it was assumed that a release can only take place in the main stream of the estuary and not in one of the tributaries. The same assumptions were used for the optimal design of the monitoring network.

As described before, the coordinates of the model grid cells do not necessarily comply with the longitudinal and lateral flow direction. To simplify the optimization problem, the source location is not described using its spherical coordinates but by its position in the longitudinal course of the estuary. For this purpose, the longitudinal course of the Thi Vai Estuary is discretized from the head to the mouth into 580 points using an equidistant distribution of 50 m. These are the same points which were considered as potential monitoring stations in the design of the monitoring network and are depicted in Figure 8.2. In addition, a table is created which contains the spherical coordinates (longitude and latitude) of each point. In the optimization process, the source location can take any value between 0 and 30 km. When a value is chosen by the optimization algorithm, the given table is used to find the spherical coordinates of the closest point. For example, the point located at KM 15 in the longitudinal course of the Thi Vai Estuary has the spherical coordinates 107.00 and 10.62. The spherical coordinates are needed inside the water quality model to define the position of the pollution source. Subsequently, the corresponding concentration distribution inside the estuary can be simulated for the given source location.

8.2.1.2 Scenario definition

In Chapter 7, two optimization approaches were applied to a simplified test case, which considered bidirectional flow conditions. To evaluate if both or at least one of the approaches presents a reliable parameter estimation technique in the Thi Vai Estuary, the approaches are applied to five synthetic pollution spill scenarios. The spill scenarios vary in the longitudinal source location, the release time and the total pollutant mass. The source parameters considered for each of the scenarios are presented in Table 8.2.

Table 8.2: Parametrization of the considered spill scenarios for pollution source identification in the Thi Vai Estuary.

Scenario	x_s	t_s	M_s
1	15.5 km	21.01. 09:00	750 kg
2	23.5 km	21.01. 12:00	975 kg
3	7.5 km	21.01. 15:00	1050 kg
4	11.5 km	21.01. 18:00	900 kg
5	19.5 km	21.01. 21:00	825 kg

The locations of the considered spill incidents are distributed between the upper and lower monitoring stations and are depicted in Figure 8.5. As explained in the previous section, the lateral source location is not considered in the analysis. It is assumed that a release can only take place from the eastern bank of the Thi Vai Estuary. The total pollutant mass released during the incidents is assumed to lie between 750 and 1000 kg. The pollutant release occurs at different points in time which are located within one tidal cycle. The release times of the pollution scenarios differ from the ones considered for the optimal monitoring network to evaluate if different pollution scenarios can also be detected by the designed monitoring network. In all considered scenarios, the freshwater inflow is set to the mean discharge at all tributaries, as tidal dynamics seem to be the main driving forces for transport and mixing in the Thi Vai Estuary.

8.2.1.3 Monitoring data

Monitoring data for the five spill incidents are generated by the calibrated Delft3D model. For a first evaluation of the optimization approaches, the data are assumed to be perfect.

The monitoring network developed in Section 8.1, consists of four monitoring stations. These are depicted in Figure 8.5. A first analysis has confirmed that all considered pollution scenarios can be detected by the monitoring network as the threshold value of $10^{-3}\,\mathrm{g\,m^{-3}}$ is exceeded at at least one monitoring station. This is an important prerequisite as PSI can only succeed if the detection of a potential spill is assured in the first place.

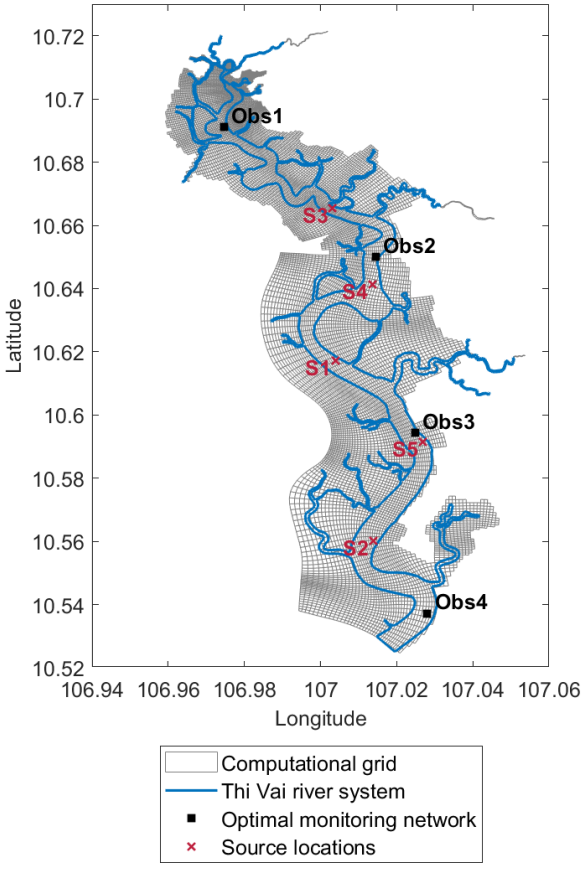

Figure 8.5: Location of optimal monitoring stations and of the considered pollution spills in the Thi Vai Estuary.

The monitoring network was developed under the assumption that the pollutant is continuously measured at the selected monitoring stations. Limitations of this assumption in practice will be further discussed in Chapter 9. However it will seldom be possible to continuously measure concentrations of various pollutants at several monitoring stations. To make the application more realistic, only a limited amount of data from one monitoring station was considered for the identification of pollution source parameters. Here, the station which initially detects the pollutant is selected for each scenario. Monitoring data covering two days following the detection time and a monitoring frequency of 1 h are used, resulting in a total of 49 data points. The considered monitoring data for each scenario are presented in Figure A.6 of the Appendix.

8.2.1.4 Boundary constraints

As described in Chapter 7, both optimization approaches require boundary constraints for the parameters to be estimated. In the case of the Thi Vai Estuary, the constraints can mainly be based on the characteristics and the collected data of the optimal monitoring network. An overview of lower and upper bounds of each pollution source parameter considered in the optimization is presented in Table 8.3.

Table 8.3: Lower and upper boundary constraints for the estimation of pollution source parameters in the Thi Vai Estuary.

Parameter	Lower bound	Upper bound
x_s	Monitoring station upstream of detection point	Monitoring station downstream of detection point
t_s	DT* - 20 h	DT*
M_s	600 kg	1200 kg

*DT: Detection time

Possible locations of a pollutant release can be determined based on the positions of the monitoring stations inside the river or estuary. In rivers, the pollution source has to be located between the monitoring station which first detects the pollution (the detection threshold is exceeded here first) and the monitoring station upstream of this station, where no detection occurred. In estuaries, due to the changing flow direction, a possible pollutant release can also take place downstream of a monitoring station and can still be detected by it during flood tide. Here, the range of possible pollutant release locations lies between the monitoring stations up- and downstream of the monitoring station, which first detects the pollution.

The upper bound for the release time is based on the minimum detection time of the pollutant plume at one of the stations in the monitoring network. The lower bound for the release time can be determined by subtracting the maximum detection time of the considered monitoring network from the minimum detection time of the spill. The considered optimal monitoring network for the Thi Vai Estuary has a maximum detection time of 19.33 h.

One option to approximate the total pollutant mass is the simultaneous measurement of the pollutant concentration and the discharge at the lower monitoring station. Based on these data the pollutant load transported through the cross-section can be determined. If the introduced substance is not conservative, a possible decrease due to decay has to be considered. However, in this work, for simplicity, the lower and upper boundary constraint for the total pollutant mass are considered to be absolute values and set to 600 and 1200 kg, respectively.

8.2.2 Results and discussion

In Table 8.4, the results of both optimization approaches for the identification of five theoretical spill incidents in the Thi Vai Estuary are presented. It can be seen that both optimization approaches generally worked well and could correctly identify the source parameters of four out of five pollution scenarios. The small errors between real and

estimated values for the longitudinal source location x_s and the release time t_s are due to the spatial and temporal discretization of the numerical transport model as explained in Chapter 7.4.

Table 8.4: Results of the simultaneous and decoupled optimization approaches for the identification of instantaneous pollutant releases in the Thi Vai Estuary considering perfect monitoring data. If the estimated grid cell does not correspond to the actual grid cell, absolute errors for x_s are marked in bold.

Scenario	Absolute error			Obj. func.	Function
	x_s [m]	t_s [min]	M_s [kg]	minimum	evaluations
Simultaneous optimization					
Scenario 1	8.31	1.67	0.00	0	4530
Scenario 2	15.99	4.58	0.00	0	4410
Scenario 3	55.14	2.84	0.00	0	4170
Scenario 4	**3162**	150.76	215.09	$3.60 \cdot 10^{-6}$	4530
Scenario 5	31.02	2.93	0.00	0	4440
Decoupled optimization					
Scenario 1	40.15	0.00	0.00	0	3809
Scenario 2	0.08	0.00	0.00	0	3751
Scenario 3	2.68	0.00	0.00	0	3934
Scenario 4	80.07	0.00	0.00	0	3839
Scenario 5	**225.09**	0.00	43.46	$5.66 \cdot 10^{-5}$	3977

The scenario, which could not be identified correctly, differed for the two optimization approaches. While the simultaneous optimization approach could not identify Scenario 4 correctly, the decoupled approach had difficulties finding the global minimum of Scenario 5. Both optimization approaches converged prematurely, which can be seen by the minimum objective function value. In the case of the decoupled approach, absolute errors between real and estimated source parameters are still small, meaning the optimization algorithm converged to a local minimum in the vicinity of the global optimum. In contrast, large deviations exist between real and estimated parameter values for Scenario 4 when using the simultaneous optimization approach. In practice, the source identification process would have led to a wrong estimation of the pollutant source.

Reasons for premature convergence are manifold. Regarding the decoupled approach it has to be considered that, due to the computational burden, a local search algorithm, namely the Nelder-Mead simplex algorithm, was used in the optimization process. The convergence of local optimization algorithms strongly depends on the initial parameter guess. In the case of the simultaneous optimization approach, the Differential Evolution algorithm was used, which is classified as a global optimization algorithm. Although global optimization algorithms have a strong global searching ability, they are not guaranteed to converge to the global minimum of the objective function.

For the convergence of both approaches, the shape of the objective function will be of major importance. Multiple local minima as well as elongated valleys and flat zones near the global minimum will cause convergence problems (Carrera and Neuman 1986b). The shape will, amongst other factors, depend on the identifiability of pollution source parameters. The results of Chapter 6.2 have shown that non-linear dependencies exist

between different source parameters, especially between the longitudinal source location x_s and the release time t_s. The strength of this interaction will be influenced by the time of release in the tidal cycle. Considering Scenario 5, the pollutant was released at maximum ebb tide, when a strong seaward current was present. In this case, both parameters are highly correlated and multiple parameter combinations will exhibit very similar objective function values, leading to a very flat shape of the objective function in the vicinity of the global minimum. This could be one of the reasons for the premature convergence of the decoupled optimization approach.

Regarding Scenario 4, the pollutant plume was detected rather late by the monitoring network, almost 7 h after its release. In contrast, scenarios 1, 2, 3, and 5 have a detection time of 5.5, 1.7, 5.4, and 2 h, respectively. The results of Chapter 6.2 have shown that the sensitivity of the model output to changes in the parameters decreases the later the plume is detected. Consequently, different spill scenarios will lead to similar concentration profiles at the considered monitoring station, complicating the correct identification of pollution source parameters. Additionally, when using a numerical transport model, poor convergence might be the result of the spatial discretization, i.e. the model grid. Different values for the longitudinal source location x_s will exhibit the same objective function value, resulting in saddle points in the objective function. Nevertheless, in the case of the chosen optimization algorithms, which are classified as derivative-free optimization methods, this should not hinder the optimization. this is also indicated by the identification results obtained for the bidirectional test case in Chapter 7.

Because both optimization approaches had trouble converging to the true global minimum in some scenarios, the influence of monitoring errors on identification results was not analysed for the Thi Vai Estuary. In this case it cannot be guaranteed that the optimization approaches really converge to the global minimum. Integration of errors should only be considered if the methods obtain reliable results when considering perfect monitoring data.

8.3 Conclusions

To identify the unknown source parameters in the case of a pollution spill, pollutant detection is the most important prerequisite. Consequently, the first part of this chapter was concerned with the design of an optimal monitoring network for the Thi Vai Estuary. For the optimization of the monitoring network, several pollution scenarios were considered. These differed not only in the source location but, due to the influence of tidal dynamics on transport and mixing processes, also in the release time. The design of the monitoring network was based on the minimization of the mean detection time, i.e. the mean time needed to detect all considered pollution spills. The mean detection time mainly depends on the number of monitoring stations installed. The more monitoring stations are considered the smaller the mean detection time. For the subsequent step, the identification of several theoretical pollution incidents in the Thi Vai Estuary, a monitoring network consisting of four monitoring stations was chosen.

To identify the source parameters of the considered spill incidents, two optimization approaches, presented in Chapter 7, were applied. These consisted of the simultaneous identification approach, which uses the Differential Evolution algorithm for the simultaneous identification of all source parameters, as well as the decoupled identification approach, in which the estimation of the release time is decoupled from the other source parameters. For the simplified bidirectional test case in Chapter 7, both approaches performed equally

well considering perfect monitoring data. For the application to the Thi Vai Estuary, five pollution scenarios were considered, which differed in the longitudinal source location, release time and total pollutant mass. In general, both approaches worked well and could correctly identify the parameters of four out of five scenarios. Only in one case, which differed between both approaches, the optimization algorithms converged prematurely. As already discussed, reasons for the premature convergence of both optimization approaches are manifold. A comprehensive analysis was not part of this work, but should be carried out in the future. Reasons can be due to the properties of the optimization algorithm as well as the shape of the objective function. The shape will be particularly influenced by the identifiability of parameters, including sensitivity and collinearity. To analyse the dependence of both approaches on the choice of initial parameter values, the optimization should be repeated several times from different starting values.

9 Summary and Outlook

9.1 Summary

The main objective of this thesis was to improve the identification of pollution source parameters (PSP) in the case of a spill incident in estuaries. It is emphasized that in this work, it is assumed that the pollutant is released instantaneously from a single point source. Consequently, the pollution spill can be described by four parameters including the longitudinal and lateral source location, the release time and the total pollutant mass. The literature review revealed that several pollution source identification (PSI) approaches have been developed and applied to rivers in recent years. In these applications, usually an analytical solution of the 1D or 2D advection-dispersion-reaction equation (ADRE) was used to simulate the transport and mixing processes in the considered river stretch. However, applications to estuaries have only rarely been discussed in the literature. Due to the tidal influence, which results in unsteady hydrodynamics, a numerical transport model is necessary to represent the transport and mixing processes in these cases. As the simulation model has to be run many times for most PSI approaches, the application of a numerical transport model results in a high computational burden.

Inverse problems like the source identification problem heavily rely on the given monitoring data. These can significantly affect parameter identifiability, and consequently the reliability of the obtained parameter estimates. However, the influence of the spatial and temporal monitoring design on identification results has been rarely evaluated up to now, both for rivers and estuaries. Consequently, the first part of this thesis focused on the analysis of the identifiability of PSP in unidirectional flow systems (e.g. rivers). A simplified test case was considered with a length of 55 km and a uniform rectangular cross-section with an area of $600\,\mathrm{m}^2$. For the simulation of transport and mixing processes, an analytical solution of the 2D ADRE was applied. In contrast to other works, the mirror-image technique was used to capture no-flux conditions at the lateral boundaries. For the identifiability analysis, the profile likelihood approach was adopted. Different monitoring designs were compared to evaluate the influence of the spatial and temporal monitoring design on the identifiability of pollution source parameters. In summary, PSP could be termed identifiable under most monitoring configurations. However, a non-linear interaction effect between the lateral source location y_s and the total pollutant mass M_s could be detected, which significantly affected parameter identifiability. The strength of this interaction depends on the position of the monitoring station within the mixing zone. The analysis further revealed that monitoring stations closer to the source and the consideration of multiple monitoring stations can reduce parameter uncertainty. A comparison between concentration time series recorded at a predetermined monitoring station and longitudinal concentration profiles showed that both provide the same amount of accuracy in pollution source parameters. Regarding the temporal design, a higher monitoring frequency leads to a higher accuracy in source parameters. It is further strongly recommended to measure the whole concentration time series at the considered monitoring stations, as a later start of the monitoring leads to higher uncertainties in the estimated parameters.

Subsequently, the analysis was extended to bidirectional flow systems (e.g. estuaries). In this case unsteady hydrodynamics had to be considered, due to the influence of tidal dynamics on the transport and mixing processes. A numerical hydrodynamic transport model was set up with the Delft3D software suite for a hypothetical test case. The test case is a simplified version of the Thi Vai Estuary and has a length of 30 km, a width of 500 m and a depth of 10 m. The boundary conditions for the test case were derived from the Thi Vai Estuary. Due to the high computational burden of the profile likelihood approach, a different approach was adopted for the evaluation of parameter identifiability in bidirectional flow. The selected approach was based on a local sensitivity analysis at multiple points in the parameter space. The approximated sensitivity matrix was further used to calculate the Fisher Information Matrix (FIM). Based on both the FIM and the sensitivity matrix, parameter sensitivity and collinearity for four reference scenarios were evaluated. The results indicated that the model output is sufficiently sensitive to changes in all source parameters including the longitudinal source location, the release time and the total pollutant mass. Therefore, the considered source parameters can be termed identifiable, at least on an individual basis. However, a strong collinearity could be detected between the longitudinal source location x_s and the release time t_s. The strength of this interaction was dependent on the time of release in the tidal cycle. For the comparison of different spatial and temporal monitoring designs, two optimality criteria based on the FIM were derived. Similar to the unidirectional test case, monitoring stations closer to the source resulted in smaller uncertainties in the estimated parameters. However, under bidirectional flow the position of the optimal monitoring locations is dependent on the time of release in the tidal cycle and can either be located up- or downstream of the source location. Regarding the temporal design, the analysis revealed that information content in the observation data is at its highest immediately after the pollutant plume arrives at the considered monitoring station. Over time, the sensitivity of the model output significantly reduces as the concentration profiles of different pollution scenarios get more and more similar. As in the unidirectional case, a higher temporal frequency can lead to smaller uncertainties in estimated pollution source parameters.

The results of the identifiability analysis provided important implications on complexities arising in the optimization of pollution source parameters. For the identification of a pollution source, several approaches exist in the literature. However, up to now, these have been only rarely applied to bidirectional flow systems like estuaries. In this work, the simulation-optimization approach was adopted, which links a pollutant transport model to an optimization algorithm. In the literature, two variants of the simulation-optimization approach have been proposed, whose performance is compared in this work. The usually applied method corresponds to the simultaneous estimation of all unknown source parameters. In a modified version, the estimation of the source parameters is decoupled from one another. Both approaches were applied to the synthetic bidirectional test case using perfect and noise perturbed monitoring data. Multiple pollution scenarios were considered, differing in the time of release in the tidal cycle. While both optimization approaches performed well if perfect monitoring data were assumed, the simultaneous optimizations approach showed signs of premature convergence in the presence of measurement noise. Calculated confidence intervals and correlation matrices showed that the time of release in the tidal cycle plays a major role in the accurate estimation of source parameters. This is in accordance with the results of the identifiability analysis, which have shown that there exists a strong dependency between the longitudinal source location and the release time. This can lead to instability problems and convergence issues during optimization.

In a final step, the simulation-optimization approach was transferred to a real-world estuary, the Thi Vai Estuary located in South Vietnam. For the simulation of pollution scenarios, a two-dimensional hydrodynamic transport model was set up with the Delft3D software suite. The numerical model, which includes a flow distance of approx. 30 km, was able to represent the complex bathymetry of the estuary including the intertidal zones which are mainly covered by mangrove forest. The model was calibrated based on monitoring data collected as part of the joint research project EWATEC-COAST. This joint research project was financed by the German Federal Ministry of Education and Research from 2012 to 2015 and managed by the Department of Hydrology, Water Management and Water Protection at the University of Braunschweig.

Initially, an optimal monitoring network was developed for the Thi Vai Estuary. Based on the results of the identifiability analysis, the mean detection time was chosen as the design criterion. Subsequently, synthetically generated monitoring data of the optimized monitoring network were used for the identification of several theoretical spill incidents in the Thi Vai Estuary. Both the simultaneous and the decoupled optimization approach were applied to the estuary. Both optimization approaches generally performed well and could correctly identify the source parameters in four out of five spill scenarios. Premature convergence in the other cases was most likely due to the complex shape of the objective function, which is influenced by the described correlation between different source parameters, as well as the spatial and temporal discretization of the numerical model.

9.2 Outlook

Up to now, the PSI approaches applied in this work could only be tested using synthetically generated monitoring data. Although in general good results could be obtained, it is not sufficient to conclude that the approaches will perform equally well when applied to real monitoring data. Consequently, in a next step the performance should be evaluated based on real monitoring data either from a tracer experiment or collected in response to a real pollution incident in an estuary. When using actual monitoring data, the assumptions used in this work for the design of the monitoring network and the application of pollution source identification approaches might not prove valid. To further improve the identification process, the following points should be investigated in the future. These include: (i) the collection of monitoring data, (ii) the pollutant transport model, (iii) the source and pollutant characteristics, and (iv) the applied optimization routine.

(i) Collection of monitoring data in practice

The results of this work have shown that the monitoring design is of major importance for the accurate identification of pollution source parameters. An optimal monitoring design can help in the early detection of a pollutant plume, and reduce uncertainties in the estimated pollution source parameters. Consequently, an optimal real-time monitoring network was designed for the Thi Vai Estuary. For the design it was assumed that the installed monitoring devices can measure the pollutant concentration continuously. This is a usually applied assumption in the literature (e.g. Telci et al. (2009) and Aral and Nam (2016)).

However, real-time monitoring devices are usually non-compound specific, and measure only routine water quality parameters like temperature, pH value, dissolved oxygen content, or turbidity (Liu et al. 2015). The pollutant concentration is usually not measured directly, as it is not clear what substance will be introduced into the water body in the

first place, and an analysis is usually very elaborate and expensive. Exceptions exist in practice, like for example gas chromatographs installed along the Rhine River (Diehl et al. 2006). However, the measured water quality parameters can usually serve as indicators that a pollution incident has occurred and additional sampling might be carried out in this case. Furthermore, the measured variables can in some cases also be used as substitute variables. El Badia and Hamdi (2007) showed that a source, emitting organic matter, represented as BOD in the model, could also be determined based on measurements of the dissolved oxygen content.

In practice, economic considerations will be particularly important for water quality monitoring. The installation of multiple automated monitoring devices is very cost and labour intensive, and will only be applied when benefits outweigh the costs. In practice, a spill incident will often only be detected by coincident, either through notifications from the public or randomly collected monitoring data. General guidelines for the optimal monitoring design in this situation have been established in this work. However, these were developed under the assumption that the location and size of the plume were known. Especially for estuaries, due to the oscillating tidal currents, further analysis regarding the localization of the pollutant plume is necessary. This is an important aspect for the positioning of monitoring stations. Additionally, the influence of the temporal monitoring design should be further investigated. A detailed analysis of the influence of the start, frequency, and duration of the monitoring as well as the corresponding minimum amount of monitoring data on identification results is still missing for PSI in estuaries.

(ii) Consideration of uncertainties in the pollutant transport model

To apply a PSI approach and to design an optimal monitoring network, an accurately calibrated transport model is of vital importance. The transport model has to be calibrated beforehand as the model parameters have a significant influence on the simulation of pollutant transport and mixing processes. A change in the model parametrization will lead to a different concentration distribution in the considered system, and consequently different concentration time series at monitoring stations or concentration profiles in the longitudinal direction.

In most works, including this thesis, it is assumed that the transport model perfectly represents the conditions inside the river or estuary. However, models are only abstractions of the physical reality and will always include uncertainties (Sun 2007). These uncertainties can be divided into different types, including input uncertainty, structural uncertainty, parameter uncertainty, and algorithmic uncertainty (Sun and Sun 2015, p. 409). Parameter uncertainty is a result of incomplete or imprecise knowledge about model parameters, including the flow velocity, dispersion coefficients and/or the decay rate. Guozhen et al. (2016) and Jiang et al. (2018) already evaluated the influence of uncertainties in model coefficients on PSI results when using an analytical solution of the ADRE in rivers. The authors came to the agreement that the longitudinal flow velocity and the dispersion coefficient will be the most important parameters. Regarding bidirectional flow systems, an analysis of the influence of uncertainties in model parametrization is still missing in the literature .

Guozhen et al. (2016) argued that uncertainties of model parameters should be included in the identification process. The authors used Bayesian inference and included prior probability distributions instead of constant values for sensitive model parameters in the source identification process. While this approach has already been successfully applied to an analytical solution for a simple river stretch, so far it has not been applied when using a numerical transport model in surface waters. For the Bayesian approach, the forward

simulation model has to be evaluated many times (up to 10,000 times), which leads to a high computational burden in the case of a numerical transport model. Surrogate models could reduce the computational time in the case of the application to groundwater systems (e.g. Borah and Bhattacharjya (2016) and Guneshwor et al. (2018)), but have not been applied to PSI in surface water yet.

When using numerical transport models, additionally the spatial discretization of the model grid has to be taken into account. This corresponds to algorithmic uncertainty. In general, Delft3D can be regarded as a far-field water quality model. Far-field water quality models usually do not have the spatial resolution that is required to predict mixing processes in the immediate mixing zone (Jirka and Weitbrecht 2005). However, the results of Chapter 6 imply that the location of optimal monitoring stations highly depends on the length of the mixing zone as it influences parameter identifiability of the lateral source location and the total pollutant mass. Up to now, an evaluation is missing, how the representation of the mixing zone inside a numerical transport model influences identification results. In the case of a numerical transport model it might be necessary to couple a near- and a far-field water quality model (Bleninger and Jirka 2004). Regarding more simple river stretches, in the literature an analytical solution of the 1D ADRE has often been used (e.g. Zhang and Xin (2017) and Wang et al. (2018)). However, a comparison of the performance of PSI between the 1D and 2D model, when monitoring stations are located inside the mixing zone is missing in the current literature.

(iii) Extension to different source and pollutant characteristics

This work was based on the assumption of an instantaneous pollutant release from a single point source. While a pollution spill usually occurs at a single point, the pollutant will often not immediately be released into the water body but instead released over a given time period. If the spill intensity is assumed to be constant over the whole release period, only the stop time of the release has to be considered as an additional source parameter. Nevertheless, the identifiability analysis should be repeated for this case. If the intensity is time variable, the whole release function might be reconstructed. Only the mathematical and the geostatistical approach have been used for this task. Both have only been applied to unidirectional flow. Boano et al. (2005) stressed the influence of the dispersion process on the recovery of the release history, which progressively diminishes the amount of information associated with the observations. Due to increased dispersion and late detection in estuaries, which are tide-dominated, the reconstruction of the entire release history might be difficult.

In this work, it was further assumed that the estuary is well-mixed, and only a vertically integrated 2D transport model was applied. In the case of a stratified water body, a 3D model needs to be used instead to correctly represent the transport and mixing processes. Overall, PSI approaches in surface water based on a 3D model have not been found in the literature. In rivers it is usually assumed that vertical mixing occurs fairly quickly (Shanahan and Gaudet 2000). However, when a substance with a density different from water (e.g. in the case of an oil spill) is considered, it will be necessary to apply a 3D model. In this case, an additional parameter, namely the source location in the vertical direction might be included in the identification process. This will also influence the optimal monitoring design, which does not only have to include the longitudinal and lateral position inside the river or estuary, but also the vertical monitoring position.

Regarding the pollutant characteristics, up to now it was assumed that the pollutant was conservative. A decay rate can be easily included, but has to be calibrated correctly. Results of Guozhen et al. (2016) and Jiang et al. (2018) show that small uncertainties in

the decay rate do not significantly affect the inversion results. However, this might depend on the monitoring design, which should be carefully investigated.

(iv) Improvement of the optimization routine

The identification results for both the bidirectional test case and the Thi Vai Estuary have shown that the optimization algorithm can converge prematurely to a local instead of a global minimum, independent of the applied optimization strategy. This is partly due to the overall complexity of the optimization problem, including the spatial and temporal discretization of the numerical transport model, as well as the high correlation between the release time and the longitudinal source location. Premature convergence might be avoided by either using a different optimization algorithm or by changing the parametrization of the applied optimization algorithm. A detailed analysis on the influence of the optimization algorithm has not been part of this study but should be evaluated in the future.

For the decoupled approach a local search method was employed, as this leads to a much faster computation when several optimization problems are considered simultaneously. However, the performance of the local search algorithm highly depends on the initial parameter guess, especially when the objective function has a complex shape with multiple local minima and/or saddle points. The decoupled optimization approach can be improved by using a global optimization algorithm or by starting the local optimization algorithm from several initial parameter guesses. This will result in a significant increase in the computational burden, a factor which is especially relevant when using a numerical transport model. Consequently, in this case, reducing the number of optimization problems by means of a more advanced selection of potential release times could reduce the computational burden.

Bibliography

Adedoja, O., Y. Hamam, B. Khalaf and R. Sadiku (2018). "Towards Development of an Optimization Model to Identify Contamination Source in a Water Distribution Network". In: *Water* 10.5, p. 579. DOI: 10.3390/w10050579.

Amirabdollahian, M. and B. Datta (2013). "Identification of Contaminant Source Characteristics and Monitoring Network Design in Groundwater Aquifers. An Overview". In: *Journal of Environmental Protection* 4.5, pp. 26–41. DOI: 10.4236/jep.2013.45A004.

Aral, M. M. and K. Nam (2016). "Optimal Monitoring Network Design for Wind-Driven and Tidal Estuaries". In: *Journal of Environmental Engineering* 142.12, p. D4015002. DOI: 10.1061/(ASCE)EE.1943-7870.0001051.

Aster, R., B. Borchers and C. H. Thurber (2013). *Parameter Estimation and Inverse Problems*. Elsevier. 359 pp. DOI: 10.1016/C2009-0-61134-X.

Atmadja, J. and A. Bagtzoglou (2001). "State of the Art Report on Mathematical Methods for Groundwater Pollution Source Identification". In: *Environmental Forensics* 2.3, pp. 205–214. DOI: 10.1006/enfo.2001.0055.

Bagtzoglou, A. C. and J. Atmadja (2005). "Mathematical Methods for Hydrologic Inversion: The Case of Pollution Source Identification". In: *Water Pollution*. Ed. by T. A. Kassim. Vol. 3. The Handbook of Environmental Chemistry. Berlin/Heidelberg: Springer-Verlag, pp. 65–96. DOI: 10.1007/b11442.

Bahadur, R. and W. B. Samuels (2015). "Modeling the Fate and Transport of a Chemical Spill in the Elk River, West Virginia". In: *Journal of Environmental Engineering* 141.7, p. 05014007. DOI: 10.1061/(ASCE)EE.1943-7870.0000930.

Banga, J. R. and E. Balsa-Canto (2008). "Parameter estimation and optimal experimental design". In: *Essays in biochemistry* 45, pp. 195–209. DOI: 10.1042/BSE0450195.

Bard, Y. (1974). *Nonlinear parameter estimation*. New York: Acad. Press. 341 pp.

Bartlett, J. M. (1998). *Quality control manual for computational estuarine modelling. Technical Report-W1 68*. Ed. by Environmental Agency, Bristol, England.

Bates, D. M. and D. G. Watts (1988). *Nonlinear Regression Analysis and Its Applications*. Hoboken, NJ, USA: John Wiley & Sons, Inc. 372 pp. DOI: 10.1002/9780470316757.

Bellman, R. and K. J. Åström (1970). "On structural identifiability". In: *Mathematical Biosciences* 7.3-4, pp. 329–339. DOI: 10.1016/0025-5564(70)90132-X.

Ben Belgacem, F., H. El Fekih and K. Souad (2013). "Detection and Location of Moving Point Sources in Contaminant Transport Models. Uniqueness and Minimal Observations". In: URL: https://hal.archives-ouvertes.fr/hal-00818370.

Berger, J. O. and M. J. Bayarri (2004). "The Interplay of Bayesian and Frequentist Analysis". In: *Statistical Science* 19.1, pp. 58–80. DOI: 10.1214/088342304000000116.

Bleninger, T. and G. Jirka (2004). "Near- and far-field model coupling methodology for wastewater discharges". In: *Environmental Hydraulics and Sustainable Water Management, Two Volume Set*. Ed. by J. Lee and K. Lam. Vol. 125. CRC Press, pp. 447–453. DOI: 10.1201/b16814-73.

Boano, F., R. Revelli and L. Ridolfi (2005). "Source identification in river pollution problems. A geostatistical approach". In: *Water Resources Research* 41.7, p. 718. DOI: 10.1029/2004WR003754.

Bode, F., T. Ferré, N. Zigelli, M. Emmert and W. Nowak (2018). "Reconnecting Stochastic Methods With Hydrogeological Applications: A Utilitarian Uncertainty Analysis and Risk Assessment Approach for the Design of Optimal Monitoring Networks". In: *Water Resources Research* 54.3, pp. 2270–2287. DOI: 10.1002/2017WR020919.

Bode, F., W. Nowak and M. Loschko (2016). "Optimization for Early-Warning Monitoring Networks in Well Catchments Should Be Multi-objective, Risk-Prioritized and Robust Against Uncertainty". In: *Transport in Porous Media* 114.2, pp. 261–281. DOI: 10.1007/s11242-015-0586-6.

Boiger, R., J. Hasenauer, S. Hroß and B. Kaltenbacher (2016). "Integration based profile likelihood calculation for PDE constrained parameter estimation problems". In: *Inverse Problems* 32.12, p. 125009. DOI: 10.1088/0266-5611/32/12/125009.

Bolker, B. M. (2008). *Ecological Models and Data in R*. Princeton: Princeton University Press. 1409 pp.

Borah, T. and R. K. Bhattacharjya (2016). "Development of an Improved Pollution Source Identification Model Using Numerical and ANN Based Simulation-Optimization Model". In: *Water Resources Management* 30.14, pp. 5163–5176. DOI: 10.1007/s11269-016-1476-6.

Brun, R., M. Kühni, H. Siegrist, W. Gujer and P. Reichert (2002). "Practical identifiability of ASM2d parameters—systematic selection and tuning of parameter subsets". In: *Water research* 36.16, pp. 4113–4127. DOI: 10.1016/S0043-1354(02)00104-5.

Brun, R., P. Reichert and H. R. Künsch (2001). "Practical identifiability analysis of large environmental simulation models". In: *Water Resources Research* 37.4, pp. 1015–1030. DOI: 10.1029/2000WR900350.

Bruner de Miranda, L., F. P. Andutta, B. Kjerfve and B. M. d. Castro Filho (2017). *Fundamentals of Estuarine Physical Oceanography*. Vol. 8. Singapore: Springer Singapore. 506 pp. DOI: 10.1007/978-981-10-3041-3.

Carrera, J. and S. P. Neuman (1986a). "Estimation of Aquifer Parameters Under Transient and Steady State Conditions: 1. Maximum Likelihood Method Incorporating Prior Information". In: *Water Resources Research* 22.2, pp. 199–210. DOI: 10.1029/WR022i002p00199.

— (1986b). "Estimation of Aquifer Parameters Under Transient and Steady State Conditions: 2. Uniqueness, Stability, and Solution Algorithms". In: *Water Resources Research* 22.2, pp. 211–227. DOI: 10.1029/WR022i002p00211.

Chadalavada, S., B. Datta and R. Naidu (2012). "Optimal Identification of Groundwater Pollution Sources Using Feedback Monitoring Information. A Case Study". In: *Environmental Forensics* 13.2, pp. 140–153. DOI: 10.1080/15275922.2012.676147.

Chapra, S. C. (1997). *Surface water quality modeling*. McGraw Hill series in water resources and environmental engineering. Boston, Mass.: WCB McGraw Hill. 844 pp.

Chatwin, P. C. and C. M. Allen (1985). "Mathematical Models of Dispersion in Rivers and Estuaries". In: *Annual Review of Fluid Mechanics* 17.1, pp. 119–149. DOI: 10.1146/annurev.fl.17.010185.001003.

Cheng, W. P. and Y. Jia (2010). "Identification of contaminant point source in surface waters based on backward location probability density function method". In: *Advances in Water Resources* 33.4, pp. 397–410. DOI: 10.1016/j.advwatres.2010.01.004.

Chiang, T.-C., C.-N. Chen and Y.-C. Lin (2013). *Parameter control mechanisms in differential evolution: A tutorial review and taxonomy*. Presentation at the IEEE Symposium Series on Computational Intelligence (SSCI 2013), Singapore.

Chin, D. A. (2013). *Water-quality engineering in natural systems. Fate and transport processes in the water environment*. 2. ed., [elektronische Ressource]. Hoboken, NJ:

Wiley. 454 pp. DOI: 10.1002/9781118459423. URL: http://onlinelibrary.wiley.com/book/10.1002/9781118459423.

Codiga, D. L. (2011). *Unified tidal analysis and prediction using the UTide matlab functions. Technical report*. Narragansett, RI: Graduate School of Oceanography, University of Rhode Island.

D'Errico, J. (2020). *Bound constrained optimization using fminsearch: fminsearchbnd*. MATLAB Central File Exchange. URL: https://de.mathworks.com/matlabcentral/fileexchange/8277 (visited on 22/04/2020).

Dalitz, C. (2017). *Construction of confidence intervals. Technical Report No. 2017-01*. Hochschule Niederrhein, Fachbereich Elektrotechnik & Informatik. URL: https://lionel.kr.hs-niederrhein.de/~dalitz/data/publications/fb03-tb-2017-01-en.pdf.

Datta, B., D. Chakrabarty and A. Dhar (2009). "Optimal Dynamic Monitoring Network Design and Identification of Unknown Groundwater Pollution Sources". In: *Water Resources Management* 23.10, pp. 2031–2049. DOI: 10.1007/s11269-008-9368-z.

Datta, B., O. Prakash, S. Campbell and G. Escalada (2013). "Efficient Identification of Unknown Groundwater Pollution Sources Using Linked Simulation-Optimization Incorporating Monitoring Location Impact Factor and Frequency Factor". In: *Water Resources Management* 27.14, pp. 4959–4976. DOI: 10.1007/s11269-013-0451-8.

Day, J. W., ed. (2013). *Estuarine ecology*. 2nd ed. Hoboken, N.J: Wiley-Blackwell. 550 pp. DOI: 10.1002/9781118412787.

Deltares (2018a). *D-Water Quality Versatile water quality modelling in 1D, 2D or 3D systems including physical, (bio)chemical and biological processes. User Manual*. Version Version 5.06.

— (2018b). *Delft3D-FLOW Simulation of multi-dimensional hydrodynamics flow and transport phenomena, including sediments. User Manual*. Version Version 3.15.

Diehl, P., T. Gerke, A. Jeuken, J. Lowis, R. Steen, J. van Steenwijk, P. Stoks and H.-G. Willemsen (2006). "Early Warning Strategies and Practices Along the River Rhine". In: *The Rhine*. Ed. by T. P. Knepper. Vol. 5L. The Handbook of Environmental Chemistry. Berlin, Heidelberg: Springer Berlin Heidelberg, pp. 99–124. DOI: 10.1007/698_5_015.

Donaldson, J. R. and R. B. Schnabel (1985). *Computational Experience with Confidence Regions and Confidence Intervals for Nonlinear Least Squares. CU-CS-302-85*.

El Badia, A., T. Ha-Duong and A. Hamdi (2005). "Identification of a point source in a linear advection–dispersion–reaction equation: application to a pollution source problem". In: *Inverse Problems* 21.3, pp. 1–17. DOI: 10.1088/0266-5611/21/3/020.

El Badia, A. and A. Hamdi (2007). "Inverse source problem in an advection–dispersion–reaction system. Application to water pollution". In: *Inverse Problems* 23.5, pp. 2103–2120. DOI: 10.1088/0266-5611/23/5/017.

FAO (2011). *The state of the world's land and water resources for food and agriculture. Managing systems at risk*. 1st ed. Milton Park Abingdon and New York NY: Earthscan. xxiii, 285.

Fischer, H. B., J. E. List, C. R. Koh, J. Imberger and N. H. Brooks (1979). *Mixing in Inland and Coastal Waters*. San Diego, CA, USA: Academic Press. 500 pp. DOI: 10.1016/C2009-0-22051-4.

Freni, G. and G. Mannina (2012). "The identifiability analysis for setting up measuring campaigns in integrated water quality modelling". In: *Physics and Chemistry of the Earth, Parts A/B/C* 42-44, pp. 52–60. DOI: 10.1016/j.pce.2011.06.001.

García, M. R., A. A. Alonso and E. Balsa-Canto (2017). "A Normalisation Strategy to Optimally Design Experiments in Computational Biology". In: *11th International Con-*

ference on Practical Applications of Computational Biology & Bioinformatics. Ed. by F. Fdez-Riverola, M. S. Mohamad, M. Rocha, J. F. de Paz and T. Pinto. Vol. 616. Advances in Intelligent Systems and Computing 616. Cham and s.l.: Springer International Publishing, pp. 126–136. DOI: 10.1007/978-3-319-60816-7_16.

Gerritsen, H., E. de Goede, F. Platzek, J. van Kester, M. Genseberger and R. Uittenbogaard (2008). *Validation document Delft3D-FLOW. A software system for 3D flow simulations*. Ed. by Deltares.

Ghane, A., M. Mazaheri and J. Mohammad Vali Samani (2016). "Location and release time identification of pollution point source in river networks based on the Backward Probability Method". In: *Journal of environmental management* 180, pp. 164–171. DOI: 10.1016/j.jenvman.2016.05.015.

Ghosh, S. N. (1998). *Tidal Hydraulic Engineering*. 1st ed. Rotterdam: CRC Press. 190 pp.

Grayman, W. M. and R. M. Males (2002). "Risk-based modeling of early warning systems for pollution accidents". In: *Water Science and Technology* 46.3, pp. 41–49. DOI: 10.2166/wst.2002.0050.

Grayman, W. M., A. H. Vicory and R. M. Males (2000). "Early Warning System for Chemical Spills on the Ohio River". In: *Security of Public Water Supplies*. Ed. by R. A. Deininger, P. Literathy and J. Bartram. Dordrecht: Springer Netherlands, pp. 91–100. DOI: 10.1007/978-94-011-4241-0_7.

Guan, J., M. M. Aral, M. L. Maslia and W. M. Grayman (2006). "Identification of Contaminant Sources in Water Distribution Systems Using Simulation–Optimization Method: Case Study". In: *Journal of Water Resources Planning and Management* 132.4, pp. 252–262. DOI: 10.1061/(ASCE)0733-9496(2006)132:4(252).

Guillaume, J. H. et al. (2019). "Introductory overview of identifiability analysis: A guide to evaluating whether you have the right type of data for your modeling purpose". In: *Environmental Modelling & Software* 119, pp. 418–432. DOI: 10.1016/j.envsoft.2019.07.007.

Gullick, R. W., W. M. Grayman, R. A. Deininger and R. M. Males (2003). "Design of Early Warning Monitoring Systems for Source Waters". In: *Journal - American Water Works Association* 95.11, pp. 58–72. DOI: 10.1002/j.1551-8833.2003.tb10493.x.

Guneshwor, L., T. I. Eldho and A. Vinod Kumar (2018). "Identification of Groundwater Contamination Sources Using Meshfree RPCM Simulation and Particle Swarm Optimization". In: *Water Resources Management* 32.4, pp. 1517–1538. DOI: 10.1007/s11269-017-1885-1.

Guozhen, W., C. Zhang, Y. Li, L. Haixing and H. Zhou (2016). "Source identification of sudden contamination based on the parameter uncertainty analysis". In: *Journal of Hydroinformatics* 18.6, pp. 919–927. DOI: 10.2166/hydro.2016.002.

Gupta, H. V., S. Sorooshian and P. O. Yapo (1999). "Status of Automatic Calibration for Hydrologic Models: Comparison with Multilevel Expert Calibration". In: *Journal of Hydrologic Engineering* 4.2, pp. 135–143. DOI: 10.1061/(ASCE)1084-0699(1999)4:2(135).

Gurarslan, G. and H. Karahan (2015). "Solving inverse problems of groundwater-pollution-source identification using a differential evolution algorithm". In: *Hydrogeology Journal* 23.6, pp. 1109–1119. DOI: 10.1007/s10040-015-1256-z.

Hadamard, J. (1902). "Sur les problèmes aux dérivées partielles et leur signification physique". In: *Princeton University Bulletin* 13, pp. 49–52.

Hahn, D. W. and M. N. Özişik (2012). *Heat conduction*. 3.ed., [elektronische Ressource]. Hoboken, NJ: Wiley. 718 pp. DOI: 10.1002/9781118411285. URL: http://site.ebrary.com/lib/alltitles/docDetail.action?docID=10593121.

Hak, D., K. Nadaoka, L. Patrick Bernado, V. Le Phu, N. Hong Quan, T. Quang Toan, N. Hieu Trung, D. van Ni and van Pham Dang Tri (2016). "Spatio-temporal variations of sea level around the Mekong Delta: their causes and consequences on the coastal environment". In: *Hydrological Research Letters* 10.2, pp. 60–66. DOI: 10.3178/hrl.10.60.

Hamdi, A. (2012). "Inverse source problem in a 2D linear evolution transport equation: detection of pollution source". In: *Inverse Problems in Science and Engineering* 20.3, pp. 401–421. DOI: 10.1080/17415977.2011.637207.

Hamdi, A. and I. Mahfoudhi (2013). "Inverse source problem in a one-dimensional evolution linear transport equation with spatially varying coefficients: application to surface water pollution". In: *Inverse Problems in Science and Engineering* 21.6, pp. 1007–1031. DOI: 10.1080/17415977.2013.764871.

Han, L. X., Y. Zhu, W. L. Jin and F. X. Zhang (2014). "Inverse problem of an instantaneous pollution source in a wide and shallow river and the analysis on inversion accuracy". In: *WATER POLLUTION 2014* (The Algarve, Portugal). Ed. by C. Brebbia. WIT Transactions on Ecology and the Environment. WIT PressSouthampton, UK, pp. 333–342. DOI: 10.2495/WP140291.

Hazart, A., J.-F. Giovannelli, S. Dubost and L. Chatellier (2014). "Inverse transport problem of estimating point-like source using a Bayesian parametric method with MCMC". In: *Signal Processing* 96, pp. 346–361. DOI: 10.1016/j.sigpro.2013.08.013.

Hicks, S. D. (2006). *Understanding tides*. Silver Spring, MD: NOAA, National Ocean Service. 83 pp. DOI: 10.25607/OBP-157.

Hill, M. C. and C. R. Tiedeman (2007). *Effective groundwater model calibration. With analysis of data, sensitivities, predictions, and uncertainty*. Hoboken, N.J: Wiley-Interscience. 455 pp. DOI: 10.1002/0470041080. URL: http://site.ebrary.com/lib/alltitles/docDetail.action?docID=10278710.

Hoang, T. C., M. C. Black, S. L. Knuteson and A. P. Roberts (2019). "Environmental Pollution, Management, and Sustainable Development: Strategies for Vietnam and Other Developing Countries". In: *Environmental management* 63.4, pp. 433–436. DOI: 10.1007/s00267-019-01144-z.

Hopmans, J. W., J. Šimůnek, N. Romano and W. Durner (2002). "3.6.2. Inverse Methods". In: *Methods of Soil Analysis*. Ed. by J. H. Dane and G. Clarke Topp. Madison, WI, USA: Soil Science Society of America, pp. 963–1008. DOI: 10.2136/sssabookser5.4.c40.

ICEM (2007). *Analysis of pollution from manufacturing sectors in Vietnam. Technical report*. Ed. by International Centre for Environmental Management. Indooroopilly, Queensland, Australia. URL: https://icem.com.au/portfolio-items/analysis-of-pollution-from-manufacturing-sectors-in-vietnam/ (visited on 11/06/2020).

Iliadis, A. (2019). "Structural identifiability and sensitivity". In: *Journal of pharmacokinetics and pharmacodynamics* 46.2, pp. 127–135. DOI: 10.1007/s10928-019-09624-9.

Jha, M. K. and B. Datta (2014). "Linked Simulation-Optimization based Dedicated Monitoring Network Design for Unknown Pollutant Source Identification using Dynamic Time Warping Distance". In: *Water Resources Management* 28.12, pp. 4161–4182. DOI: 10.1007/s11269-014-0737-5.

Ji, Z.-G. (2017). *Hydrodynamics and water quality. Modeling rivers, lakes, and estuaries*. Second edition. Hoboken NJ: John Wiley and Sons Inc. 581 pp.

Jiang, J., Y. Chen and B. Wang (2019). "Pollution Source Identification for River Chemical Spills by Modular-Bayesian Approach: A Retrospective Study on the 'Landmark' Spill Incident in China". In: *Hydrology* 6.3, p. 74. DOI: 10.3390/hydrology6030074.

Jiang, J., F. Han, Y. Zheng, N. Wang and Y. Yuan (2018). "Inverse uncertainty characteristics of pollution source identification for river chemical spill incidents by stochastic analysis". In: *Frontiers of Environmental Science & Engineering* 12.5, p. 205. DOI: 10.1007/s11783-018-1081-4.

Jin, X., R. S. Ranjithan and G. Mahinthakumar (2014). "A Monitoring Network Design Procedure for Three-Dimensional (3D) Groundwater Contaminant Source Identification". In: *Environmental Forensics* 15.1, pp. 78–96. DOI: 10.1080/15275922.2013.873095.

Jing, L., J. Kong, Q. Wang and Y. Yao (2018). "An Improved Contaminant Source Identification Method for Sudden Water Pollution Accident in Coaster Estuaries". In: *Journal of Coastal Research* 85, pp. 946–950. DOI: 10.2112/SI85-190.1.

Jirka, G. H. and V. Weitbrecht (2005). "Mixing Models for Water Quality Management in Rivers: Continuous and Instantaneous Pollutant Releases". In: *Water Quality Hazards and Dispersion of Pollutants*. Ed. by W. Czernuszenko and P. M. Rowinski. Boston, MA: Springer Science+Business Media Inc. DOI: 10.1007/0-387-23322-9_1.

Kathirgamanathan, P., R. McKibbin and R. McLachlan (2002). "Source Term Estimation of Pollution from an Instantaneous Point Source". In: *Research Letters in the Information and Mathematical Sciences* 3, pp. 59–67. URL: https://www.massey.ac.nz/~rmclachl/SourceTermEstimation.pdf.

Knobloch, R., J. Mlýnek and R. Srb (2017). "The classic differential evolution algorithm and its convergence properties". In: *APPLICATIONS OF MATHEMATICS* 62.2, pp. 197–208. DOI: 10.21136/AM.2017.0274-16.

Krause, P., D. P. Boyle and F. Bäse (2005). "Comparison of different efficiency criteria for hydrological model assessment". In: *Advances in Geosciences* 5, pp. 89–97. DOI: 10.5194/adgeo-5-89-2005.

Kreutz, C., A. Raue, D. Kaschek and J. Timmer (2013). "Profile likelihood in systems biology". In: *The FEBS journal* 280.11, pp. 2564–2571. DOI: 10.1111/febs.12276.

Kreutz, C., A. Raue and J. Timmer (2015). "Statistics for Model Calibration". In: *Multiple Shooting and Time Domain Decomposition Methods. MuS-TDD, Heidelberg, May 6-8, 2013*. Ed. by T. Carraro, M. Geiger, S. Körkel and R. Rannacher. Vol. 9. Contributions in Mathematical and Computational Sciences 9. Cham: Springer, pp. 355–375. DOI: 10.1007/978-3-319-23321-5_14.

Larson, J., M. Menickelly and S. M. Wild (2019). "Derivative-free optimization methods". In: *Acta Numerica* 28, pp. 287–404. DOI: 10.1017/S0962492919000060.

Le, T. T. H., M. Lorenz, S. Zeunert, C. V. Nguyen and G. Meon (2017). "Räumliche und zeitliche Variabilität der Wassermenge und Wasserqualität des Thi-Vai-Einzugsgebietes in Südvietnam – Datenanalyse eines Monitoringprogramms –". In: *Hydrologie & Wasserbewirtschaftung* 61.6, pp. 370–382. DOI: 10.5675/HyWa_2017,6_1.

Lee, Y., C. Park and M. Lee (2018). "Identification of a Contaminant Source Location in a River System Using Random Forest Models". In: *Water* 10.4, p. 391. DOI: 10.3390/w10040391.

Legates, D. R. and G. J. McCabe (1999). "Evaluating the use of "goodness-of-fit" Measures in hydrologic and hydroclimatic model validation". In: *Water Resources Research* 35.1, pp. 233–241. DOI: 10.1029/1998WR900018.

Li, Z., P. Lu, D. Zhang and T. Zhang (2018). "Practical Identifiability Analysis and Optimal Experimental Design for the Parameter Estimation of the ASM2d-Based EBPR Anaerobic Submodel". In: *Mathematical Problems in Engineering* 2018.3, pp. 1–9. DOI: 10.1155/2018/9201085.

Li, Z., X.-Z. Mao, T. S. Li and S. Zhang (2016). "Estimation of river pollution source using the space-time radial basis collocation method". In: *Advances in Water Resources* 88, pp. 68–79. DOI: 10.1016/j.advwatres.2015.11.019.

Liu, S. and P. Auckenthaler (2014). "Optimal sensor placement for event detection and source identification in water distribution networks". In: *Journal of Water Supply: Research and Technology-Aqua* 63.1, pp. 51–57. DOI: 10.2166/aqua.2013.106.

Liu, S., H. Che, K. Smith and C. Chen (2015). "A method of detecting contamination events using multiple conventional water quality sensors". In: *Environmental monitoring and assessment* 187.1, p. 4189. DOI: 10.1007/s10661-014-4189-4.

Liu, X. and Z. Zhai (2008). "Location identification for indoor instantaneous point contaminant source by probability-based inverse Computational Fluid Dynamics modeling". In: *Indoor air* 18.1, pp. 2–11. DOI: 10.1111/j.1600-0668.2007.00499.x.

Lorenz, M. (2015). "Entwicklung eines ökohydrologischen Modellsystems auf der Einzugsgebietsskala und Anwendung in den sommerfeuchten Tropen". Dissertation. Technische Universität Braunschweig. 274 pp.

Lorenz, M., S. Zeunert, H. Q. Nguyen and G. Meon (2017). "Ökohydrologische Modellierung eines Einzugsgebietes in den sommerfeuchten Tropen im Kontext von Klimawandel und anthropogener Entwicklung". In: *Hydrologie & Wasserbewirtschaftung* 61.6, pp. 408–423. DOI: 10.5675/HyWa_2017,6_4.

Maier, H. R., S. Razavi, Z. Kapelan, L. S. Matott, J. Kasprzyk and B. A. Tolson (2019). "Introductory overview: Optimization using evolutionary algorithms and other metaheuristics". In: *Environmental Modelling & Software* 114, pp. 195–213. DOI: 10.1016/j.envsoft.2018.11.018.

Maiwald, T. et al. (2016). "Driving the Model to Its Limit: Profile Likelihood Based Model Reduction". In: *PloS one* 11.9, e0162366. DOI: 10.1371/journal.pone.0162366.

Malcherek, A. (2018). *Gezeiten und Wellen. In Küsteningenieurwesen und Ozeanographie*. 2. Auflage. Wiesbaden: Springer Vieweg. 452 pp. DOI: 10.1007/978-3-658-19303-4.

Marsili-Libelli, S. and E. Giusti (2008). "Water quality modelling for small river basins". In: *Environmental Modelling & Software* 23.4, pp. 451–463. DOI: 10.1016/j.envsoft.2007.06.008.

Marsili-Libelli, S., M. B. Beck, P. Brunner, B. Croke, J. Guillaume, A. Jakeman, J. Jakeman, K. Keesman and H. Stigter (2014). "Practical identifiability analysis of environmental models". In: *Proceedings of the 7th International Congress on Environmental Modelling and Software*. 7th International Congress on Environmental Modelling and Software (San Diego, USA). Ed. by D. Ames, N. Quinn and A. Rizzoli. San Diego, CA, USA, pp. 681–693. URL: http://hdl.handle.net/1885/54328.

Martin, J. L., S. C. McCutcheon and R. W. Schottman (1999). *Hydrodynamics and Transport for Water Quality Modeling*. Boca Raton, Florida: CRC Press. 1817 pp.

Mazaheri, M., J. Mohammad Vali Samani and H. M. V. Samani (2015). "Mathematical Model for Pollution Source Identification in Rivers". In: *Environmental Forensics* 16.4, pp. 310–321. DOI: 10.1080/15275922.2015.1059391.

McDowell, D. M. and B. A. O'Connor (1977). *Hydraulic behaviour of estuaries*. Civil engineering hydraulics series. London: Macmillan.

Meeker, W. Q. and L. A. Escobar (1995). "Teaching about Approximate Confidence Regions Based on Maximum Likelihood Estimation". In: *The American Statistician* 49.1, p. 48. DOI: 10.2307/2684811.

Meon, G., M. Lorenz, A. Koch, S. Zeunert, T. T. H. Le, M. Pätsch and H. Q. Nguyen (2017). "Entwicklung einer Basisversion eines Managementsystems für die regionale Wasserwirtschaft einer Küstenzone in Vietnam". In: *Hydrologie & Wasserbewirtschaftung* 61.6, pp. 437–449. DOI: 10.5675/HYWA_2017,6_6.

Miao, H., X. Xia, A. S. Perelson and H. Wu (2011). "On identifiability of nonlinear ODE models and applications in viral dynamics". In: *SIAM review. Society for Industrial and Applied Mathematics* 53.1, pp. 3–39. DOI: 10.1137/090757009.

Millar, R. B. (2011). *Maximum likelihood estimation and inference. With examples in R, SAS, and ADMB*. Statistics in practice. Chichester West Sussex: Wiley. xvi, 357.

Murray, B. (2016). *Vietnamese factory caught dumping industrial waste*. Ed. by Anadolu Agency. URL: https://www.aa.com.tr/en/asia-pacific/vietnamese-factory-caught-dumping-industrial-waste-/715068 (visited on 02/12/2019).

Nelder, J. A. and R. Mead (1965). "A Simplex Method for Function Minimization". In: *The Computer Journal* 7.4, pp. 308–313. DOI: 10.1093/comjnl%2F7.4.308.

Neupauer, R. M. and J. L. Wilson (1999). "Adjoint method for obtaining backward-in-time location and travel time probabilities of a conservative groundwater contaminant". In: *Water Resources Research* 35.11, pp. 3389–3398. DOI: 10.1029/1999WR900190.

— (2001). "Adjoint-derived location and travel time probabilities for a multidimensional groundwater system". In: *Water Resources Research* 37.6, pp. 1657–1668. DOI: 10.1029/2000WR900388.

— (2003). "Backward location and travel time probabilities for a decaying contaminant in an aquifer". In: *Journal of Contaminant Hydrology* 66.1-2, pp. 39–58. DOI: 10.1016/S0169-7722(03)00024-X.

— (2004). "Numerical implementation of a backward probabilistic model of ground water contamination". In: *Ground water* 42.2, pp. 175–189. DOI: 10.1111/j.1745-6584.2004.tb02666.x.

Nguyen, H. P. and H. T. Pham (2012). "The Dark Side of Development in Vietnam". In: *Journal of Macromarketing* 32.1, pp. 74–86. DOI: 10.1177/0276146711423666.

Nocedal, J. and S. J. Wright (2006). *Numerical optimization*. 2nd ed. Springer series in operations research. New York: Springer. xxii, 664.

Olivier, A. and A. W. Smyth (2017). "On the Performance of Online Parameter Estimation Algorithms in Systems with Various Identifiability Properties". In: *Frontiers in Built Environment* 3, p. 380. DOI: 10.3389/fbuil.2017.00014.

Park, C., I. T. Telci, S.-H. Kim and M. M. Aral (2014). "Designing an optimal water quality monitoring network for river systems using constrained discrete optimization via simulation". In: *Engineering Optimization* 46.1, pp. 107–129. DOI: 10.1080/0305215X.2012.748049.

Park, J., K. T. Kim and W. H. Lee (2020). "Recent Advances in Information and Communications Technology (ICT) and Sensor Technology for Monitoring Water Quality". In: *Water* 12.2, p. 510. DOI: 10.3390/w12020510.

Parolin, R. d. S., A. J. d. Silva Neto, P. P. G. W. Rodrigues and O. Llanes Santiago (2015). "Estimation of a contaminant source in an estuary with an inverse problem approach". In: *Applied Mathematics and Computation* 260, pp. 331–341. DOI: 10.1016/j.amc.2015.03.054.

Price, K. V., R. M. Storn and J. A. Lampinen (2005). *Differential evolution. A practical approach to global optimization*. Natural computing series. Berlin and New York: Springer. xix, 538.

Prilop, K., H. Q. Nguyen, M. Lorenz, H. Le, T. H. Le and G. Meon (2014). "Integrated water quality monitoring of the Thi Vai River: An assessment of historical and current situation". In: *EWATEC–COAST: Contributions to 4th International Conference for Environment and Natural Resources - ICENR 2014*. Ed. by G. Meon, M. Pätsch, N. van Phuoc and N. Hong Quan. 1st ed. HYWAG Schriftenreihe. Göttingen: Cuvillier Verlag.

Pritchard, D. W. (1967). "What is an estuary: a physical viewpoint". In: *Estuaries*. Ed. by G. H. Lauff. 83. Washington D.C.: American Association for the Advancement of Science, pp. 3–5.

Pugh, D. T. (1987). *Tides, surges and mean sea level*. Chichester: Wiley. 472 pp.

Rathi, S. and R. Gupta (2015). "A critical review of sensor location methods for contamination detection in water distribution networks". In: *Water Quality Research Journal of Canada* 50.2, pp. 95–108. DOI: 10.2166/wqrjc.2014.011.

Raue, A., V. Becker, U. Klingmüller and J. Timmer (2010). "Identifiability and observability analysis for experimental design in nonlinear dynamical models". In: *Chaos: An Interdisciplinary Journal of Nonlinear Science* 20.4, p. 045105. DOI: 10.1063/1.3528102.

Raue, A., C. Kreutz, T. Maiwald, J. Bachmann, M. Schilling, U. Klingmüller and J. Timmer (2009). "Structural and practical identifiability analysis of partially observed dynamical models by exploiting the profile likelihood". In: *Bioinformatics (Oxford, England)* 25.15, pp. 1923–1929. DOI: 10.1093/bioinformatics/btp358.

Raue, A., J. Karlsson, M. P. Saccomani, M. Jirstrand and J. Timmer (2014). "Comparison of approaches for parameter identifiability analysis of biological systems". In: *Bioinformatics (Oxford, England)* 30.10, pp. 1440–1448. DOI: 10.1093/bioinformatics/btu006.

Raue, A., C. Kreutz, F. J. Theis and J. Timmer (2013). "Joining forces of Bayesian and frequentist methodology: a study for inference in the presence of non-identifiability". In: *Philosophical transactions. Series A, Mathematical, physical, and engineering sciences* 371.1984, p. 20110544. DOI: 10.1098/rsta.2011.0544.

Reichert, P. and P. Vanrolleghem (2001). "Identifiability and uncertainty analysis of the river water quality model no. 1 (RWQM1)". In: *Water Science and Technology* 43.7, pp. 329–338.

Ren, N. Q. et al. (2007). "Modeling the nitrobenzene spill in the Songhua River". In: *Water Supply* 7.2, pp. 115–123. DOI: 10.2166/ws.2007.046.

Rios, L. M. and N. V. Sahinidis (2013). "Derivative-free optimization: a review of algorithms and comparison of software implementations". In: *Journal of Global Optimization* 56.3, pp. 1247–1293. DOI: 10.1007/s10898-012-9951-y.

Savenije, H. (2012). *Salinity and Tides in Alluvial Estuaries*. 2. Auflage. 208 pp. URL: salinityandtides.com.

Schenk, J., E. Poeter and W. Navidi (2018). "Demystifying Fisher Information: What Observation Data Reveal about Our Models". In: *Ground water* 56.4, pp. 547–556. DOI: 10.1111/gwat.12668.

Schwaab, M., J. E. C. Biscaia, J. L. Monteiro and J. C. Pinto (2008). "Nonlinear parameter estimation through particle swarm optimization". In: *Chemical Engineering Science* 63.6, pp. 1542–1552. DOI: 10.1016/j.ces.2007.11.024.

Seth, A., K. A. Klise, J. D. Siirola, T. Haxton and C. D. Laird (2016). "Testing Contamination Source Identification Methods for Water Distribution Networks". In: *Journal of Water Resources Planning and Management* 142.4, p. 04016001. DOI: 10.1061/(ASCE)WR.1943-5452.0000619.

Shahmohammadi, A. and K. B. McAuley (2019). "Sequential Model-Based A-Optimal Design of Experiments When the Fisher Information Matrix Is Noninvertible". In: *Industrial & Engineering Chemistry Research* 58.3, pp. 1244–1261. DOI: 10.1021/acs.iecr.8b03047.

Shanahan, P. and S. C. Gaudet (2000). "Mixing and transport of pollutants in surface water". In: *Standard handbook of environmental science, health, and technology*. Ed.

by J. H. Lehr and J. K. Lehr. McGraw-Hill standard handbooks. New York, NY: McGraw-Hill.

Šimůnek, J. and J. W. Hopmans (2002). "1.7 Parameter Optimization and Nonlinear Fitting". In: *Methods of Soil Analysis*. Ed. by J. H. Dane and G. Clarke Topp. Madison, WI, USA: Soil Science Society of America, pp. 139–157. DOI: 10.2136/sssabookser5.4.c7.

Skaggs, T. H. and Z. J. Kabala (1994). "Recovering the release history of a groundwater contaminant". In: *Water Resources Research* 30.1, pp. 71–79. DOI: 10.1029/93WR02656.

Snodgrass, M. F. and P. K. Kitanidis (1997). "A geostatistical approach to contaminant source identification". In: *Water Resources Research* 33.4, pp. 537–546. DOI: 10.1029/96WR03753.

Stollberg, R. (2012). "Groundwater Contaminant Source Zone Identification at an Industrial and Abandoned Mining Site – A Forensic Backward-In-Time Modelling Approach". Dissertation. Martin Luther Universität Halle-Wittenberg. 203 pp.

Storey, M. V., B. van der Gaag and B. P. Burns (2011). "Advances in on-line drinking water quality monitoring and early warning systems". In: *Water research* 45.2, pp. 741–747. DOI: 10.1016/j.watres.2010.08.049.

Storn, R. and K. Price (1997). "Differential Evolution - A Simple and Efficient Heuristic for global Optimization over Continuous Spaces". In: *Journal of Global Optimization* 11.4, pp. 341–359. DOI: 10.1023/A:1008202821328.

Sun, A. Y. (2007). "A robust geostatistical approach to contaminant source identification". In: *Water Resources Research* 43.2, p. 225. DOI: 10.1029/2006WR005106.

Sun, N.-Z. and A. Sun (2015). *Model Calibration and Parameter Estimation*. New York, NY: Springer New York. 638 pp. DOI: 10.1007/978-1-4939-2323-6.

Sun, N.-Z. and A. Y. Sun (2006). "Inverse methods for parameter estimations". In: *Encyclopedia of hydrological sciences. EHS*. Ed. by M. G. Anderson. John Wiley & Sons, Ltd. DOI: 10.1002/0470848944.hsa154c.

Sun, N.-Z. and W. W.-G. Yeh (1990). "Coupled inverse problems in groundwater modeling: 2. Identifiability and experimental design". In: *Water Resources Research* 26.10, pp. 2527–2540. DOI: 10.1029/WR026i010p02527.

Telci, I. T. and M. M. Aral (2011). "Contaminant Source Location Identification in River Networks Using Water Quality Monitoring Systems for Exposure Analysis". In: *Water Quality, Exposure and Health* 2.3-4, pp. 205–218. DOI: 10.1007/s12403-011-0039-6.

Telci, I. T., K. Nam, J. Guan and M. M. Aral (2009). "Optimal water quality monitoring network design for river systems". In: *Journal of environmental management* 90.10, pp. 2987–2998. DOI: 10.1016/j.jenvman.2009.04.011.

Thomann, R. V. and J. A. Mueller (1987). *Principles of surface water quality modeling and control*. New York: HarperCollinsPublishers Inc. 644 pp.

Tran, D. T. L. (2008). *ENVIRONMENT-VIETNAM: River Pollution Scandal a Wake-up Call*. Ed. by IPS Inter Press Agency. URL: http://www.ipsnews.net/2008/12/environment-vietnam-river-pollution-scandal-a-wake-up-call/ (visited on 02/12/2019).

Trang, D. (2017). *Timeline: The Formosa Environmental Disaster*. Ed. by The Vietnamese. URL: https://www.thevietnamese.org/2017/11/timeline-the-formosa-environmental-disaster/ (visited on 02/12/2019).

Tryby, M. E., M. Propato and S. R. Ranjithan (2010). "Monitoring Design for Source Identification in Water Distribution Systems". In: *Journal of Water Resources Planning and Management* 136.6, pp. 637–646. DOI: 10.1061/(ASCE)WR.1943-5452.0000080.

US EPA (1990). *Technical Guidance Manual for Performing Waste Load Allocations, Book III: Estuaries. Part 1: Estuaries and Waste Load Allocation Models*. Washington D.C.

van Genuchten, M. T., F. J. Leij, T. H. Skaggs, N. Toride, S. A. Bradford and E. M. Pontedeiro (2013). "Exact analytical solutions for contaminant transport in rivers 1. The equilibrium advection-dispersion equation". In: *Journal of Hydrology and Hydromechanics* 61.2, pp. 146–160. DOI: 10.2478/johh-2013-0020.

van Ravenzwaaij, D., P. Cassey and S. D. Brown (2018). "A simple introduction to Markov Chain Monte-Carlo sampling". In: *Psychonomic bulletin & review* 25.1, pp. 143–154. DOI: 10.3758/s13423-016-1015-8.

VietNamNews (2011). "Untreated waste water found pouring into river". In: *VietNamNews*. URL: https://vietnamnews.vn/environment/214119/untreated-waste-water-found-pouring-into-river.html (visited on 11/06/2020).

Visvanathan, C. and M. Padmasri (2010). "Introduction: Water environment in Southeast Asia: Where do we stand today?" In: *Southeast Asian water environment. Volume 4*. Ed. by K. Fukushi, F. Kurisu, K. Oguma, H. Furumai and P. Fontanos. London: IWA Publishing, pp. 1–10.

Vugrin, K. W., L. P. Swiler, R. M. Roberts, N. J. Stucky-Mack and S. P. Sullivan (2007). "Confidence region estimation techniques for nonlinear regression in groundwater flow: Three case studies". In: *Water Resources Research* 43.3, p. 1796. DOI: 10.1029/2005WR004804.

Wagner, D. E., R. M. Neupauer and C. Cichowitz (2015). "Adjoint-Based Probabilistic Source Characterization in Water-Distribution Systems with Transient Flows and Imperfect Sensors". In: *Journal of Water Resources Planning and Management* 141.9, p. 04015003. DOI: 10.1061/(ASCE)WR.1943-5452.0000508.

Wahde, M. (2008). *Biologically inspired optimization methods. An introduction*. Southampton UK and Boston MA: WIT Press. 218 pp.

Walter, E. and L. Pronzato (1996). "On the identifiability and distinguishability of nonlinear parametric models". In: *Mathematics and Computers in Simulation* 42.2-3, pp. 125–134. DOI: 10.1016/0378-4754(95)00123-9.

Wang, H. and X. Jin (2013). "Characterization of groundwater contaminant source using Bayesian method". In: *Stochastic Environmental Research and Risk Assessment* 27.4, pp. 867–876. DOI: 10.1007/s00477-012-0622-9.

Wang, J., J. Zhao, X. Lei and H. Wang (2018). "New approach for point pollution source identification in rivers based on the backward probability method". In: *Environmental pollution* 241, pp. 759–774. DOI: 10.1016/j.envpol.2018.05.093.

Wang, Z. and J. Liu (2012). "Identification of the pollution source from one-dimensional parabolic equation models". In: *Applied Mathematics and Computation* 219.8, pp. 3403–3413. DOI: 10.1016/j.amc.2008.03.014.

Weise, T. (2009). *Global Optimization Algorithms - Theory and Application*. Second Edition. Self-Published. 820 pp. URL: http://www.it-weise.de.

Willmott, C. J., S. G. Ackleson, R. E. Davis, J. J. Feddema, K. M. Klink, D. R. Legates, J. O'Donnell and C. M. Rowe (1985). "Statistics for the evaluation and comparison of models". In: *Journal of Geophysical Research* 90.C5, p. 8995. DOI: 10.1029/JC090iC05p08995.

Willmott, C. J., S. M. Robeson and K. Matsuura (2012). "A refined index of model performance". In: *International Journal of Climatology* 32.13, pp. 2088–2094. DOI: 10.1002/joc.2419.

Witkowski, W. R. and J. J. Allen (1993). "Approximation of parameter uncertainty in nonlinear optimization-based parameter estimation schemes". In: *AIAA Journal* 31.5, pp. 947–950. DOI: 10.2514/3.11709.

Wolanski, E. and M. Elliott (2015). *Estuarine Ecohydrology. An Introduction*. 2nd ed. Burlington: Elsevier Science. 334 pp.

World Bank Group (2019). *Vietnam: Toward a safe, clean and resilient water system*. World Bank, Washington, D.C. URL: https://openknowledge.worldbank.org/handle/10986/31770.

Yang, H., D. Shao, B. Liu, J. Huang and X. Ye (2016). "Multi-point source identification of sudden water pollution accidents in surface waters based on differential evolution and Metropolis–Hastings–Markov Chain Monte Carlo". In: *Stochastic Environmental Research and Risk Assessment* 30.2, pp. 507–522. DOI: 10.1007/s00477-015-1191-5.

Zeunert, S., M. Lorenz, H. Q. Nguyen and G. Meon (2017). "Modellgestützte Untersuchungen der Auswirkungen des Klimawandels und fortschreitender anthropogener Entwicklungen auf die Wasserqualität des tropischen Thi-Vai-Ästuars". In: *Hydrologie & Wasserbewirtschaftung* 61.6, pp. 424–436. DOI: 10.5675/HyWa_2017,6_5.

Zeunert, S. and G. Meon (2020). "Influence of the spatial and temporal monitoring design on the identification of an instantaneous pollutant release in a river". In: *Advances in Water Resources*. DOI: 10.1016/j.advwatres.2020.103788.

Zhang, J., L. Zeng, C. Chen, D. Chen and L. Wu (2015). "Efficient Bayesian experimental design for contaminant source identification". In: *Water Resources Research* 51.1, pp. 576–598. DOI: 10.1002/2014WR015740.

Zhang, S.-P. and X.-P. Xin (2017). "Pollutant source identification model for water pollution incidents in small straight rivers based on genetic algorithm". In: *Applied Water Science* 7.4, pp. 1955–1963. DOI: 10.1007/s13201-015-0374-z.

Zhu, X., Y. Yue, P. W. H. Wong, Y. Zhang and J. Tan (2018). "Optimum Water Quality Monitoring Network Design for Bidirectional River Systems". In: *International journal of environmental research and public health* 15.2. DOI: 10.3390/ijerph15020195.

A Appendix

A.1 Unidirectional test case (River)

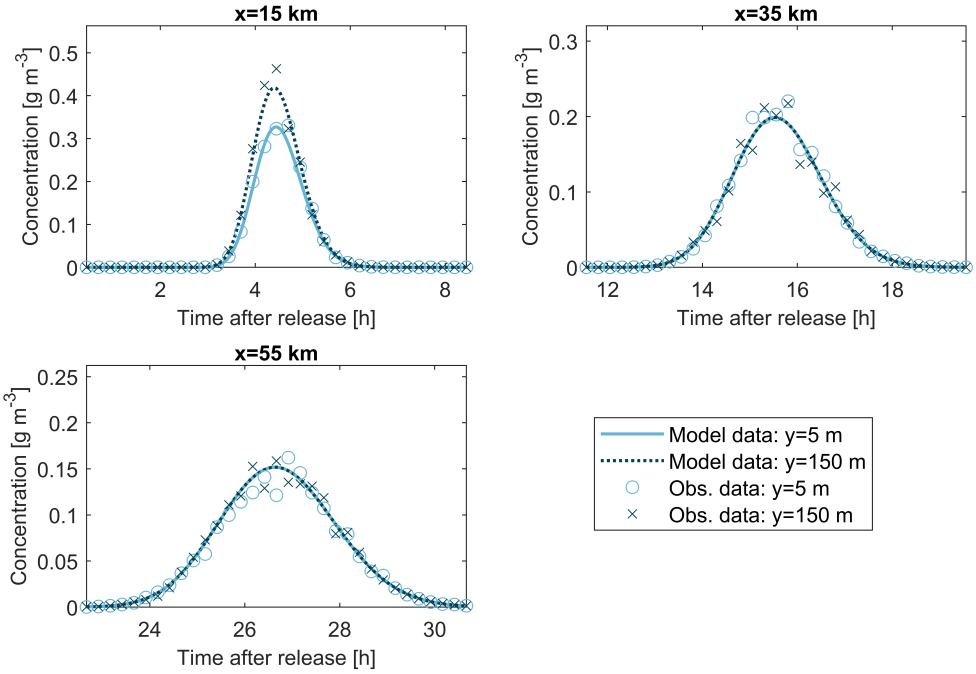

Figure A.1: Simulated concentration time series and considered noise-perturbed monitoring data at the monitoring stations of the cross-sections A, B, and C for the reference scenario of the unidirectional test case.

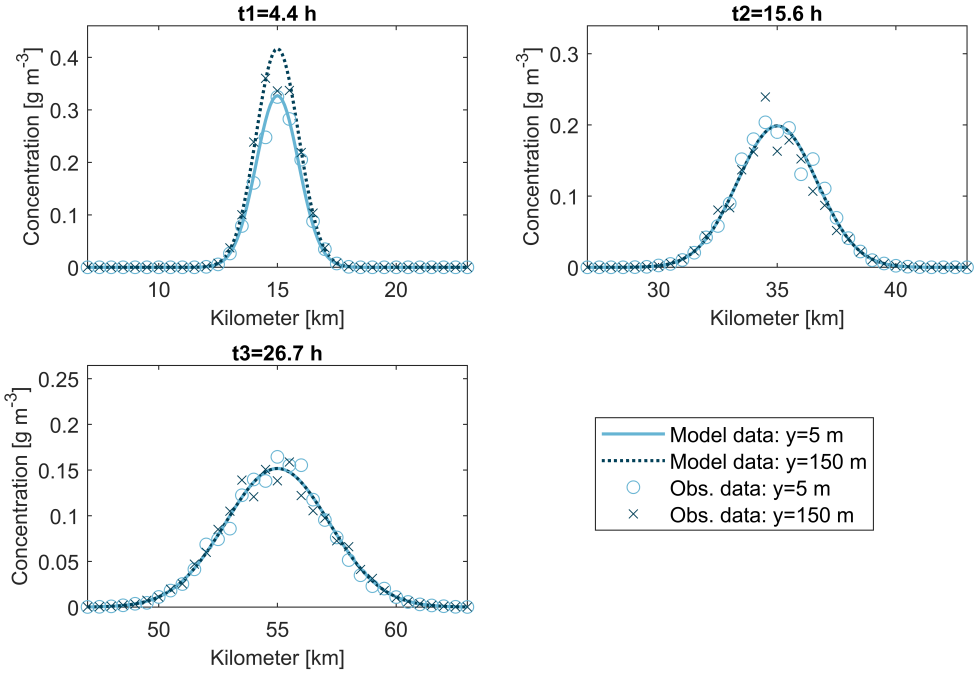

Figure A.2: Simulated longitudinal concentration profiles and considered noise-perturbed monitoring data for the longitudinal measurement campaigns at times t1, t2 and t3 for the reference scenario of the unidirectional test case.

A.2 Bidirectional test case (Estuary)

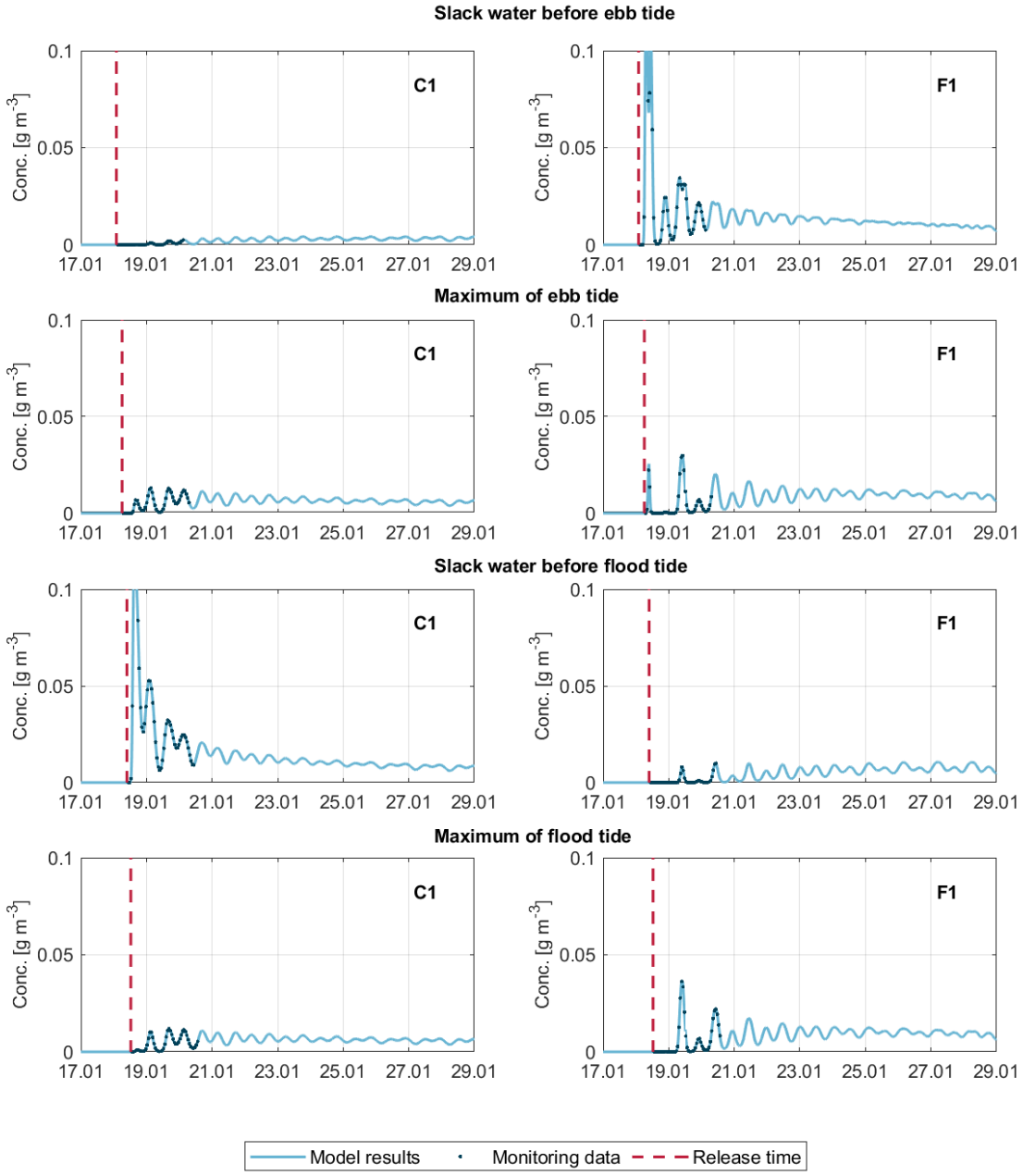

Figure A.3: Simulated concentration time series and considered monitoring data for PSI at the stations C1 and F1 for the bidirectional test case.

A.3 Thi Vai Estuary

A.3.1 Evaluation of monitoring data

Table A.1: Discharge characteristics of the tributaries flowing into the Thi Vai Estuary, derived using the simulated discharge of the hydrological model PANTA RHEI from 1998 to 2013.

	Bung Mon	**Suoi Ca**	**Cau Vac**	**Ben Ngu**	**Muong**	**Total**
Q_{10}	1.1	0.4	0.8	0.4	0.8	3.6
Q_{25}	1.4	0.6	1.1	0.5	1.1	4.7
Q_{50}	2.4	1.2	2.1	0.8	2.0	8.6
Q_{75}	5.0	4.0	4.9	1.5	4.3	19.8
Q_{90}	9.7	11.0	8.6	2.8	9.1	41.3
Q_{mean}	4.3	4.1	3.7	1.4	4.0	17.6
Q_{dry}	1.6	1.0	1.2	0.6	1.3	5.7
Q_{wet}	6.8	7.0	6.1	2.1	6.1	28.2

Table A.2: Amplitudes and phases of the most important tidal constituents in the Thi Vai Estuary calculated with the MATLAB program UTide.

(a) Amplitude [m]

Constituent	**Vung Tau**	**Cai Mep**	**Vedan**	**Long Tho**
M2	0.78	0.91	1.03	0.99
K1	0.60	0.62	0.64	0.58
O1	0.45	0.46	0.46	0.40
S2	0.30	0.35	0.41	0.37
SA	0.21	0.22	0.23	0.20
P1	0.19	0.20	0.20	0.16
N2	0.17	0.19	0.21	0.19
K2	0.10	0.11	0.13	0.15
F	0.96	0.86	0.77	0.72

(b) Phase [deg]

Constituent	**Vung Tau**	**Cai Mep**	**Vedan**	**Long Tho**
M2	38	47	55	59
K1	312	316	319	320
O1	262	267	269	271
S2	80	91	100	106
SA	354	354	354	357
P1	308	313	317	322
N2	15	25	34	40
K2	95	106	116	124

A.3.2 Optimal monitoring network

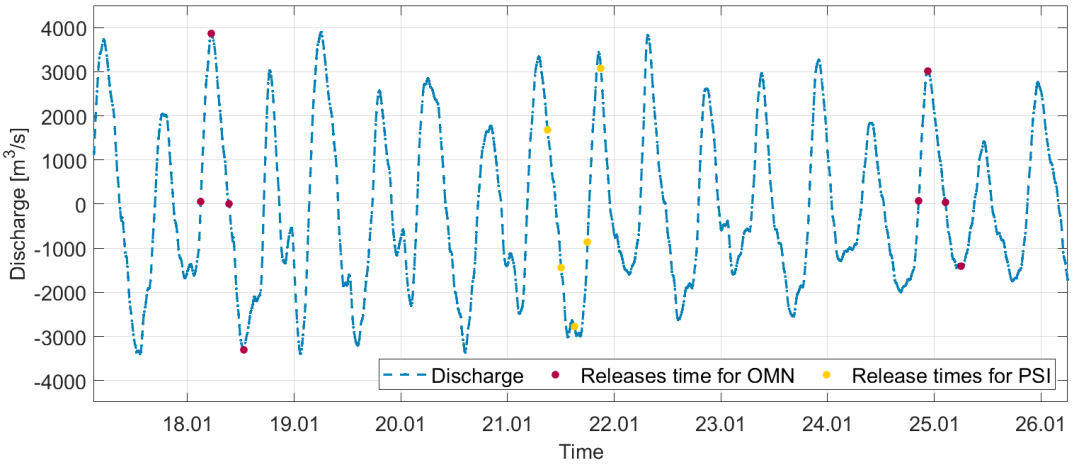

Figure A.4: Considered release times for the design of an optimal monitoring network and pollution source identification in the Thi Vai Estuary as well as the corresponding discharge time series in the middle section of the Thi Vai Estuary.

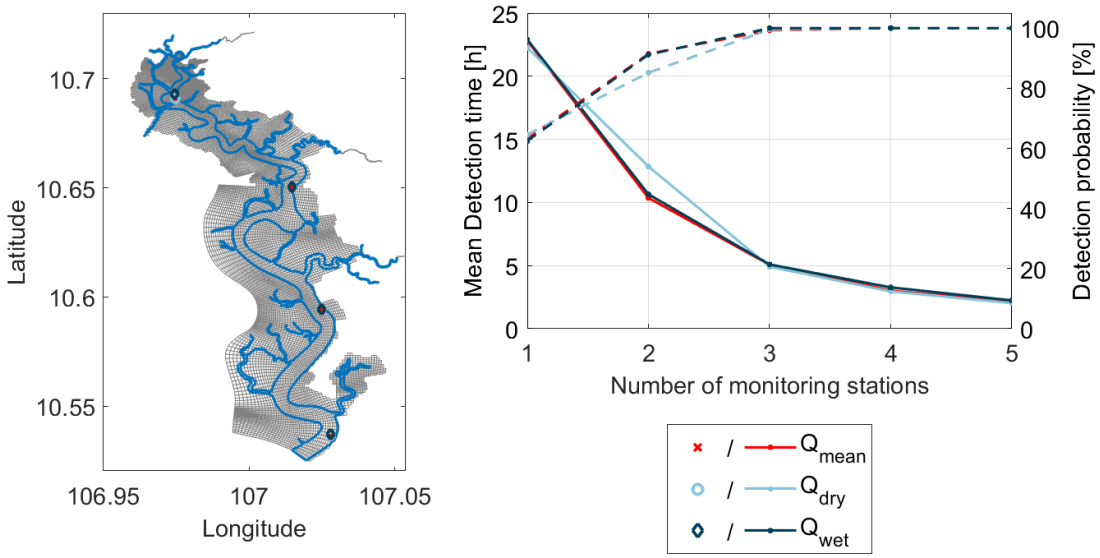

Figure A.5: Influence of the freshwater inflow on the design of the monitoring network for the Thi Vai Estuary.

A.3.3 Pollution source identification

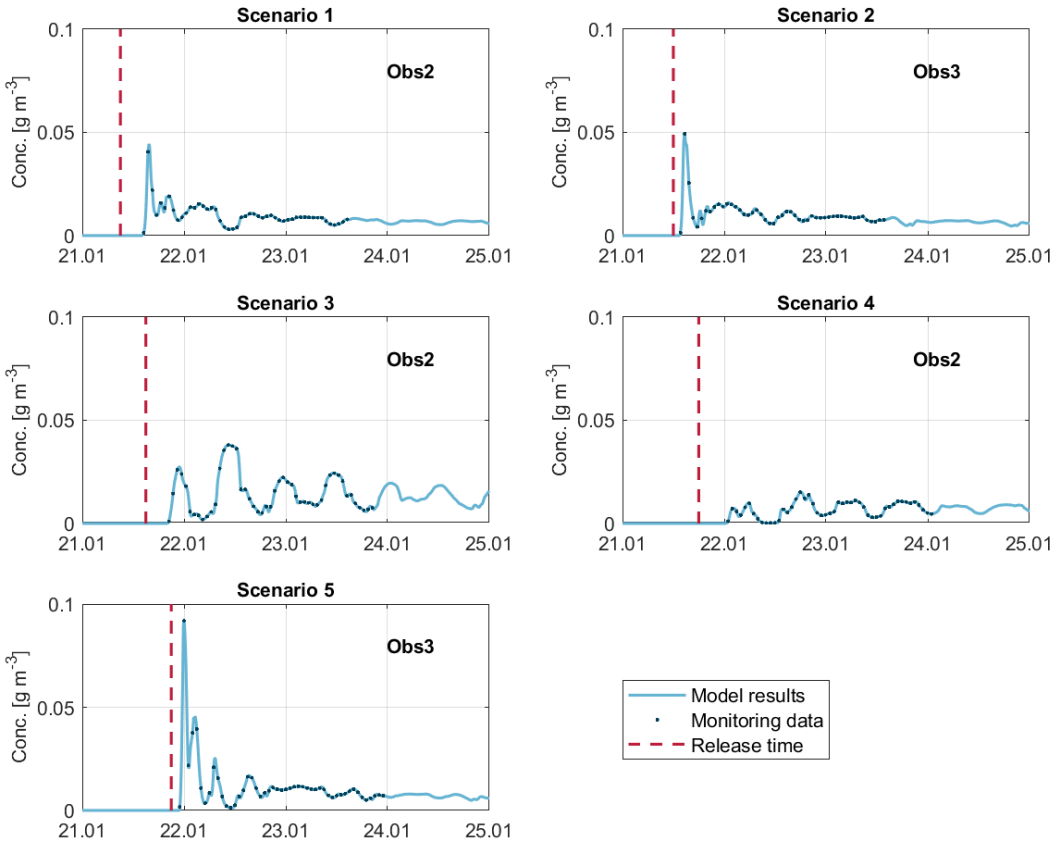

Figure A.6: Simulated concentration time series and considered monitoring data used for pollution source identification in the Thi Vai Estuary.

List of Figures

List of Tables

List of Abbreviations and Symbols

Abbreviations

ACO	Ant Colony Optimization
ADCP	Acoustic Doppler Current Profiler
ADRE	Advection-Dispersion-Reaction Equation
ANN	Artificial Neural Network
ASFS	Adaptive Sequential Feature Selection
BGA	Basic Genetic Algorithm
BLP	Backward Location Probability
BOD	Biological Oxygen Demand
BPM	Backward Probability Method
BTTP	Backward Travel Time Probability
DE	Differential Evolution
DO	Dissolved Oxygen
DONRE	Department of Environment and Resources
DT	Detection Time
DRAM	Delayed Rejection and Adaptive Metropolis algorithm
EPA	Environmental Protection Agency
EWS	Early-Warning System
FIM	Fisher Information Matrix
FLP	Forward Location Probability
GA	Genetic Algorithm
GPS	Generalized Pattern Search
GUI	Graphical User Interface
IER	Institute for Environmental Resources
MADS	Mesh Adaptive Direct Search
MAE	Mean Absolute Error
MET	Maximum Ebb Tide
MFT	Maximum Flood Tide
MLE	Maximum Likelihood Estimator
MCMC	Markov Chain Monte Carlo
MH-MCMC	Metropolis-Hastings Markov Chain Monte Carlo
MOPSO	Multi-Objective Particle Swarm Optimization
OED	Optimal Experimental Design
PBIAS	Percent Bias

PL	Profile Likelihood
PSI	Pollution Source Identification
PSO	Particle Swarm Optimization
PSP	Pollution Source Parameters
RBF	Radial Basis Function
RMSE	Root Mean Squared Error
SET	Slack water before Ebb Tide
SFT	Slack water before Flood Tide
SSE	Summed Squared Errors
SWMM	Storm Water Management Model
UHSLC	Research Quality Database of the University of Hawaii Sea Level Center
UTide	Unified Tidal Analysis and Prediction
WDS	Water Distribution System

Latin Uppercase Symbols

A_i	[m]	amplitude of the the ith tidal constituent
CM	–	correlation matrix
CR	–	crossover rate
D	–	distance metric
D_m	$[\mathrm{m^2\,s^{-1}}]$	molecular diffusion coefficient
$D_{t,x}$	$[\mathrm{m^2\,s^{-1}}]$	turbulent diffusion coefficient in x-direction
D_x	$[\mathrm{m^2\,s^{-1}}]$	dispersion coefficient in x-direction
D_y	$[\mathrm{m^2\,s^{-1}}]$	dispersion coefficient in y-direction
FIM	–	Fisher Information Matrix
F	–	tidal form factor
F	–	scaling factor for mutation
F_x, F_y	$[\mathrm{m\,s^{-2}}]$	horizontal Reynolds stresses
J_x	$[\mathrm{g\,m^{-2}\,s^{-1}}]$	mass flux in x-direction
K	–	parameter subset
M	–	number of installed monitoring stations
M_s	[g]	total released pollutant mass
N	–	number of tidal constituents
N	–	number of potential monitoring stations
NP	–	number of individuals in the population
O_i	–	ith observed value
$\overline{O}$	–	mean of the observed values
Q	$[\mathrm{m\,s^{-1}}]$	contributions per unit area
P_i	–	ith model predicted value
P_x, P_y	$[\mathrm{kg\,m^{-2}\,s^{-2}}]$	horizontal pressure terms
R	–	reliability of the monitoring system

S	$[\mathrm{g\,m^{-3}\,s^{-1}}]$	sinks and sources term of a transport model
S	–	number of pollution scenarios
S	–	sensitivity or Jacobian matrix
$\overline{S}$	–	scaled sensitivity matrix
$\tilde{S}$	–	normalized sensitivity matrix
$\tilde{S_K}$	–	submatrix of $\tilde{S}$
T_i	[h]	tidal period of the ith tidal constituent
W	[m]	river width
W	–	weight matrix for pollution scenarios
X	–	monitoring network

Latin Lowercase Symbols

c	$[\mathrm{g\,m^{-3}}]$	solute/pollutant concentration
c_{obs}	$[\mathrm{g\,m^{-3}}]$	observed pollutant concentration
c_{sim}	$[\mathrm{g\,m^{-3}}]$	simulated pollutant concentration
c_{th}	$[\mathrm{g\,m^{-3}}]$	concentration threshold
d	–	measurement data
d	[m]	depth below the reference plane
d_1	–	modified index of agreement
d_2	–	index of agreement
df	–	degrees of freedom
f	$[\mathrm{s^{-1}}]$	Coriolis parameter
$f(\theta)$	–	model output
h	[m]	river/water depth
k	$[\mathrm{d^{-1}}]$	process coefficient/decay rate
n	–	number of measurement data
p	–	number of unknown parameters
r	–	correlation coefficient
s_{ij}	–	coefficient of the sensitivity matrix S
$\tilde{s}_{ij}$	–	coefficient of the normalized sensitivity matrix $\tilde{S}$
s_{θ_j}	–	scaling factor related to the uncertainty in the initial value of the jth parameter value
s_{y_i}	–	estimate of the standard deviation of the ith measurement
$\overline{s}_{ij}$	–	coefficient of the scaled sensitivity matrix $\overline{S}$
t	[s]	time
$\overline{t}_d$	[s]	mean detection time
$t_{d,s}$	[s]	detection time for a single scenario
t_s	[s]	pollutant release time
$u_{i,g}$	–	trial vector
$v_{i,g}$	–	mutant vector
v_x	$[\mathrm{m\,s^{-1}}]$	depth-averaged flow velocity in x-direction

v_y	$[\mathrm{m\,s^{-1}}]$	depth-averaged flow velocity in y-direction
w_s	–	weight assigned to the sth scenario
x	[m]	x-coordinate
$x_{i,g}$	–	target vector
x_{obs}	m	x-coordinate of the monitoring location
x_s	[m]	x-coordinate of the source location
y	[m]	y-coordinate
y_{obs}	m	y-coordinate of the monitoring location
y_s	[m]	y-coordinate of the source location

Greek Uppercase Symbols

$\Delta\theta$	–	perturbation factor
Σ_ϵ	–	error covariance matrix
Σ_p	–	covariance matrix of the parameter estimates

Greek Lowercase Symbols

α	–	significance level
δ_s	–	indicator variable
ϵ	–	measurement error
ϵ_{rel}	–	relative measurement error
ζ	[m]	water level above a reference plane
ζ_0	[m]	mean height of water level above a reference plane
η_0	[m]	residual tidal signal
θ	[-]	parameter vector
θ^*	[-]	true parameter vector
$\hat{\theta}$	[-]	estimated parameter vector
λ	–	eigenvalue
λ_{min}	–	smallest eigenvalue
λ_{max}	–	largest eigenvalue
ρ	$[\mathrm{kg\,m^{-3}}]$	water density
σ	–	standard deviation
σ_i	–	standard deviation of the ith measurement error
σ_{rel}	–	relative standard deviation
τ	–	backward time
τ_{bx}, τ_{by}	$[\mathrm{kg\,m^{-1}\,s^{-2}}]$	bed shear stresses
τ_{sx}, τ_{sy}	$[\mathrm{kg\,m^{-1}\,s^{-2}}]$	free surface (wind) stresses
ϕ_i	$[^\circ]$	phase of the ith tidal constituent
ψ	–	adjoint state
ω_i	$[^\circ\,\mathrm{h^{-1}}]$	angular frequency of the ith tidal constituent